Constraints on New Physics from Neutrino and Other Particle Experiments

Yee Kao

Dissertation submitted to the Faculty of the Virginia Polytechnic Institute and State University in partial fulfillment of the requirements for the degree of

Doctor of Philosophy
in
Physics

Tatsu Takeuchi, Chair
Djordje Minic
Tetsuro Mizutani
Mark Pitt

December 07, 2010
Blacksburg, Virginia

Keywords: High Energy Physics, Elementary Particles, Neutrino, Physics Beyond Standard Model

Constraints on New Physics from Neutrino and Other Particle Experiments

Yee Kao

(ABSTRACT)

In this thesis we analyze a number of past, current, and future experiments to extract information on physics beyond standard model. We use the Jacobi method to derive a set of simplified expressions for the probabilities of neutrino oscillations in matter. Using the proposed Fermilab-HyperK experiment, we place constraints on models beyond the Standard Model such as models with generation distinguishing Z', models containing various types of leptoquarks, R-parity violating supersymmetry models, models with extended Higgs sector. In several cases, we find that the limits thus thus obtained could be competitive with those expected from direct searches at the Large Hadron Collider.

We then consider the possible effects of new physics beyond the Standard Model on precision measurements. In particular, we look at recent Bell/Babar results on the $B \to \tau\nu$ branching fraction, and the bounds on $\tau^- \to \ell^- K_S^0$ ($\ell = e$ or μ) from Babar. As a general framework of analyzing new physics beyond the Standard Model, we discuss what constraints can be placed on R-parity violating SUSY from these experiments. To complete our analysis, we update the single-coupling bounds on R-parity violating supersymmetry using the most up to date data as of October 2009. In addition to the data listed in the latest Review of Particle Properties [116], we utilize a new measurement of the weak charge of cesium-133 [103], and preliminary τ-decay branching fractions from Babar [104]. Analysis of semileptonic D-decay is improved by the inclusion of experimentally measured form-factors into the calculation of the Standard Model predictions.

Acknowledgements

First of all, I would like to express my greatest gratitude to my adviser, Dr. Tatsu Takeuchi, whose advising, guidance, and support were of tremendous help for me throughout all the years that I have been in graduate school at Virginia Tech. I have learned a lot from him in various areas of math and physics because he is an amazing teacher. His patience and ability to explain complex matters in the most simple and clear manner have inspired me since the very beginning of my graduate study.

I would also like to thank Dr. Djordje Minic, Dr. Tetsuro Mizutani, Dr. Mark Pitt, and Dr. Patrick Huber for the energy and effort they put in reading this manuscript. Also, I thank my collaborators Minako Honda, Naotoshi Okamura, and Alexey Pronin. It has been my pleasure working with you.

I am very grateful to Dr. Marvin Blecher, Dr. Kyungwha Park, Dr. Eric Sharpe, Dr. Rahul Kulkarni, and Dr. John Simonetti for all the physics they have taught me and all the help they have given me. And a special thanks to Chris Thomas, who went out of her way to ensure everything ran smoothly during my time here at Blacksburg and even before I came here.

I would like to thank Andrew Fenley and Zack Lewis for accompanying me all these years, as fellow students and as friends. And thank you to Elizabeth Chin, whose support and encouragement have helped me through many difficult times during this endeavor.

Last but not least, I would like to thank my parents and grandparents, who have provided support throughout my education, and my uncles and aunts, who always looked out for me as if I was one of their own children. This would not have been possible without you.

Contents

List of Figures

List of Tables

Chapter 1

Introduction

The standard model (SM) of particle physics describes the behavior of elementary particles, namely their electromagnetic, weak, and strong interactions. Numerous particle experiments have been performed and no significant deviations from the SM prediction has been found. However, many questions remain unanswered. For instance, the SM does not tell us why neutrinos have mass, why their masses are so small, why there are mixings between different flavors, why the mixing in the lepton sector is so different than the mixing in the quark sector, and what the origin of the matter-antimatter asymmetry of the universe is. These questions are all related to neutrinos, and I believe the key to answering them lies in a better understanding of neutrino physics.

In the SM, neutrinos are assumed to be massless. However, the solar neutrino deficit observed by the Homestake experiment suggests that neutrinos do have mass and the deficit is caused by neutrino oscillation. To understand the properties of neutrinos, numerous experiments have been performed and more are being planned. Neutrino oscillation parameters have been measured through solar, atmospheric, reactor, and accelerator neutrino experiments. Some of these parameters are now better constrained, while others remain primary objectives for future experiments.

Prior to the discovery of neutrino oscillations, the only information we had on flavor mixing was that among the quarks. Now with the additional information on the neutrino mixing angles, we have more clues that may one day lead us to the understanding of what flavor is, and why different flavors mix. However, neutrino flavor mixing angles have been found to be very different from that of the quarks. For instance, the neutrino mixing angle θ_{23} can be as large as 45° but the largest quark mixing angle θ_{13} is only 12°. On the other hand, we still do not know the size of the neutrino mixing angle θ_{13}, only its upper limit. Several experiments are either taking data or being planned to address these issues, such as the Daya Bay experiment. When more experimental data become available, we can extract information on why there are mixings and what flavor is.

Results from neutrino experiments may also have several implications on cosmology. Our universe is dominated by particles and not anti-particles, which could be explained by violation of CP-symmetry. Some of the neutrino experiments can potentially measure the CP violating phase δ_{CP}, thus give us clues to what origin of the matter-antimatter asymmetry is. Furthermore, since the neutrinos are so abundant in the universe, the absolute value of their masses have a significant impact on how the universe evolved. It is puzzling that neutrino masses are so small

compared to other fermions. From astronomical observations, we found out that neutrino masses are at least three orders of magnitude smaller than charged leptons. Although neutrino oscillation experiments do not measure the absolute scale of individual neutrino masses, they are sensitive to mass-squared differences between different neutrino flavors. These extra information can still help us understand where particle masses come from.

One popular mechanism that generates small neutrino masses is the seesaw mechanism. It requires a set of heavy right-handed neutrinos, which are included in various models beyond the SM. These models, along with many other models beyond the SM can have effects that will show up at low energies. In a long-baseline neutrino experiment, neutrinos interact with matter inside of Earth through either neutral current or charged current interactions. It is possible that additional contributions from new physics can affect the neutrino oscillation probabilities. Therefore, we can utilize neutrino oscillation experiments to probe physics beyond the SM, especially that certain types of interactions are invisible to the LHC.

Numerous models beyond the SM have been proposed in attempts to explain the smallness of neutrino masses and other puzzles of the SM. In addition to neutrino oscillation experiments and direct searches at the LHC, these new physics can also be seen at various other experiments. While we wait for the results from the LHC, we should also look at existing experimental data. The amount of data and the precision of these experiments means that even the smallest deviation from the SM could still be detected.

In this thesis, I present a set of simplified formulae for matter effects of neutrino oscillation. Then I discuss the potential bounds on serval models beyond the SM obtainable from neutrino oscillation experiments. Finally, I discuss the constraints on new physics from various precision measurements, such as Bell, Babar, and other particle experiments.

1.1 Neutrino Oscillation

New physics can affect neutrino oscillation experiments through matter effects. To describe the matter effects, a set of rather complicated formulae involving the mixing angles and mass-squared differences is used. This is adequate if we were calculating the oscillation probabilities numerically. Analytically, it is not very clear from these formulae how the oscillation in matter depends on the vacuum parameter, not to mention if we want to incorporate effects from new physics. In an effort to understand how these new physics will affect neutrino oscillation, we developed a set of simplified formulae for neutrino oscillation probabilities using the Jacobi method. Utilizing these formulae, the dependence of oscillation probabilities in matter on mixing angles and mass-squared-differences in vacuum becomes transparent. We show in chapter 2 that matter effects can be described as shifts in certain neutrino mixing angles.

It was shown in [34] that long baseline neutrino oscillation experiments could be sensitive to physics beyond the SM. In particular, new physics that are not universal in the neutral current interactions. As an example, we consider a hypothetical experiment in which a muon neutrino beam from Fermilab is sent to the proposed Hyper-Kamiokande detector in Japan. This experiment can potentially place a constraint on universality violation at the 1% level after 5 years of data taking.

Various models of physics beyond SM violates lepton We analyzed how various physics beyond the SM can affect the matter effects on neutrino oscillation. We considered models such as Z',

topcolor assisted technicolor, leptoquarks, R-parity violating SUSY, and models with extended Higgs sector. Base on the example above, we were able to extract potential constraints on these models.

1.2 Precision Measurements from Belle/Babar

It is puzzling that the couplings in the SM are so small compared to Planck scale. One of the possible solutions is to introduce extra particles through SUSY. Each SM particles now have a corresponding superpartner. Many models beyond the SM or GUTs have lepton- and baryon-number violating processes. A good example is the SUSY with R-parity violating couplings. The RPV SUSY contains many different types of processes. Therefore using RPV SUSY as a general framework, we calculate bounds on various combinations of RPV couplings (Chapter 4), and bounds on single RPV couplings (Chapter 5). These bounds can then be translated to bounds on other models beyond the SM.

Certain RPV couplings can be constrained using recent Belle and Babar τ-decay data

$B \to \tau\nu_\tau$ To extract the effects from new physics, we first look at the SM prediction. Although the error is not very small, we use the value of V_{ub} from charmless semileptonic B-decays and the value f_B from unquenched lattice QCD for these values are unaffected by RPV. From the recent Babar measurement we place constraints on either t-channel sdown exchange or s-channel selectron exchange.

$\tau^- \to l^- K_S^0$ RPV can also generate tau lepton-flavor-violating decays. Since there exist no SM contribution, the recent Babar measurement for the upper limit of such process translate directly to into bounds on new physics. In the RPV SUSY framework, we place bounds on sup exchange and sneutrino exchange.

1.3 Various Other Experiments

To complete our analysis, we update the single-coupling bounds from the R-parity violating SUSY framework. We survey the data from various measurements and analyze the constraints on new physics. The measurements include lepton and meson decay ratios, CKM matrix elements, the weak charge of atomic nuclei, and neutrinoless double beta decay.

1.3.1 CKM unitarity

The CKM matrix element V_{ud} is affected by RPV coupling. Using the values of V_{us} and V_{ub} and the unitarity condition, we can extract the constraints on λ'_{11k} and λ_{12k}.

1.3.2 Semi-leptonic D and leptonic D_s-decay

To investigate the effects of RPV on D-decay and D_S-decay, we need a good prediction for the SM process. We present in the appendix a detailed calculation of the form-factors for the matrix elements base on various good experimental data from FOCUS, Belle, Babar, and CLEO. This was not done in preceding analyses and we show that the differences could be significant in some cases.

1.3.3 Atomic parity violation

RPV can have effect on atomic parity violation experiments through the muon decay constant G_μ. Using the latest result of the weak charge of cesium-133, we place bounds on λ'_{11k}, λ'_{1j1}, and λ_{12k}.

1.3.4 Neutrinoless double beta decay

In addition to providing a probe of lepton number violation and the scale of neutrino masses, neutrinoless double beta decay can also probe new physics that may not be visible at LHC. Many experiments have been looking for neutrinoless double beta decay and so far no concrete evidence have been found. This puts an extremely tight constraint on the underlying mechanism, whether it is heavy Majorana neutrinos, R-parity violating SUSY, or other models of physics beyond the SM.

Chapter 2

Neutrino Oscillation

In this chapter we present simple analytical approximations to matter-effect corrected effective neutrino mixing angles and effective mass-squared-differences. The expressions clarify the dependence of oscillation probabilities in matter to the mixing angles and mass-squared-differences in vacuum, and are useful for analyzing long-baseline neutrino oscillation experiments.

2.1 Introduction

Since the proposal of neutrino existence, numerous experiments have been done to investigate their properties. One of the challenges experimentalists encounter is that neutrinos interact very weakly, therefore are very difficult to detect. But, it is also this same property that allows us to probe deeper into the stars and further out to distant astronomical objects where traditional optical and radio observations would have failed.

One major discovery has brought neutrino physics to another level: neutrino oscillation. This can be best explained by nonzero neutrino masses and that the neutrino mass eigenstates are different from neutrino flavor eigenstates. Several long-baseline (LBL) neutrino oscillation experiments are in progress and many more being proposed to better determining the neutrino oscillation parameters, namely: neutrino mass-squared differences, neutrino mixing angels, and CP violating phase. Since the neutrino beams of LBL experiments necessarily traverse the Earth, the understanding of matter effects is crucial in extracting the vacuum oscillation parameters from the measured oscillation probabilities in matter.

The calculation of matter effects requires the diagonalization of the modified Hamiltonian, which is a 3×3 matrix that depends on both energy and matter density. This can be done numerically on a computer with ease, but the dependence of the oscillation probabilities on the vacuum parameters is not transparent. It is also possible to write down exact analytical expressions for the effective oscillation parameters in terms of those in vacuum, but the expressions are too complicated to be illuminating.

In this chapter, we present simple approximate expressions for the matter-effect modified effective mass-squared-differences and mixing angels in terms of vacuum parameters. They are simple enough to be used by hand, yet accurate in a wide energy range.

2.2 Neutrino Oscillation

2.2.1 The MNS Matrix

Neutrinos are created in their flavor eigenstates, but they propagate in theirs mass eigenstates. Since the mass eigenstates and flavor eigenstates of the neutrinos are not the same, oscillation may occur. The flavor eigenstates $|\nu_\alpha\rangle(\alpha = e, \mu, \tau)$ are related to the mass eigenstates $|\nu_i\rangle(i = 1, 2, 3)$ via the Maskawa-Nakagawa-Sakata(MNS) matrix:

$$(V_{MNS})_{\alpha i} \equiv \langle \nu_\alpha | \nu_i \rangle, \quad |\nu_i\rangle = \sum_{\alpha=e,\mu,\tau} (V_{MNS})_{\alpha i} |\nu_\alpha\rangle, \quad |\nu_\alpha\rangle = \sum_{i=1,2,3} (V_{MNS})^*_{\alpha i} |\nu_i\rangle. \tag{2.2.1}$$

A popular parametrization is given by

$$V_{MNS} = U\mathcal{P}, \tag{2.2.2}$$

with

$$\begin{aligned} U &= \begin{bmatrix} 1 & 0 & 0 \\ 0 & c_{23} & s_{23} \\ 0 & -s_{23} & c_{23} \end{bmatrix} \begin{bmatrix} c_{13} & 0 & c_{13}e^{-i\delta} \\ 0 & 1 & 0 \\ -s_{13}e^{i\delta} & 0 & c_{13} \end{bmatrix} \begin{bmatrix} c_{12} & s_{12} & 0 \\ -s_{12} & c_{12} & 0 \\ 0 & 0 & 1 \end{bmatrix} \\ &= \begin{bmatrix} c_{12}c_{13} & s_{12}c_{13} & s_{13}e^{-i\delta} \\ -s_{12}c_{23} - c_{12}s_{13}s_{23}e^{i\delta} & c_{12}c_{23} - s_{12}s_{13}s_{23}e^{i\delta} & c_{13}s_{23} \\ s_{12}s_{23} - c_{12}s_{13}c_{23}e^{i\delta} & -c_{12}s_{23} - s_{12}s_{13}c_{23}e^{i\delta} & c_{13}c_{23} \end{bmatrix}, \end{aligned} \tag{2.2.3}$$

$$\mathcal{P} = \mathrm{diag}(e^{i\alpha_1/2}, e^{i\alpha_2/2}, 1), \tag{2.2.4}$$

where $s_{ij} \equiv \sin\theta_{ij}$ and $c_{ij} \equiv \cos\theta_{ij}$. Without loss of generality, we can adopt the convention $0 \le \theta_{ij} \le \pi/2$, $0 \le \delta < 2\pi$.

2.2.2 Oscillations

Consider a neutrino state that is created initially at $x = 0$ with flavor α and energy E. It can be written in terms of a linear combination of mass eigenstates with mass m_i:

$$|\nu_{\alpha,\mathrm{ini}}(x=0)\rangle = |\nu_\alpha\rangle = \sum_{i=1}^{3} (V_{\mathrm{MNS}})^*_{\alpha i} |\nu_i\rangle. \tag{2.2.5}$$

At $x = L$, it becomes

$$|\nu_{\alpha,\mathrm{ini}}(x=L)\rangle = \sum_{i=1}^{3} e^{ip_iL} (V_{\mathrm{MNS}})^*_{\alpha i} |\nu_i\rangle. \tag{2.2.6}$$

Since neutrinos have very small masses, we can expand momentum p_i in powers of m_i^2/E^2:

$$p_i = \sqrt{E^2 - m_i^2} = E\left[1 - \frac{1}{2}\left(\frac{m_i^2}{E^2}\right) - \frac{1}{8}\left(\frac{m_i^2}{E^2}\right)^2 + \cdots\right]. \tag{2.2.7}$$

Neglecting terms inside the brackets that are $\mathcal{O}([m_i^2/E^2]^2)$ or higher, we find

$$|\nu_{\alpha,\mathrm{ini}}(x=L)\rangle = e^{iEL}\sum_{i=1}^{3}\exp\left(-i\frac{m_i^2}{2E}L\right)(V_{\mathrm{MNS}})^*_{\alpha i}|\nu_i\rangle. \tag{2.2.8}$$

The amplitude of observing neutrino of flavor β at $x = L$ is then, after dropping the irrelevant overall phase,

$$\begin{aligned}
&\langle\nu_\beta|\nu_{\alpha,\mathrm{ini}}(x=L)\rangle && (2.2.9)\\
&= \left[\sum_{j=1}^{3}\nu_j|(V_{\mathrm{MNS}})_{\beta j}\right]\left[\sum_{i=1}^{3}\left(-i\frac{m_i^2}{2E}L\right)(V_{\mathrm{MNS}})^*_{\alpha i}|\nu_i\rangle\right] && (2.2.10)\\
&= \sum_{i,j=1}^{3}(V_{\mathrm{MNS}})_{\beta j}\exp\left(-i\frac{m_i^2}{2E}L\right)(V_{\mathrm{MNS}})^*_{\alpha i}\langle\nu_j|\nu_i\rangle && (2.2.11)\\
&= \sum_{j=1}^{3}(V_{\mathrm{MNS}})_{\beta j}\exp\left(-i\frac{m_i^2}{2E}L\right)(V_{\mathrm{MNS}})^*_{\alpha j}, && (2.2.12)
\end{aligned}$$

and the probability of oscillation from $|\nu_\alpha\rangle$ to $|\nu_\beta\rangle$ with neutrino energy E and baseline L is then

$$\begin{aligned}
P(\nu_\alpha\to\nu_\beta) &= \left|\sum_{j=1}^{3}(V_{MNS})_{\beta j}\exp\left(-i\frac{m_j^2}{2E}L\right)(V_{MNS})^*_{\alpha j}\right|^2\\
&= \delta_{\alpha\beta} - 4\sum_{i>j}\Re(U^*_{\alpha i}U_{\beta i}U_{\alpha j}U^*_{\beta j})\sin^2\frac{\Delta_{ij}}{2} + 2\sum_{i>j}\Im(U^*_{\alpha i}U_{\beta i}U_{\alpha j}U^*_{\beta j})\sin\Delta_{ij},
\end{aligned}$$

where

$$\Delta_{ij}\equiv\frac{\delta m_{ij}^2}{2E}L = 2.534\frac{\delta m_{ij}^2(\mathrm{eV}^2)}{E(\mathrm{GeV})}L(\mathrm{km}), \qquad \delta m_{ij}^2\equiv m_i^2 - m_j^2. \tag{2.2.13}$$

Since

$$\Delta_{32} = \Delta_{31} - \Delta_{21}, \tag{2.2.14}$$

only two of the three Δ_{ij}'s in Eq. (2.2.13) are independent. Eliminating Δ_{32} from Eq. (2.2.13), we obtain

$$\begin{aligned}
P(\nu_\alpha\to\nu_\alpha) &= 1 - 4|U_{\alpha 2}|^2\left(1-|U_{\alpha 2}|^2\right)\sin^2\frac{\Delta_{21}}{2} - 4|U_{\alpha 3}|^2\left(1-|U_{\alpha 3}|^2\right)\sin^2\frac{\Delta_{31}}{2}\\
&\quad + 2|U_{\alpha 2}|^2|U_{\alpha 3}|^2\left(4\sin^2\frac{\Delta_{21}}{2}\sin^2\frac{\Delta_{31}}{2} + \sin\Delta_{21}\sin\Delta_{31}\right),
\end{aligned} \tag{2.2.15}$$

for the $\alpha = \beta$ case, and

$$\begin{aligned}
P(\nu_\alpha\to\nu_\beta) &= 4|U_{\alpha 2}|^2|U_{\beta 2}|^2\sin^2\frac{\Delta_{21}}{2} + 4|U_{\alpha 3}|^2|U_{\beta 3}|^2\sin^2\frac{\Delta_{31}}{2}\\
&\quad + 2\Re(U^*_{\alpha i}U_{\beta i}U_{\alpha j}U^*_{\beta j})\left(4\sin^2\frac{\Delta_{21}}{2}\sin^2\frac{\Delta_{31}}{2} + \sin\Delta_{21}\sin\Delta_{31}\right)\\
&\quad + 4J_{(\alpha,\beta)}\left(\sin^2\frac{\Delta_{21}}{2}\sin\Delta_{31} - \sin^2\frac{\Delta_{31}}{2}\sin\Delta_{21}\right)
\end{aligned} \tag{2.2.16}$$

for the $\alpha \neq \beta$ case, where $J_{(\alpha,\beta)}$ is the Jarskog invariant:

$$\begin{aligned} J_{(\alpha,\beta)} &= +\Im(U^*_{\alpha1}U_{\beta1}U_{\alpha2}U^*_{\beta2}) + \Im(U^*_{\alpha2}U_{\beta2}U_{\alpha3}U^*_{\beta3}) + \Im(U^*_{\alpha3}U_{\beta3}U_{\alpha1}U^*_{\beta1}) \\ &\quad -\Im(U^*_{\alpha2}U_{\beta2}U_{\alpha1}U^*_{\beta1}) - \Im(U^*_{\alpha1}U_{\beta1}U_{\alpha3}U^*_{\beta3}) - \Im(U^*_{\alpha3}U_{\alpha3}U_{\alpha2}U^*_{\beta2}) \\ &= -J_{(\beta,\alpha)}. \end{aligned} \tag{2.2.17}$$

Using the parameterization given in Eq. (2.2.3), we have

$$J_{(\mu,\tau)} = -J_{(\tau,\mu)} = J_{(\tau,e)} = -J_{(e,\tau)} = J_{(e,\mu)} = -J_{(\mu,e)} = A\sin\delta, \tag{2.2.18}$$

with

$$A = s_{12}c_{12}s_{13}c^2_{13}s_{23}c_{23}. \tag{2.2.19}$$

The oscillation probabilities for the anti-neutrinos are obtained by replacing $U_{\alpha i}$ with its complex conjugate, which only amounts to flipping the sign of δ in the parameterization of Eq. (2.2.3). From Eq. (2.2.15) we can see that $P(\bar{\nu}_\alpha \to \bar{\nu}_\alpha) = P(\nu_\alpha \to \nu_\alpha)$, which is to be expected from the CPT theorem. For flavor changing oscillations, however, only the Jarskog term in Eq. (2.2.16) changes sign.

2.2.3 Current Experimental Bounds

When $|\Delta_{21}| \ll |\Delta_{31}| = O(1)$, the expressions given above can be expanded in Δ_{21} to yield

$$\begin{aligned} &P(\nu_\alpha \to \nu_\alpha) \\ &= 1 - 4\,|U_{\alpha3}|^2\left(1-|U_{\alpha3}|^2\right)\sin^2\frac{\Delta_{31}}{2} + \left(2\,|U_{\alpha2}|^2|U_{\alpha3}|^2\sin\Delta_{31}\right)\Delta_{21} \\ &\quad + |U_{\alpha2}|^2\left\{2|U_{\alpha3}|^2\sin^2\frac{\Delta_{31}}{2} - \left(1-|U_{\alpha2}|^2\right)\right\}\Delta^2_{21} - \left(\frac{1}{3}\,|U_{\alpha2}|^2|U_{\alpha3}|^2\sin\Delta_{31}\right)\Delta^3_{21} + O(\Delta^4_{21}) \\ &= 1 - 4\,|U_{\alpha3}|^2\left(1-|U_{\alpha3}|^2\right)\sin^2\left(\frac{\Delta_{31}-\kappa_{\alpha\alpha}\Delta_{21}}{2}\right) \\ &\quad - |U_{\alpha1}|^2|U_{\alpha2}|^2\left(1+\frac{|U_{\alpha3}|^2}{1-|U_{\alpha3}|^2}\cos\Delta_{31}\right)\Delta^2_{21} \\ &\quad - |U_{\alpha1}|^2|U_{\alpha2}|^2|U_{\alpha3}|^2\left\{\frac{1+|U_{\alpha2}|^2-|U_{\alpha3}|^2}{3(1-|U_{\alpha3}|^2)^2}\sin\Delta_{31}\right\}\Delta^3_{21} + O(\Delta^4_{21})\,, \end{aligned} \tag{2.2.20}$$

$$\begin{aligned} &P(\nu_\alpha \to \nu_\beta) \\ &= 4\,|U_{\alpha3}|^2|U_{\beta3}|^2\sin^2\frac{\Delta_{31}}{2} \\ &\quad + \left\{2\,\Re\left(U^*_{\alpha3}U_{\beta3}U_{\alpha2}U^*_{\beta2}\right)\sin\Delta_{31} - 4\,J_{(\alpha,\beta)}\sin^2\frac{\Delta_{31}}{2}\right\}\Delta_{21} \\ &\quad + \left\{|U_{\alpha2}|^2|U_{\beta2}|^2 + 2\Re\left(U^*_{\alpha3}U_{\beta3}U_{\alpha2}U^*_{\beta2}\right)\sin^2\frac{\Delta_{31}}{2} + J_{(\alpha,\beta)}\sin\Delta_{31}\right\}\Delta^2_{21} \\ &\quad + \frac{1}{3}\left\{2J_{(\alpha,\beta)}\sin^2\frac{\Delta_{31}}{2} - \Re\left(U^*_{\alpha3}U_{\beta3}U_{\alpha2}U^*_{\beta2}\right)\sin\Delta_{31}\right\}\Delta^3_{21} + O(\Delta^4_{21}) \\ &= 4\left(|U_{\alpha3}|^2|U_{\beta3}|^2 - J_{(\alpha,\beta)}\Delta_{21}\right)\sin^2\left(\frac{\Delta_{31}-\kappa_{\alpha\beta}\Delta_{21}}{2}\right) \end{aligned}$$

$$+\left\{\frac{J^2_{(\alpha,\beta)}}{|U_{\alpha3}|^2|U_{\beta3}|^2}-2|U_{\alpha3}|^2|U_{\beta3}|^2\kappa_{\alpha\beta}\,(1-\kappa_{\alpha\beta})\sin^2\frac{\Delta_{31}}{2}-J_{(\alpha,\beta)}\,(1-2\kappa_{\alpha\beta})\sin\Delta_{31}\right\}\Delta^2_{21}$$
$$-\frac{1}{3}\left\{3J_{(\alpha,\beta)}\kappa^2_{\alpha\beta}+2J_{(\alpha,\beta)}(1-3\kappa^2_{\alpha\beta})\sin^2\frac{\Delta_{31}}{2}-|U_{\alpha3}|^2|U_{\beta3}|^2\kappa_{\alpha\beta}(1-\kappa^2_{\alpha\beta})\sin\Delta_{31}\right\}\Delta^3_{21}$$
$$+O(\Delta^4_{21})\;, \tag{2.2.21}$$

where

$$\kappa_{\alpha\alpha}\equiv\frac{|U_{\alpha2}|^2}{1-|U_{\alpha3}|^2}\;,\qquad \kappa_{\alpha\beta}\equiv-\frac{\Re\left(U^*_{\alpha3}U_{\beta3}U_{\alpha2}U^*_{\beta2}\right)}{|U_{\alpha3}|^2|U_{\beta3}|^2}\;. \tag{2.2.22}$$

Neglecting terms of order $O(\Delta^2_{21})$ and higher, we obtain the following simplified expressions for a few specific processes:

$$\begin{aligned}
P(\nu_e\to\nu_e) &= 1-4s^2_{13}(1-s^2_{13})\sin^2\left(\frac{\Delta_{31}-s^2_{12}\Delta_{21}}{2}\right)\\
&= 1-\sin^2(2\theta_{\rm rct})\sin^2\left(\frac{\Delta_{31}-s^2_{12}\Delta_{21}}{2}\right)\;,\\
P(\nu_\mu\to\nu_\mu) &= 1-4c^2_{13}s^2_{23}(1-c^2_{13}s^2_{23})\sin^2\left(\frac{\Delta_{31}-\kappa_{\mu\mu}\Delta_{21}}{2}\right)\\
&= 1-\sin^2(2\theta_{\rm atm})\sin^2\left(\frac{\Delta_{31}-\kappa_{\mu\mu}\Delta_{21}}{2}\right)\;,\\
P(\nu_\mu\to\nu_e) &= 4(c^2_{13}s^2_{13}s^2_{23}-J_{(\mu,e)}\Delta_{21})\sin^2\left(\frac{\Delta_{31}-\kappa_{\mu e}\Delta_{21}}{2}\right)\\
&= 4(\sin^2\theta_{\rm rct}\,\sin^2\theta_{\rm atm}-A\sin\delta\,\Delta_{21})\sin^2\left(\frac{\Delta_{31}-\kappa_{\mu e}\Delta_{21}}{2}\right)\;,
\end{aligned} \tag{2.2.23}$$

where

$$\begin{aligned}
A &= \frac{1}{8}\sin(2\theta_{12})\sin(2\theta_{\rm rct})\sin(2\theta_{\rm atm})\sqrt{1-\tan^2\theta_{\rm rct}\tan^2\theta_{\rm atm}}\;,\\
\kappa_{\mu\mu} &= c^2_{12}-(c^2_{12}-s^2_{12})\tan^2\theta_{\rm rct}\tan^2\theta_{\rm atm}-\left(\frac{2A}{\cos^2\theta_{\rm rct}\cos^2\theta_{\rm atm}}\right)\cos\delta\;,\\
\kappa_{\mu e} &= s^2_{12}-\left(\frac{A}{\sin^2\theta_{\rm rct}\sin^2\theta_{atm}}\right)\cos\delta\;.
\end{aligned} \tag{2.2.24}$$

We have made the identifications

$$\begin{aligned}
\sin\theta_{\rm atm} &= s_{23}c_{13} = \sin\theta_{23}\cos\theta_{13}\;,\\
\sin\theta_{\rm rct} &= s_{13} = \sin\theta_{13}\;,
\end{aligned} \tag{2.2.25}$$

where $\theta_{\rm atm}$ and $\theta_{\rm rct}$ are the mixing angles extracted from atmospheric [3] and reactor [4] neutrino oscillation experiments, respectively, based on two-flavor oscillation analyses.

Solar Neutrino Experiments

The SNO Collaboration's two-neutrino oscillation analysis including all the solar neutrino data and KamLAND data:

$$\delta m^2_{\rm sol} = 7.59^{+0.20}_{-0.21}\times10^{-5}\;{\rm eV}^2\;,$$

$\lvert\delta m^2_{31}\rvert$ (eV^2)	$\varepsilon = \sqrt{\frac{\delta m^2_{21}}{\lvert\delta m^2_{31}\rvert}}$	Upper bound on θ_{13}
2.0×10^{-3}	$0.20 \sim 0.21$	0.23
2.5×10^{-3}	$0.18 \sim 0.19$	0.21
3.0×10^{-3}	$0.16 \sim 0.17$	0.19

Table 2.1: Comparison of the size of the ratio $\delta m^2_{21}/|\delta m^2_{31}|$ and the 90% confidence limit on θ_{13}.

$$\tan^2\theta_{\rm sol} \;=\; 0.457^{+0.040}_{-0.029}\;. \tag{2.2.26}$$

The sign of $\delta m^2_{21} = m^2_2 - m^2_1$ is known to be positive since $m^2_2 > m^2_1$ is required for the MSW effect [18] to work.

Atmospheric Neutrino Experiments

The current experimental bounds on atmospheric neutrinos from Super-Kamiokande at the 90% confidence level are

$$\begin{aligned} |\delta m^2_{31}| &= (1.9 \sim 3.0) \times 10^{-3}\ {\rm eV}^2\;, \\ \sin^2(2\theta_{\rm atm}) &> 0.90\;. \end{aligned} \tag{2.2.27}$$

Only the absolute value of δm^2_{31} is known since $P(\nu_\mu \to \nu_\mu) = 1 - \sin^2(2\theta_{\rm atm})\sin^2(\Delta_{31}/2)$ at leading order in Δ_{21}.

Reactor Experiments

The 90% confidence limit on $\theta_{\rm rct} = \theta_{13}$ from the CHOOZ experiment, which measured $P(\bar\nu_e \to \bar\nu_e) = 1 - \sin^2(2\theta_{\rm rct})\sin^2(\Delta_{31}/2)$, is

$$\sin^2(2\theta_{rct}) \;< 0.19 \qquad \text{for } |\delta m^2_{31}| = 2.0 \times 10^{-3}\ {\rm eV}^2\;. \tag{2.2.28}$$

Accelerator Experiments

The K2K experiment searched the $\nu_\mu \to \nu_e$ channel $P(\nu_\mu \to \nu_e) = \sin^2(2\theta_{13}) \cdot \sin^2(\theta_{23}) \cdot \sin^2(\Delta_{31}/2)$, and the 90% CL upper limit was obtained for

$$\sin^2(2\theta_{13}) < 0.26 \qquad \text{at } |\delta m^2_{31}| = 2.8 \times 10^{-3}{\rm eV}^2\;. \tag{2.2.29}$$

2.2.4 The Sizes of θ_{13}, θ_{12}, and θ_{23}

If we allow both δm^2_{21} and $|\delta m^2_{31}|$ to move within their respective 90% confidence limits given in Eqs. (2.2.27) and (2.2.26), the ratio of the two is in the range

$$\frac{\delta m^2_{21}}{|\delta m^2_{31}|} = 0.038 \sim 0.041\;. \tag{2.2.30}$$

Thus, the approximation $\Delta_{21} \ll |\Delta_{31}|$ that was used above is justified. The square-root of this ratio, which we will call ε, is in the range

$$\varepsilon \equiv \sqrt{\frac{\delta m^2_{21}}{|\delta m^2_{31}|}} = 0.20 \; . \tag{2.2.31}$$

Note that ε is roughly in the same range as that of the 90% upper bound on θ_{13} which can be obtained from Eq. (2.2.28). In fact, the two numbers are positively correlated as shown in TABLE I.

While we currently have no experimental lower bound on θ_{13}, many analyses of LBL experiments only consider cases where $\sin^2(2\theta_{13}) > 0.04$, which corresponds to $\theta_{13} > 0.1$, since smaller values of θ_{13} would put $P(\nu_\mu \to \nu_e)$ below detectable range. Therefore, we will assume that θ_{13} is of order ε in the following. However, the formulae we derive below can be applied as is to cases in which θ_{13} is smaller, since we only use the size of θ_{13} to decide when terms containing s_{13} can be neglected. A smaller θ_{13} will simply make those terms even more negligible.

The 90% confidence limits on the solar mixing angle given in Eq. (2.2.26) translates into

$$\theta_{12} = 0.579^{+0.020}_{-0.015} = (0.184^{+0.006}_{-0.005})\pi \; , \tag{2.2.32}$$

and

$$\begin{aligned} s_{12} &= 0.53 \sim 0.56 \; , \\ c_{12} &= 0.83 \sim 0.85 \; , \\ \sin(2\theta_{12}) &= 0.90 \sim 0.93 \; , \\ \cos(2\theta_{12}) &= 0.36 \sim 0.43 \; . \end{aligned} \tag{2.2.33}$$

Being sines and cosines, the upper end of these ranges are always smaller than one. However, s_{12}, c_{12}, and $\sin(2\theta_{12})$ are still much larger than ε so we will treat them, and also θ_{12}, as numbers of order 1. On the other hand, $\cos(2\theta_{12})$ is only slightly larger than ε. Its range is roughly equal to that of 2ε. Therefore, we can consider $\cos(2\theta_{12})/2$ as a number of order ε.

The 90% confidence limits on the atmospheric mixing angle given in Eq. (2.2.27) translates to

$$\theta_{\rm atm} = 0.62 \sim 0.95 = (0.25 \pm 0.05)\pi \; . \tag{2.2.34}$$

Though we made the identification $\sin\theta_{\rm atm} = s_{23}c_{13}$ in Eq. (2.2.25), the limits on θ_{23} are virtually identical to those of $\theta_{\rm atm}$ due to the smallness of θ_{13}. We can therefore assume

$$\begin{aligned} s_{23} &= 0.58 \sim 0.81 \; , \\ c_{23} &= 0.58 \sim 0.81 \; , \\ \sin(2\theta_{23}) &> 0.95 \; , \\ |\cos(2\theta_{23})| &< 0.32 \; . \end{aligned} \tag{2.2.35}$$

As in the case of θ_{12}, we can assume s_{23}, c_{23}, $\sin(2\theta_{23})$, and θ_{23} to be numbers of order 1, while $\cos(2\theta_{23})$ is of order ε or smaller.

2.3 Matter Effects

In long baseline experiments, neutrinos inevitably travel through Earth. Thus we have to modify the hamiltonian to take into account matter effects:

$$H = U \begin{bmatrix} 0 & 0 & 0 \\ 0 & \delta m^2_{21} & 0 \\ 0 & 0 & \delta m^2_{31} \end{bmatrix} U^\dagger + \begin{bmatrix} a & 0 & 0 \\ 0 & 0 & 0 \\ 0 & 0 & 0 \end{bmatrix} . \tag{2.3.1}$$

The factor a is due to the interaction of the $|\nu_e\rangle$ component of the neutrinos with the electrons in matter via W-exchange:

$$a = 2\sqrt{2} G_F N_e E = 7.63 \times 10^{-5} (\text{eV})^2 \left(\frac{\rho}{\text{g/cm}^3}\right) \left(\frac{E}{\text{GeV}}\right) , \tag{2.3.2}$$

where N_e is the electron number density along the baseline, and E is the energy of the neutrinos. Note that a is E-dependent, which means that both $\tilde{U}$ and $\tilde{\Delta}_{ij}$ are also E-dependent. It is also assumed that $E \ll M_W$ since the W-exchange interaction is approximated by a point-like four-fermion interaction in deriving this expression.

To see the effect of a, we introduce the matrix

$$\mathcal{Q} = \text{diag}(1, 1, e^{i\delta}) . \tag{2.3.3}$$

The matrix $\mathcal{Q}$ serves to separate out the dependance of H' on the CP violating phase δ:

$$\begin{aligned}
H &= U \left(\begin{bmatrix} 0 & 0 & 0 \\ 0 & \delta m^2_{21} & 0 \\ 0 & 0 & \delta m^2_{31} \end{bmatrix} + U^\dagger \begin{bmatrix} a & 0 & 0 \\ 0 & 0 & 0 \\ 0 & 0 & 0 \end{bmatrix} U \right) U^\dagger \\
&= U\mathcal{Q} \left(\mathcal{Q}^\dagger \begin{bmatrix} 0 & 0 & 0 \\ 0 & \delta m^2_{21} & 0 \\ 0 & 0 & \delta m^2_{31} \end{bmatrix} \mathcal{Q} + \mathcal{Q}^\dagger U^\dagger \begin{bmatrix} a & 0 & 0 \\ 0 & 0 & 0 \\ 0 & 0 & 0 \end{bmatrix} U\mathcal{Q} \right) \mathcal{Q}^\dagger U^\dagger \\
&= U\mathcal{Q} \left(\begin{bmatrix} 0 & 0 & 0 \\ 0 & \delta m^2_{21} & 0 \\ 0 & 0 & \delta m^2_{31} \end{bmatrix} + a\mathcal{Q}^\dagger \begin{bmatrix} U^*_{e1}U_{e1} & U^*_{e1}U_{e2} & U^*_{e1}U_{e3} \\ U^*_{e2}U_{e1} & U^*_{e2}U_{e2} & U^*_{e2}U_{e3} \\ U^*_{e3}U_{e1} & U^*_{e3}U_{e2} & U^*_{e3}U_{e3} \end{bmatrix} \mathcal{Q} \right) \mathcal{Q}^\dagger U^\dagger \\
&= U\mathcal{Q} \left(\begin{bmatrix} 0 & 0 & 0 \\ 0 & \delta m^2_{21} & 0 \\ 0 & 0 & \delta m^2_{31} \end{bmatrix} + a \begin{bmatrix} c^2_{12}c^2_{13} & c_{12}s_{12}c^2_{13} & c_{12}c_{13}s_{13} \\ c_{12}s_{12}c^2_{13} & s^2_{12}c^2_{13} & s_{12}c_{13}s_{13} \\ c_{12}c_{13}s_{13} & s_{12}c_{13}s_{13} & s^2_{13} \end{bmatrix} \right) \mathcal{Q}^\dagger U^\dagger \\
&= U\mathcal{Q} \begin{bmatrix} ac^2_{12}c^2_{13} & ac_{12}s_{12}c^2_{13} & ac_{12}c_{13}s_{13} \\ ac_{12}s_{12}c^2_{13} & as^2_{12}c^2_{13} + \delta m^2_{21} & as_{12}c_{13}s_{13} \\ ac_{12}c_{13}s_{13} & as_{12}c_{13}s_{13} & as^2_{13} + \delta m^2_{31} \end{bmatrix} \mathcal{Q}^\dagger U^\dagger \\
&= U\mathcal{Q}H'\mathcal{Q}^\dagger U^\dagger,
\end{aligned} \tag{2.3.4}$$

where

$$H' = \begin{bmatrix} ac^2_{12}c^2_{13} & ac_{12}s_{12}c^2_{13} & ac_{12}c_{13}s_{13} \\ ac_{12}s_{12}c^2_{13} & as^2_{12}c^2_{13} + \delta m^2_{21} & as_{12}c_{13}s_{13} \\ ac_{12}c_{13}s_{13} & as_{12}c_{13}s_{13} & as^2_{13} + \delta m^2_{31} \end{bmatrix} . \tag{2.3.5}$$

Our strategy is to approximately diagonalize H' through the Jacobi method using $\varepsilon = \sqrt{\delta m^2_{21}/|\delta m^2_{31}|}$ as the expansion parameter. Corrections to the eigenvalues of H' of order $\varepsilon^3|\delta m^2_{31}|$ and higher, and those to the elements of $\tilde{U}$ of order ε^3 and higher will be neglected. For $\varepsilon = 0.15 \sim 0.24$, we have $\varepsilon^3 = 0.0034 \sim 0.014$.

We can diagonalize H' with some matrix R:

$$H' = R \begin{bmatrix} \lambda_1 & 0 & 0 \\ 0 & \lambda_2 & 0 \\ 0 & 0 & \lambda_3 \end{bmatrix} R^\dagger, \tag{2.3.6}$$

so that

$$\begin{aligned} H &= U\mathcal{Q}H'\mathcal{Q}^\dagger U^\dagger \\ &= U\mathcal{Q}R \begin{bmatrix} \lambda_1 & 0 & 0 \\ 0 & \lambda_2 & 0 \\ 0 & 0 & \lambda_3 \end{bmatrix} R^\dagger \mathcal{Q}^\dagger U^\dagger \\ &= \tilde{U} \begin{bmatrix} \lambda_1 & 0 & 0 \\ 0 & \lambda_2 & 0 \\ 0 & 0 & \lambda_3 \end{bmatrix} \tilde{U}^\dagger, \end{aligned} \tag{2.3.7}$$

where

$$\tilde{U} = U\mathcal{Q}R \equiv \begin{bmatrix} \tilde{c}_{12}\tilde{c}_{13} & \tilde{s}_{12}\tilde{c}_{13} & \tilde{s}_{13}e^{-i\tilde{\delta}} \\ -\tilde{s}_{12}\tilde{c}_{23} - \tilde{c}_{12}\tilde{s}_{13}\tilde{s}_{23}e^{i\tilde{\delta}} & \tilde{c}_{12}\tilde{c}_{23} - \tilde{s}_{12}\tilde{s}_{13}\tilde{s}_{23}e^{i\tilde{\delta}} & \tilde{c}_{13}\tilde{s}_{23} \\ \tilde{s}_{12}\tilde{s}_{23} - \tilde{c}_{12}\tilde{s}_{13}\tilde{c}_{23}e^{i\tilde{\delta}} & -\tilde{c}_{12}\tilde{s}_{23} - \tilde{s}_{12}\tilde{s}_{13}\tilde{c}_{23}e^{i\tilde{\delta}} & \tilde{c}_{13}\tilde{c}_{23} \end{bmatrix} \tag{2.3.8}$$

contains effective neutrino mixing angles in matter, and λ_i are effective neutrino mass squared. Analogous to neutrino oscillation in vacuum, eq.(2.2.13), neutrino oscillation in matter can be described by simply replacing $U_{\alpha\beta}$ and m_i^2 with $\tilde{U}_{\alpha\beta}$ and λ_i respectively:

$$P(\nu_\alpha \to \nu_\beta)_{\text{matter}} = \delta_{\alpha\beta} - 4\sum_{i>j} \Re(\tilde{U}^*_{\alpha i}\tilde{U}_{\beta i}\tilde{U}_{\alpha j}\tilde{U}^*_{\beta j}) \sin^2 \frac{\tilde{\Delta}_{ij}}{2} + 2\sum_{i>j} \Im(\tilde{U}^*_{\alpha i}\tilde{U}_{\beta i}\tilde{U}_{\alpha j}\tilde{U}^*_{\beta j}) \sin \tilde{\Delta}_{ij}, \tag{2.3.9}$$

where $\tilde{\Delta}_{ij} \equiv \lambda_i - \lambda_j$.

2.4 Approximated Formulae

To obtain approximated formulae for neutrino oscillation with matter effects, we use the Jacobi method to obtain an approximation to the diagonalization matrix R. We find that the formulae we obtain after two rotations are sufficiently accurate.

Using the Jacobi method, we find that H' is partially diagonalized by a rotation of the 1-2 submatrix followed by a rotation of the 2-3 submatrix. The rotation in the 1-2 components is given by

$$V = \begin{bmatrix} c_\varphi & s_\varphi & 0 \\ -s_\varphi & c_\varphi & 0 \\ 0 & 0 & 1 \end{bmatrix}, \tag{2.4.1}$$

where

$$c_\varphi = \cos\varphi\ , \quad s_\varphi = \sin\varphi\ , \quad \varphi = \frac{1}{2}\tan^{-1}\frac{ac_{13}^2\sin 2\theta_{12}}{\delta m_{21}^2 - ac_{13}^2\cos 2\theta_{12}}\ . \tag{2.4.2}$$

And the rotation in the 2-3 components is given by

$$W = \begin{bmatrix} 1 & 0 & 0 \\ 0 & c_\phi & s_\phi \\ 0 & -s_\phi & c_\phi \end{bmatrix}, \tag{2.4.3}$$

where

$$c_\phi = \cos\phi\ , \quad s_\phi = \sin\phi\ , \quad \phi = \frac{1}{2}\tan^{-1}\left(\frac{as'_{12}\sin 2\theta_{13}}{\delta m_{31}^2 + as_{13}^2 - \lambda'_2}\right)\ , \tag{2.4.4}$$

and

$$s'_{12} \;=\; \sin\theta'_{12} = \sin(\theta_{12}+\varphi), \qquad \lambda'_2 = \frac{(as_{12}^2c_{13}^2 + \delta m_{21}^2)c_\varphi^2 - (ac_{12}^2c_{13}^2)s_\varphi^2}{c_\varphi^2 - s_\varphi^2}. \tag{2.4.5}$$

The Hamiltonian is then approximately diagonalized as

$$\begin{aligned} W^\dagger V^\dagger H' V W &= W^\dagger V^\dagger \mathcal{Q}^\dagger U^\dagger H U \mathcal{Q} V W \\ \equiv U'^\dagger H U' &= \begin{bmatrix} \lambda''_1 & -ac'_{12}c_{13}s_{13}\sin\phi_{23} & ac'_{12}c_{13}s_{13}\cos\phi_{23} \\ -ac'_{12}c_{13}s_{13}\sin\phi_{23} & \lambda''_2 & 0 \\ ac'_{12}c_{13}s_{13}\cos\phi_{23} & 0 & \lambda''_3 \end{bmatrix}, \end{aligned} \tag{2.4.6}$$

where

$$\begin{aligned} U' &= U\mathcal{Q}VW \\ &= \begin{bmatrix} 1 & 0 & 0 \\ 0 & c_{23} & s_{23} \\ 0 & -s_{23} & c_{23} \end{bmatrix} \begin{bmatrix} c_{13} & 0 & s_{13}e^{-i\delta} \\ 0 & 1 & 0 \\ -s_{13}e^{i\delta} & 0 & c_{13} \end{bmatrix} \begin{bmatrix} c_{12} & s_{12} & 0 \\ -s_{12} & c_{12} & 0 \\ 0 & 0 & 1 \end{bmatrix} \begin{bmatrix} 1 & 0 & 0 \\ 0 & 1 & 0 \\ 0 & 0 & e^{i\delta} \end{bmatrix} \begin{bmatrix} c_\varphi & s_\varphi & 0 \\ -s_\varphi & c_\varphi & 0 \\ 0 & 0 & 1 \end{bmatrix} W \\ &= \begin{bmatrix} 1 & 0 & 0 \\ 0 & c_{23} & s_{23} \\ 0 & -s_{23} & c_{23} \end{bmatrix} \begin{bmatrix} c_{13} & 0 & s_{13}e^{-i\delta} \\ 0 & 1 & 0 \\ -s_{13}e^{i\delta} & 0 & c_{13} \end{bmatrix} \begin{bmatrix} c_{12} & s_{12} & 0 \\ -s_{12} & c_{12} & 0 \\ 0 & 0 & 1 \end{bmatrix} \begin{bmatrix} c_\varphi & s_\varphi & 0 \\ -s_\varphi & c_\varphi & 0 \\ 0 & 0 & 1 \end{bmatrix} \begin{bmatrix} 1 & 0 & 0 \\ 0 & 1 & 0 \\ 0 & 0 & e^{i\delta} \end{bmatrix} W \\ &= \begin{bmatrix} 1 & 0 & 0 \\ 0 & c_{23} & s_{23} \\ 0 & -s_{23} & c_{23} \end{bmatrix} \begin{bmatrix} c_{13} & 0 & s_{13}e^{-i\delta} \\ 0 & 1 & 0 \\ -s_{13}e^{i\delta} & 0 & c_{13} \end{bmatrix} \begin{bmatrix} c'_{12} & s'_{12} & 0 \\ -s'_{12} & c'_{12} & 0 \\ 0 & 0 & 1 \end{bmatrix} \begin{bmatrix} 1 & 0 & 0 \\ 0 & 1 & 0 \\ 0 & 0 & e^{i\delta} \end{bmatrix} \begin{bmatrix} 1 & 0 & 0 \\ 0 & c_\phi & s_\phi \\ 0 & -s_\phi & c_\phi \end{bmatrix} \\ &= \begin{bmatrix} c_{13}c'_{12} & c_{13}s'_{12}c_\phi - s_{13}s_\phi & c_{13}s'_{12}s_\phi + s_{13}c_\phi \\ -c_{23}s'_{12} - s_{23}s_{13}c'_{12}e^{i\delta} & c_{23}c'_{12}c_\phi - s_{23}(s_{13}s'_{12}c_\phi + c_{13}s_\phi)e^{i\delta} & c_{23}c'_{12}s_\phi - s_{23}(s_{13}s'_{12}s_\phi - c_{13}c_\phi)e^{i\delta} \\ s_{23}s'_{12} - c_{23}s_{13}c'_{12}e^{i\delta} & -s_{23}c'_{12}c_\phi - c_{23}(s_{13}s'_{12}c_\phi + c_{13}s_\phi)e^{i\delta} & -s_{23}c'_{12}s_\phi - c_{23}(s_{13}s'_{12}s_\phi - c_{13}c_\phi)e^{i\delta} \end{bmatrix} \end{aligned} \tag{2.4.7}$$

By comparing eq.(2.4.6) with

$$\tilde{U}^\dagger H \tilde{U} = \begin{bmatrix} \tilde{\lambda}_1 & 0 & 0 \\ 0 & \tilde{\lambda}_2 & 0 \\ 0 & 0 & \tilde{\lambda}_3 \end{bmatrix}\ , \tag{2.4.8}$$

we can make the following identifications:

$$\tilde{U} \approx U' \quad , \quad \tilde{\lambda}_i \approx \lambda''_i \text{ , and} \qquad \tilde{\Delta}_{ij} \equiv \tilde{\lambda}_i - \tilde{\lambda}_j \approx \lambda''_i - \lambda''_j \tag{2.4.9}$$

The approximated neutrino oscillation formulae can be obtained by replacing the effective mixing matrix $\tilde{U}$ and the mass-squared differences $\tilde{\Delta}$ in eq.(2.3.9) with the above approximated ones. However, further simplification can be made as follows.

2.4.1 Simplified Effective Mixing Angles

Instead of using the approximated effective mixing matrix U' given in eq. (2.4.7), it is possible to absorb matter effects into shifts in the three mixing angles and the CP violating phase so that the vacuum oscillation formulae, eq.(2.2.23), can be used as is. We derive the expressions for each of these parameters in the following.

$\tilde{\theta}_{13}$

Comparing the (1,3) elements of the matrices $\tilde{U}$ and U', we can make the identification

$$\begin{aligned} \tilde{s}_{13} &= c_{13}s'_{12}s_\phi + s_{13}c_\phi \\ &= c_{13}s'_{12}s_\phi + s'_{12}s_{13}c_\phi + (1-s'_{12})s_{13}c_\phi \\ &= s'_{12}(c_{13}s_\phi + s_{13}c_\phi) + (1-s'_{12})s_{13}c_\phi \\ &= s'_{12}s'_{13} + (1-s'_{12})s_{13}c_\phi, \end{aligned} \tag{2.4.10}$$

where $(1-s'_{12})s_{13}c_\phi$ is of order $\mathcal{O}(\epsilon^2)$ or smaller. Therefore,

$$\begin{aligned} \tilde{\theta}_{13} &\approx \sin^{-1}[s'_{12}s'_{13}] \\ &= \sin^{-1}\left[s'_{13}\sqrt{1-(c'_{12})^2}\right]. \end{aligned} \tag{2.4.11}$$

Since c'_{12} is of $\mathcal{O}(\epsilon)$ or smaller, we can expand

$$\begin{aligned} \tilde{\theta}_{13} &\approx \sin^{-1}(\sin\theta'_{13}) - \frac{\sin\theta'_{13}}{\sqrt{1-\sin^2\theta'_{13}}}\frac{(c'_{12})^2}{2} + \mathcal{O}\left(\epsilon^4\right) \\ &\approx \theta'_{13} - \tan\theta'_{13}\frac{(c'_{12})^2}{2}\,. \end{aligned} \tag{2.4.12}$$

$\tilde{\theta}_{12}$

Next, looking at the (1,1) and (1,2) elements, we find

$$\begin{aligned} \tan\tilde{\theta_{12}} &= \frac{\tilde{s}_{12}\tilde{c}_{13}}{\tilde{c}_{12}\tilde{c}_{13}} \\ &= \frac{c_{13}s'_{12}c_\phi - s_{13}s_\phi}{c_{13}c'_{12}} \\ &= \frac{(c_{13}c_\phi - s_{13}s_\phi)s'_{12} - s_{13}(1-s'_{12})s_\phi}{c_{13}c'_{12}} \\ &= \left(\frac{c'_{13}}{c_{13}}\right)\left[\tan\theta'_{12} + \frac{1}{\cos^2\theta'_{12}}\left\{-\frac{s_{13}c'_{12}(1-s'_{12})s_\phi}{c'_{13}}\right\}\right]. \end{aligned} \tag{2.4.13}$$

The factor $s_{13}c'_{12}s_\phi/c'_{13}$ is of order ϵ^4 or smaller. Therefore,

$$\tan\tilde{\theta}_{12} = \left(\frac{c'_{13}}{c_{13}}\right)\tan\left[\theta'_{12} + O(\epsilon^4)\right]. \tag{2.4.14}$$

Since $\theta'_{13} = \theta_{13} + \phi$, we can expect the ratio c'_{13}/c_{13} to be roughly equal to one when ϕ is small, and consequently, $\tilde{\theta}_{12} \approx \theta'_{12}$. Indeed, if $\delta m^2_{31} > 0$ with $a/|\delta m^2_{31}| \leq O(\epsilon)$, or $\delta m^2_{31} < 0$ with any a, then $s_\phi \leq O(\epsilon)$, and we find

$$1 - \frac{c'_{13}}{c_{13}} = (1 - c_\phi) + s_\phi \tan\theta_{13} \leq O(\epsilon^2). \tag{2.4.15}$$

In these cases, we can treat $(1 - c'_{13}/c_{13}$ as a small quantity and expand

$$\tilde{\theta}_{12} = \theta'_{12} + s'_{12}c'_{12}\left(1 - \frac{c'_{13}}{c_{13}}\right) + \cdots = \theta'_{12} + O(\epsilon^4). \tag{2.4.16}$$

The $\delta m^2_{31} > 0$ case with $a/|\delta m^2_{31}| = O(1)$ or $a/|\delta m^2_{31}| = O(\epsilon^{-1})$ must be considered separately. First taking the reciprocal of both sides of Eq. (2.4.14), we obtain

$$\cot\tilde{\theta}_{12} = \frac{c_{13}}{c'_{13}}\cot\theta'_{12}, \tag{2.4.17}$$

where we have dropped the shift in θ'_{12} on the right hand side which is of order $\epsilon^{7,8}$ in these particular cases. Recall that when $a/|\delta m^2_{31}| = O(\epsilon^{0,-1})$, we have

$$\theta'_{12} = \frac{\pi}{2} - \frac{\delta m^2_{21}}{2a}\sin(2\theta_{12} + O(\epsilon^{4,5}), \tag{2.4.18}$$

while

$$\frac{c_{13}}{c'_{13}} = O(\epsilon^{0,-2}). \tag{2.4.19}$$

Therefore, from Eq. (2.4.17) we find

$$\begin{aligned}
\tan\left(\frac{\pi}{2} - \tilde{\theta}_{12}\right) &= \frac{c_{13}}{c'_{13}}\tan\left(\frac{\pi}{2} - \theta'_{12}\right) \\
&= \frac{c_{13}}{c'_{13}}\tan\left(\frac{\delta m^2_{21}}{2a}\sin(2\theta_{12}) + O(\epsilon^{4,5})\right) \\
&= \frac{c_{13}}{c'_{13}}\left(\frac{\delta m^2_{21}}{2a}\sin(2\theta_{12})\right) + O(\epsilon^{4,3}) \\
&= \tan\left(\frac{c_{13}}{c'_{13}}\frac{\delta m^2_{21}}{2a}\sin(2\theta_{12}) + O(\epsilon^{4,5}\right),
\end{aligned} \tag{2.4.20}$$

from which we can conclude

$$\tilde{\theta}_{12} = \frac{\pi}{2} - \frac{c_{13}}{c'_{13}}\left(\frac{\delta m^2_{21}}{2a}\right)\sin(2\theta_{12} + O(\epsilon^{4,3}). \tag{2.4.21}$$

$\tilde{\theta}_{23}$

Next, using the relation

$$s_{13}s'_{12}s_\phi - c_{13}c_\phi \;=\; -(c_{13}c_\phi - s_{13}s_\phi) - s_{13}(1-s'_{12})s_\phi \;=\; -c'_{13} + O(\varepsilon^4)\;, \tag{2.4.22}$$

we simplify the $(2,3)$ and $(3,3)$ elements of U' as

$$\begin{aligned} c_{23}c'_{12}s_\phi - s_{23}(s_{13}s'_{12}s_\phi - c_{13}c_\phi)e^{i\delta} &= c_{23}c'_{12}s_\phi + s_{23}c'_{13}e^{i\delta} + O(\varepsilon^4)\;, \\ -s_{23}c'_{12}s_\phi - c_{23}(s_{13}s'_{12}s_\phi - c_{13}c_\phi)e^{i\delta} &= -s_{23}c'_{12}s_\phi + c_{23}c'_{13}e^{i\delta} + O(\varepsilon^4)\;. \end{aligned} \tag{2.4.23}$$

Then, using the fact that $c'_{12}s_\phi = O(\varepsilon^2)$ or smaller, we find

$$\begin{aligned} &|c_{23}c'_{12}s_\phi - s_{23}(s_{13}s'_{12}s_\phi - c_{13}c_\phi)e^{i\delta}| \\ &\quad= \sqrt{s_{23}^2{c'_{13}}^2 + 2s_{23}c_{23}c'_{13}c'_{12}s_\phi\cos\delta + c_{23}^2{c'_{12}}^2s_\phi^2 + O(\varepsilon^4)} \\ &\quad= \sqrt{s_{23}^2{c'_{13}}^2 + 2s_{23}c_{23}c'_{13}c'_{12}s_\phi\cos\delta + O(\varepsilon^4)} \\ &\quad= s_{23}c'_{13} + c_{23}c'_{12}s_\phi\cos\delta + O(\varepsilon^4) \\ &|-s_{23}c'_{12}s_\phi - c_{23}(s_{13}s'_{12}s_\phi - c_{13}c_\phi)e^{i\delta}| \\ &\quad= \sqrt{c_{23}^2{c'_{13}}^2 - 2s_{23}c_{23}c'_{13}c'_{12}s_\phi\cos\delta + s_{23}^2{c'_{12}}^2s_\phi^2 + O(\varepsilon^4)} \\ &\quad= \sqrt{c_{23}^2{c'_{13}}^2 - 2s_{23}c_{23}c'_{13}c'_{12}s_\phi\cos\delta + O(\varepsilon^4)} \\ &\quad= c_{23}c'_{13} - s_{23}c'_{12}s_\phi\cos\delta + O(\varepsilon^4) \end{aligned} \tag{2.4.24}$$

Therefore, we can make the identification

$$\begin{aligned} \tan\tilde{\theta}_{23} &= \frac{\tilde{c}_{13}\tilde{s}_{23}}{\tilde{c}_{13}\tilde{c}_{23}} \\ &= \frac{s_{23}c'_{13} + c_{23}c'_{12}s_\phi\cos\delta}{c_{23}c'_{13} - s_{23}c'_{12}s_\phi\cos\delta} + O(\varepsilon^4) \\ &= \frac{t_{23} + \left(\dfrac{c'_{12}s_\phi}{c'_{13}}\right)\cos\delta}{1 - t_{23}\left(\dfrac{c'_{12}s_\phi}{c'_{13}}\right)\cos\delta} + O(\varepsilon^4) \\ &= \tan\left[\theta_{23} + \left(\frac{c'_{12}s_\phi}{c'_{13}}\right)\cos\delta\right] + O(\varepsilon^4)\;, \end{aligned} \tag{2.4.25}$$

and we obtain

$$\tilde{\theta}_{23} = \theta_{23} + \left(\frac{c'_{12}s_\phi}{c'_{13}}\right)\cos\delta + O(\varepsilon^4)\;. \tag{2.4.26}$$

The factor $c'_{12}s_\phi/c'_{13}$ is of order ε^3 or smaller if $\delta m^2_{31} > 0$ with $a/|\delta m^2_{31}| \le O(\varepsilon)$, or $\delta m^2_{31} < 0$ with any a. In those cases, we have

$$\tilde{\theta}_{23} = \theta_{23} + O(\varepsilon^3)\;. \tag{2.4.27}$$

For the case of $\delta m^2_{31} > 0$ with $a/|\delta m^2_{31}| \ge O(1)$, we can expand c'_{12} and approximate

$$\tilde{\theta}_{23} = \theta_{23} + \frac{s_\phi}{c'_{13}}\left(\frac{\delta m^2_{21}}{2a}\right)\sin(2\theta_{12})\cos\delta + O(\varepsilon^4)\;. \tag{2.4.28}$$

2.4.2 Two Rotations and then Commute Through

When θ_{13} is not too small, we can further approximate the mixing matrix by first commuting matrix V through $\mathcal{Q}$:

$$
\begin{aligned}
& U' \\
= \quad & U\mathcal{Q}VW \\
= \quad & \begin{bmatrix} 1 & 0 & 0 \\ 0 & c_{23} & s_{23} \\ 0 & -s_{23} & c_{23} \end{bmatrix} \begin{bmatrix} c_{13} & 0 & s_{13}e^{-i\delta} \\ 0 & 1 & 0 \\ -s_{13}e^{i\delta} & 0 & c_{13} \end{bmatrix} \begin{bmatrix} c_{12} & s_{12} & 0 \\ -s_{12} & c_{12} & 0 \\ 0 & 0 & 1 \end{bmatrix} \begin{bmatrix} 1 & 0 & 0 \\ 0 & 1 & 0 \\ 0 & 0 & e^{i\delta} \end{bmatrix} \begin{bmatrix} c_\varphi & s_\varphi & 0 \\ -s_\varphi & c_\varphi & 0 \\ 0 & 0 & 1 \end{bmatrix} W \\
\approx \quad & \begin{bmatrix} 1 & 0 & 0 \\ 0 & c_{23} & s_{23} \\ 0 & -s_{23} & c_{23} \end{bmatrix} \begin{bmatrix} c_{13} & 0 & s_{13}e^{-i\delta} \\ 0 & 1 & 0 \\ -s_{13}e^{i\delta} & 0 & c_{13} \end{bmatrix} \begin{bmatrix} c_{12} & s_{12} & 0 \\ -s_{12} & c_{12} & 0 \\ 0 & 0 & 1 \end{bmatrix} \begin{bmatrix} c_\varphi & s_\varphi & 0 \\ -s_\varphi & c_\varphi & 0 \\ 0 & 0 & 1 \end{bmatrix} \begin{bmatrix} 1 & 0 & 0 \\ 0 & 1 & 0 \\ 0 & 0 & e^{i\delta} \end{bmatrix} W \\
= \quad & \begin{bmatrix} 1 & 0 & 0 \\ 0 & c_{23} & s_{23} \\ 0 & -s_{23} & c_{23} \end{bmatrix} \begin{bmatrix} c_{13} & 0 & s_{13}e^{-i\delta} \\ 0 & 1 & 0 \\ -s_{13}e^{i\delta} & 0 & c_{13} \end{bmatrix} \begin{bmatrix} c'_{12} & s'_{12} & 0 \\ -s'_{12} & c'_{12} & 0 \\ 0 & 0 & 1 \end{bmatrix} \begin{bmatrix} 1 & 0 & 0 \\ 0 & 1 & 0 \\ 0 & 0 & e^{i\delta} \end{bmatrix} W,
\end{aligned}
$$

where the extra 1-2 rotation from matter effects is now absorbed into the vacuum mixing angle θ_{12}:

$$\theta'_{12} = \theta_{12} + \varphi \ , \tag{2.4.29}$$

and we can identify it with the effective mixing angle

$$\tilde{\theta}_{12} \approx \theta'_{12} = \theta_{12} + \phi \tag{2.4.30}$$

If $\theta'_{12} \approx \pi/2$,

$$\begin{bmatrix} c'_{12} & s'_{12} & 0 \\ -s'_{12} & c'_{12} & 0 \\ 0 & 0 & 1 \end{bmatrix} \approx \begin{bmatrix} 0 & 1 & 0 \\ -1 & 0 & 0 \\ 0 & 0 & 1 \end{bmatrix}, \tag{2.4.31}$$

then we can commute the $2-3$ rotation matrix W through:

$$
\begin{aligned}
\begin{bmatrix} c'_{12} & s'_{12} & 0 \\ -s'_{12} & c'_{12} & 0 \\ 0 & 0 & 1 \end{bmatrix} \begin{bmatrix} 1 & 0 & 0 \\ 0 & c_\phi & s_\phi \\ 0 & -s_\phi & c_\phi \end{bmatrix} \quad & \approx \quad \begin{bmatrix} 0 & 1 & 0 \\ -1 & 0 & 0 \\ 0 & 0 & 1 \end{bmatrix} \begin{bmatrix} 1 & 0 & 0 \\ 0 & c_\phi & s_\phi \\ 0 & -s_\phi & c_\phi \end{bmatrix} \\
& = \quad \begin{bmatrix} c_\phi & 0 & s_\phi \\ 0 & 1 & 0 \\ -s_\phi & 0 & c_\phi \end{bmatrix} \begin{bmatrix} 0 & 1 & 0 \\ -1 & 0 & 0 \\ 0 & 0 & 1 \end{bmatrix} \\
& \approx \quad \begin{bmatrix} c_\phi & 0 & s_\phi \\ 0 & 1 & 0 \\ -s_\phi & 0 & c_\phi \end{bmatrix} \begin{bmatrix} c'_{12} & s'_{12} & 0 \\ -s'_{12} & c'_{12} & 0 \\ 0 & 0 & 1 \end{bmatrix}.
\end{aligned} \tag{2.4.32}
$$

The mixing matrix becomes:

$$
\begin{aligned}
&U' \\
&= \begin{bmatrix} 1 & 0 & 0 \\ 0 & c_{23} & s_{23} \\ 0 & -s_{23} & c_{23} \end{bmatrix} \begin{bmatrix} c_{13} & 0 & s_{13}e^{-i\delta} \\ 0 & 1 & 0 \\ -s_{13}e^{i\delta} & 0 & c_{13} \end{bmatrix} \begin{bmatrix} c'_{12} & s'_{12} & 0 \\ -s'_{12} & c'_{12} & 0 \\ 0 & 0 & 1 \end{bmatrix} \begin{bmatrix} 1 & 0 & 0 \\ 0 & 1 & 0 \\ 0 & 0 & e^{i\delta} \end{bmatrix} \begin{bmatrix} 1 & 0 & 0 \\ 0 & c_\phi & s_\phi \\ 0 & -s_\phi & c_\phi \end{bmatrix} \\
&= \begin{bmatrix} 1 & 0 & 0 \\ 0 & c_{23} & s_{23} \\ 0 & -s_{23} & c_{23} \end{bmatrix} \begin{bmatrix} c_{13} & 0 & s_{13}e^{-i\delta} \\ 0 & 1 & 0 \\ -s_{13}e^{i\delta} & 0 & c_{13} \end{bmatrix} \begin{bmatrix} c'_{12} & s'_{12} & 0 \\ -s'_{12} & c'_{12} & 0 \\ 0 & 0 & 1 \end{bmatrix} \begin{bmatrix} 1 & 0 & 0 \\ 0 & c_\phi & s_\phi \\ 0 & -s_\phi & c_\phi \end{bmatrix} \begin{bmatrix} 1 & 0 & 0 \\ 0 & 1 & 0 \\ 0 & 0 & e^{i\delta} \end{bmatrix} \\
&\approx \begin{bmatrix} 1 & 0 & 0 \\ 0 & c_{23} & s_{23} \\ 0 & -s_{23} & c_{23} \end{bmatrix} \begin{bmatrix} c_{13} & 0 & s_{13}e^{-i\delta} \\ 0 & 1 & 0 \\ -s_{13}e^{i\delta} & 0 & c_{13} \end{bmatrix} \begin{bmatrix} c_\phi & 0 & s_\phi \\ 0 & 1 & 0 \\ -s_\phi & 0 & c_\phi \end{bmatrix} \begin{bmatrix} c'_{12} & s'_{12} & 0 \\ -s'_{12} & c'_{12} & 0 \\ 0 & 0 & 1 \end{bmatrix} \begin{bmatrix} 1 & 0 & 0 \\ 0 & 1 & 0 \\ 0 & 0 & e^{i\delta} \end{bmatrix} \\
&= \begin{bmatrix} 1 & 0 & 0 \\ 0 & c_{23} & s_{23} \\ 0 & -s_{23} & c_{23} \end{bmatrix} \begin{bmatrix} c'_{13} & 0 & s'_{13}e^{-i\delta} \\ 0 & 1 & 0 \\ -s'_{13}e^{i\delta} & 0 & c'_{13} \end{bmatrix} \begin{bmatrix} c'_{12} & s'_{12} & 0 \\ -s'_{12} & c'_{12} & 0 \\ 0 & 0 & 1 \end{bmatrix} \begin{bmatrix} 1 & 0 & 0 \\ 0 & 1 & 0 \\ 0 & 0 & e^{i\delta} \end{bmatrix} \\
&= U'',
\end{aligned}
\tag{2.4.33}
$$

where the $2-3$ rotation is absorbed into mixing angle θ_{13} and becomes effective mixing angle

$$\theta'_{13} = \theta_{13} + \phi, \tag{2.4.34}$$

and

$$U'' = \begin{bmatrix} c'_{12}c'_{13} & s'_{12}c'_{13} & s'_{13}e^{-i\delta} \\ -s'_{12}c_{23} - c'_{12}s'_{13}s_{23}e^{i\delta} & c'_{12}c_{23} - s'_{12}s'_{13}s_{23}e^{i\delta} & c'_{13}s_{23} \\ s'_{12}s_{23} - c'_{12}s'_{13}c_{23}e^{i\delta} & -c'_{12}s_{23} - s'_{12}s'_{13}c_{23}e^{i\delta} & c'_{13}c_{23} \end{bmatrix}, \tag{2.4.35}$$

where

$$\begin{aligned} c'_{12} &= \cos\theta'_{12} = \cos(\theta_{12} + \varphi) \qquad & s'_{12} &= \sin\theta'_{12} = \sin(\theta_{12} + \varphi) \\ c'_{13} &= \cos\theta'_{13} = \cos(\theta_{13} + \phi) \qquad & s'_{13} &= \sin\theta'_{13} = \sin(\theta_{13} + \phi). \end{aligned}$$

The approximated oscillation probabilities can be obtain by replacing the mixing matrix U in eq.(2.2.13) with the approximated mixing matrix U'':

$$P(\nu_\alpha \to \nu_\beta)_{\text{matter}} \approx \delta_{\alpha\beta} - 4\sum_{i>j} \Re(U''^*_{\alpha i} U''_{\beta i} U''_{\alpha j} U''^*_{\beta j}) \sin^2 \frac{\Delta''_{ij}}{2} + 2\sum_{i>j} \Im(U''^*_{\alpha i} U''_{\beta i} U''_{\alpha j} U''^*_{\beta j}) \sin\Delta''_{ij}, \tag{2.4.36}$$

where

$$\Delta''_{ij} = \lambda'_i - \lambda'_j \tag{2.4.37}$$

and

$$\begin{aligned}\lambda'_1 &= \frac{(\delta m^2_{21}+a)-\sqrt{(\delta m^2_{21}-a)^2+4a\delta m^2_{21}s^2_{12}}}{2}\\ \lambda'_2 &= \frac{(\delta m^2_{21}+a)+\sqrt{(\delta m^2_{21}-a)^2+4a\delta m^2_{21}s^2_{12}}}{2}\\ \lambda'_3 &= \delta m^2_{31}\end{aligned} \tag{2.4.38}$$

for $a/|\delta m^2_{13}| < \mathrm{O}(\epsilon)$,

$$\begin{aligned}\lambda'_1 &= \delta m^2_{21}c^2_{12}\\ \lambda'_2 &= \frac{(\delta m^2_{31}+a)-\sqrt{(\delta m^2_{31}-a)^2+4a\delta m^2_{31}s^2_{12}}}{2}\\ \lambda'_2 &= \frac{(\delta m^2_{31}+a)+\sqrt{(\delta m^2_{31}-a)^2+4a\delta m^2_{31}s^2_{12}}}{2}\end{aligned} \tag{2.4.39}$$

for $a/|\delta m^2_{13}| > \mathrm{O}(1)$. Fig.**??** is a sample calculation using approximated formula compared to the exact formula.

This approximation breaks down when ϕ is closer to $\pi/2$ than θ'_{12}. Instead of eq.(2.4.32), we now have

$$\begin{bmatrix} c'_{12} & s'_{12} & 0\\ -s'_{12} & c'_{12} & 0\\ 0 & 0 & 1\end{bmatrix}\begin{bmatrix} 1 & 0 & 0\\ 0 & c_\phi & s_\phi\\ 0 & -s_\phi & c_\phi\end{bmatrix} \approx \begin{bmatrix} c'_{12} & s'_{12} & 0\\ -s'_{12} & c'_{12} & 0\\ 0 & 0 & 1\end{bmatrix}\begin{bmatrix} 1 & 0 & 0\\ 0 & 0 & 1\\ 0 & -1 & 0\end{bmatrix}, \tag{2.4.40}$$

and this approximation breaks down. So the condition for this approximation to work is

$$\begin{aligned}\theta'_{12} &> \phi.\\ \theta_{12}+\varphi &> \phi.\end{aligned} \tag{2.4.41}$$

where

$$\begin{aligned}\varphi &= \frac{1}{2}\tan^{-1}\frac{ac^2_{12}\sin 2\theta_{12}}{\delta m^2_{21}-ac^2_{12}\cos 2\theta_{12}}\\ &\approx \frac{1}{2}\tan^{-1}\frac{a\sin 2\theta_{12}}{\delta m^2_{21}-a\cos 2\theta_{12}}.\end{aligned} \tag{2.4.42}$$

Expanding $\tan^{-1}$ when it's argument is large, we get

$$\begin{aligned}\varphi &\approx \frac{1}{2}\left(\frac{\pi}{2}-\frac{\delta m^2_{21}-a\cos 2\theta_{12}}{a\sin 2\theta_{12}}\right)\\ &\approx \frac{1}{2}\left(\frac{\pi}{2}-\cot 2\theta_{12}\right).\end{aligned} \tag{2.4.43}$$

On the other hand,

$$\begin{aligned}\phi &= \frac{1}{2}\tan^{-1}\frac{as'_{12}\sin 2\theta_{13}}{\delta m^2_{31}+as^2_{13}-\lambda'_2}\\ &\approx \frac{1}{2}\tan^{-1}\frac{a\sin 2\theta_{13}}{\delta m^2_{31}-a\cos 2\theta_{13}}.\end{aligned} \tag{2.4.44}$$

Expand it around 0 we get

$$\begin{aligned}\phi &\approx \frac{1}{2}\left(\pi + \frac{a\sin 2\theta_{13}}{\delta m^2_{31} - a\cos 2\theta_{13}}\right) \\ &\approx \frac{1}{2}\left(\pi + \tan 2\theta_{13}\right). \end{aligned} \tag{2.4.45}$$

So now eq.(2.4.41) becomes

$$\begin{aligned}\theta_{12} + \frac{1}{2}\left(\frac{\pi}{2} - \cot 2\theta_{12}\right) &< \frac{1}{2}\left(\pi + \tan 2\theta_{13}\right) \\ \theta_{13} &< \frac{1}{2}\tan^{-1}\left(\theta_{12} - \frac{\pi}{2} + \cot 2\theta_{12}\right) = 1.4 \end{aligned} \tag{2.4.46}$$

2.5 Inverted Hierarchy

Following the same procedure as the normal hierarchy case, the Hamiltonian for the inverted hierarchy case, $\delta m^2_{31} < 0$, can be approximately diagonalized by a 1-2 rotation, V, followed by a 2-3 rotation,W.

2.5.1 Effective mixing angles

θ_{13}

Comparing the (1,3) elements of the matrices, we can make the identification

$$\begin{aligned}\tilde{s}_{13} &= c_{13}s'_{12}s_\phi + s_{13}c_\phi \\ &= (c_{13}s_\phi + s_{13}c_\phi) - (1 - s'_{12})s_\phi c_{13} \\ &= s'_{13} + c'_{13}\left\{-\frac{(1-s'_{12})s_\phi c_{13}}{c'_{13}}\right\}, \end{aligned} \tag{2.5.1}$$

where we have defined

$$s'_{13} = \sin\theta'_{13}\,, \qquad c'_{13} = \cos\theta'_{13}\,, \qquad \theta'_{13} = \theta_{13} + \phi\,. \tag{2.5.2}$$

Note that the factor $(1 - s'_{12})s_\phi/c'_{13}$ is of order ε^3 or smaller regardless of the value of a, as shown in Table **??**. Therefore,

$$\sin\tilde{\theta}_{13} = \sin\left[\theta'_{13} + O(\varepsilon^3)\right]\,, \tag{2.5.3}$$

which implies

$$\tilde{\theta}_{13} = \theta'_{13} + O(\varepsilon^3)\,. \tag{2.5.4}$$

θ_{12}

Next, looking at the $(1,1)$ and $(1,2)$ elements, we find

$$\begin{aligned}\tan\tilde{\theta}_{12} &= \frac{\tilde{s}_{12}\tilde{c}_{13}}{\tilde{c}_{12}\tilde{c}_{13}} \\ &= \frac{c_{13}s'_{12}c_\phi - s_{13}s_\phi}{c_{13}c'_{12}} \end{aligned}$$

$$
\begin{aligned}
&= \frac{(c_{13}c_\phi - s_{13}s_\phi)s'_{12} - s_{13}(1-s'_{12})s_\phi}{c_{13}c'_{12}} \\
&= \left(\frac{c'_{13}}{c_{13}}\right)\left[\tan\theta'_{12} + \frac{1}{\cos^2\theta'_{12}}\left\{-\frac{s_{13}c'_{12}(1-s'_{12})s_\phi}{c'_{13}}\right\}\right] . \qquad (2.5.5)
\end{aligned}
$$

From Table **??**, we find that the factor $s_{13}c'_{12}(1-s'_{12})s_\phi/c'_{13}$ is of order ε^4 or smaller for all a. Therefore,

$$\tan\tilde{\theta}_{12} = \left(\frac{c'_{13}}{c_{13}}\right)\tan\left[\theta'_{12} + O(\varepsilon^4)\right] . \qquad (2.5.6)$$

Since $\theta'_{13} = \theta_{13} + \phi$, we can expect the ratio c'_{13}/c_{13} to be roughly equal to one when ϕ is small, and consequently, $\tilde{\theta}_{12} \approx \theta'_{12}$. Indeed, if $\delta m^2_{31} > 0$ with $a/|\delta m^2_{31}| \leq O(\varepsilon)$, or $\delta m^2_{31} < 0$ with any a, then $s_\phi \leq O(\varepsilon)$, and we find

$$1 - \frac{c'_{13}}{c_{13}} = (1-c_\phi) + s_\phi\tan\theta_{13} \leq O(\varepsilon^2) . \qquad (2.5.7)$$

In these cases, we can treat $(1 - c'_{13}/c_{13})$ as a small quantity and expand

$$\tilde{\theta}_{12} \;=\; \theta'_{12} + s'_{12}c'_{12}\left(1 - \frac{c'_{13}}{c_{13}}\right) + \cdots \;=\; \theta'_{12} + O(\varepsilon^4) . \qquad (2.5.8)$$

The $\delta m^2_{31} > 0$ case with $a/|\delta m^2_{31}| = O(1)$ or $a/|\delta m^2_{31}| = O(\varepsilon^{-1})$ must be considered separately. First, taking the reciprocal of both sides of Eq. (2.5.6), we obtain

$$\cot\tilde{\theta}_{12} = \frac{c_{13}}{c'_{13}}\cot\theta'_{12} , \qquad (2.5.9)$$

where we have dropped the shift in θ'_{12} on the right hand side which is of order $\varepsilon^{7,8}$ in these particular cases. (cf. Table **??**.) Recall that when $a/|\delta m^2_{31}| = O(\varepsilon^{0,-1})$, we have

$$\theta'_{12} = \frac{\pi}{2} - \frac{\delta m^2_{21}}{2a}\sin(2\theta_{12}) + O(\varepsilon^{4,5}) , \qquad (2.5.10)$$

while

$$\frac{c_{13}}{c'_{13}} = O(\varepsilon^{0,-2}) . \qquad (2.5.11)$$

Therefore, from Eq. (2.5.9) we find

$$
\begin{aligned}
\tan\left(\frac{\pi}{2} - \tilde{\theta}_{12}\right) &= \frac{c_{13}}{c'_{13}}\tan\left(\frac{\pi}{2} - \theta'_{12}\right) \\
&= \frac{c_{13}}{c'_{13}}\tan\left(\frac{\delta m^2_{21}}{2a}\sin(2\theta_{12}) + O(\varepsilon^{4,5})\right) \\
&= \frac{c_{13}}{c'_{13}}\left(\frac{\delta m^2_{21}}{2a}\sin(2\theta_{12})\right) + O(\varepsilon^{4,3}) \\
&= \tan\left(\frac{c_{13}}{c'_{13}}\frac{\delta m^2_{21}}{2a}\sin(2\theta_{12}) + O(\varepsilon^{4,3})\right) , \qquad (2.5.12)
\end{aligned}
$$

from which we can conclude

$$\tilde{\theta}_{12} = \frac{\pi}{2} - \frac{c_{13}}{c'_{13}}\left(\frac{\delta m^2_{21}}{2a}\right)\sin(2\theta_{12}) + O(\varepsilon^{4,3}) . \qquad (2.5.13)$$

θ_{23}

Next, using the relation

$$s_{13}s'_{12}s_\phi - c_{13}c_\phi \;=\; -(c_{13}c_\phi - s_{13}s_\phi) - s_{13}(1-s'_{12})s_\phi \;=\; -c'_{13} + O(\varepsilon^4)\;, \tag{2.5.14}$$

we simplify the $(2,3)$ and $(3,3)$ elements of U' as

$$\begin{aligned} c_{23}c'_{12}s_\phi - s_{23}(s_{13}s'_{12}s_\phi - c_{13}c_\phi)e^{i\delta} &= c_{23}c'_{12}s_\phi + s_{23}c'_{13}e^{i\delta} + O(\varepsilon^4)\;, \\ -s_{23}c'_{12}s_\phi - c_{23}(s_{13}s'_{12}s_\phi - c_{13}c_\phi)e^{i\delta} &= -s_{23}c'_{12}s_\phi + c_{23}c'_{13}e^{i\delta} + O(\varepsilon^4)\;. \end{aligned} \tag{2.5.15}$$

Then, using the fact that $c'_{12}s_\phi = O(\varepsilon^2)$ or smaller, we find

$$\begin{aligned} &|c_{23}c'_{12}s_\phi - s_{23}(s_{13}s'_{12}s_\phi - c_{13}c_\phi)e^{i\delta}| \\ &\quad= \sqrt{s_{23}^2{c'_{13}}^2 + 2s_{23}c_{23}c'_{13}c'_{12}s_\phi\cos\delta + c_{23}^2{c'_{12}}^2s_\phi^2 + O(\varepsilon^4)} \\ &\quad= \sqrt{s_{23}^2{c'_{13}}^2 + 2s_{23}c_{23}c'_{13}c'_{12}s_\phi\cos\delta + O(\varepsilon^4)} \\ &\quad= s_{23}c'_{13} + c_{23}c'_{12}s_\phi\cos\delta + O(\varepsilon^4) \\ &|-s_{23}c'_{12}s_\phi - c_{23}(s_{13}s'_{12}s_\phi - c_{13}c_\phi)e^{i\delta}| \\ &\quad= \sqrt{c_{23}^2{c'_{13}}^2 - 2s_{23}c_{23}c'_{13}c'_{12}s_\phi\cos\delta + s_{23}^2{c'_{12}}^2s_\phi^2 + O(\varepsilon^4)} \\ &\quad= \sqrt{c_{23}^2{c'_{13}}^2 - 2s_{23}c_{23}c'_{13}c'_{12}s_\phi\cos\delta + O(\varepsilon^4)} \\ &\quad= c_{23}c'_{13} - s_{23}c'_{12}s_\phi\cos\delta + O(\varepsilon^4) \end{aligned} \tag{2.5.16}$$

Therefore, we can make the identification

$$\begin{aligned} \tan\tilde\theta_{23} &= \frac{\tilde c_{13}\tilde s_{23}}{\tilde c_{13}\tilde c_{23}} \\ &= \frac{s_{23}c'_{13} + c_{23}c'_{12}s_\phi\cos\delta}{c_{23}c'_{13} - s_{23}c'_{12}s_\phi\cos\delta} + O(\varepsilon^4) \\ &= \frac{t_{23} + \left(\dfrac{c'_{12}s_\phi}{c'_{13}}\right)\cos\delta}{1 - t_{23}\left(\dfrac{c'_{12}s_\phi}{c'_{13}}\right)\cos\delta} + O(\varepsilon^4) \\ &= \tan\left[\theta_{23} + \left(\frac{c'_{12}s_\phi}{c'_{13}}\right)\cos\delta\right] + O(\varepsilon^4)\;, \end{aligned} \tag{2.5.17}$$

and we obtain

$$\tilde\theta_{23} = \theta_{23} + \left(\frac{c'_{12}s_\phi}{c'_{13}}\right)\cos\delta + O(\varepsilon^4)\;. \tag{2.5.18}$$

The factor $c'_{12}s_\phi/c'_{13}$ is of order ε^3 or smaller if $\delta m^2_{31} > 0$ with $a/|\delta m^2_{31}| \le O(\varepsilon)$, or $\delta m^2_{31} < 0$ with any a. In those cases, we have

$$\tilde\theta_{23} = \theta_{23} + O(\varepsilon^3)\;. \tag{2.5.19}$$

For the case of $\delta m^2_{31} > 0$ with $a/|\delta m^2_{31}| \ge O(1)$, we can expand c'_{12} and approximate

$$\tilde\theta_{23} = \theta_{23} + \frac{s_\phi}{c'_{13}}\left(\frac{\delta m^2_{21}}{2a}\right)\sin(2\theta_{12})\cos\delta + O(\varepsilon^4)\;. \tag{2.5.20}$$

δ

Finally, we calculate the CP violating phase. The Jarskog invariant of U' is

$$\begin{aligned} J' &= (c_{13}s'_{12}s_\phi + s_{13}c_\phi)(c_{13}s'_{12}c_\phi - s_{13}s_\phi)(c_{13}c'_{12})s_{23}c_{23}\sin\delta \\ &= \tilde{s}_{13}(\tilde{c}_{13}\tilde{s}_{12})(\tilde{c}_{13}\tilde{c}_{12})s_{23}c_{23}\sin\delta \\ &= (\tilde{s}_{13}\tilde{c}^2_{13}\tilde{s}_{12}\tilde{c}_{12})s_{23}c_{23}\sin\delta\ . \end{aligned} \tag{2.5.21}$$

On the other hand, the Jarskog invariant of $\tilde{U}$ is

$$\tilde{J} = \tilde{s}_{13}\tilde{c}^2_{13}\tilde{s}_{12}\tilde{c}_{12}\tilde{s}_{23}\tilde{c}_{23}\sin\tilde{\delta}\ . \tag{2.5.22}$$

Comparison with J' shows that

$$\sin(2\tilde{\theta}_{23})\sin\tilde{\delta} = \sin(2\theta_{23})\sin\delta\ , \tag{2.5.23}$$

which is actually an exact relation as discussed in Ref. [22]. Since $\tilde{\theta}_{23} = \theta_{23} + O(\varepsilon^3)$ when $\delta m^2_{31} > 0$ with $a/|\delta m^2_{31}| \leq O(\varepsilon)$, or $\delta m^2_{31} < 0$ with any a, for these cases we have

$$\tilde{\delta} = \delta + O(\varepsilon^3)\ . \tag{2.5.24}$$

For the case $\delta m^2_{31} > 0$ with $a/|\delta m^2_{31}| \geq O(1)$, we can use Eq. (2.5.20) to obtain

$$\tilde{\delta} = \delta - \frac{s_\phi}{c'_{13}}\left(\frac{\delta m^2_{21}}{a}\right)\frac{\sin(2\theta_{12})}{\tan(2\theta_{23})}\sin\delta + O(\varepsilon^6)\ . \tag{2.5.25}$$

2.5.2 Summary of Neutrino Results and Sample Calculation

Let us summarize the results of the two previous subsections.

Approximate values of the effective mixing angles in matter can be obtained from the relations

$$\begin{aligned} \tilde{\theta}_{13} &\approx \theta'_{13} - \tan\theta'_{13}\frac{(c'_{12})^2}{2}, \\ \tan\tilde{\theta}_{12} &\approx \frac{c'_{13}}{c_{13}}\tan\theta'_{12}\ , \\ \tilde{\theta}_{23} &\approx \theta_{23} + \left(\frac{c'_{12}s_\phi}{c'_{13}}\right)\cos\delta\ , \\ \sin(2\tilde{\theta}_{23})\sin\tilde{\delta} &= \sin(2\theta_{23})\sin\delta\ , \end{aligned} \tag{2.5.26}$$

where

$$\begin{aligned} \theta'_{12} &= \theta_{12} + \varphi\ , \\ \theta'_{13} &= \theta_{13} + \phi\ , \end{aligned} \tag{2.5.27}$$

and the angles φ and ϕ were defined in Eqs. (**??**) and (**??**), respectively. The a-dependence of φ and ϕ for the sample case of $\tan^2\theta_{12} = 0.4$, $\sin^2(2\theta_{13}) = 0.16$, $\delta m^2_{21} = 8.2\times10^{-5}\mathrm{eV}^2$, and $|\delta m^2_{31}| = 2.5\times10^{-3}\mathrm{eV}^2$ is shown in Fig 2.5.1 with gray solid lines. In the figure, the angles are in units of π, and they are plotted against the variable α defined as:

$$\alpha \equiv \log_{1/\varepsilon}\frac{a}{|\delta m^2_{31}|}\ , \qquad \frac{a}{|\delta m^2_{31}|} = \varepsilon^{-\alpha}\ . \tag{2.5.28}$$

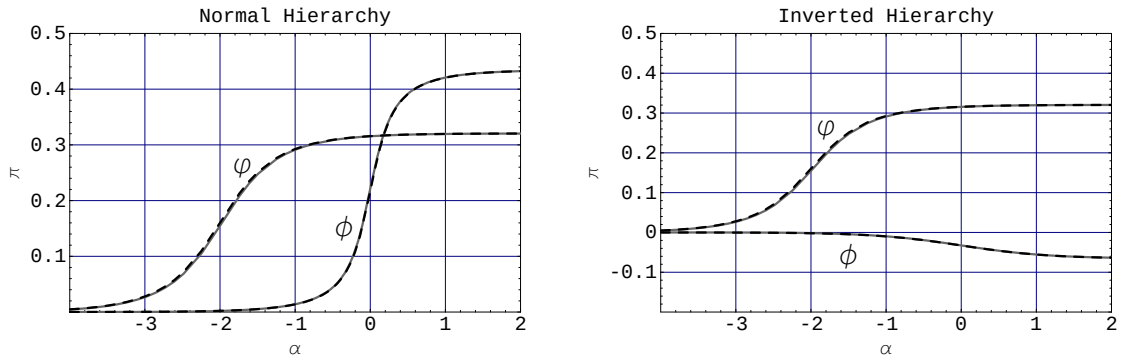

Figure 2.5.1: The exact (gray solid line) and approximate (black dashed line) values of φ and ϕ plotted against $\alpha = \log_{1/\varepsilon}(a/|\delta m^2_{31}|)$. The parameter choice was $\tan^2\theta_{12} = 0.4$, $\sin^2(2\theta_{13}) = 0.16$, $\delta m^2_{21} = 8.2 \times 10^{-5}\text{eV}^2$ and $|\delta m^2_{31}| = 2.5 \times 10^{-3}\text{eV}^2$.

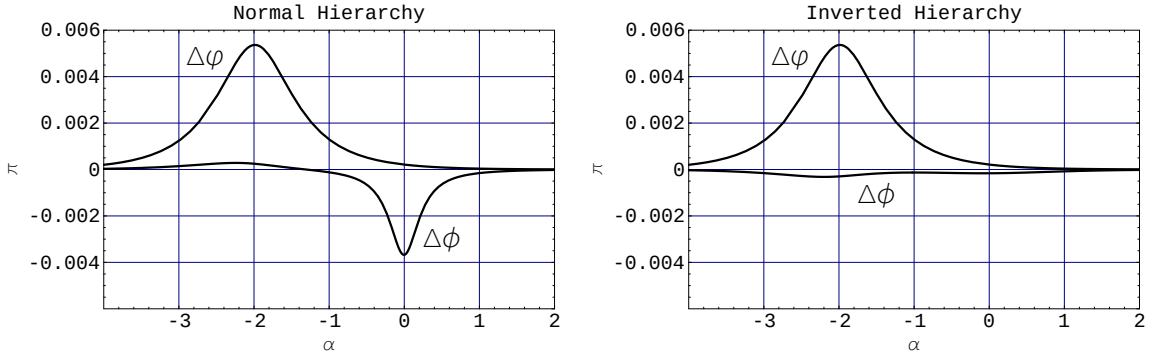

Figure 2.5.2: $\Delta\varphi = \varphi_{\text{approx}} - \varphi_{\text{exact}}$ and $\Delta\phi = \phi_{\text{approx}} - \phi_{\text{exact}}$ plotted against $\alpha = \log_{1/\varepsilon}(a/|\delta m^2_{31}|)$ for the same parameter choice as Fig. 2.5.1.

$\alpha = 0$ corresponds to $a = |\delta m^2_{31}|$, and $\alpha = -2$ corresponds to $a = \delta m^2_{21}$.

When either $\delta m^2_{31} > 0$ (normal hierarchy) with $\alpha \lesssim -1$, which corresponds to $a/|\delta m^2_{31}| \leq O(\varepsilon)$, or $\delta m^2_{31} < 0$ (inverted hierarchy) with any α, the angle ϕ is small, and Eq. (2.5.26) reduces to

$$\begin{aligned} \tilde{\theta}_{13} &\approx \theta'_{13} = \theta_{13} + \phi \,, \\ \tilde{\theta}_{12} &\approx \theta'_{12} = \theta_{12} + \varphi \,, \\ \tilde{\theta}_{23} &\approx \theta_{23} \,, \\ \tilde{\delta} &\approx \delta \,. \end{aligned} \tag{2.5.29}$$

For the $\delta m^2_{31} > 0$ case (normal hierarchy) with $\alpha \gtrsim 0$, which corresponds to $a/|\delta m^2_{31}| \geq O(1)$, the angles can be approximated as

$$\begin{aligned} \tilde{\theta}_{13} &\approx \theta'_{13} \,, \\ \tilde{\theta}_{12} &\approx \frac{\pi}{2} - \frac{c_{13}}{c'_{13}} \left(\frac{\delta m^2_{21}}{2a} \right) \sin(2\theta_{12}) \,, \\ \tilde{\theta}_{23} &\approx \theta_{23} + \frac{s_\phi}{c'_{13}} \left(\frac{\delta m^2_{21}}{2a} \right) \sin(2\theta_{12}) \cos\delta \,, \\ \tilde{\delta} &\approx \delta - \frac{s_\phi}{c'_{13}} \left(\frac{\delta m^2_{21}}{a} \right) \frac{\sin(2\theta_{12})}{\tan(2\theta_{23})} \sin\delta \,. \end{aligned} \tag{2.5.30}$$

To make use of these expressions, we must first calculate φ and ϕ, and then $\theta'_{12} = \theta_{12} + \varphi$ and $\theta'_{13} = \theta_{13} + \phi$. Simple approximations to φ and ϕ are provided by

$$\tan 2\varphi \approx \frac{a \sin 2\theta_{12}}{\delta m^2_{21} - a \cos 2\theta_{12}} \,, \qquad \tan 2\phi \approx \frac{a \sin 2\theta_{13}}{\delta m^2_{31} - a \cos 2\theta_{13}} \,. \tag{2.5.31}$$

The approximate values of φ and ϕ obtained from these expressions are also shown in Fig. 2.5.1 with black dashed lines. As is clear from the figure, the graphs of the exact and approximate values are virtually indistinguishable at this scale. In Fig. 2.5.2 we plot the differences between the approximate and exact values of φ and ϕ:

$$\Delta\varphi \equiv \varphi_{\text{approx}} - \varphi_{\text{exact}} \,, \qquad \Delta\phi \equiv \phi_{\text{approx}} - \phi_{\text{exact}} \,. \tag{2.5.32}$$

The maximum deviation from the exact values occur at the level-crossing points $\alpha = -2$ and $\alpha = 0$ (there is no level-crossing at $\alpha = 0$ when $\delta m^2_{31} < 0$) but even then, it is a mere fraction of a percent of π. Using Eq. (2.5.31), we can also obtain simple approximate formulae for $\theta'_{12} = \theta_{12} + \varphi$ and $\theta'_{13} = \theta_{13} + \phi$:

$$\tan 2\theta'_{12} \approx \frac{\delta m^2_{21} \sin 2\theta_{12}}{\delta m^2_{21} \cos 2\theta_{12} - a} \,, \qquad \tan 2\theta'_{13} \approx \frac{\delta m^2_{31} \sin 2\theta_{13}}{\delta m^2_{31} \cos 2\theta_{13} - a} \,. \tag{2.5.33}$$

These allow us to calculate θ'_{12} and θ'_{13} directly without going through φ and ϕ. Eqs. (2.5.31) and (2.5.33) provide a quick and easy way to obtain the input angles necessary to utilize Eqs. (2.5.26), (2.5.29), and (2.5.30).

To demonstrate the accuracy of these approximations, we present a sample calculation using the following parameter choice:

$$\delta m^2_{21} = 8.2 \times 10^{-5}\,\text{eV}^2 \,,$$

$$\begin{aligned} |\delta m^2_{31}| &= 2.5 \times 10^{-3}\,\mathrm{eV}^2\ , \\ \tan^2\theta_{12} &= 0.4\ , \\ \sin^2(2\theta_{13}) &= 0.16\ , \\ \theta_{23} &= 0.2\,\pi\ , \\ \delta &= 0.25\,\pi\ . \end{aligned} \tag{2.5.34}$$

The values of δm^2_{21}, $|\delta m^2_{31}|$, and $\tan^2\theta_{12}$ are the experimental central values. The value of $\sin^2(2\theta_{13})$ is taken to be the 90% upper limit corresponding to our choice of $|\delta m^2_{31}|$ so that the $O(\theta_{13})$ terms that we neglect are maximized. The value of θ_{23} is also chosen to be one of the 90% confidence limits since if we set θ_{23} to the experimentally preferred central value of 0.25π, then the shift of $\tilde{\delta}$ away from δ would be suppressed. Similarly, we chose $\delta = 0.25\pi$ so that both $\tilde{\theta}_{23}$ and $\tilde{\delta}$ will be shifted from their vacuum values.

We first consider the normal hierarchy case ($\delta m^2_{31} > 0$). In Fig. 2.5.3a, we plot the exact values of $\tilde{\theta}_{12}$, $\tilde{\theta}_{13}$, $\tilde{\theta}_{23}$, and $\tilde{\delta}$ calculated numerically with gray solid lines, together with the approximate values obtained from Eq. (2.5.26), using Eqs. (2.5.31) and (2.5.33) to calculate the input angles, with dashed black lines. Fig. 2.5.3b shows the errors:

$$\Delta\theta_{ij} \equiv \tilde{\theta}_{ij,\mathrm{approx}} - \tilde{\theta}_{ij,\mathrm{exact}}\ , \qquad \Delta\delta \equiv \tilde{\delta}_{\mathrm{approx}} - \tilde{\delta}_{\mathrm{exact}}\ . \tag{2.5.35}$$

$\Delta\theta_{12}$ and $\Delta\theta_{13}$ are indicated with solid gray lines, while $\Delta\theta_{23}$ and $\Delta\delta$ are indicated with dashed black lines. The errors are never larger than a fraction of a percent of π, and comparison with Fig. 2.5.2 makes it apparent that the majority of it was inherited from having calculated φ and ϕ using Eq. (2.5.31). In Figs. 2.5.4a and 2.5.5a, we plot the exact values against the approximate values obtained using Eqs. (2.5.29) and (2.5.30), respectively, together with the errors in Figs. 2.5.4b and 2.5.5b. Clearly, the approximations using Eqs. (2.5.29) and (2.5.30) are good in their respective ranges of applicability.

For the inverted hierarchy case ($\delta m^2_{31} < 0$), we only need to consider Eq. (2.5.29). In Fig. 2.5.6a, we show the comparison between the numerically calculated exact values and the approximate values obtained from Eq. (2.5.29). The errors are shown in Fig. 2.5.6b.

The approximate values for the mass-squared eigenvalues are given by

$$\begin{aligned} \lambda_1 &\approx \lambda'_-\ , \\ \lambda_2 &\approx \lambda''_-\ , \\ \lambda_3 &\approx \lambda''_+\ , \end{aligned} \tag{2.5.36}$$

for $\delta m^2_{31} > 0$ (normal hierarchy), and by

$$\begin{aligned} \lambda_1 &\approx \lambda'_-\ , \\ \lambda_2 &\approx \lambda''_+\ , \\ \lambda_3 &\approx \lambda''_-\ , \end{aligned} \tag{2.5.37}$$

for $\delta m^2_{31} < 0$ (inverted hierarchy), where $\lambda'_\pm$ and $\lambda''_\pm$ are defined in Eqs, (**??**) and (**??**), respectively. The accuracy of this approximation is illustrated in Fig 2.5.7 using the parameter values of Eq. (2.5.34), where the exact numerically calculated values of $\delta\lambda_{21} = \lambda_2 - \lambda_1$ and $|\delta\lambda_{31}| = |\lambda_3 - \lambda_1|$ are plotted against those obtained from the above approximate expressions. The vertical axis is plotted using the same log-scale as the horizontal axis where $|\delta m^2_{31}|$ corresponds to 0 and δm^2_{21} corresponds to -2. Since a log-scale plot does not reflect the absolute accuracy of each $\delta\lambda_{ij}$, in

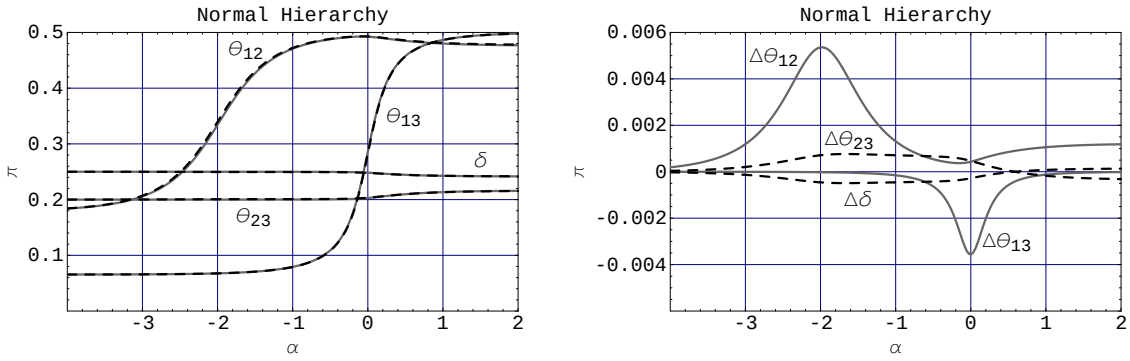

Figure 2.5.3: (a) The exact values of $\tilde{\theta}_{12}$, $\tilde{\theta}_{13}$, $\tilde{\theta}_{23}$, and $\tilde{\delta}$ (solid gray lines) plotted against their approximate values (black dashed lines) obtained using Eq. (2.5.26), with Eqs. (2.5.31) and (2.5.33), as functions of $\alpha = \log_{1/\varepsilon}(a/|\delta m^2_{31}|)$. (b) The differences $\Delta\theta_{12} = \tilde{\theta}_{12,\text{approx}} - \tilde{\theta}_{12,\text{exact}}$ and $\Delta\theta_{13} = \tilde{\theta}_{13,\text{approx}} - \tilde{\theta}_{13,\text{exact}}$ (solid gray lines), and the differences $\Delta\theta_{23} = \tilde{\theta}_{23,\text{approx}} - \tilde{\theta}_{23,\text{exact}}$ and $\Delta\delta = \tilde{\delta}_{\text{approx}} - \tilde{\delta}_{\text{exact}}$ (black dashed lines) of this approximation plotted against α.

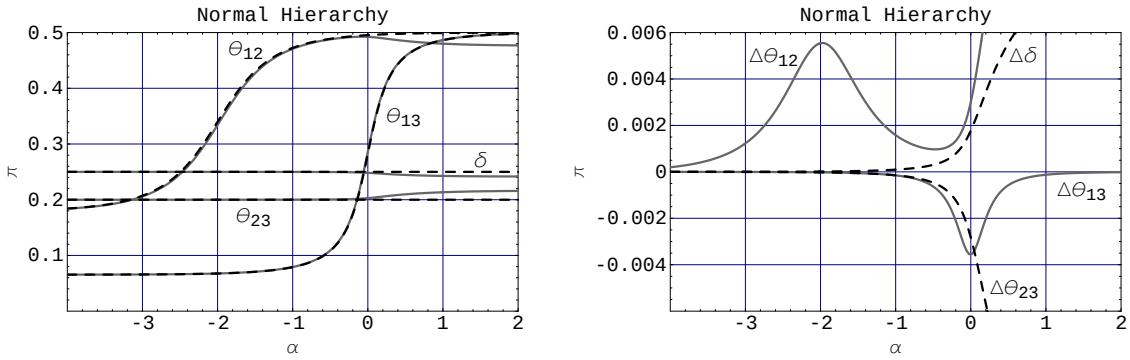

Figure 2.5.4: (a) The exact values of $\tilde{\theta}_{12}$, $\tilde{\theta}_{13}$, $\tilde{\theta}_{23}$, and $\tilde{\delta}$ (solid gray lines) plotted against their approximate values (black dashed lines) obtained using Eq. (2.5.29) as functions of $\alpha = \log_{1/\varepsilon}(a/|\delta m^2_{31}|)$. (b) $\Delta\theta_{12}$ and $\Delta\theta_{13}$ (solid gray lines), and $\Delta\theta_{23}$ and $\Delta\delta$ (black dashed lines) of this approximation plotted as functions of α. This approximation is applicable when $\alpha \lesssim -1$.

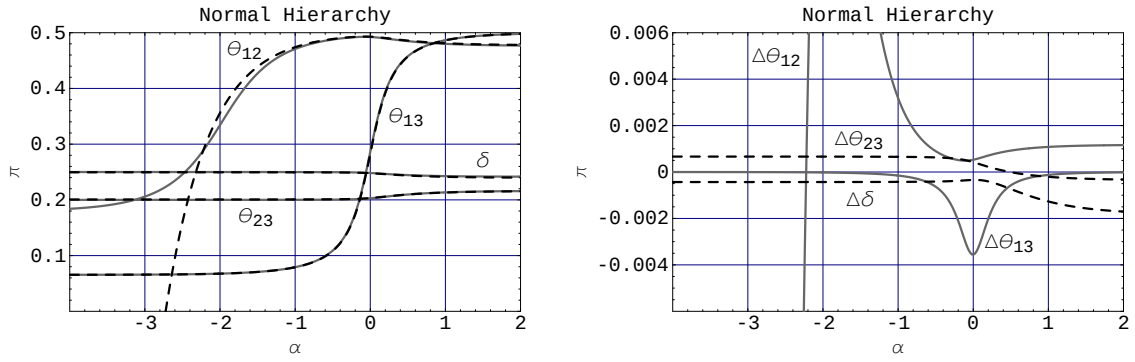

Figure 2.5.5: (a) The exact values of $\tilde{\theta}_{12}$, $\tilde{\theta}_{13}$, $\tilde{\theta}_{23}$, and $\tilde{\delta}$ (solid gray lines) plotted against their approximate values (black dashed lines) obtained using Eq. (2.5.30) as functions of $\alpha = \log_{1/\varepsilon}(a/|\delta m^2_{31}|)$. (b) $\Delta\theta_{12}$ and $\Delta\theta_{13}$ (solid gray lines), and $\Delta\theta_{23}$ and $\Delta\delta$ (black dashed lines) of this approximation plotted as functions of α. This approximation is applicable when $\alpha \gtrsim 0$.

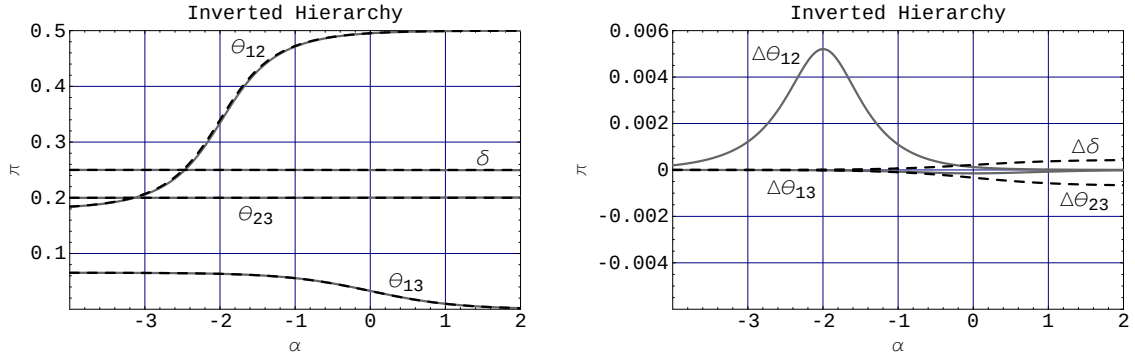

Figure 2.5.6: (a) The exact values of $\tilde{\theta}_{12}$, $\tilde{\theta}_{13}$, $\tilde{\theta}_{23}$, and $\tilde{\delta}$ (solid gray lines) plotted against their approximate values (black dashed lines) obtained using Eq. (2.5.29) as functions of $\alpha = \log_{1/\varepsilon}(a/|\delta m^2_{31}|)$ for the inverted hierarchy case ($\delta m^2_{31} < 0$). (b) $\Delta\theta_{12}$ and $\Delta\theta_{13}$ (solid gray lines), and $\Delta\theta_{23}$ and $\Delta\delta$ (black dashed lines) of this approximation plotted as functions of α.

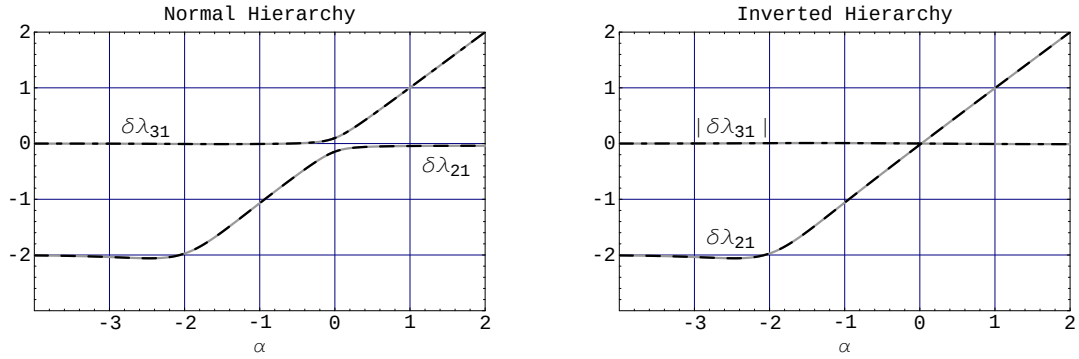

Figure 2.5.7: The exact and approximate values of $\log_{1/\varepsilon}(\delta\lambda_{21}/|\delta m^2_{31}|)$ and $\log_{1/\varepsilon}(|\delta\lambda_{31}|/|\delta m^2_{31}|)$ for the parameter set of Eq. (2.5.34) plotted against $\alpha = \log_{1/\varepsilon}(a/|\delta m^2_{31}|)$. The exact values are in gray solid lines, whereas the approximate values are in black dashed ($\delta\lambda_{21}$) and black dot-dashed ($|\delta\lambda_{31}|$) lines.

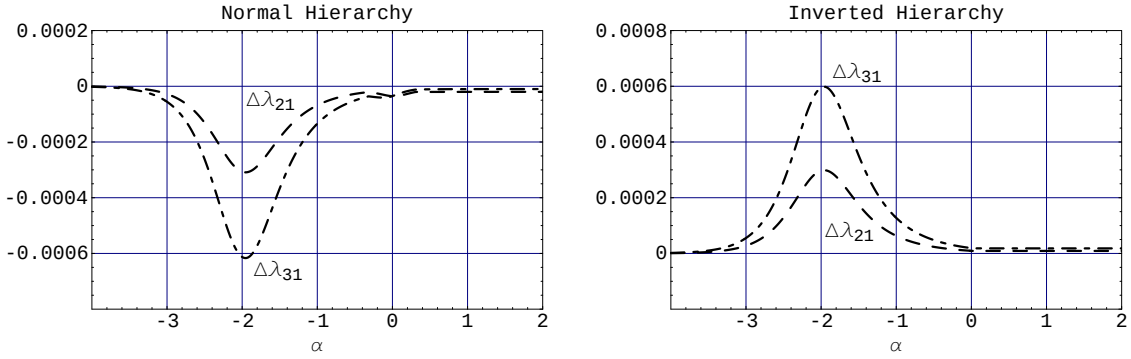

Figure 2.5.8: The rescaled errors $\Delta\lambda_{21}$ (dashed) and $\Delta\lambda_{31}$ (dot-dashed), as defined in Eq. (2.5.38), for the approximation of Fig. 2.5.7.

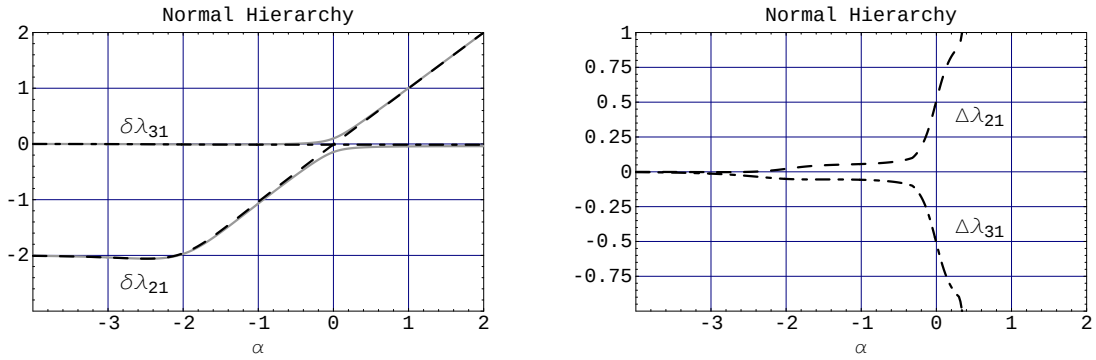

Figure 2.5.9: Comparison of exact and approximate values using Eq. (2.5.40) for the normal hierarchy case. The approximation is applicable when $\alpha \lesssim -1$.

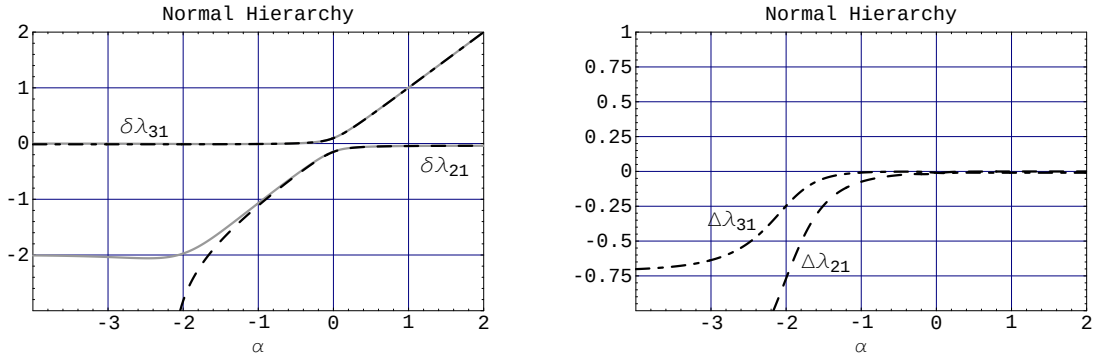

Figure 2.5.10: Comparison of exact and approximate values using Eq. (2.5.41) for the normal hierarchy case. The approximation is applicable when $\alpha \gtrsim -1$.

Fig. 2.5.8 we plot the difference between the exact and approximate values of $\delta\lambda_{ij}$ normalized to $\delta\lambda_{\rm min,exact}$:

$$\Delta\lambda_{i1} \equiv \frac{\delta\lambda_{i1,\rm approx} - \delta\lambda_{i1,\rm exact}}{\delta\lambda_{\rm min,exact}} \ , \qquad (i = 2, 3) \ , \tag{2.5.38}$$

where

$$\delta\lambda_{\rm min,exact} \equiv \min(\delta\lambda_{21,\rm exact}, |\delta\lambda_{31,\rm exact}|, |\delta\lambda_{32,\rm exact}|) \ . \tag{2.5.39}$$

This tells us how large the errors are compared to $\delta\lambda_{\rm min}$, which is typically used to expand the oscillation probabilities in. As is evident from the figures, the approximation is excellent.

When either $\delta m^2_{31} > 0$ (normal hierarchy) with $\alpha \lesssim -1$, *i.e.* $a/|\delta m^2_{31}| \leq O(\varepsilon)$, or $\delta m^2_{31} < 0$ (inverted hierarchy) with any a, the λ's can be further approximated by

$$\begin{aligned}
\lambda_1 &\approx \frac{(a + \delta m^2_{21}) - \sqrt{(a - \delta m^2_{21})^2 + 4a\,\delta m^2_{21} s^2_{12}}}{2} \ , \\
\lambda_2 &\approx \frac{(a + \delta m^2_{21}) + \sqrt{(a - \delta m^2_{21})^2 + 4a\,\delta m^2_{21} s^2_{12}}}{2} \ , \\
\lambda_3 &\approx \delta m^2_{31} \ .
\end{aligned} \tag{2.5.40}$$

For the $\delta m^2_{31} > 0$ (normal hierarchy) case with $\alpha \gtrsim -1$, *i.e.* $a/|\delta m^2_{31}| \geq O(\varepsilon)$, we can use

$$\begin{aligned}
\lambda_1 &\approx \delta m^2_{21} c^2_{12} \ , \\
\lambda_2 &\approx \frac{(a + \delta m^2_{31}) - \sqrt{(a - \delta m^2_{31})^2 + 4a\,\delta m^2_{31} s^2_{13}}}{2} \ , \\
\lambda_3 &\approx \frac{(a + \delta m^2_{31}) + \sqrt{(a - \delta m^2_{31})^2 + 4a\,\delta m^2_{31} s^2_{13}}}{2} \ .
\end{aligned} \tag{2.5.41}$$

This second approximation introduces errors of $O(\varepsilon^2|\delta m^2_{31}|)$ in the λ's. However, since $\delta\lambda_{21} \geq O(\varepsilon|\delta m^2_{31}|)$ in this range, an error of this size is tolerable. The accuracy of these approximations is illustrated in Figs. 2.5.9 and 2.5.10 for the $\delta m^2_{31} > 0$ case, and Fig. 2.5.11 for the $\delta m^2_{31} < 0$ case. Though the accuracy is not as good as when Eqs. (2.5.36) and (2.5.37), with Eqs. (**??**) and (**??**), are used, it is sufficient for most practical purposes.

2.6 Anti-Neutrino: Normal Hierarchy

Matter effects for anti-neutrinos can be treated in an analogous fashion. The effective Hamiltonian for anti-neutrino in matter is

$$\bar{H} = U^* \begin{bmatrix} 0 & 0 & 0 \\ 0 & \delta m^2_{21} & 0 \\ 0 & 0 & \delta m^2_{31} \end{bmatrix} U^{\rm T} + \begin{bmatrix} -a & 0 & 0 \\ 0 & 0 & 0 \\ 0 & 0 & 0 \end{bmatrix} \ . \tag{2.6.1}$$

Following the general procedure we employed for the neutrinos, we begin by separating out the CP violating phase δ:

$$\begin{aligned}
\bar{H} &= U^* \left(\begin{bmatrix} 0 & 0 & 0 \\ 0 & \delta m^2_{21} & 0 \\ 0 & 0 & \delta m^2_{31} \end{bmatrix} + U^{\mathrm{T}} \begin{bmatrix} -a & 0 & 0 \\ 0 & 0 & 0 \\ 0 & 0 & 0 \end{bmatrix} U^* \right) U^{\mathrm{T}} \\
&= U^*\mathcal{Q}^* \left(\mathcal{Q} \begin{bmatrix} 0 & 0 & 0 \\ 0 & \delta m^2_{21} & 0 \\ 0 & 0 & \delta m^2_{31} \end{bmatrix} \mathcal{Q}^* + \mathcal{Q}U^{\mathrm{T}} \begin{bmatrix} -a & 0 & 0 \\ 0 & 0 & 0 \\ 0 & 0 & 0 \end{bmatrix} U^*\mathcal{Q}^* \right) \mathcal{Q}U^{\mathrm{T}} \\
&= U^*\mathcal{Q}^* \left(\begin{bmatrix} 0 & 0 & 0 \\ 0 & \delta m^2_{21} & 0 \\ 0 & 0 & \delta m^2_{31} \end{bmatrix} + a\mathcal{Q} \begin{bmatrix} U^*_{e1}U_{e1} & U^*_{e1}U_{e2} & U^*_{e1}U_{e3} \\ U^*_{e2}U_{e1} & U^*_{e2}U_{e2} & U^*_{e2}U_{e3} \\ U^*_{e3}U_{e1} & U^*_{e3}U_{e2} & U^*_{e3}U_{e3} \end{bmatrix} \mathcal{Q}^* \right) \mathcal{Q}U^{\mathrm{T}} \\
&= U^*\mathcal{Q}^* \left(\begin{bmatrix} 0 & 0 & 0 \\ 0 & \delta m^2_{21} & 0 \\ 0 & 0 & \delta m^2_{31} \end{bmatrix} - a \begin{bmatrix} c^2_{12}c^2_{13} & c_{12}s_{12}c^2_{13} & c_{12}c_{13}s_{13} \\ c_{12}s_{12}c^2_{13} & s^2_{12}c^2_{13} & s_{12}c_{13}s_{13} \\ c_{12}c_{13}s_{13} & s_{12}c_{13}s_{13} & s^2_{13} \end{bmatrix} \right) \mathcal{Q}U^{\mathrm{T}} \\
&= U^*\mathcal{Q}^* \begin{bmatrix} ac^2_{12}c^2_{13} & ac_{12}s_{12}c^2_{13} & ac_{12}c_{13}s_{13} \\ ac_{12}s_{12}c^2_{13} & as^2_{12}c^2_{13} + \delta m^2_{21} & as_{12}c_{13}s_{13} \\ ac_{12}c_{13}s_{13} & as_{12}c_{13}s_{13} & as^2_{13} + \delta m^2_{31} \end{bmatrix} \mathcal{Q}U^{\mathrm{T}} \\
&= U^*\mathcal{Q}^*\bar{H}'\mathcal{Q}U^{\mathrm{T}}, \qquad (2.6.2)
\end{aligned}$$

where

$$\bar{H}' = \begin{bmatrix} ac^2_{12}c^2_{13} & ac_{12}s_{12}c^2_{13} & ac_{12}c_{13}s_{13} \\ ac_{12}s_{12}c^2_{13} & as^2_{12}c^2_{13} + \delta m^2_{21} & as_{12}c_{13}s_{13} \\ ac_{12}c_{13}s_{13} & as_{12}c_{13}s_{13} & as^2_{13} + \delta m^2_{31} \end{bmatrix} . \qquad (2.6.3)$$

This matrix is diagonalized by some matrix $\bar{R}$:

$$\bar{H}' = \bar{R}^* \begin{bmatrix} \bar{\lambda}_1 & 0 & 0 \\ 0 & \bar{\lambda}_2 & 0 \\ 0 & 0 & \bar{\lambda}_3 \end{bmatrix} \bar{R}^{\mathrm{T}} , \qquad (2.6.4)$$

so that

$$\begin{aligned}
\bar{H} &= U^*\mathcal{Q}^*\bar{R}^* \begin{bmatrix} \bar{\lambda}_1 & 0 & 0 \\ 0 & \bar{\lambda}_2 & 0 \\ 0 & 0 & \bar{\lambda}_3 \end{bmatrix} \bar{R}^{\mathrm{T}}\mathcal{Q}^{\mathrm{T}}U^{\mathrm{T}} \\
&= \tilde{U}^{\mathrm{T}} \begin{bmatrix} \bar{\lambda}_1 & 0 & 0 \\ 0 & \bar{\lambda}_2 & 0 \\ 0 & 0 & \bar{\lambda}_3 \end{bmatrix} \tilde{U}^* , \qquad (2.6.5)
\end{aligned}$$

where

$$\tilde{U} = \begin{bmatrix} 1 & 0 & 0 \\ 0 & \tilde{c}_{23} & \tilde{s}_{23} \\ 0 & -\tilde{s}_{23} & \tilde{c}_{23} \end{bmatrix} \begin{bmatrix} \tilde{c}_{13} & 0 & \tilde{s}_{13}e^{-i\tilde{\delta}} \\ 0 & 1 & 0 \\ -\tilde{s}_{13}e^{i\tilde{\delta}} & 0 & \tilde{c}_{13} \end{bmatrix} \begin{bmatrix} \tilde{c}_{12} & \tilde{s}_{12} & 0 \\ -\tilde{s}_{12} & \tilde{c}_{12} & 0 \\ 0 & 0 & 1 \end{bmatrix}$$

$$= \begin{bmatrix} \overset{\frown}{c}_{12}\overset{\frown}{c}_{13} & \overset{\frown}{s}_{12}\overset{\frown}{c}_{13} & \overset{\frown}{s}_{13}e^{-i\overset{\frown}{\delta}} \\ -\overset{\frown}{s}_{12}\overset{\frown}{c}_{23} - \overset{\frown}{c}_{12}\overset{\frown}{s}_{13}\overset{\frown}{s}_{23}e^{i\overset{\frown}{\delta}} & \overset{\frown}{c}_{12}\overset{\frown}{c}_{23} - \overset{\frown}{s}_{12}\overset{\frown}{s}_{13}\overset{\frown}{s}_{23}e^{i\overset{\frown}{\delta}} & \overset{\frown}{c}_{13}\overset{\frown}{s}_{23} \\ \overset{\frown}{s}_{12}\overset{\frown}{s}_{23} - \overset{\frown}{c}_{12}\overset{\frown}{s}_{13}\overset{\frown}{c}_{23}e^{i\overset{\frown}{\delta}} & -\overset{\frown}{c}_{12}\overset{\frown}{s}_{23} - \overset{\frown}{s}_{12}\overset{\frown}{s}_{13}\overset{\frown}{c}_{23}e^{i\overset{\frown}{\delta}} & \overset{\frown}{c}_{13}\overset{\frown}{c}_{23} \end{bmatrix} . \tag{2.6.6}$$

Next, by using the Jacobi method, we found that the $\bar{H}'$ can be approximately diagonalized by a 1-2 rotation followed by a 1-3 rotation:

$$\begin{aligned} \bar{W}^{\rm T}\bar{V}^{\rm T}\bar{H}'\bar{V}\bar{W} &= \bar{W}^{\rm T}\bar{V}^{\rm T}\mathcal{Q}U^{\rm T}\bar{H}U^*\mathcal{Q}^*\bar{V}\bar{W} \\ &\equiv \bar{U}'^{\rm T}\bar{H}\bar{U}'^* , \end{aligned} \tag{2.6.7}$$

where

$$\begin{aligned} &\bar{U}' \\ &= U\bar{V}Q\,\bar{W} \\ &= \begin{bmatrix} 1 & 0 & 0 \\ 0 & c_{23} & s_{23} \\ 0 & -s_{23} & c_{23} \end{bmatrix} \begin{bmatrix} c_{13} & 0 & s_{13}e^{-i\delta} \\ 0 & 1 & 0 \\ -s_{13}e^{i\delta} & 0 & c_{13} \end{bmatrix} \begin{bmatrix} c_{12} & s_{12} & 0 \\ -s_{12} & c_{12} & 0 \\ 0 & 0 & 1 \end{bmatrix} \begin{bmatrix} \bar{c}_\varphi & \bar{s}_\varphi & 0 \\ -\bar{s}_\varphi & \bar{c}_\varphi & 0 \\ 0 & 0 & 1 \end{bmatrix} Q\,\bar{W} \\ &= \begin{bmatrix} 1 & 0 & 0 \\ 0 & c_{23} & s_{23} \\ 0 & -s_{23} & c_{23} \end{bmatrix} \begin{bmatrix} c_{13} & 0 & s_{13}e^{-i\delta} \\ 0 & 1 & 0 \\ -s_{13}e^{i\delta} & 0 & c_{13} \end{bmatrix} \begin{bmatrix} \bar{c}'_{12} & \bar{s}'_{12} & 0 \\ -\bar{s}'_{12} & \bar{c}'_{12} & 0 \\ 0 & 0 & 1 \end{bmatrix} \begin{bmatrix} 1 & 0 & 0 \\ 0 & 1 & 0 \\ 0 & 0 & e^{i\delta} \end{bmatrix} \begin{bmatrix} \bar{c}_\phi & 0 & \bar{s}_\phi \\ 0 & 1 & 0 \\ -\bar{s}_\phi & 0 & \bar{c}_\phi \end{bmatrix} \\ &= \begin{bmatrix} c_{13}\bar{c}'_{12}\bar{c}_\phi - s_{13}\bar{s}_\phi & c_{13}\bar{s}'_{12} & s_{13}\bar{c}_\phi + c_{13}\bar{c}'_{12}\bar{s}_\phi \\ -c_{23}\bar{s}'_{12}\bar{c}_\phi - s_{23}(c_{13}\bar{s}_\phi + s_{13}\bar{c}'_{12}\bar{c}_\phi)e^{i\delta} & c_{23}\bar{c}'_{12} - s_{23}s_{13}\bar{s}'_{12}e^{i\delta} & -c_{23}\bar{s}'_{12}\bar{s}_\phi + s_{23}(c_{13}\bar{c}_\phi - s_{13}\bar{c}'_{12}\bar{s}_\phi)e^{i\delta} \\ s_{23}\bar{s}'_{12}\bar{c}_\phi - c_{23}(c_{13}\bar{s}_\phi + s_{13}\bar{c}'_{12}\bar{c}_\phi)e^{i\delta} & -s_{23}\bar{c}'_{12} - c_{23}s_{13}\bar{s}'_{12}e^{i\delta} & s_{23}\bar{s}'_{12}\bar{s}_\phi + c_{23}(c_{13}\bar{c}_\phi - s_{13}\bar{c}'_{12}\bar{s}_\phi)e^{i\delta} \end{bmatrix} \end{aligned} \tag{2.6.8}$$

Identification of this matrix with $\overset{\frown}{U}$ in eq. (2.6.6) (up to phases that can be absorbed into redefinitions of the charged lepton fields and the Majorana phases of the neutrinos) yields

$$\begin{aligned} \overset{\frown}{\theta}_{13} &\approx \bar{\theta}'_{13} , \\ \tan\overset{\frown}{\theta}_{12} &\approx \frac{c_{13}}{\bar{c}'_{13}}\tan\bar{\theta}'_{12} , \\ \overset{\frown}{\theta}_{23} &\approx \theta_{23} - \left(\frac{\bar{s}'_{12}\bar{s}_\phi}{\bar{c}'_{13}}\right)\cos\delta , \\ \sin(2\overset{\frown}{\theta}_{23})\sin\overset{\frown}{\delta} &\approx \sin(2\theta_{23})\sin\delta , \end{aligned} \tag{2.6.9}$$

where

$$\bar{s}'_{13} = \sin\bar{\theta}'_{13} , \qquad \bar{c}'_{13} = \cos\bar{\theta}'_{13} , \qquad \bar{\theta}'_{13} \equiv \theta_{13} + \bar{\phi} . \tag{2.6.10}$$

Since the angle $\bar{\phi}$ is small we can simply the above relations to the above relations simplify to

$$\begin{aligned} \overset{\frown}{\theta}_{13} &\approx \bar{\theta}'_{13} = \theta_{13} + \bar{\phi} , \\ \overset{\frown}{\theta}_{12} &\approx \bar{\theta}'_{12} = \theta_{12} + \bar{\varphi} , \\ \overset{\frown}{\theta}_{23} &\approx \theta_{23} , \\ \overset{\frown}{\delta} &\approx \delta . \end{aligned} \tag{2.6.11}$$

2.7 Anti-Neutrino: Inverted Hierarchy

In the case of inverted hierarchy, we followed the same procedure as the case of normal hierarchy. When $a/|\delta m^2_{31}| \leq O(\epsilon)|$, the angle $\bar{\phi}$ is again small and we can simplify the effective mixing angles to

$$\begin{aligned} \overset{\frown}{\theta}_{13} &\approx \bar{\theta}'_{13} = \theta_{13} + \bar{\phi} \,, \\ \overset{\frown}{\theta}_{12} &\approx \bar{\theta}'_{12} = \theta_{12} + \bar{\varphi} \,, \\ \overset{\frown}{\theta}_{23} &\approx \theta_{23} \,, \\ \overset{\frown}{\delta} &\approx \delta \,. \end{aligned} \tag{2.7.1}$$

When $a/|\delta m^2_{31}| \leq O(1)$, we can approximate

$$\begin{aligned} \overset{\frown}{\theta}_{13} &\approx \bar{\theta}'_{13} \,, \\ \overset{\frown}{\theta}_{12} &\approx \frac{c_{13}}{\bar{c}'_{13}} \left(\frac{\delta m^2_{21}}{2a} \right) \sin(2\theta_{12}) \,, \\ \overset{\frown}{\theta}_{23} &\approx \theta_{23} - \frac{\bar{s}_\phi}{\bar{c}'_{13}} \left(\frac{\delta m^2_{21}}{2a} \right) \sin(2\theta_{12}) \cos\delta \,, \\ \overset{\frown}{\delta} &\approx \delta + \frac{\bar{s}_\phi}{\bar{c}'_{13}} \left(\frac{\delta m^2_{21}}{a} \right) \frac{\sin(2\theta_{12})}{\tan(2\theta_{23})} \sin\delta \,. \end{aligned} \tag{2.7.2}$$

2.8 Sample Calculation of Oscillation Probabilities

	L (km)	ρ (g/cm^3)	E (GeV)	$\alpha = \log_{1/\varepsilon}(a/\lvert\delta m^2_{31}\rvert)$	$\lvert\Delta_{31}\rvert$	Reference
T2K (JPARC → Super-K)	295	2.6	$0.25 \sim 2$	$-2.3 \sim -1.1$	$(0.3 \sim 2.4)\pi$	[10]
JPARC → Korea	1000	2.7	$1 \sim 6$	$-1.5 \sim -0.4$	$(0.3 \sim 2.0)\pi$	[15, 16]
BNL → Home Stake	2540	3.4	$2 \sim 10$	$-0.9 \sim 0$	$(0.5 \sim 2.6)\pi$	[11]

Table 2.2: The three cases for which we calculate the probabilities for the processes $\nu_\mu \to \nu_\mu$ and $\nu_\mu \to \nu_e$. The ranges of α and $|\Delta_{31}|$ were calculated assuming $\delta m^2_{21} = 8.2 \times 10^{-5}\,\text{eV}^2$ and $|\delta m^2_{31}| = 2.5 \times 10^{-3}\,\text{eV}^2$. ρ is the average matter density along the baseline calculated using the Preliminary Earth Reference Model (PREM) [26].

The accuracy of our approximation in calculating the effective mixing angles and effective mass-squared differences translates directly into the accuracy in calculating the oscillation probabilities. To illustrate this, we calculate the probabilities for the processes $\nu_\mu \to \nu_\mu$ and $\nu_\mu \to \nu_e$ for the three cases listed in Table 2.2. The energy ranges listed include the energies at which $|\Delta_{31}| = \pi$, around where the first oscillation peak occurs. The ranges of the matter effect parameter $\alpha = \log_{1/\varepsilon}(a/|\delta m^2_{31}|)$ for the three cases are roughly $-2 \sim -1$, $-1.5 \sim -0.5$, and $-1 \sim 0$, so together they cover the range $-2 \sim 0$.

Since $\alpha < 0$ for all three cases, the effective mixing angles are well approximated by Eq. (2.5.29). For the effective mass-squared differences, we use Eq. (2.5.40) which is applicable to $\alpha \lesssim -1$ for the $L = 295\,\text{km}$ case, and Eq. (2.5.41) which is applicable to $\alpha \gtrsim -1$ for the $L = 2540\,\text{km}$ case.

The $L = 1000\,\text{km}$ case is a bit problematic since neither Eq. (2.5.40) nor (2.5.41) can be used throughout the entire range $\alpha = -1.5 \sim -0.5$, Eq. (2.5.40) being applicable only to the low

energy end, and Eq. (2.5.41) being applicable only to the high energy end. Using Eqs. (2.5.36) and (2.5.37), with Eqs. (**??**) and (**??**), which are applicable to all energies, would solve our problem and lead to approximate oscillation probabilities that are virtually indistinguishable from their exact values. However, we would like to illustrate the power (and limitations) of our much simpler expressions in Eqs. (2.5.40) and (2.5.41). Here, we will use Eq. (2.5.40) since the first oscillation peak occurs towards the lower end of the energy range.

In Figs. 2.8.1 through 2.8.6, we plot the approximate versus the exact oscillation probabilities for both the $\delta m^2_{31} > 0$ (normal hierarchy) and $\delta m^2_{31} < 0$ (inverted hierarchy) cases. The vacuum parameters were set to the values listed in Eq. (2.5.34) except for the CP violating phase. For $\nu_\mu \to \nu_e$, the four cases $\delta = 0$, $\frac{\pi}{2}$, π, and $\frac{3\pi}{2}$ were plotted. For $\nu_\mu \to \nu_\mu$, which depends only very weakly on δ, only the $\delta = 0$ case is shown.

The $L = 295\,\text{km}$ case is shown in Figs. 2.8.1 and 2.8.2. As is clear from the figures, our approximate values are completely indistinguishable from the exact values, the difference being less than a fraction of a percent throughout the energy range considered. For the $L = 1000\,\text{km}$ case shown in Figs. 2.8.3 and 2.8.4, deviations can be seen toward the high energy end as expected, but the difference is still well under control. For the $L = 2540\,\text{km}$ case shown in Figs. 2.8.5 and 2.8.6, the difference between the exact and approximate values is again less that a percent in the range $E = 2 \sim 10\,\text{GeV}$ where the approximation is applicable, but becomes large below $E = 2\,\text{GeV}$.

2.9 Qualitative Analysis

Let us now use our approximation to see whether we can understand various qualitative features of the oscillation probabilities we plotted.

Since the three cases we considered in the previous section cover the range $\alpha = -2 \sim 0$, let us take the midpoint $\alpha \sim -1$ and further simplify our expressions to those applicable there. The approximations for the effective mixing angles for the neutrinos can be obtained from Eqs. (**??**), (**??**), and (2.5.29):

$$\begin{aligned}
\tilde{\theta}_{12} &\approx \frac{\pi}{2} - \frac{\delta m^2_{21}}{2a}\sin(2\theta_{12})\,, \\
\tilde{\theta}_{13} &\approx \frac{\theta_{13}}{\left(1 - \dfrac{a}{\delta m^2_{31}}\right)}, \\
\tilde{\theta}_{23} &\approx \theta_{23}\,, \\
\tilde{\delta} &\approx \delta\,.
\end{aligned} \tag{2.9.1}$$

In Fig. 2.9.1 we plot these approximations against the exact values. Though the approximation for θ_{13} breaks down for the normal hierarchy case as $\alpha \to 0$, these expressions nevertheless capture the essential behavior of the effective mixing angles throughout the range $-2 < \alpha < 0$. They and are also numerically accurate for most of this range. In fact, for the inverted hierarchy case, the approximations of $\tilde{\theta}_{13}$, $\tilde{\theta}_{23}$ and $\tilde{\delta}$ are valid for all α. From Eq. (**??**), the approximations for the effective mass-squared differences are

$$\lambda_1 \approx \delta m^2_{21}\, c^2_{12}\,,$$

$$\begin{aligned} \lambda_2 &\approx a + \delta m^2_{21}\, s^2_{12}\ , \\ \lambda_3 &\approx \delta m^2_{31}\ . \end{aligned} \tag{2.9.2}$$

These expressions are compared against the exact values in Fig. 2.9.2, and we can again conclude that they are fairly accurate for most of the range $-2 < \alpha < 0$, except very near the endpoints.

For the anti-neutrinos, the effective mixing angles when $\alpha \sim -1$ are approximated by

$$\begin{aligned} \breve{\theta}_{12} &\approx \frac{\delta m^2_{21}}{2a} \sin(2\theta_{12})\ , \\ \breve{\theta}_{13} &\approx \frac{\theta_{13}}{\left(1 + \dfrac{a}{\delta m^2_{31}}\right)}\ , \\ \breve{\theta}_{23} &\approx \theta_{23}\ , \\ \breve{\delta} &\approx \delta\ . \end{aligned} \tag{2.9.3}$$

The accuracy of these expressions is shown in Fig. 2.9.3. In contrast to the neutrino case, the approximations for $\breve{\theta}_{13}$, $\breve{\theta}_{23}$ and $\breve{\delta}$ are applicable to all a for the normal hierarchy case, and the approximation for $\breve{\theta}_{13}$ breaks down as $\alpha \to 0$ for the inverted hierarchy case. The approximations for the effective mass-squared differences are given by

$$\begin{aligned} \bar{\lambda}_1 &\approx -a + \delta m^2_{21}\, s^2_{12}\ , \\ \bar{\lambda}_2 &\approx \delta m^2_{21}\, c^2_{12}\ , \\ \bar{\lambda}_3 &\approx \delta m^2_{31}\ , \end{aligned} \tag{2.9.4}$$

with the accuracy shown in Fig. (2.9.4). As in the neutrino case, we can conclude that these approximations capture the essential behavior of the effective mixing angles and mass squared differences throughout the range $-2 < \alpha < 0$, and are also numerically accurate except near the endpoints.

Let us now apply these approximations to the oscillation probabilities $P(\nu_\mu \to \nu_\mu)$ and $P(\nu_\mu \to \nu_e)$ in matter, and their anti-neutrino counterparts. First, recall from Eqs. (2.2.23) and (2.2.24) that these probabilities in vacuum are given by

$$\begin{aligned} P(\nu_\mu \to \nu_\mu) &= 1 - \sin^2(2\theta_{\rm atm}) \sin^2\left(\frac{\Delta_{31} - \kappa_{\mu\mu}\Delta_{21}}{2}\right) + O(\Delta^2_{21})\ , \\ P(\nu_\mu \to \nu_e) &= 4 \sin^2\theta_{13}\, \sin^2\theta_{\rm atm} \big\{1 - (B \sin\delta)\, \Delta_{21}\big\} \sin^2\left(\frac{\Delta_{31} - \kappa_{\mu e}\Delta_{21}}{2}\right) + O(\Delta^2_{21})\ , \end{aligned} \tag{2.9.5}$$

where

$$\begin{aligned} \sin\theta_{\rm atm} &= s_{23} c_{13}\ , \\ A &= \frac{1}{8} \sin(2\theta_{12}) \sin(2\theta_{13}) \sin(2\theta_{\rm atm}) \sqrt{1 - \tan^2\theta_{13} \tan^2\theta_{\rm atm}} \\ &= \frac{1}{8} \times O(1) \times 2O(\varepsilon) \times O(1) \times \sqrt{1 - O(\varepsilon^2)} \\ &= \frac{1}{4} O(\varepsilon)\ , \end{aligned}$$

$$\begin{aligned} B &\equiv \frac{A}{\sin^2\theta_{13}\sin^2\theta_{\rm atm}} = \frac{1}{2}\,O(\varepsilon^{-1})\,, \\ \kappa_{\mu\mu} &= c_{12}^2 - \cos(2\theta_{12})\tan^2\theta_{13}\tan^2\theta_{\rm atm} - \left(\frac{2A}{\cos^2\theta_{13}\cos^2\theta_{\rm atm}}\right)\cos\delta \\ &= \frac{1}{2}\,O(1) - 2O(\varepsilon^3) - O(\varepsilon)\cos\delta \\ &= \frac{1}{2}\,O(1) - O(\varepsilon)\cos\delta\,, \\ \kappa_{\mu e} &= s_{12}^2 - B\cos\delta \\ &= \frac{1}{2}\,O(1) - \frac{1}{2}\,O(\varepsilon^{-1})\cos\delta\,. \end{aligned} \tag{2.9.6}$$

The oscillation probabilities for the anti-neutrinos are obtained by flipping the sign of $\sin\delta$.

Note that the first oscillation peak occurs at a distance/energy of $|\Delta_{31}| \approx \pi$. Since $\Delta_{21}/|\Delta_{31}| = \delta m_{21}^2/|\delta m_{31}^2| = \varepsilon^2$, the $O(\Delta_{21}^2)$ terms in Eq. (2.9.5) are of $O(\pi^2\varepsilon^4)$ which justifies our dropping them at those distance/energies. Note also that the coefficient of $\cos\delta$ in $\kappa_{\mu e}$ is $B = \frac{1}{2}O(\varepsilon^{-1})$, which when multiplied by Δ_{21} is of $O(\varepsilon)$. The exact same product of parameters, $B\Delta_{21} = O(\varepsilon)$, appears in the coefficient of $\sin\delta$ in the oscillation envelope of $P(\nu_\mu \to \nu_e)$. Therefore, a measurement of $P(\nu_\mu \to \nu_e)$ can, in principle, constrain $\cos\delta$ from the position of the peak, and $\sin\delta$ from the height of the peak, provided it is accurate enough to discern these $O(\varepsilon)$ corrections. In contrast, the coefficient of $\cos\delta$ in $\kappa_{\mu\mu}$ is $O(\varepsilon)$, rendering the $\cos\delta$ term in $\kappa_{\mu\mu}\Delta_{21}$ negligible, and we conclude that $P(\nu_\mu \to \nu_\mu)$ is insensitive to δ.

Of course, actual long-baseline experiments can only measure oscillation probabilities in matter. The effective Δ_{31}'s in matter for the neutrinos and anti-neutrinos are

$$\begin{aligned} \tilde{\Delta}_{31} &\approx \left(\Delta_{31} - \Delta_{21}c_{12}^2\right)\,, \\ \breve{\Delta}_{31} &\approx \left(\Delta_{31} + \frac{a}{2E}L - \Delta_{21}s_{12}^2\right)\,, \end{aligned} \tag{2.9.7}$$

respectively, so they are both the same order as Δ_{31}. The effective Δ_{21}'s, on the other hand, are

$$\begin{aligned} \tilde{\Delta}_{21} &\approx \left(\frac{a}{2E}L - \Delta_{21}\cos 2\theta_{12}\right) \approx \frac{a}{2E}L = (\sqrt{2}G_F N_e)L\,, \\ \breve{\Delta}_{21} &\approx \left(\frac{a}{2E}L + \Delta_{21}\cos 2\theta_{12}\right) \approx \frac{a}{2E}L = (\sqrt{2}G_F N_e)L\,, \end{aligned} \tag{2.9.8}$$

so they are enhanced by a factor of $a/\delta m_{21}^2$ relative to Δ_{21}. Therefore, at the first oscillation peak where $|\Delta_{31}| \approx \pi$, we can expect $\tilde{\Delta}_{21}$ and $\breve{\Delta}_{21}$ to be of order $\pi a/|\delta m_{31}^2|$.

Note that the value of $\tilde{\Delta}_{21} \approx \breve{\Delta}_{21} \approx (\sqrt{2}G_F N_e)L$ does not depend on the energy E. It is determined solely by the baseline length L, once the matter density ρ is fixed. ($N_e = N_A\rho/2$ where N_A is the Avogadro number.) For the three examples we considered in the previous section, we find

$$(\sqrt{2}G_F N_e)L = \begin{cases} 0.15 & (\rho = 2.6\,{\rm g/cm^3}\,, L = 295\,{\rm km})\,, \\ 0.5 & (\rho = 2.7\,{\rm g/cm^3}\,, L = 1000\,{\rm km})\,, \\ 1.7 & (\rho = 3.4\,{\rm g/cm^3}\,, L = 2540\,{\rm km})\,. \end{cases} \tag{2.9.9}$$

Since we would like to use the analog of Eq. (2.9.5) to analyze the oscillation probabilities in matter, we would like maintain the condition

$$\tilde{\Delta}_{21},\ \breve{\Delta}_{21} < 1\,, \tag{2.9.10}$$

so that an expansion in $\tilde{\Delta}_{21}$ or $\overset{\smile}{\Delta}_{21}$ is justified. The $L = 2540\,\mathrm{km}$ case is clearly problematic and must be treated separately. We will therefore first restrict our attention to the cases in which the $|\Delta_{31}| = \pi$ condition occurs in the region $-2 < \alpha \lesssim -1$, so that $\tilde{\Delta}_{21} \approx \overset{\smile}{\Delta}_{21} \lesssim O(\pi\varepsilon) = 0.47 \sim 0.75$.

Even with this restriction, $\tilde{\Delta}_{21}$ and $\overset{\smile}{\Delta}_{21}$ can still be enhanced considerably when $|\Delta_{31}| = \pi$ occurs at $\alpha \approx -1$. One may naively anticipate that this enhancement will enhance the coefficients of $\sin\delta$ and $\cos\delta$ in $P(\nu_\mu \to \mu_e)$, thereby facilitate the detection of δ. At the same time, it could also enhance the $O(\tilde{\Delta}_{21}^2)$ and $O(\overset{\smile}{\Delta}_{21}^{\,2})$ terms in the oscillation probabilities and invalidate their complete neglect. However, it turns out that these are not the case.

Let us first look at the ν_μ and $\bar{\nu}_\mu$ survival probabilities in matter which are obtained by replacing all the quantities in the vacuum probability with their tilded and anti-tilded counterparts:

$$\begin{aligned}
&\tilde{P}(\nu_\mu \to \nu_\mu) \\
&= 1 - \sin^2(2\tilde{\theta}_{\rm atm}) \sin^2\left(\frac{\tilde{\Delta}_{31} - \tilde{\kappa}_{\mu\mu}\tilde{\Delta}_{21}}{2}\right) \\
&\quad - |\tilde{U}_{\mu 1}|^2 |\tilde{U}_{\mu 2}|^2 \left(1 + \frac{|\tilde{U}_{\mu 3}|^2}{1 - |\tilde{U}_{\mu 3}|^2} \cos\tilde{\Delta}_{31}\right) \tilde{\Delta}_{21}^2 \\
&\quad - |\tilde{U}_{\mu 1}|^2 |\tilde{U}_{\mu 2}|^2 |\tilde{U}_{\mu 3}|^2 \left\{\frac{1 + |\tilde{U}_{\mu 2}|^2 - |\tilde{U}_{\mu 3}|^2}{3(1 - |\tilde{U}_{\mu 3}|^2)^2} \sin\tilde{\Delta}_{31}\right\} \tilde{\Delta}_{21}^3 + O(\tilde{\Delta}_{21}^4)\,, \qquad (2.9.11) \\
&\overset{\smile}{P}(\bar{\nu}_\mu \to \bar{\nu}_\mu) \\
&= 1 - \sin^2(2\overset{\smile}{\theta}_{\rm atm}) \sin^2\left(\frac{\overset{\smile}{\Delta}_{31} - \overset{\smile}{\kappa}_{\mu\mu}\overset{\smile}{\Delta}_{21}}{2}\right) \\
&\quad - |\overset{\smile}{U}_{\mu 1}|^2 |\overset{\smile}{U}_{\mu 2}|^2 \left(1 + \frac{|\overset{\smile}{U}_{\mu 3}|^2}{1 - |\overset{\smile}{U}_{\mu 3}|^2} \cos\overset{\smile}{\Delta}_{31}\right) \overset{\smile}{\Delta}_{21}^{\,2} \\
&\quad - |\overset{\smile}{U}_{\mu 1}|^2 |\overset{\smile}{U}_{\mu 2}|^2 |\overset{\smile}{U}_{\mu 3}|^2 \left\{\frac{1 + |\overset{\smile}{U}_{\mu 2}|^2 - |\overset{\smile}{U}_{\mu 3}|^2}{3(1 - |\overset{\smile}{U}_{\mu 3}|^2)^2} \sin\overset{\smile}{\Delta}_{31}\right\} \overset{\smile}{\Delta}_{21}^{\,3} + O(\overset{\smile}{\Delta}_{21}^{\,4})\,. \qquad (2.9.12)
\end{aligned}$$

We have kept terms up to $\tilde{\Delta}_{21}^3$ and $\overset{\smile}{\Delta}_{21}^{\,3}$ explicitly to evaluate their sizes. Using the approximations of Eqs. (2.9.1) and (2.9.3), the effective MNS matrix elements that appear in these expressions can be evaluated to be

$$\begin{aligned}
|\tilde{U}_{\mu 1}|^2 &= |\tilde{s}_{12}\tilde{c}_{23} + \tilde{c}_{12}\tilde{s}_{13}\tilde{s}_{23}e^{i\tilde{\delta}}|^2 = \frac{1}{2}O(1)\,, \\
|\tilde{U}_{\mu 2}|^2 &= |\tilde{c}_{12}\tilde{c}_{23} - \tilde{s}_{12}\tilde{s}_{13}\tilde{s}_{23}e^{i\tilde{\delta}}|^2 \approx O(\varepsilon^2)\,, \\
|\tilde{U}_{\mu 3}|^2 &= (\tilde{c}_{13}\tilde{s}_{23})^2 = \frac{1}{2}O(1)\,. \qquad (2.9.13)
\end{aligned}$$

for the neutrinos, and

$$\begin{aligned}
|\overset{\smile}{U}_{\mu 1}|^2 &= |\overset{\smile}{s}_{12}\overset{\smile}{c}_{23} + \overset{\smile}{c}_{12}\overset{\smile}{s}_{13}\overset{\smile}{s}_{23}e^{i\overset{\smile}{\delta}}|^2 \approx O(\varepsilon^2)\,, \\
|\overset{\smile}{U}_{\mu 2}|^2 &= |\overset{\smile}{c}_{12}\overset{\smile}{c}_{23} - \overset{\smile}{s}_{12}\overset{\smile}{s}_{13}\overset{\smile}{s}_{23}e^{i\overset{\smile}{\delta}}|^2 = \frac{1}{2}O(1)\,,
\end{aligned}$$

$$|\overset{\frown}{U}_{\mu 3}|^2 \;=\; (\overset{\frown}{c}_{13}\overset{\frown}{s}_{23})^2 \;=\; \frac{1}{2}O(1)\;, \tag{2.9.14}$$

for the anti-neutrinos. This shows that the $\tilde{\Delta}^2_{21}$, $\overset{\frown}{\Delta}{}^2_{21}$ and $\tilde{\Delta}^3_{21}$, $\overset{\frown}{\Delta}{}^3_{21}$ terms are suppressed by $|\tilde{U}_{\mu 2}|^2 = O(\varepsilon^2)$ for the neutrinos, and by $|\overset{\frown}{U}_{\mu 1}|^2 = O(\varepsilon^2)$ for the anti-neutrinos, canceling out the enhancements of $\tilde{\Delta}_{21}$, $\overset{\frown}{\Delta}_{21}$ over Δ_{21}, and reducing these higher order terms to $O(\pi^2\varepsilon^4)$, which is the same order as the $O(\Delta^2_{21})$ terms that were neglected for the vacuum case. The fact that $\cos\tilde{\Delta}_{31} \approx -1$ and $\sin\tilde{\Delta}_{31} \approx 0$ near the first oscillation peak also helps in suppressing these terms. Therefore, to a very good approximation, we can use the expressions

$$\begin{aligned}
\tilde{P}(\nu_\mu \to \nu_\mu) &= 1 - \sin^2(2\tilde{\theta}_{\rm atm})\sin^2\left(\frac{\tilde{\Delta}_{31} - \tilde{\kappa}_{\mu\mu}\tilde{\Delta}_{21}}{2}\right)\;, \\
\overset{\frown}{P}(\bar{\nu}_\mu \to \bar{\nu}_\mu) &= 1 - \sin^2(2\overset{\frown}{\theta}_{\rm atm})\sin^2\left(\frac{\overset{\frown}{\Delta}_{31} - \overset{\frown}{\kappa}_{\mu\mu}\overset{\frown}{\Delta}_{21}}{2}\right)\;.
\end{aligned} \tag{2.9.15}$$

Looking at the remaining parameters in these expressions, we find

$$\begin{aligned}
\sin\tilde{\theta}_{\rm atm} &= \tilde{c}_{13}\tilde{s}_{23} \;=\; c_{13}s_{23}\left[1 + O(\varepsilon^3)\right] \;\approx\; \sin\theta_{\rm atm}\;, \\
\tilde{A} &= \frac{1}{8}\sin(2\tilde{\theta}_{12})\sin(2\tilde{\theta}_{13})\sin(2\tilde{\theta}_{\rm atm})\sqrt{1 - \tan^2\tilde{\theta}_{13}\tan^2\tilde{\theta}_{\rm atm}} \\
&\approx \frac{1}{4}\left(\frac{\delta m^2_{21}}{a}\right)\left(1 + \frac{a}{\delta m^2_{31}}\right)\theta_{13} \\
&= \frac{1}{4}\,O(\varepsilon^2)\;, \\
\tilde{\kappa}_{\mu\mu} &= \tilde{c}^2_{12} - \cos(2\tilde{\theta}_{12})\tan^2\tilde{\theta}_{13}\tan^2\tilde{\theta}_{\rm atm} - \left(\frac{2\tilde{A}}{\cos^2\tilde{\theta}_{13}\cos^2\tilde{\theta}_{\rm atm}}\right)\cos\tilde{\delta} \\
&= O(\varepsilon^2) - O(\varepsilon^2)\cos\delta\;,
\end{aligned} \tag{2.9.16}$$

for the neutrinos, and

$$\begin{aligned}
\sin\overset{\frown}{\theta}_{\rm atm} &= \overset{\frown}{c}_{13}\overset{\frown}{s}_{23} \;=\; c_{13}s_{23}\left[1 + O(\varepsilon^3)\right] \;\approx\; \sin\theta_{\rm atm}\;, \\
\overset{\frown}{A} &\approx \frac{1}{8}\sin(2\overset{\frown}{\theta}_{12})\sin(2\overset{\frown}{\theta}_{13})\sin(2\overset{\frown}{\theta}_{\rm atm})\sqrt{1 - \tan^2\overset{\frown}{\theta}_{13}\tan^2\overset{\frown}{\theta}_{\rm atm}} \\
&\approx \frac{1}{4}\left(\frac{\delta m^2_{21}}{a}\right)\left(1 - \frac{a}{\delta m^2_{31}}\right)\theta_{13} \;=\; \frac{1}{4}\,O(\varepsilon^2)\;, \\
\overset{\frown}{\kappa}_{\mu\mu} &= \cos^2\overset{\frown}{\theta}_{12} - \cos(2\overset{\frown}{\theta}_{12})\tan^2\overset{\frown}{\theta}_{13}\tan^2\overset{\frown}{\theta}_{\rm atm} - \left(\frac{2\overset{\frown}{A}}{\cos^2\overset{\frown}{\theta}_{13}\cos^2\overset{\frown}{\theta}_{\rm atm}}\right)\cos\overset{\frown}{\delta} \\
&= O(1) - O(\varepsilon^2)\cos\delta\;,
\end{aligned} \tag{2.9.17}$$

for the anti-neutrinos. (Recall that $\sin(2\theta_{12}) = 1 - 2O(\varepsilon^2)$ and $\sin(2\theta_{\rm atm}) = 1 - \frac{1}{2}O(\varepsilon^2)$.) This shows that the coefficient of $\cos\delta$ in $\tilde{\kappa}_{\mu\mu}$ ($\overset{\frown}{\kappa}_{\mu\mu}$) is suppressed by one power of ε relative to $\kappa_{\mu\mu}$. Consequently, the ν_μ and $\bar{\nu}_\mu$ survival probabilities remain insensitive to the CP violating phase δ, despite the enhancements of $\tilde{\Delta}_{21}$, $\overset{\frown}{\Delta}_{21}$ over Δ_{21}. Looking at the arguments of the sines more

carefully, we find

$$\begin{aligned}
\Delta_{31} - \kappa_{\mu\mu}\Delta_{21} &= \left(\Delta_{31} - c_{12}^2\Delta_{21}\right) + O(\varepsilon^3\Delta_{31}) \,, \\
\tilde{\Delta}_{31} - \tilde{\kappa}_{\mu\mu}\tilde{\Delta}_{21} &\approx \left(\Delta_{31} - c_{12}^2\Delta_{21}\right) - \tilde{c}_{12}^2\left(\frac{a}{2E}L - \Delta_{21}\cos 2\theta_{12}\right) \\
&= \left(\Delta_{31} - c_{12}^2\Delta_{21}\right) + O(\varepsilon^3\Delta_{31}) \,, \\
\overset{\smile}{\Delta}_{31} - \overset{\smile}{\kappa}_{\mu\mu}\overset{\smile}{\Delta}_{21} &\approx \left(\Delta_{31} + \frac{a}{2E}L - \Delta_{21}s_{12}^2\right) - \overset{\smile}{c}_{12}^2\left(\frac{a}{2E}L + \Delta_{21}\cos 2\theta_{12}\right) \\
&= \left(\Delta_{31} + \frac{a}{2E}L - \Delta_{21}s_{12}^2\right) - \left(\frac{a}{2E}L + \Delta_{21}\cos 2\theta_{12}\right) + O(\varepsilon^3\Delta_{31}) \\
&= \left(\Delta_{31} - c_{12}^2\Delta_{21}\right) + O(\varepsilon^3\Delta_{31}) \,. \qquad (2.9.18)
\end{aligned}$$

Since $\sin(2\theta_{\rm atm}) \approx \sin(2\tilde{\theta}_{\rm atm}) \approx \sin(2\overset{\smile}{\theta}_{\rm atm})$, we conclude

$$\tilde{P}(\nu_\mu \to \nu_\mu) \approx P(\nu_\mu \to \nu_\mu) = P(\bar{\nu}_\mu \to \bar{\nu}_\mu) \approx \overset{\smile}{P}(\bar{\nu}_\mu \to \bar{\nu}_\mu) \,. \qquad (2.9.19)$$

That is, the ν_μ and $\bar{\nu}_\mu$ survival probabilities are insensitive to matter effects and their values in matter are the same as their values in vacuum. In Fig. 2.9.5 we compare the exact numerical values of these probabilities calculated for our example parameter set Eq. (2.5.34) with $\delta m_{31}^2 > 0$. As can be seen, the differences among these probabilities are extremely small, and our approximation has allowed us to understand this analytically.

Next, let us consider the $\nu_\mu \to \nu_e$ and $\bar{\nu}_\mu \to \bar{\nu}_e$ oscillation probabilities. They are

$$\begin{aligned}
&\tilde{P}(\nu_\mu \to \nu_e) \\
&= 4\sin^2\tilde{\theta}_{13}\sin^2\tilde{\theta}_{\rm atm}\left[\left\{1 - (\tilde{B}\sin\tilde{\delta})\tilde{\Delta}_{21}\right\}\sin^2\left(\frac{\tilde{\Delta}_{31} - \tilde{\kappa}_{\mu e}\tilde{\Delta}_{21}}{2}\right)\right. \\
&\quad + \frac{1}{4}\left\{(\tilde{B}\sin\tilde{\delta})^2 - 2\tilde{\kappa}_{\mu e}(1-\tilde{\kappa}_{\mu e})\sin^2\frac{\tilde{\Delta}_{31}}{2} - (\tilde{B}\sin\tilde{\delta})(1-2\tilde{\kappa}_{\mu e})\sin\tilde{\Delta}_{31}\right\}\tilde{\Delta}_{21}^2 \\
&\quad - \frac{1}{12}\left\{3(\tilde{B}\sin\tilde{\delta})\tilde{\kappa}_{\mu e}^2 + 2(\tilde{B}\sin\tilde{\delta})(1-3\tilde{\kappa}_{\mu e}^2)\sin^2\frac{\tilde{\Delta}_{31}}{2} - \tilde{\kappa}_{\mu e}(1-\tilde{\kappa}_{\mu e}^2)\sin\tilde{\Delta}_{31}\right\}\tilde{\Delta}_{21}^3 \\
&\quad \left. + O(\tilde{\Delta}_{21}^4)\right] \,, \qquad (2.9.20)
\end{aligned}$$

$$\begin{aligned}
&\overset{\smile}{P}(\bar{\nu}_\mu \to \bar{\nu}_e) \\
&= 4\sin^2\overset{\smile}{\theta}_{13}\sin^2\overset{\smile}{\theta}_{\rm atm}\left[\left\{1 + (\overset{\smile}{B}\sin\overset{\smile}{\delta})\overset{\smile}{\Delta}_{21}\right\}\sin^2\left(\frac{\overset{\smile}{\Delta}_{31} - \overset{\smile}{\kappa}_{\mu e}\overset{\smile}{\Delta}_{21}}{2}\right)\right. \\
&\quad + \frac{1}{4}\left\{(\overset{\smile}{B}\sin\overset{\smile}{\delta})^2 - 2\overset{\smile}{\kappa}_{\mu e}(1-\overset{\smile}{\kappa}_{\mu e})\sin^2\frac{\overset{\smile}{\Delta}_{31}}{2} + (\overset{\smile}{B}\sin\overset{\smile}{\delta})(1-2\overset{\smile}{\kappa}_{\mu e})\sin\overset{\smile}{\Delta}_{31}\right\}\overset{\smile}{\Delta}_{21}^2 \\
&\quad + \frac{1}{12}\left\{3(\overset{\smile}{B}\sin\overset{\smile}{\delta})\overset{\smile}{\kappa}_{\mu e}^2 + 2(\overset{\smile}{B}\sin\overset{\smile}{\delta})(1-3\overset{\smile}{\kappa}_{\mu e}^2)\sin^2\frac{\overset{\smile}{\Delta}_{31}}{2} + \overset{\smile}{\kappa}_{\mu e}(1-\overset{\smile}{\kappa}_{\mu e}^2)\sin\overset{\smile}{\Delta}_{31}\right\}\overset{\smile}{\Delta}_{21}^3 \\
&\quad \left. + O(\overset{\smile}{\Delta}_{21}^4)\right] \,, \qquad (2.9.21)
\end{aligned}$$

From Eq. (2.9.16) we obtain

$$\begin{aligned}\tilde{B} &= \frac{\tilde{A}}{\sin^2\tilde{\theta}_{13}\sin^2\tilde{\theta}_{atm}} \approx \frac{1}{2}\left(\frac{\delta m^2_{21}}{a}\right)\left(1-\frac{a}{\delta m^2_{31}}\right)\frac{1}{\theta_{13}} = \frac{1}{2}O(1)\,,\\ \tilde{\kappa}_{\mu e} &= \tilde{s}^2_{12}-\tilde{B}\cos\tilde{\delta} \approx 1-\frac{1}{2}O(1)\cos\delta\,,\end{aligned}$$

and from Eq. (2.9.17) we obtain

$$\begin{aligned}\breve{B} &= \frac{\breve{A}}{\sin^2\breve{\theta}_{13}\sin^2\breve{\theta}_{atm}} \approx \frac{1}{2}\left(\frac{\delta m^2_{21}}{a}\right)\left(1+\frac{a}{\delta m^2_{31}}\right)\frac{1}{\theta_{13}} = \frac{1}{2}O(1)\,,\\ \breve{\kappa}_{\mu e} &= \breve{s}^2_{12}-\breve{B}\cos\breve{\delta} = \frac{1}{4}O(\varepsilon^2)-\frac{1}{2}O(1)\cos\delta \approx -\frac{1}{2}O(1)\cos\delta\,.\end{aligned}$$

Therefore, the expressions inside the curly brackets in the $\tilde{\Delta}^2_{21}$, $\breve{\Delta}^2_{21}$ and $\tilde{\Delta}^3_{21}$, $\breve{\Delta}^3_{21}$ terms are roughly of order one, with factors of 1/4 and 1/12 in front suppressing them. And since the entire expression is multiplied by $\sin^2\tilde{\theta}_{13} = O(\varepsilon^2)$, $\sin^2\breve{\theta}_{13} = O(\varepsilon^2)$ from outside the square brackets, these terms are of $O(\pi^2\varepsilon^4)$ and are negligible.

Therefore, to a good approximation, we can use the expressions

$$\begin{aligned}\tilde{P}(\nu_\mu\to\nu_e) &= 4\sin^2\tilde{\theta}_{13}\sin^2\tilde{\theta}_{\rm atm}\left\{1-(\tilde{B}\sin\tilde{\delta})\tilde{\Delta}_{21}\right\}\sin^2\left(\frac{\tilde{\Delta}_{31}-\tilde{\kappa}_{\mu e}\tilde{\Delta}_{21}}{2}\right)\,,\\ \breve{P}(\bar{\nu}_\mu\to\bar{\nu}_e) &= 4\sin^2\breve{\theta}_{13}\sin^2\breve{\theta}_{\rm atm}\left\{1+(\breve{B}\sin\breve{\delta})\breve{\Delta}_{21}\right\}\sin^2\left(\frac{\breve{\Delta}_{31}-\breve{\kappa}_{\mu e}\breve{\Delta}_{21}}{2}\right)\,,\end{aligned} \quad (2.9.22)$$

where the arguments of the sine functions are given by

$$\begin{aligned}&\tilde{\Delta}_{31}-\tilde{\kappa}_{\mu e}\tilde{\Delta}_{21}\\ &\approx \tilde{\Delta}_{31}-\left(\tilde{s}^2_{12}-\tilde{B}\cos\tilde{\delta}\right)\tilde{\Delta}_{21}\\ &\approx (\Delta_{31}-c^2_{12}\Delta_{21})-\left\{1-\frac{1}{2}\left(\frac{\delta m^2_{21}}{a\theta_{13}}\right)\left(1-\frac{a}{\delta m^2_{31}}\right)\cos\delta\right\}\left(\frac{a}{2E}L-\Delta_{21}\cos 2\theta_{12}\right)\\ &= \Delta_{31}\left[1-\left(\frac{a}{\delta m^2_{31}}\right)+\frac{1}{2\theta_{13}}\left(\frac{\delta m^2_{21}}{\delta m^2_{31}}\right)\cos\delta+O(\varepsilon^2)\right]\\ &= \Delta_{31}\left[1+{\rm sign}(\delta m^2_{31})\left(-\frac{a}{|\delta m^2_{31}|}+\frac{\varepsilon^2}{2\theta_{13}}\cos\delta\right)+O(\varepsilon^2)\right]\,,\\ &\breve{\Delta}_{31}-\breve{\kappa}_{\mu e}\breve{\Delta}_{21}\\ &\approx \breve{\Delta}_{31}-\left(\breve{s}^2_{12}-\breve{B}\cos\breve{\delta}\right)\breve{\Delta}_{21}\\ &\approx \left(\Delta_{31}+\frac{a}{2E}L-s^2_{12}\Delta_{21}\right)-\left\{-\frac{1}{2}\left(\frac{\delta m^2_{21}}{a\theta_{13}}\right)\left(1+\frac{a}{\delta m^2_{31}}\right)\cos\delta\right\}\left(\frac{a}{2E}L+\Delta_{21}\cos 2\theta_{12}\right)\\ &= \Delta_{31}\left[1+\left(\frac{a}{\delta m^2_{31}}\right)+\frac{1}{2\theta_{13}}\left(\frac{\delta m^2_{21}}{\delta m^2_{31}}\right)\cos\delta+O(\varepsilon^2)\right]\\ &= \Delta_{31}\left[1+{\rm sign}(\delta m^2_{31})\left(\frac{a}{|\delta m^2_{31}|}+\frac{\varepsilon^2}{2\theta_{13}}\cos\delta\right)+O(\varepsilon^2)\right]\,,\end{aligned} \quad (2.9.23)$$

while the amplitudes are given by

$$\begin{aligned}
&4\sin^2\tilde{\theta}_{13}\sin^2\tilde{\theta}_{\rm atm}\left\{1-(\tilde{B}\sin\tilde{\delta})\tilde{\Delta}_{21}\right\}\\
&\quad\approx\ 2\theta_{13}^2\left(1+\frac{2a}{\delta m^2_{31}}\right)\left[1-\left\{\frac{1}{2}\left(\frac{\delta m^2_{21}}{a\theta_{13}}\right)\left(1-\frac{a}{\delta m^2_{31}}\right)\sin\delta\right\}\left(\frac{a}{2E}L-\Delta_{21}\cos 2\theta_{12}\right)\right]\\
&\quad=\ 2\theta_{13}^2\left[1+\frac{2a}{\delta m^2_{31}}-\frac{1}{2\theta_{13}}\left(\frac{\delta m^2_{21}}{\delta m^2_{31}}\right)\Delta_{31}\sin\delta+O(\varepsilon^2)\right]\\
&\quad=\ 2\theta_{13}^2\left[1+\frac{2a}{\delta m^2_{31}}-\frac{\varepsilon^2}{2\theta_{13}}|\Delta_{31}|\sin\delta+O(\varepsilon^2)\right]\ ,\\
&4\sin^2\breve{\theta}_{13}\sin^2\breve{\theta}_{\rm atm}\left\{1+(\breve{B}\sin\breve{\delta})\breve{\Delta}_{21}\right\}\\
&\quad\approx\ 2\theta_{13}^2\left(1-\frac{2a}{\delta m^2_{31}}\right)\left[1+\left\{\frac{1}{2}\left(\frac{\delta m^2_{21}}{a\theta_{13}}\right)\left(1+\frac{a}{\delta m^2_{31}}\right)\sin\delta\right\}\left(\frac{a}{2E}L+\Delta_{21}\cos 2\theta_{12}\right)\right]\\
&\quad=\ 2\theta_{13}^2\left[1-\frac{2a}{\delta m^2_{31}}+\frac{1}{2\theta_{13}}\left(\frac{\delta m^2_{21}}{\delta m^2_{31}}\right)\Delta_{31}\sin\delta+O(\varepsilon^2)\right]\\
&\quad=\ 2\theta_{13}^2\left[1-\frac{2a}{\delta m^2_{31}}+\frac{\varepsilon^2}{2\theta_{13}}|\Delta_{31}|\sin\delta+O(\varepsilon^2)\right]\ .
\end{aligned}\tag{2.9.24}$$

From these simple expressions, we can discern a few facts about ν_e ($\bar{\nu}_e$) appearance experiments.

Roughly speaking, the positions of the oscillation peaks will provide information on the combination

$$\mathrm{sign}(\delta m^2_{31})\left(\mp\frac{a}{|\delta m^2_{31}|}+\frac{\varepsilon^2}{2\theta_{13}}\cos\delta\right)\ ,\tag{2.9.25}$$

while the heights of the oscillation peaks will provide information on the combination

$$2\theta_{13}^2\left[1\pm\left\{\mathrm{sign}(\delta m^2_{31})\frac{2a}{|\delta m^2_{31}|}-\frac{\varepsilon^2}{2\theta_{13}}|\Delta_{31}|\sin\delta\right\}\right]\ ,\tag{2.9.26}$$

where the upper signs are for the neutrinos, and the lower signs are for the anti-neutrinos. If the oscillation peaks occur in an energy region in which

$$\frac{a}{|\delta m^2_{31}|}\ll\frac{\varepsilon^2}{2\theta_{13}}\ ,\tag{2.9.27}$$

($\alpha\sim-2$) then the $a/|\delta m^2_{31}|$ terms in these expressions can be neglected. Then, measuring the height of the peak (or just the total ν_e or $\bar{\nu}_e$ flux using a narrow band beam) will allow us to constrain $\sin\delta$, provided that θ_{13} is well known from future reactor experiments [27, 28]. If θ_{13} is not well-known, then measuring the peak heights for both the neutrino and anti-neutrino will allow us to constrain both θ_{13} and $\sin\delta$. If one also measures the position of the peaks, either using a wide band beam or by changing the beam energy, then one can also extract information on the product

$$\mathrm{sign}(\delta m^2_{31})\cos\delta\ ,\tag{2.9.28}$$

but neither $\mathrm{sign}(\delta m^2_{31})$ nor the sign of $\cos\delta$ can be uniquely determined, even if both neutrino and anti-neutrino beams are used [29].

These features are clearly visible in Fig. 2.8.2, which shows the probabilities to be probed by the T2K experiment [10]. In phase 2 of T2K, the oscillation event rates for both neutrinos and

anti-neutrinos are to be measured, the difference from which we can extract $\sin\delta$. However, this does not provide any information on $\cos\delta$. It was proposed in Ref. [30] to measure the event rates using several beams of different energy, and thereby obtain some information on the peak position of the oscillation spectrum, but the sign of $\cos\delta$ cannot be uniquely determined unless the sign of δm^2_{31} is known [31]. (These difficulties can be best seen visually by utilizing the Minakata-Nunokawa plot [32].)

On the other hand, if the oscillation peaks occur in an energy region in which

$$\frac{a}{|\delta m^2_{31}|} \approx \frac{\varepsilon^2}{2\theta_{13}} \; , \tag{2.9.29}$$

($\alpha \sim -1$) then the measurement of the peak height by itself may not be able to determine either $\mathrm{sign}(\delta m^2_{31})$ or $\sin\delta$, even if θ_{13} were accurately known. In particular, there will be a degeneracy between the two cases in which $\mathrm{sign}(\delta m^2_{31})$ and $\sin\delta$ are both positive, and both negative, as can be clearly seen in Fig. 2.8.4. Measuring peak heights for both the neutrino and anti-neutrino will not help use here since they both depend on the same linear combination of $a/\delta m^2_{31}$ and $\sin\delta$, though it will help us in determining θ_{13}. If one also measures the position of the peak, then the degeneracy in $\mathrm{sign}(\delta m^2_{31})$ and $\cos\delta$ which existed for the previous case can be lifted, except when $\delta \approx 0$ for the neutrino case, and $\delta \approx \pi$ for the anti-neutrino case. Due to these shortcomings in performing a single experiment at either $\alpha \sim -1$ or $\alpha \sim -2$, various scenarios have been suggested which utilize two detectors set up at different baseline lengths [14, 15, 16, 17].

For the $L = 2540\,\mathrm{km}$ case, an expansion in $\tilde{\Delta}_{21}$ is no longer permissible. The approximation we used above for $\tilde{\theta}_{13}$ also breaks down as $\alpha \to 0$. We can nevertheless simplify the expressions for the oscillation probabilities and understand their behavior analytically. As an example, consider the oscillation probability $\tilde{P}(\nu_\mu \to \nu_e)$, the full expression of which is

$$\begin{aligned}
\tilde{P}(\nu_\mu \to \nu_e) \;=\; & 4\,|\tilde{U}_{\mu 2}|^2|\tilde{U}_{e2}|^2 \sin^2\frac{\tilde{\Delta}_{21}}{2} + 4\,|\tilde{U}_{\mu 3}|^2|\tilde{U}_{e3}|^2 \sin^2\frac{\tilde{\Delta}_{31}}{2} \\
& + 2\,\Re(\tilde{U}^*_{\mu 3}\tilde{U}_{e3}\tilde{U}_{\mu 2}\tilde{U}^*_{e2}) \left(4\sin^2\frac{\tilde{\Delta}_{21}}{2}\sin^2\frac{\tilde{\Delta}_{31}}{2} + \sin\tilde{\Delta}_{21}\sin\tilde{\Delta}_{31} \right) \\
& + 4\,\tilde{J}_{(\mu,e)} \left(\sin^2\frac{\tilde{\Delta}_{21}}{2}\sin\tilde{\Delta}_{31} - \sin^2\frac{\tilde{\Delta}_{31}}{2}\sin\tilde{\Delta}_{21} \right) \; .
\end{aligned} \tag{2.9.30}$$

Using the approximations in Eq. (2.9.1), except the one for $\tilde{\theta}_{13}$, we find

$$\begin{aligned}
|\tilde{U}_{\mu 2}|^2|\tilde{U}_{e2}|^2 &\approx s^2_{23}\tilde{s}^2_{13}\tilde{c}^2_{13} - 2\tilde{A}\cos\delta \; , \\
|\tilde{U}_{\mu 3}|^2|\tilde{U}_{e3}|^2 &\approx s^2_{23}\tilde{s}^2_{13}\tilde{c}^2_{13} \; , \\
\Re(\tilde{U}^*_{\mu 3}\tilde{U}_{e3}\tilde{U}_{\mu 2}\tilde{U}^*_{e2}) &\approx -s^2_{23}\tilde{s}^2_{13}\tilde{c}^2_{13} + \tilde{A}\cos\delta \; , \\
\tilde{J}_{(\mu,e)} &\approx \tilde{A}\sin\delta \; ,
\end{aligned} \tag{2.9.31}$$

where

$$\tilde{A} \approx \left(\frac{\delta m^2_{21}}{2a}\right) \sin(2\theta_{12}) s_{23}c_{23}\tilde{s}_{13}\tilde{c}^2_{13} \; . \tag{2.9.32}$$

Terms of order $(\delta m^2_{21}/a)^2$ and higher have been neglected. Substituting into Eq. (2.9.30), we

$a/\lvert\delta m^2_{31}\rvert$			$O(\varepsilon^3)$	$O(\varepsilon^2)$	$O(\varepsilon)$	$O(1)$	$O(\varepsilon^{-1})$
ν	$\tilde{\theta}_{12}$		$\approx \theta_{12}$	$\nearrow$	$\approx \frac{\pi}{2}$		
	$\tilde{\theta}_{13}$	$\delta m^2_{31} > 0$	$\approx \theta_{13}$			$\nearrow$	$\approx \frac{\pi}{2}$
		$\delta m^2_{31} < 0$	$\approx \theta_{13}$			$\searrow$	≈ 0
$\bar{\nu}$	$\breve{\theta}_{12}$		$\approx \theta_{12}$	$\searrow$	≈ 0		
	$\breve{\theta}_{13}$	$\delta m^2_{31} > 0$	$\approx \theta_{13}$			$\searrow$	≈ 0
		$\delta m^2_{31} < 0$	$\approx \theta_{13}$			$\nearrow$	$\approx \frac{\pi}{2}$

Table 2.3: The dependence of the effective mixing angles on $a/|\delta m^2_{31}|$.

obtain

$$\begin{aligned}
\tilde{P}(\nu_\mu \to \nu_e) &\approx 4 s^2_{23} \tilde{s}^2_{13} \tilde{c}^2_{13} \sin^2 \frac{\tilde{\Delta}_{32}}{2} + 8 \tilde{A} \sin \frac{\tilde{\Delta}_{32}}{2} \sin \frac{\tilde{\Delta}_{21}}{2} \cos\left(\frac{\tilde{\Delta}_{31}}{2} + \delta \right) \\
&\approx \left[s_{23} \sin(2\tilde{\theta}_{13}) \sin \frac{\tilde{\Delta}_{32}}{2} + c_{23} \tilde{c}_{13} \left(\frac{\delta m^2_{21}}{a} \right) \sin(2\theta_{12}) \sin \frac{\tilde{\Delta}_{21}}{2} \cos\left(\frac{\tilde{\Delta}_{31}}{2} + \delta \right) \right]^2 \\
&\approx \frac{1}{2} \left[\sin(2\tilde{\theta}_{13}) \sin \frac{\tilde{\Delta}_{32}}{2} + \tilde{c}_{13} \left(\frac{\delta m^2_{21}}{a} \right) \sin \frac{\tilde{\Delta}_{21}}{2} \cos\left(\frac{\tilde{\Delta}_{31}}{2} + \delta \right) \right]^2 , \qquad (2.9.33)
\end{aligned}$$

where we have used $\sin(2\theta_{12}) = 1 - 2O(\varepsilon)$, and $\sin(2\theta_{23}) = 1 - \frac{1}{2}O(\varepsilon^2)$. Now, the a-dependence of $\tilde{\theta}_{13}$ is different depending on the sign of δm^2_{31}. If $\delta m^2_{31} > 0$ (normal hierarchy), $\tilde{\theta}_{13}$ increases monotonically from θ_{13} toward $\frac{\pi}{2}$ as a increases with energy, and passes through $\frac{\pi}{4}$ around $a \approx |\delta m^2_{31}|$. If $\delta m^2_{31} < 0$ (inverted hierarchy), $\tilde{\theta}_{13}$ decreases monotonically from θ_{13} toward 0 as a increase with energy, and is about $\theta_{13}/2$ around $a \approx |\delta m^2_{31}|$. (cf. Table 2.3) Therefore, if $\delta m^2_{31} > 0$, then the coefficient of the first term in the brackets of Eq. (2.9.33) is maximized around $a \approx |\delta m^2_{31}|$. If the oscillation peak where $\tilde{\Delta}_{32} \approx \pi$ matches that energy, one can expect a maximum oscillation probability as large as $\frac{1}{2}$. (Note that this maximum probability is determined by θ_{23} and is independent of the value of θ_{13} in vacuum.) On the other hand, if $\delta m^2_{31} < 0$, then the same coefficient is suppressed to $O(\varepsilon)$, and the oscillation probability with be suppressed by a factor of $O(\varepsilon^2)$. This difference is evident in Fig. 2.8.6. (In both cases, the second term in the brackets interferes with the first term giving the probability a weak δ-dependence.) Due to this clear difference, measuring the ν_e appearance probability at the first oscillation peak at a baseline length of $L = 2540\,\mathrm{km}$ has been proposed as an unambiguous method to determine the sign of δm^2_{31} [11].

Comparing the $L = 295\,\mathrm{km}$, $L = 1000\,\mathrm{km}$, and $L = 2540\,\mathrm{km}$ cases considered above, we can discern a generic trend that the oscillation probability $\tilde{P}(\nu_\mu \to \nu_e)$ (or $\breve{P}(\bar{\nu}_\mu \to \bar{\nu}_e)$) is more sensitive to the CP violating phase δ at lower energies (shorter baselines), and more sensitive to the mass hierarchy (sign of δm^2_{31}) at higher energies (longer baselines). This can be understood as follows. First, the angle $\tilde{\theta}_{13}$, which has a different energy dependence depending on the sign of δm^2_{31}, enters $\tilde{P}(\nu_\mu \to \nu_e)$ dominantly in the combination

$$\sin\tilde{\theta}_{13} \sin\tilde{\theta}_{\mathrm{atm}} = \sin\tilde{\theta}_{13} \cos\tilde{\theta}_{13} \sin\tilde{\theta}_{23}$$

$$
\begin{aligned}
&= \frac{1}{2}\sin(2\tilde{\theta}_{13})\sin\tilde{\theta}_{23} \\
&\approx \frac{1}{2}\sin(2\tilde{\theta}_{13})\sin\theta_{23}\ . \qquad (2.9.34)
\end{aligned}
$$

Therefore, $\sin(2\tilde{\theta}_{13})$ determines the sensitivity of $\tilde{P}(\nu_\mu \to \nu_e)$ on the behavior of $\tilde{\theta}_{13}$. On the other hand, the size of CP violation is governed by the Jarskog invariant,

$$\tilde{J} = \tilde{A}\sin\tilde{\delta}\ , \qquad (2.9.35)$$

where

$$
\begin{aligned}
\tilde{A} &= \tilde{s}_{12}\tilde{c}_{12}\tilde{s}_{13}\tilde{c}_{13}^2\tilde{s}_{23}\tilde{c}_{23} \\
&= \frac{1}{4}\sin(2\tilde{\theta}_{12})\sin(2\tilde{\theta}_{23})\tilde{s}_{13}(1-\tilde{s}_{13}^2) \\
&\approx \frac{1}{4}\sin(2\tilde{\theta}_{12})\sin(2\theta_{23})\tilde{s}_{13}(1-\tilde{s}_{13}^2)\ . \qquad (2.9.36)
\end{aligned}
$$

In our convention where the mixing angles are in the first quadrant, $\tilde{A}$ is bounded by

$$0 \ \le\ \tilde{A}\ \le\ \frac{1}{6\sqrt{3}} \equiv A_{\rm max}\ . \qquad (2.9.37)$$

In Fig. 2.9.6, we plot the α-dependence of $\sin(2\tilde{\theta}_{13})$, $\sin(2\tilde{\theta}_{12})$, $\tilde{s}_{13}(1-\tilde{s}_{31}^2)$, and $\tilde{A}/A_{\rm max}$, and their anti-neutrino counterparts, for the input parameters of Eq. (2.5.34). It is clear from the figure that the differences in $\sin(2\tilde{\theta}_{13})$ and $\sin(2\widecheck{\theta}_{13})$ between the $\delta m^2_{31} > 0$ and $\delta m^2_{31} < 0$ cases is most prominent at $\alpha \approx 0$ where there exists a large peak in one case which is absent in the other. This is due to the fact $\tilde{\theta}_{13}$ ($\widecheck{\theta}_{13}$) crosses $\pi/4$ at $a \approx |\delta m^2_{31}|$ when $\delta m^2_{31} > 0$ ($\delta m^2_{31} < 0$). (cf. Table 2.3.) Therefore, experiments that are performed closer to $\alpha = 0$ are more sensitive to $\mathrm{sign}(\delta m^2_{31})$. On the other hand, the α-dependence of $\tilde{A}$ ($\widecheck{A}$) is dominated by that of $\sin(2\tilde{\theta}_{12})$ ($\sin(2\widecheck{\theta}_{12})$ which starts out as a number of $O(1)$ at low α, but drops off quickly toward zero as α is increased from -2 to -1. Therefore, experiments that are performed at $\alpha \lesssim -2$ are more sensitive to δ than those performed at $\alpha \gtrsim -1$.

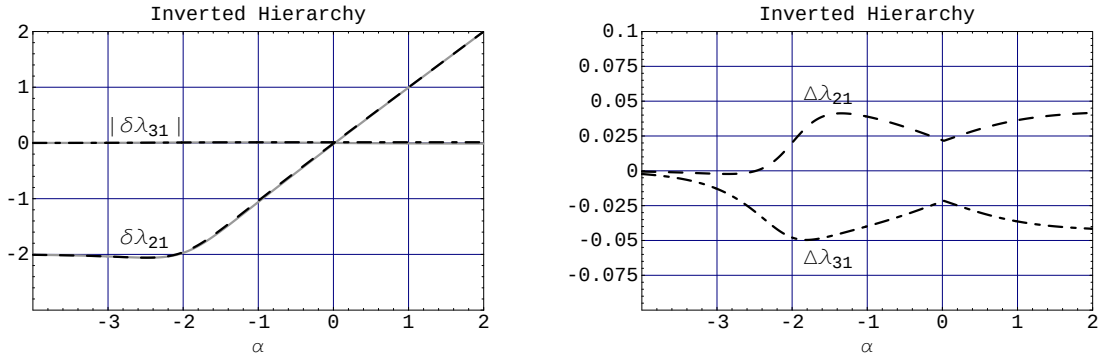

Figure 2.5.11: Comparison of exact and approximate values using Eq. (2.5.40) for the inverted hierarchy case.

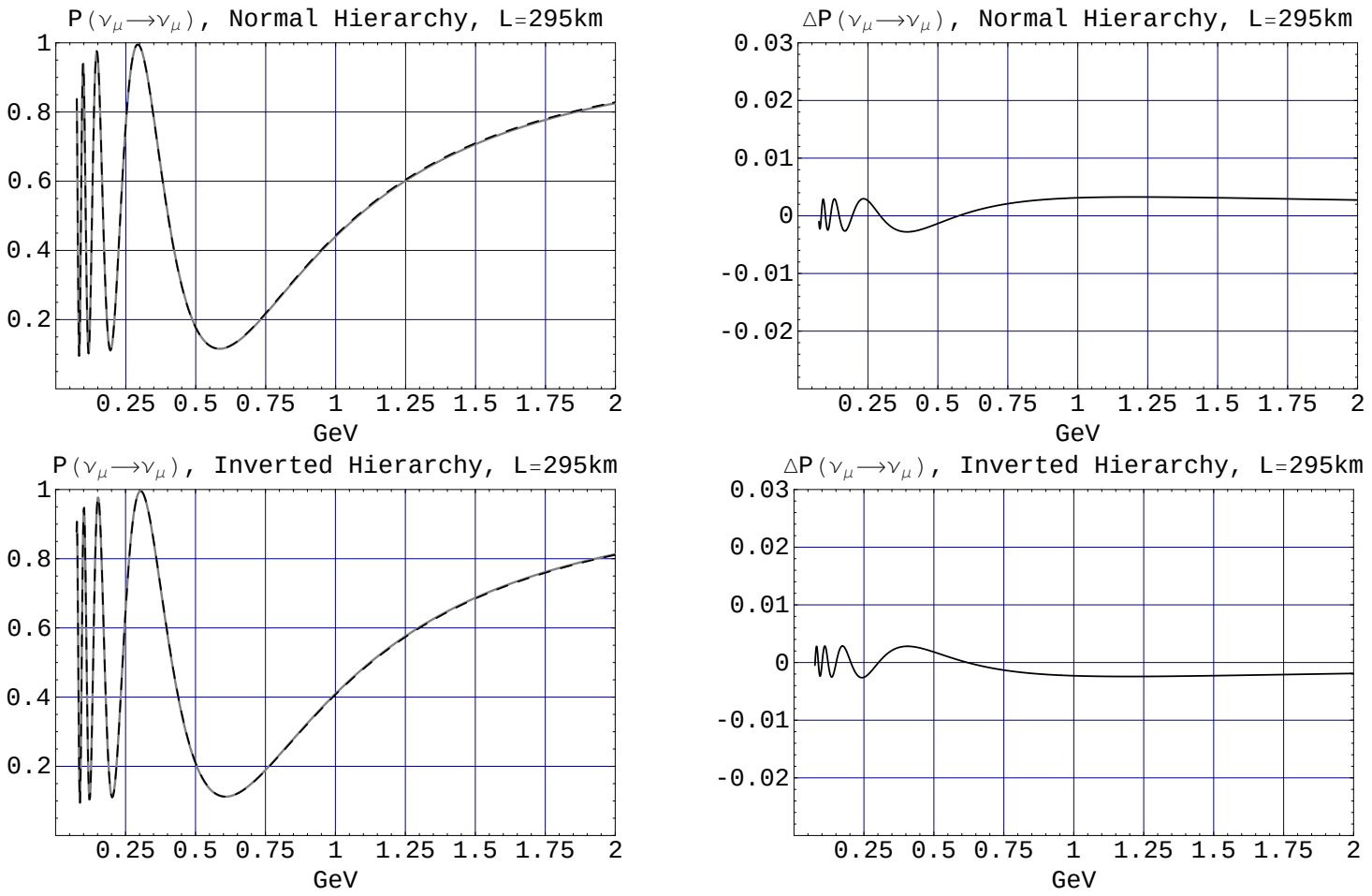

Figure 2.8.1: Comparison of exact (solid gray line) and approximate (black dashed line) values of $P(\nu_\mu \to \nu_\mu)$ for the $L = 295\,\text{km}$ case. The approximate value was calculated using Eq. (2.5.29) for the mixing angles, and Eq. (2.5.40) for the mass-squared differences. The CP violating phase δ was set to zero. The difference $\Delta P \equiv P_{\text{approx}} - P_{\text{exact}}$ is plotted on the right.

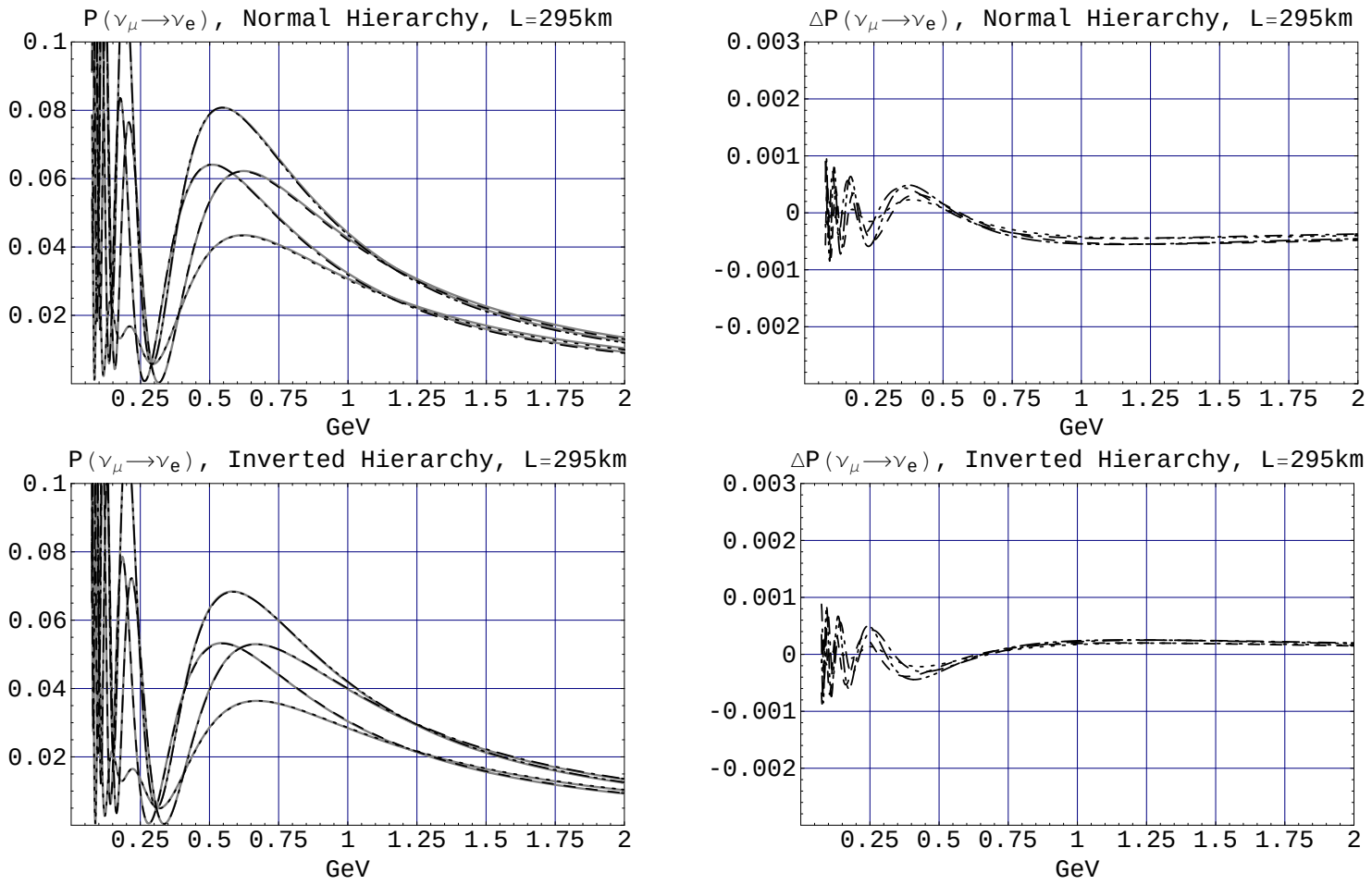

Figure 2.8.2: Comparison of exact and approximate values of $P(\nu_\mu \to \nu_e)$ for the $L = 295\,\text{km}$ case for several different values of the CP violating phase δ. The approximate values were calculated using Eq. (2.5.29) for the mixing angles, and Eq. (2.5.40) for the mass-squared differences. The exact values are given by the solid gray lines, while the approximate values are the black dashed ($\delta = 0$), dotted ($\delta = \pi/2$), dot-dashed ($\delta = \pi$), and double-dot-dashed ($\delta = 3\pi/2$) lines.

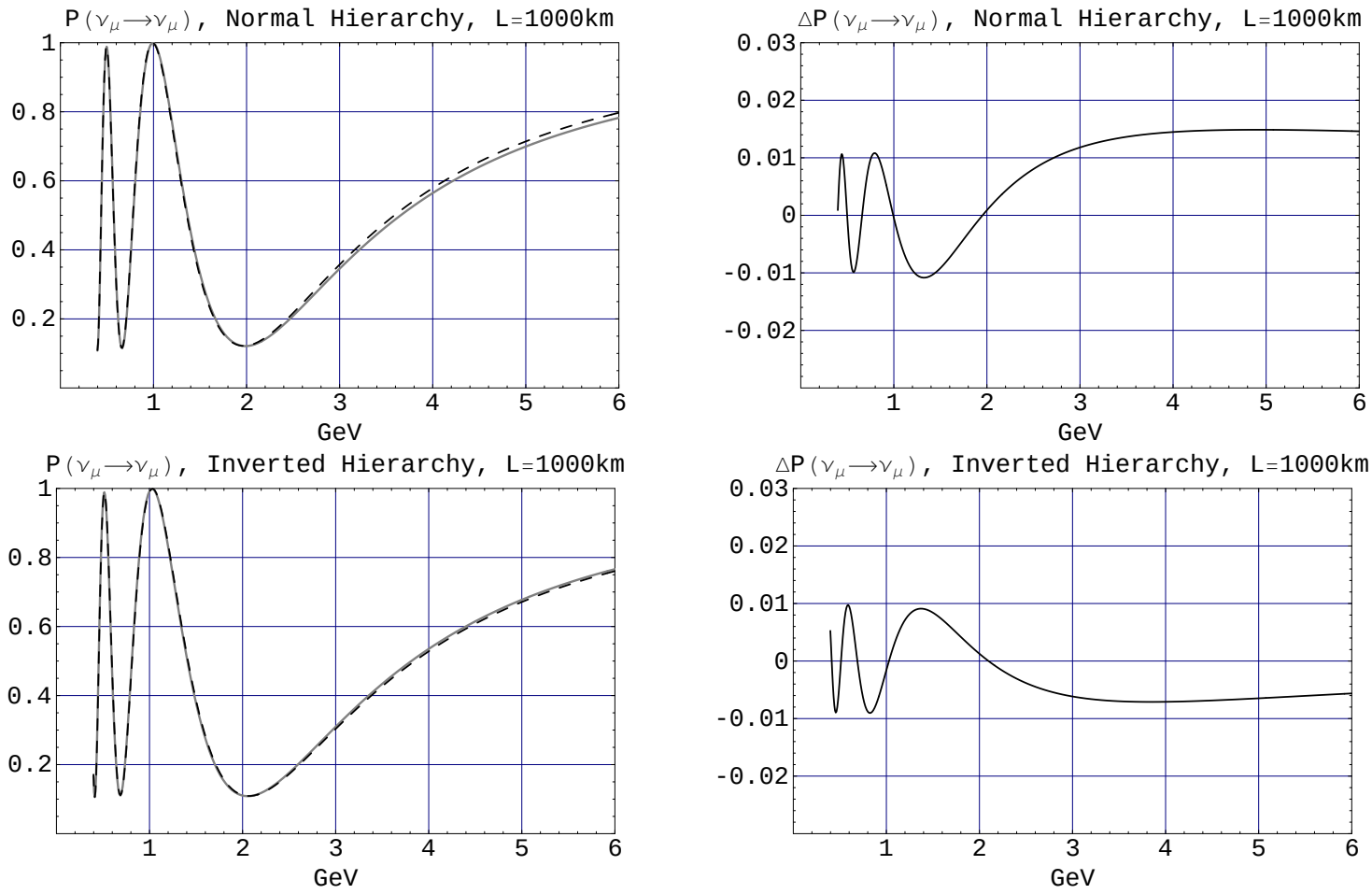

Figure 2.8.3: Comparison of exact (solid gray line) and approximate (black dashed line) values of $P(\nu_\mu \to \nu_\mu)$ for the $L = 1000\,\text{km}$ case. The approximate value was calculated using Eq. (2.5.29) for the mixing angles, and Eq. (2.5.40) for the mass-squared differences. The CP violating phase δ was set to zero. The difference $\Delta P \equiv P_{\text{approx}} - P_{\text{exact}}$ is plotted on the right.

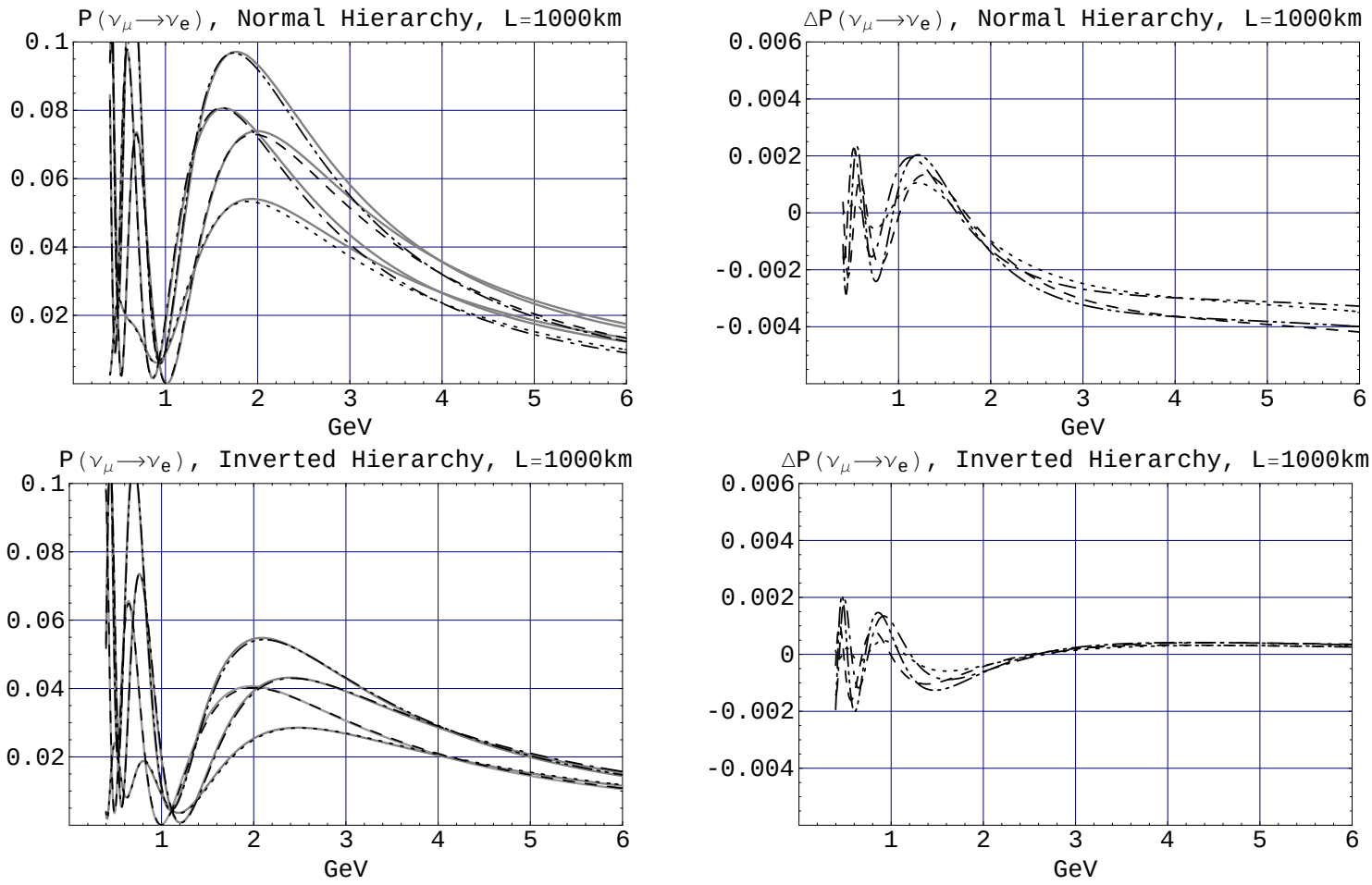

Figure 2.8.4: Comparison of exact and approximate values of $P(\nu_\mu \to \nu_e)$ for the $L = 1000\,\text{km}$ case for several different values of the CP violating phase δ. The approximate values were calculated using Eq. (2.5.29) for the mixing angles, and Eq. (2.5.40) for the mass-squared differences. The exact values are given by the solid gray lines, while the approximate values are the black dashed ($\delta = 0$), dotted ($\delta = \pi/2$), dot-dashed ($\delta = \pi$), and double-dot-dashed ($\delta = 3\pi/2$) lines.

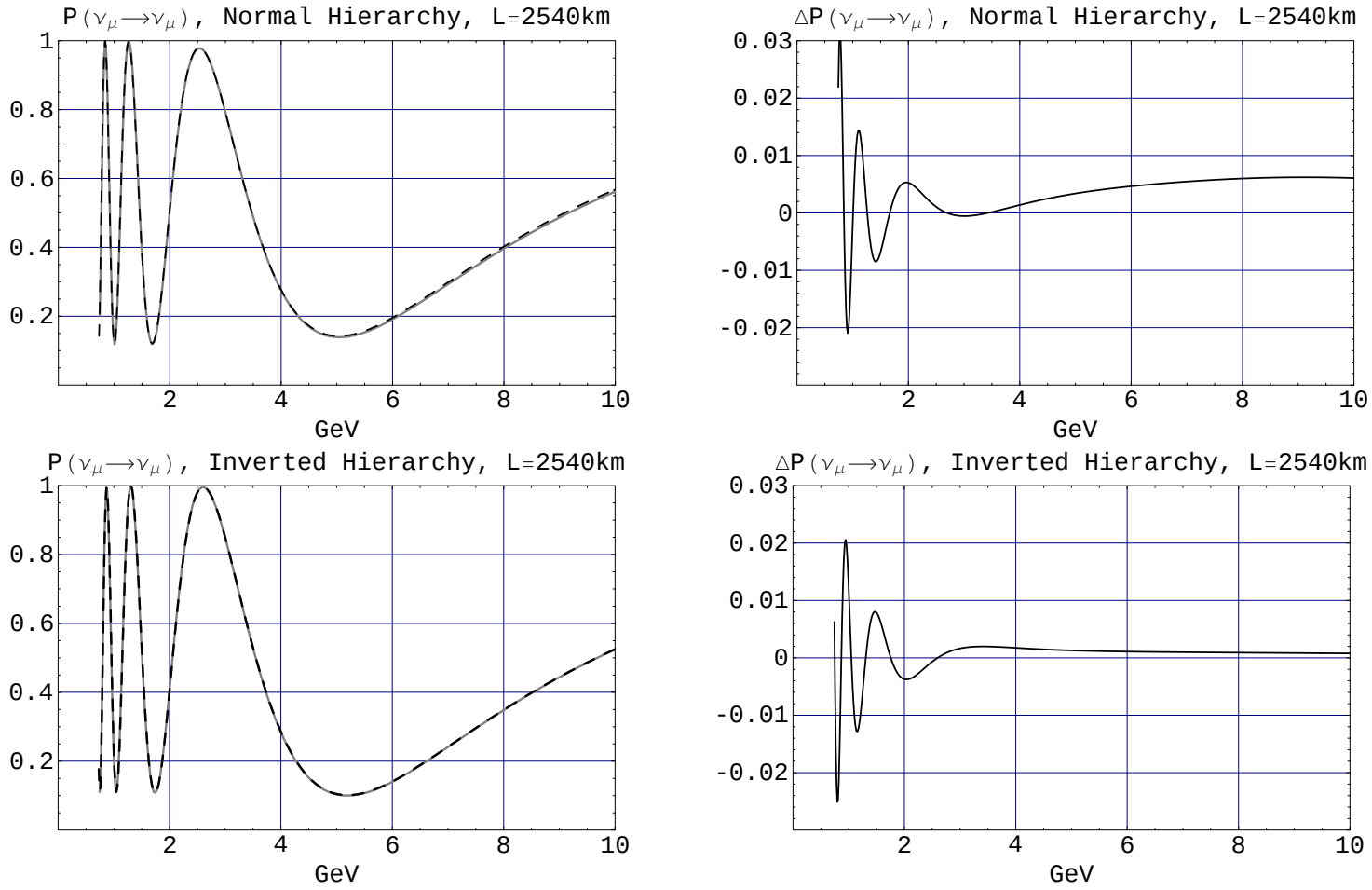

Figure 2.8.5: Comparison of exact (solid gray line) and approximate (black dashed line) values of $P(\nu_\mu \to \nu_\mu)$ for the $L = 2540\,\text{km}$ case. The approximate value was calculated using Eq. (2.5.29) for the mixing angles, and Eq. (2.5.41) for the mass-squared differences. The CP violating phase δ was set to zero.

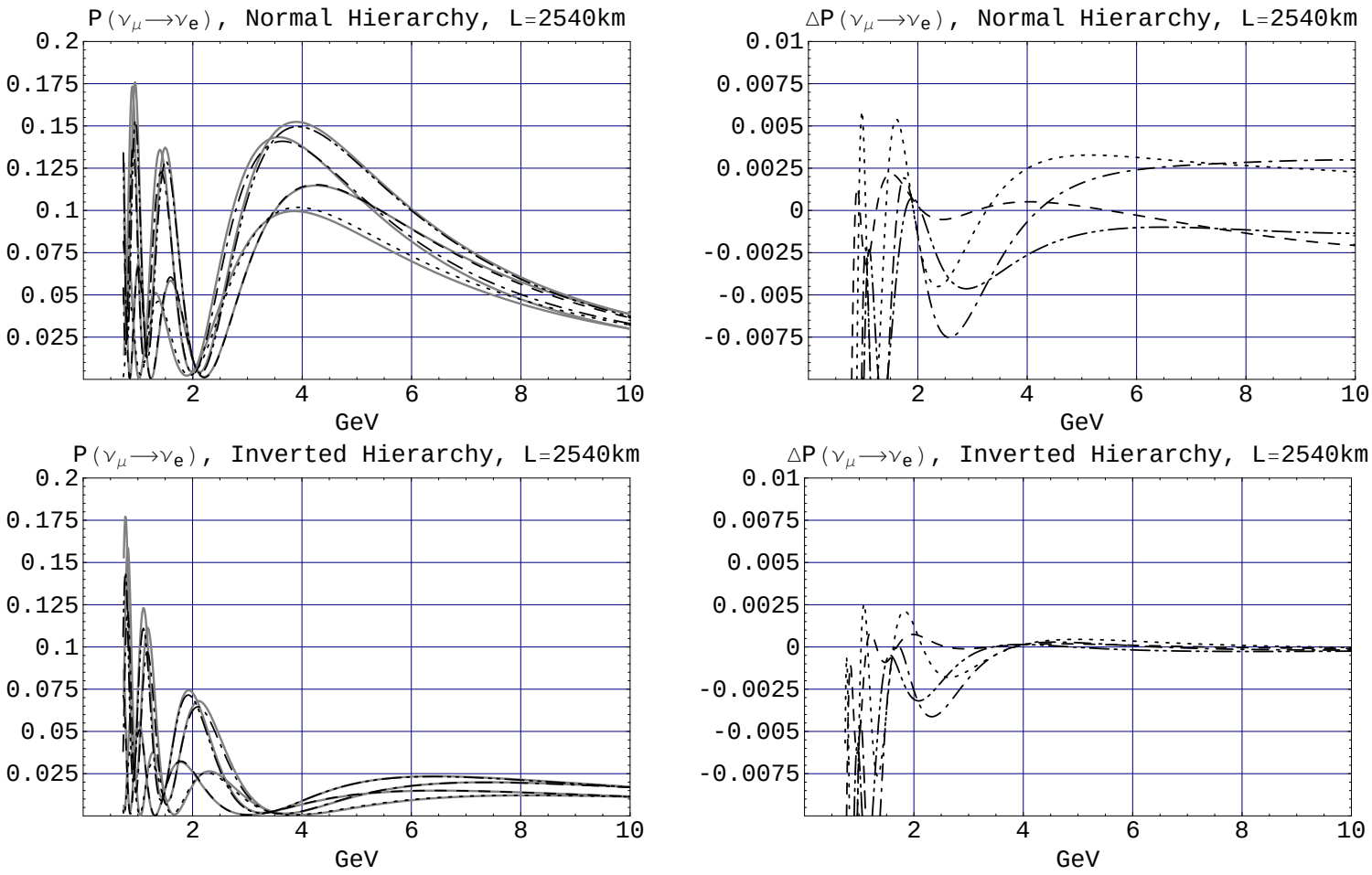

Figure 2.8.6: Comparison of exact and approximate values of $P(\nu_\mu \to \nu_e)$ for the $L = 2540\,\text{km}$ case for several different values of the CP violating phase δ. The approximate values were calculated using Eq. (2.5.29) for the mixing angles, and Eq. (2.5.41) for the mass-squared differences. The exact values are given by the solid gray lines, while the approximate values are the black dashed ($\delta = 0$), dotted ($\delta = \pi/2$), dot-dashed ($\delta = \pi$), and double-dot-dashed ($\delta = 3\pi/2$) lines.

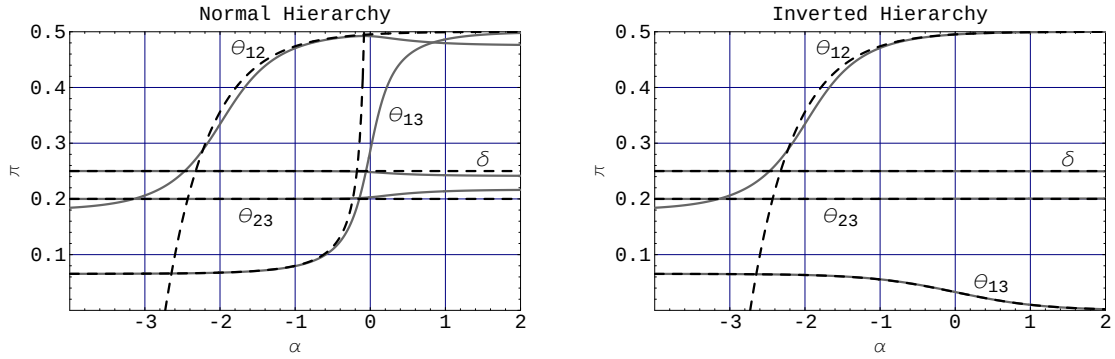

Figure 2.9.1: The exact values of $\tilde{\theta}_{12}$, $\tilde{\theta}_{13}$, $\tilde{\theta}_{23}$, and $\tilde{\delta}$ (solid gray lines) plotted as functions of $\alpha = \log_{1/\varepsilon}(a/|\delta m^2_{31}|)$ against their approximate values (black dashed lines) obtained using Eq. (2.9.1). The $\delta m^2_{31} > 0$ (normal hierarchy) case is shown on the left, and the $\delta m^2_{31} < 0$ (inverted hierarchy) case is shown on the right. The input parameters are those of Eq. (2.5.34).

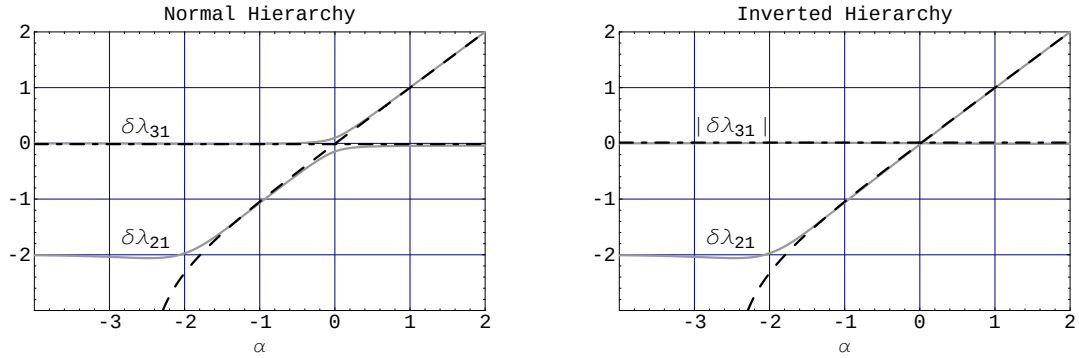

Figure 2.9.2: The exact values of $\log_{1/\varepsilon}(\delta\lambda_{21}/|\delta m^2_{31}|)$ and $\log_{1/\varepsilon}(\delta\lambda_{31}/|\delta m^2_{31}|)$ (solid gray lines) plotted as functions of $\alpha = \log_{1/\varepsilon}(a/|\delta m^2_{31}|)$ against their approximate values (black dashed and dot-dashed lines) obtained using Eq. (2.9.2). The input parameters are those of Eq. (2.5.34).

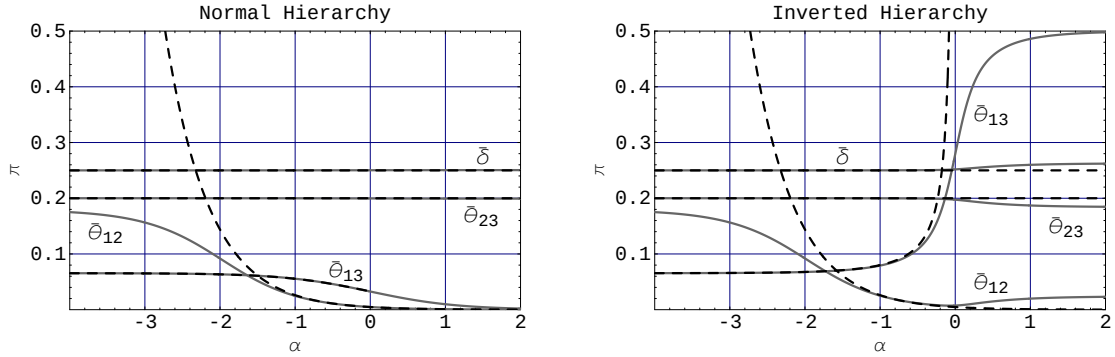

Figure 2.9.3: The exact values of $\breve{\theta}_{12}$, $\breve{\theta}_{13}$, $\breve{\theta}_{23}$, and $\breve{\delta}$ (solid gray lines) plotted as functions of $\alpha = \log_{1/\varepsilon}(a/|\delta m^2_{31}|)$ against their approximate values (black dashed lines) obtained using Eq. (2.9.3). The $\delta m^2_{31} > 0$ (normal hierarchy) case is shown on the left, and the $\delta m^2_{31} < 0$ (inverted hierarchy) case is shown on the right. The input parameters are those of Eq. (2.5.34).

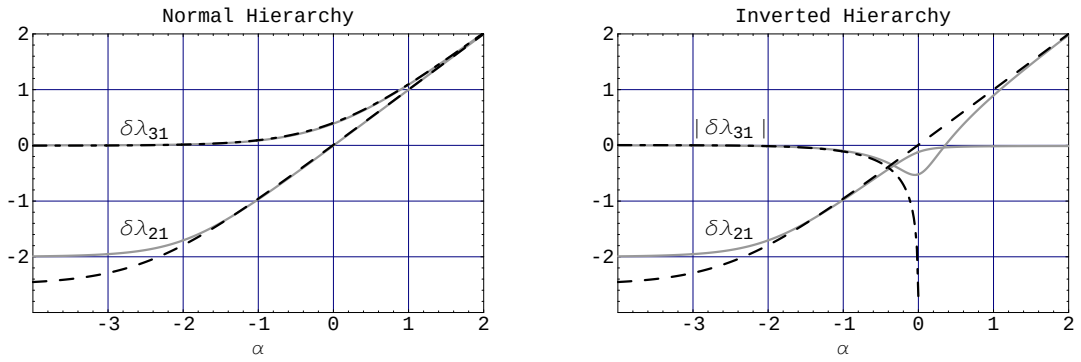

Figure 2.9.4: The exact values of $\log_{1/\varepsilon}(\delta\bar{\lambda}_{21}/|\delta m^2_{31}|)$ and $\log_{1/\varepsilon}(|\delta\bar{\lambda}_{31}|/|\delta m^2_{31}|)$ (solid gray lines) plotted as functions of $\alpha = \log_{1/\varepsilon}(a/|\delta m^2_{31}|)$ against their approximate values (black dashed and dot-dashed lines), obtained using Eq. (2.9.4). The input parameters are those of Eq. (2.5.34).

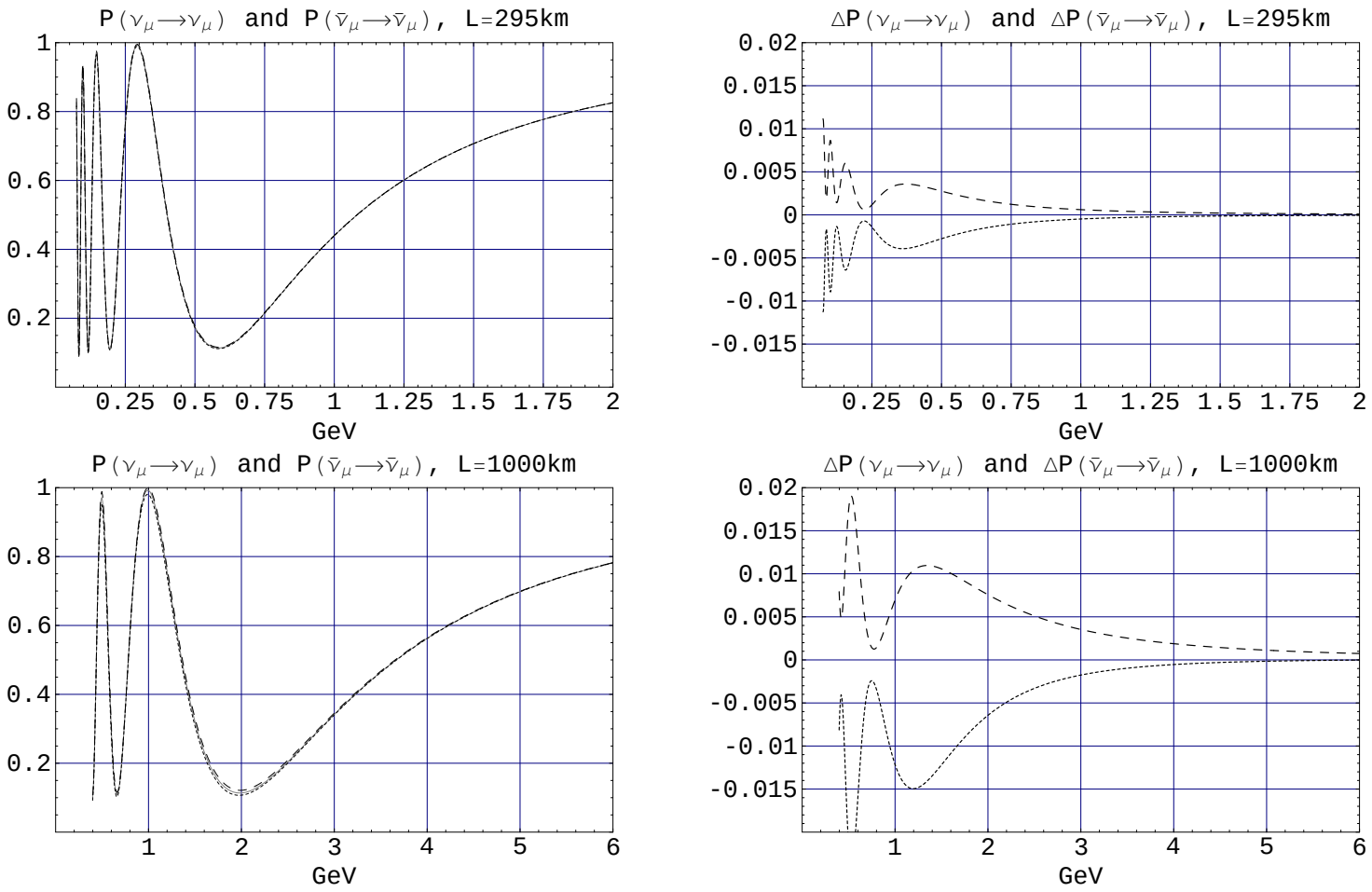

Figure 2.9.5: Comparison of the ν_μ and $\bar{\nu}_\mu$ survival probabilities in vacuum and in matter. On the left, $P(\nu_\mu \to \nu_\mu) = P(\bar{\nu}_\mu \to \bar{\nu}_\mu)$ is the solid gray line, $\tilde{P}(\nu_\mu \to \nu_\mu)$ is the dashed black line, and $\widetilde{\bar{P}}(\bar{\nu}_\mu \to \bar{\nu}_\mu)$ is the dotted black line. On the right, the difference $\Delta P(\nu_\mu \to \nu_\mu) = \tilde{P}(\nu_\mu \to \nu_\mu) - P(\nu_\mu \to \nu_\mu)$ is the dashed black line, and the difference $\Delta P(\bar{\nu}_\mu \to \bar{\nu}_\mu) = \widetilde{\bar{P}}(\bar{\nu}_\mu \to \bar{\nu}_\mu) - P(\bar{\nu}_\mu \to \bar{\nu}_\mu)$ is the dotted black line. The input parameters are those listed in Eq. (2.5.34) with $\delta m^2_{31} > 0$.

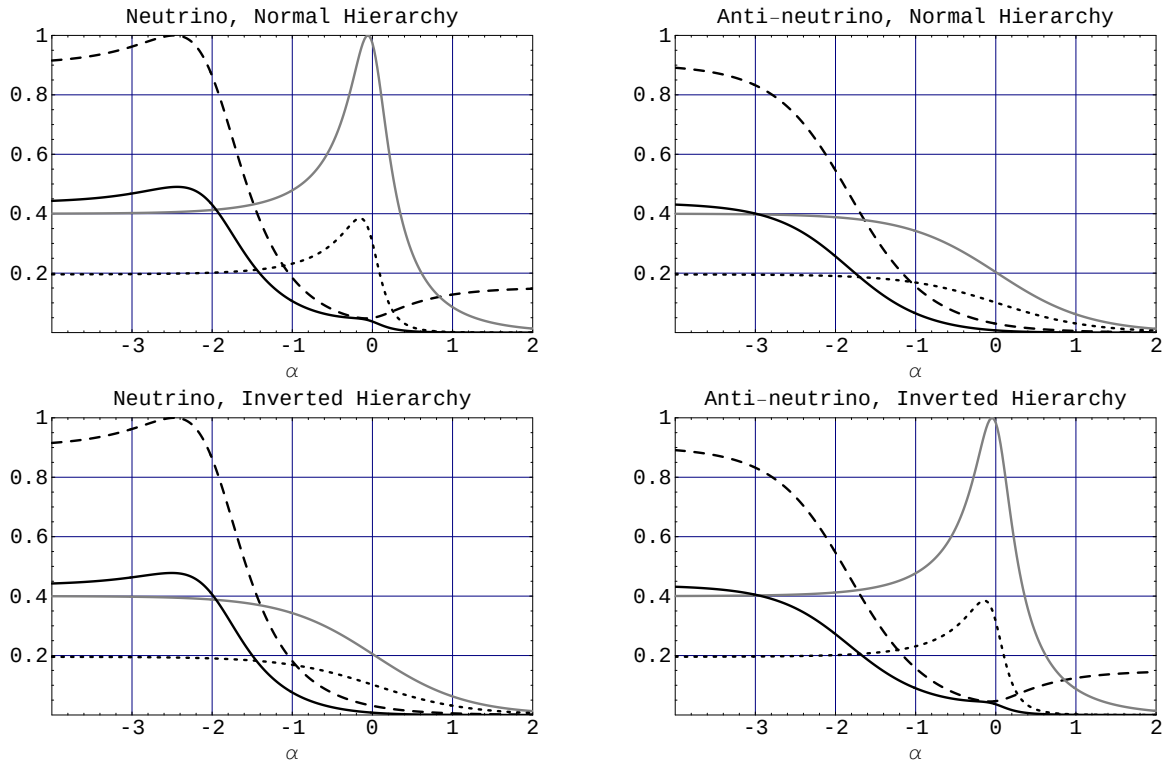

Figure 2.9.6: The dependence of $\sin(2\tilde{\theta}_{13})$, $\sin(2\widecheck{\theta}_{13})$ (solid gray lines), $\sin(2\tilde{\theta}_{12})$, $\sin(2\widecheck{\theta}_{12})$ (dashed black lines), $\tilde{s}_{13}(1-\tilde{s}^2_{13})$, $\widecheck{s}_{13}(1-\widecheck{s}^2_{13})$ (dotted black lines), and $\tilde{A}/A_{\rm max}$, $\widecheck{A}/A_{\rm max}$ (solid black lines) on $\alpha = \log_{1/\varepsilon}(a/|\delta m^2_{31}|)$. The input parameters were those listed in Eq. (2.5.34).

Chapter 3

Constraints on New Physics from Long Baseline Neutrino Experiments

It has been shown previously [34] that a long-baseline neutrino (LBL) oscillation experiments would be able to constraint certain types of new physics beyond the Standard Model, provided that the vacuum value of $\sin^2 2\theta_{23}$ is not too close to one. In this chapter, we give an example of a LBL experiment in which the Fermilab-NUMI bean in its high-energy mode [35] is aimed at the planned Hyper-Kamiokande detector [36] and discuss the potential constraints it can placed on new physics.

3.1 Introduction

When considering matter effects on neutrino oscillation, it is customary to consider only the W-exchange interaction of the ν_e with the electrons in matter. However, if new interactions beyond the Standard Model (SM) that distinguish among the three generations of neutrinos exist, they can lead to extra matter effects via radiative corrections to the $Z\nu\nu$ vertex, which effectively violate neutral current universality, or via the direct exchange of new particles between the neutrinos and matter particles [37].

Many models of physics beyond the SM introduce interactions which distinguish among generations: gauged $L_\alpha - L_\beta$ [38] and gauged $B - \alpha L_e - \beta L_\mu - \gamma L_\tau$ [39, 40, 41, 42] models introduce Z's and Higgs sectors which distinguish among the three generations of leptons; topcolor assisted technicolor treats the third generation differently from the first two to explain the large top mass [44, 45]; R-parity violating couplings in supersymmetric models couple fermions/sfermions from different generations [46, 47, 48].

The effective Hamiltonian that governs neutrino oscillation in the presence of neutral-current lepton universality violation, or new physics that couples to the different generations differently, is given by [34]

$$H = \tilde{U} \begin{bmatrix} \lambda_1 & 0 & 0 \\ 0 & \lambda_2 & 0 \\ 0 & 0 & \lambda_3 \end{bmatrix} \tilde{U}^\dagger = U \begin{bmatrix} 0 & 0 & 0 \\ 0 & \delta m^2_{21} & 0 \\ 0 & 0 & \delta m^2_{31} \end{bmatrix} U^\dagger + \begin{bmatrix} a & 0 & 0 \\ 0 & 0 & 0 \\ 0 & 0 & 0 \end{bmatrix} + \begin{bmatrix} b_e & 0 & 0 \\ 0 & b_\mu & 0 \\ 0 & 0 & b_\tau \end{bmatrix} . \quad (3.1.1)$$

In this expression, U is the MNS matrix [49],

$$a = 2EV_{CC} \ , \qquad V_{CC} = \sqrt{2}G_F N_e = N_e \frac{g^2}{4M_W^2} \ , \tag{3.1.2}$$

is the usual matter effect due to W-exchange between ν_e and the electrons [18], and b_e, b_μ, b_τ are the extra matter effects which we assume to be flavor diagonal and non-equal. The matter effect terms in this Hamiltonian can always be written as

$$\begin{aligned} &\begin{bmatrix} a & 0 & 0 \\ 0 & 0 & 0 \\ 0 & 0 & 0 \end{bmatrix} + \begin{bmatrix} b_e & 0 & 0 \\ 0 & b_\mu & 0 \\ 0 & 0 & b_\tau \end{bmatrix} \\ &= \begin{bmatrix} \left(a + b_e - \dfrac{b_\mu + b_\tau}{2}\right) & 0 & 0 \\ 0 & \left(\dfrac{b_\mu - b_\tau}{2}\right) & 0 \\ 0 & 0 & -\left(\dfrac{b_\mu - b_\tau}{2}\right) \end{bmatrix} + \left(\frac{b_\mu + b_\tau}{2}\right) \begin{bmatrix} 1 & 0 & 0 \\ 0 & 1 & 0 \\ 0 & 0 & 1 \end{bmatrix} \end{aligned} \tag{3.1.3}$$

The unit matrix term does not contribute to neutrino oscillation so it can be dropped. We define the parameter ξ as

$$\frac{b_\tau - b_\mu}{a} = \xi \ . \tag{3.1.4}$$

Then, the effective Hamiltonian can be written as

$$H = \tilde{U} \begin{bmatrix} \lambda_1 & 0 & 0 \\ 0 & \lambda_2 & 0 \\ 0 & 0 & \lambda_3 \end{bmatrix} \tilde{U}^\dagger = U \begin{bmatrix} 0 & 0 & 0 \\ 0 & \delta m_{21}^2 & 0 \\ 0 & 0 & \delta m_{31}^2 \end{bmatrix} U^\dagger + a \begin{bmatrix} 1 & 0 & 0 \\ 0 & -\xi/2 & 0 \\ 0 & 0 & +\xi/2 \end{bmatrix} \ , \tag{3.1.5}$$

where we have absorbed the extra b-terms in the $(1,1)$ element into a.

The extra ξ-dependent contribution in Eq. (3.1.5) can manifest itself when $a > |\delta m_{31}^2|$ (*i.e.* $E \gtrsim 10\,\mathrm{GeV}$ for typical matter densities in the Earth) in the ν_μ and $\bar{\nu}_\mu$ survival probabilities as [34]

$$\begin{aligned} P(\nu_\mu \to \nu_\mu) &\approx 1 - \sin^2\left(2\theta_{23} - \frac{a\xi}{\delta m_{31}^2}\right) \sin^2 \frac{\Delta}{2} \ , \\ P(\bar{\nu}_\mu \to \bar{\nu}_\mu) &\approx 1 - \sin^2\left(2\theta_{23} + \frac{a\xi}{\delta m_{31}^2}\right) \sin^2 \frac{\Delta}{2} \ , \end{aligned} \tag{3.1.6}$$

where

$$\Delta \approx \Delta_{31} c_{13}^2 - \Delta_{21} c_{12}^2 \ , \qquad \Delta_{ij} = \frac{\delta m_{ij}^2}{2E} L \ , \qquad c_{ij} = \cos\theta_{ij} \ , \tag{3.1.7}$$

and the CP violating phase δ has been set to zero. As is evident from these expressions, the small shift due to ξ will be invisible if the value of $\sin^2 2\theta_{23}$ is too close to one. However, if the value of $\sin^2 2\theta_{23}$ is as low as $\sin^2 2\theta_{23} = 0.92$ (the current 90% lower bound [50]), and if ξ is as large as $\xi = 0.025$ (the central value from CHARM/CHARM II [51]), then the shift in the survival probability at the first oscillation dip can be as large as $\sim 40\%$. If the Fermilab-NUMI beam in

its high-energy mode [35] were aimed at a declination angle of 46° toward the planned Hyper-Kamiokande detector [36] in Kamioka, Japan (baseline 9120 km), such a shift would be visible after just one year of data taking, assuming a Mega-ton fiducial volume and 100% efficiency. The absence of any shift after 5 years of data taking would constrain ξ to [34]

$$|\xi| \leq \xi_0 \equiv 0.005 \,, \tag{3.1.8}$$

at the 99% confidence level.

We new look at how this potential limit on ξ would translate into constraints on new physics, in particular, on the couplings and masses of new particles. As mentioned above, the models must be those that distinguish among different generations. We consider the following four classes of models:

1. Models with a generation distinguishing Z' boson. This class includes gauged $L_e - L_\mu$, gauged $L_e - L_\tau$, gauged $B - \alpha L_e - \beta L_\mu - \gamma L_\tau$, and topcolor assisted technicolor.

2. Models with leptoquarks (scalar and vector). This class includes various Grand Unification Theory (GUT) models and extended technicolor (ETC).

3. The Supersymmetric Standard Model with R-parity violation.

4. Extended Higgs models. This class includes the Babu model, the Zee model, and various models with triplet Higgs, as well as the generation distinguishing Z' models listed above.

These classes will be discussed one by one in sections II through V. The constraints on these models will be compared with existing ones from LEP/SLD, the Tevatron, and other low energy experiments, and with those expected from direct searches for the new particles at the LHC. Concluding remarks will be presented in section VI.

3.2 Models with an extra Z' boson

Z' generically refers to any electrically neutral gauge boson corresponding to a flavor-diagonal generator of some new gauge group. Here, we are interested in models in which the Z' couples differently to different generations. The models we will consider are (A) gauged $L_e - L_\mu$ and $L_e - L_\tau$, (B) gauged $B - \alpha L_e - \beta L_\mu - \gamma L_\tau$, with $\alpha + \beta + \gamma = 3$, and (C) topcolor assisted technicolor.

3.2.1 Gauged $L_e - L_\mu$ and $L_e - L_\tau$

In Ref. [38], it was pointed out that the charges $L_e - L_\mu$, $L_e - L_\tau$, and $L_\mu - L_\tau$ are anomaly free within the particle content of the Standard Model, and therefore can be gauged. Models with these symmetries are recently receiving renewed attention in attempts to explain the large mixing angles observed in the neutrino sector [52]. Of these, gauged $L_e - L_\mu$ and $L_e - L_\tau$ affect neutrino oscillation in matter. These models necessarily possess a Higgs sector which also distinguishes among different lepton generations [53], but we will only consider the effect of the the extra gauge boson in this section and relegate the effect of the Higgs sector to a more generic discussion in section V.

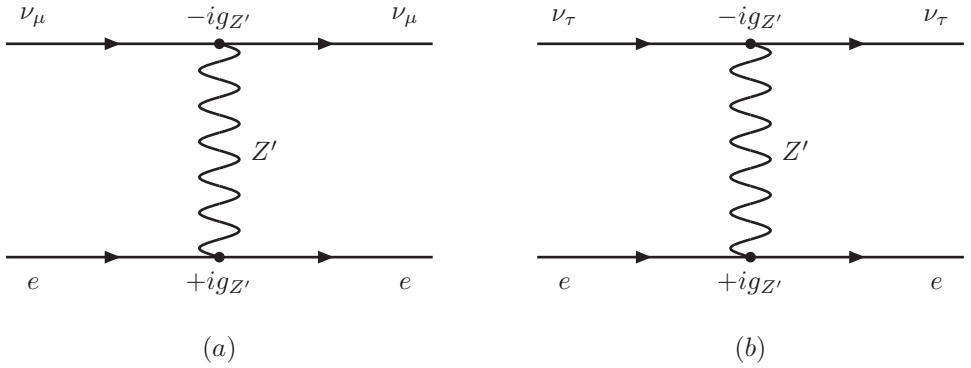

Figure 3.2.1: Diagrams that contribute to neutrino oscillation matter effects in (a) the gauged $L_e - L_\mu$ model, and (b) the gauged $L_e - L_\tau$ model.

The interaction Lagrangian for gauged $L_e - L_\ell$ ($\ell = \mu$ or τ) is given by

$$\mathcal{L} = g_{Z'} \left(\overline{e}\gamma^\mu e - \overline{\ell}\gamma^\mu \ell + \overline{\nu_{eL}}\gamma^\mu \nu_{eL} - \overline{\nu_{\ell L}}\gamma^\mu \nu_{\ell L} \right) Z'_\mu \, . \tag{3.2.1}$$

The diagrams that affect neutrino propagation in matter are shown in Fig. 3.2.1. (The exchange of the Z' between the ν_e and the electrons do not lead to new matter effects.) The forward scattering amplitude of the left-handed neutrino $\nu_{\ell L}$ ($\ell = \mu, \tau$) is

$$i\mathcal{M} = (ig_{Z'})(-ig_{Z'}) \langle \nu_{\ell L} | \overline{\nu_{\ell L}} \gamma^\mu \nu_{\ell L} | \nu_{\ell L} \rangle \left(\frac{ig_{\mu\nu}}{M^2_{Z'}} \right) \langle e | \overline{e} \gamma^\nu e | e \rangle \, . \tag{3.2.2}$$

The electrons in matter are non-relativistic, so only the time-like components of the currents need to be considered. Replacing $\langle e|\overline{e}\gamma^0 e|e\rangle = \langle e|e^\dagger e|e\rangle$ with N_e, the number density of electrons in matter, and $\langle \nu_{\ell L}|\overline{\nu_{\ell L}}\gamma^0 \nu_{\ell L}|\nu_{\ell L}\rangle = \langle \nu_{\ell L}|\nu^\dagger_{\ell L}\nu_{\ell L}|\nu_{\ell L}\rangle$ with $\phi^\dagger_{\nu_\ell}\phi_{\nu_\ell}$, where ϕ_{ν_ℓ} is the wave function of the left-handed neutrino $\nu_{\ell L}$, we obtain

$$i\mathcal{M} \;=\; i\frac{g^2_{Z'}}{M^2_{Z'}} \left(\phi^\dagger_{\nu_\ell}\phi_{\nu_\ell} \right) N_e \;\equiv\; -iV_{\nu_\ell} \left(\phi^\dagger_{\nu_\ell}\phi_{\nu_\ell} \right) \, . \tag{3.2.3}$$

Therefore, the effective potential felt by the neutrinos as they traverse matter can be identified as

$$V_{\nu_\ell} = -\frac{g^2_{Z'}}{M^2_{Z'}} N_e \, . \tag{3.2.4}$$

The effective ξ's for the $L_e - L_\mu$ and $L_e - L_\tau$ cases are

$$\begin{aligned} \xi_{L_e - L_\mu} &= -\frac{V_{\nu_\mu}}{V_{CC}} = +4\,\frac{(g^2_{Z'}/M^2_{Z'})}{(g^2/M^2_W)} = +\frac{1}{\sqrt{2}G_F}\left(\frac{g_{Z'}}{M_{Z'}}\right)^2 , \\ \xi_{L_e - L_\tau} &= +\frac{V_{\nu_\tau}}{V_{CC}} = -4\,\frac{(g^2_{Z'}/M^2_{Z'})}{(g^2/M^2_W)} = -\frac{1}{\sqrt{2}G_F}\left(\frac{g_{Z'}}{M_{Z'}}\right)^2 . \end{aligned} \tag{3.2.5}$$

Ignoring potential contributions from the Higgs sector, a bound on ξ of $|\xi| \leq \xi_0 = 0.005$ from Eq. (3.1.8) translates into:

$$\frac{M_{Z'}}{g_{Z'}} \geq \sqrt{\frac{1}{\sqrt{2}G_F\xi_0}} \approx 3500\,\text{GeV} \, , \tag{3.2.6}$$

	Λ_- (TeV) from $e^+e^- \to e^+e^-$	Λ_+ (TeV) from $e^+e^- \to \mu^+\mu^-$	Λ_+ (TeV) from $e^+e^- \to \tau^+\tau^-$	Reference
L3	10.1	14.4	7.6	[54]
OPAL	10.6	12.7	8.6	[55]
DELPHI	13.9	12.2	15.8	[56]
ALEPH	12.5	10.5	12.8	[57]

Table 3.1: The 95% confidence level lower bounds on the compositeness scale $\Lambda^{\pm}$ (TeV) from leptonic LEP/LEP2 data. Dividing by $\sqrt{4\pi}$ converts these limits to those on $(M_{Z'}/g_{z'})$.

for both the $L_e - L_\mu$ and $L_e - L_\tau$ cases.

The Z' in gauged $L_e - L_\ell$ ($\ell = \mu, \tau$) cannot be sought for at the LHC since they only couple to leptons. However, they can be produced in e^+e^- collisions and subsequently decay into e^+e^- or $\ell^+\ell^-$ pairs, and stringent contraints already exist from LEP/LEP2. The exchange of the Z' induces the following effective four-fermion interactions, relevant to e^+e^- colliders, among the charged leptons at energies far below the Z' mass:

$$\mathcal{L} = -\frac{g_{Z'}^2}{2M_{Z'}^2}\left(\overline{e}\gamma_\mu e\right)\left(\overline{e}\gamma^\mu e\right) + \frac{g_{z'}^2}{M_{Z'}^2}\left(\overline{e}\gamma_\mu e\right)\left(\overline{\ell}\gamma^\mu \ell\right) \ . \tag{3.2.7}$$

The LEP collaborations fit their data to

$$\mathcal{L} = -\frac{4\pi}{2\Lambda_-^2}\left(\overline{e}\gamma_\mu e\right)\left(\overline{e}\gamma^\mu e\right) + \frac{4\pi}{\Lambda_+^2}\left(\overline{e}\gamma_\mu e\right)\left(\overline{\ell}\gamma^\mu \ell\right) \ , \tag{3.2.8}$$

with the 95% confidence limits on $\Lambda_\pm$ shown in Table 3.1. The strongest constraint for the $L_e - L_\mu$ case comes from the $e^+e^- \to \mu^+\mu^-$ channel of L3, which translates to

$$\frac{M_{Z'}}{g_{Z'}} \geq 4.1\,\text{TeV} \ , \tag{3.2.9}$$

while that for the $L_e - L_\tau$ case comes from the $e^+e^- \to \tau^+\tau^-$ channel of DELPHI, which translates to

$$\frac{M_{Z'}}{g_{Z'}} \geq 4.5\,\text{TeV} \ . \tag{3.2.10}$$

Though these are the 95% confidence limits while that given in Eq. (3.2.6) is the 99% limit, it is clear that the bound on ξ will not lead to any improvement of already existing bounds from LEP/LEP2.

3.2.2 Gauged $B - (\alpha L_e + \beta L_\mu + \gamma L_\tau)$

In Refs. [39, 40, 41, 42], extensions of the SM gauge group to $SU(3)_C \times SU(2)_L \times U(1)_Y \times U(1)_X$ with $X = B - (\alpha L_e + \beta L_\mu + \gamma L_\tau)$ were considered. Again, the motivation was to explain the observed pattern of neutrino masses and mixings. The cases $(\alpha, \beta, \gamma) = (0, 0, 3)$, $(3, 0, 0)$, and $(0, \frac{3}{2}, \frac{3}{2})$ were considered, respectively, in Refs. [39], [40], and [41]. In all cases, the condition

$$\alpha + \beta + \gamma = 3 \tag{3.2.11}$$

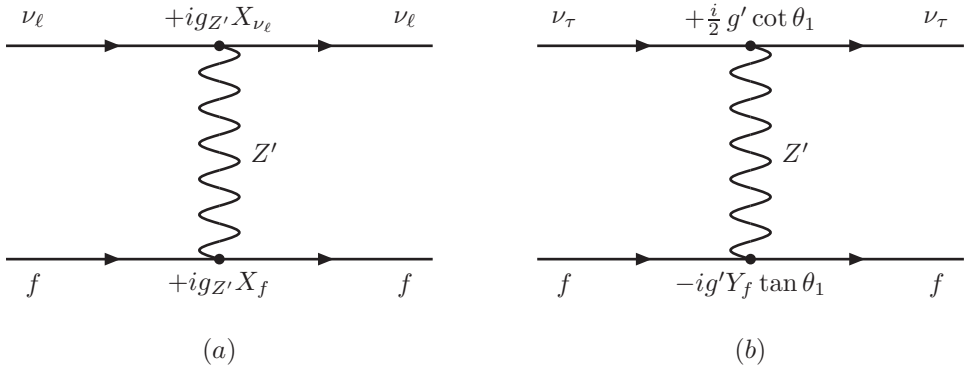

Figure 3.2.2: Diagrams that contribute to neutrino oscillation matter effects in (a) the gauged $X = B - \alpha L_e - \beta L_\mu - \gamma L_\tau$ model, $\ell = \{e, \mu, \tau\}$, $f = \{u, d, e\}$, and (b) topcolor assisted technicolor, $f = \{u_L, u_R, d_L, d_R, e_L, e_R\}$.

is required for anomaly cancellation within the SM plus right-handed neutrinos[1]. When $\alpha \neq \beta \neq \gamma$, the $U(1)_X$ gauge boson, *i.e.* the Z', couples to the three lepton generations differently, and can lead to extra neutrino oscillation matter effects. As in the gauged $L_e - L_\ell$ case, the Higgs sectors of these models also necessarily distinguish among the lepton generations, but we relegate the discussion of their effects to section V.

For generic values of (α, β, γ), the Z' couples to the quarks and leptons as

$$\mathcal{L}_{Z'} = g_{Z'} J_X^\mu Z'_\mu \,, \tag{3.2.12}$$

where

$$\begin{aligned} J_X^\mu &= \sum_f X_f (\bar{f}\gamma^\mu f) \\ &= \frac{1}{3}\sum_q (\,\bar{q}\gamma^\mu q\,) - \alpha\,(\,\bar{e}\gamma^\mu e + \overline{\nu_e}\gamma^\mu\nu_e\,) - \beta\,(\,\bar{\mu}\gamma^\mu\mu + \overline{\nu_\mu}\gamma^\mu\nu_\mu\,) - \gamma\,(\,\bar{\tau}\gamma^\mu\tau + \overline{\nu_\tau}\gamma^\mu\nu_\tau\,)\ . \end{aligned} \tag{3.2.13}$$

The forward scattering amplitude of the left-handed neutrino $\nu_{\ell L}$ ($\ell = e, \mu, \tau$) on matter fermion F ($F = p, n, e$) due to Z'-exchange (*cf.* Fig. 3.2.2a) is

$$i\mathcal{M}_F \;=\; (+ig_{Z'}X_{\nu_\ell})(+ig_{Z'})\,\langle\nu_{\ell L}|\overline{\nu_\ell}\gamma^\mu\nu_\ell|\nu_{\ell L}\rangle\left(\frac{ig_{\mu\nu}}{M_{Z'}^2}\right)\langle F|J_X^\nu|F\rangle\ . \tag{3.2.14}$$

Again, we can assume that the matter fermions are non-relativistic, so that only the time-like components of the currents need be considered. Then, we can make the replacements

$$\begin{aligned} \langle e|J_X^0|e\rangle &= -\alpha\langle e|e^\dagger e|e\rangle \;\to\; -\alpha N_e\ , \\ \langle p|J_X^0|p\rangle &= \frac{1}{3}\langle p|\left(u^\dagger u + d^\dagger d\right)|p\rangle \;\to\; \frac{1}{3}\left(2N_p + N_p\right) \;=\; N_p\ , \\ \langle n|J_X^0|n\rangle &= \frac{1}{3}\langle n|\left(u^\dagger u + d^\dagger d\right)|n\rangle \;\to\; \frac{1}{3}\left(N_n + 2N_n\right) \;=\; N_n\ , \end{aligned} \tag{3.2.15}$$

and

$$\langle\nu_{\ell L}|\overline{\nu_\ell}\gamma^0\nu_\ell|\nu_{\ell L}\rangle \;=\; \langle\nu_{\ell L}|\left(\nu_{\ell L}^\dagger\nu_{\ell L} + \nu_{\ell R}^\dagger\nu_{\ell R}\right)|\nu_{\ell L}\rangle \;=\; \langle\nu_{\ell L}|\nu_{\ell L}^\dagger\nu_{\ell L}|\nu_{\ell L}\rangle \;\to\; \phi_{\nu_\ell}^\dagger\phi_{\nu_\ell}\ , \tag{3.2.16}$$

[1]Only the right-handed neutrinos with non-zero X charge need to be included for anomaly cancellation.

which gives us

$$i\mathcal{M}_F \;=\; -iX_{\nu_\ell}\frac{g_{Z'}^2}{M_{Z'}^2}\left(\phi^\dagger_{\nu_\ell}\phi_{\nu_\ell}\right)\left(X_F N_F\right)\,, \tag{3.2.17}$$

where we have defined $X_p = X_n = 1$. Summing over $F = p, n, e$, we find:

$$\begin{aligned} i\mathcal{M} \;&=\; i\sum_{F=p,n,e}\mathcal{M}_F \\ &=\; -iX_{\nu_\ell}\frac{g_{Z'}^2}{M_{Z'}^2}\left(\phi^\dagger_{\nu_\ell}\phi_{\nu_\ell}\right)\left(\,N_p + N_n - \alpha N_e\,\right) \;=\; -i\,V_{\nu_\ell}\left(\phi^\dagger_{\nu_\ell}\phi_{\nu_\ell}\right)\,, \end{aligned} \tag{3.2.18}$$

where

$$V_{\nu_\ell} \equiv +X_{\nu_\ell}\frac{g_{Z'}^2}{M_{Z'}^2}\left(N_n + N_p - \alpha N_e\right) \tag{3.2.19}$$

can be identified as the effective potential experienced by the left-handed neutrino $\nu_{\ell L}$ as it travels through matter. Since the Earth is electrically neutral and is mostly composed of lighter elements, we can make the approximation $N_n \approx N_p = N_e \equiv N$, in which case

$$V_{\nu_\ell} \approx -X_{\nu_\ell}\frac{g_{Z'}^2}{M_{Z'}^2}(\alpha - 2)N\,. \tag{3.2.20}$$

The effective ξ is then

$$\xi_{(\alpha,\beta,\gamma)} \;=\; \frac{V_{\nu_\tau} - V_{\nu_\mu}}{V_{CC}} \;=\; -4(\alpha-2)(\beta-\gamma)\frac{(g_{Z'}/M_{Z'})^2}{(g/M_W)^2}\,. \tag{3.2.21}$$

When $\alpha = 2$, the contribution of the matter electrons is cancelled by those of the matter nucleons and $\xi_{(2,\beta,\gamma)}$ vanishes, regardless of the values of β and γ. When $\beta = \gamma$, the matter effects on ν_μ and ν_τ will be the same, again resulting in $\xi_{(\alpha,\beta,\beta)} = 0$, regardless of the value of α.

In Fig. 3.2.3, we plot the dependence of $\xi_{Z'}$ on the Z' mass for selected values of $g_{Z'}$ for the case $\alpha = \beta = 0$, $\gamma = 3$, namely, the Z' couples to $B - 3L_\tau$. In this case

$$\xi_{(0,0,3)} \;=\; -24\,\frac{(g_{Z'}/M_{Z'})^2}{(g/M_W)^2} \;=\; -\frac{6}{\sqrt{2}G_F}\left(\frac{g_{Z'}}{M_{Z'}}\right)^2\,. \tag{3.2.22}$$

Ignoring the possible contribution of the Higgs sector, a bound on ξ of $|\xi| \le \xi_0 = 0.005$ from Eq. (3.1.8) translates into:

$$\frac{M_{Z'}}{g_{Z'}} \ge \sqrt{\frac{6}{\sqrt{2}G_F\xi_0}} \approx 8500\,\mathrm{GeV}\,. \tag{3.2.23}$$

More generically, the bound on the Z' mass is

$$\frac{M_{Z'}}{g_{Z'}} \;\ge\; \sqrt{\frac{|(\alpha-2)(\beta-\gamma)|}{\sqrt{2}\,G_F\xi_0}} \;\approx\; \sqrt{|(\alpha-2)(\beta-\gamma)|}\times(3500\,\mathrm{GeV})\,. \tag{3.2.24}$$

This bound is plotted in Fig. 3.2.4 as a function of β for three different values of $g_{Z'}$, and two different values of α. The value of γ is fixed by the anomaly cancellation condition, Eq. (3.2.11), to $\gamma = 3 - \alpha - \beta$. The region of the $(\beta, M_{Z'})$ parameter space below each curve will be excluded.

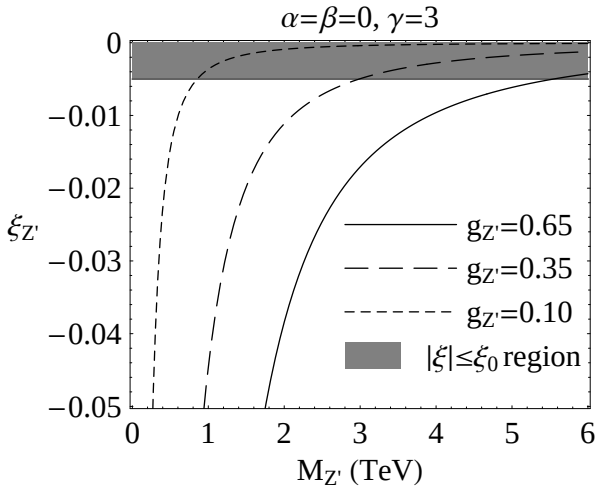

Figure 3.2.3: $\xi_{Z'}$ dependence on the Z' mass for the special case $\alpha = \beta = 0$, $\gamma = 3$.

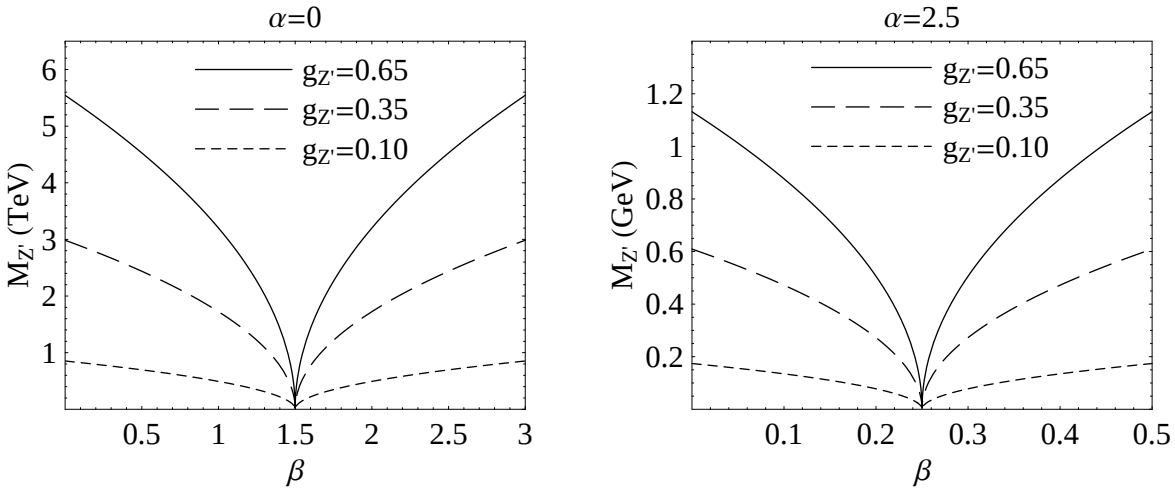

Figure 3.2.4: Lower bounds on Z' mass.

Let us now look at existing bounds. We limit our attention to the $\alpha = 0$ case, i.e. the Z' couples to $B - \beta L_\mu - \gamma L_\tau$, with $\beta + \gamma = 3$. In this case, the Z' can be produced in $p\bar{p}$ collisions and subsequently decay into $\mu^+\mu^-$ or $\tau^+\tau^-$ pairs. The exchange of the Z' in this case leads to the following four-fermion interactions, relevant to $p\bar{p}$ colliders, between the charged leptons and the light quarks at energies way below the Z' mass:

$$\mathcal{L} = +\frac{\beta g_{Z'}^2}{3M_{Z'}^2}\left(\bar{u}\gamma^\mu u + \bar{d}\gamma^\mu d\right)\left(\bar{\mu}\gamma_\mu \mu\right) + \frac{\gamma g_{Z'}^2}{3M_{Z'}^2}\left(\bar{u}\gamma^\mu u + \bar{d}\gamma^\mu d\right)\left(\bar{\tau}\gamma_\mu \tau\right) \ . \tag{3.2.25}$$

D0 has searched for the contact interaction

$$\mathcal{L} = +\frac{4\pi}{\Lambda_+^2}\left(\bar{u}\gamma^\mu u + \bar{d}\gamma^\mu d\right)\left(\bar{\mu}\gamma_\mu \mu\right) \tag{3.2.26}$$

(α, β, γ)	$g_{Z'}$	2σ (95%) limit from LEP/SLD [42]	95% limit from CDF [60]/D0 [59]	limit from $\lvert\xi\rvert \leq \xi_0$ (99%)
$(0, 0, 3)$	0.65	580 GeV	~ 1 TeV	5500 GeV
	0.35	220 GeV	~ 0.6 TeV	3000 GeV
$(0, \frac{3}{2}, \frac{3}{2})$	0.65	500 GeV	880 GeV	—
	0.35	—	470 GeV	—

Table 3.2: Current and possible lower bounds on the Z' mass in gauged $B - \alpha L_3 - \beta L_\mu - \gamma L_\tau$ models.

in its dimuon production data [59] and has set a 95% confidence level limit of

$$\Lambda_+ \geq 6.88\,\text{TeV} \; . \tag{3.2.27}$$

This translates into

$$\frac{M_{Z'}}{g_{Z'}} \geq \sqrt{|\beta|} \times (1.1\,\text{TeV}) \; . \tag{3.2.28}$$

CDF has searched for the production of a Z' followed by its decay into $\tau^+\tau^-$ pairs [60] and has set a 95% confidence level lower bound of

$$M_{Z'} \geq 400\,\text{GeV} \tag{3.2.29}$$

for a sequential Z' (i.e. a Z' with the exact same couplings to the fermions as the SM Z). Rescaling to account for the difference in couplings, we estimate

$$\frac{M_{Z'}}{g_{Z'}} \gtrsim \sqrt{|\gamma|} \times (1\,\text{TeV}) \; . \tag{3.2.30}$$

Limits on this model also exist from a global analysis of loop effects in LEP/SLD data [42], but they are weaker than the direct search limits from the Tevatron. In Table 3.2, we compare the bounds from LEP/SLD, CDF/D0, and the potential bounds from a measurement of ξ for two choices of (α, β, γ), and two choices for the value of $g_{Z'}$. For the $(\alpha, \beta, \gamma) = (0, 0, 3)$ case, we can expect a significant improvement over current bounds.

The sensitivity of the LHC to Z's has been analyzed assuming Z' decay into e^+e^- or $\mu^+\mu^-$ pairs, or 2 jets [62]. For a sequential Z', the LHC is sensitive to masses as heavy as 5 TeV with 100 fb^{-1} of integrated luminosity. The Z' of the $(\alpha, \beta, \gamma) = (0, 0, 3)$ model, however, decays mostly into $\tau^+\tau^-$, which will not provide as clean a signal as decays into the lighter charged lepton pairs. Ref. [43] estimates that if $g_{Z'} \sim g' \approx 0.35$, then the LHC reach will be up to about 1 TeV with 100 fb^{-1}. If this estimate is correct, the potential bound on $M_{Z'}$ from neutrino oscillation may be better than that from the LHC. A complete detector analysis may show that the actual reach of the LHC is somewhat higher, but even then we can expect the neutrino oscillation bound to be competitive with the LHC bound for the $(0, 0, 3)$ model.

3.2.3 Topcolor Assisted Technicolor

Another example of a model with a Z' which distinguishes among different generations is topcolor assisted technicolor [44, 45]. Models of this class are hybrids of topcolor and technicolor: the topcolor interactions generate the large top-mass (and a fraction of the W and Z masses), while the technicolor interactions generate (the majority of) the W and Z masses. The models include

	$SU(3)_s$	$SU(3)_w$	$U(1)_s$	$U(1)_w$	$SU(2)_L$
$(t,b)_L$	3	1	$\frac{1}{6}$	0	2
$(t,b)_R$	3	1	$\left(\frac{2}{3},-\frac{1}{3}\right)$	0	1
$(\nu_\tau,\tau^-)_L$	1	1	$-\frac{1}{2}$	0	2
τ_R^-	1	1	-1	0	1
$(c,s)_L$, $(u,d)_L$	1	3	0	$\frac{1}{6}$	2
$(c,s)_R$, $(u,d)_R$	1	3	0	$\left(\frac{2}{3},-\frac{1}{3}\right)$	1
$(\nu_\mu,\mu^-)_L$, $(\nu_e,e^-)_L$	1	1	0	$-\frac{1}{2}$	2
μ_R^-, e_R^-	1	1	0	-1	1

Table 3.3: Charge assignments of the ordinary fermions. The $U(1)$ charges are equal to the SM hypercharges normalized to $Q_{em} = I_3 + Y$.

a Z' in the topcolor sector, the interactions of which helps the top to condense, but prevents the bottom from doing so also. To extract the interactions of this Z' relevant to our discussion, we need to look at the model in some detail.

Though there are several different versions of topcolor assisted technicolor, we consider here the simplest in which the quarks and leptons transform under the gauge group

$$SU(3)_s \times SU(3)_w \times U(1)_s \times U(1)_w \times SU(2)_L \tag{3.2.31}$$

with coupling constants g_{3s}, g_{3w}, g_{1s}, g_{1w}, and g. It is assumed that $g_{3s} \gg g_{3w}$ and $g_{1s} \gg g_{1w}$. $SU(2)_L$ is the usual weak-isospin gauge group of the SM with coupling constant g. The charge assignments of the three generation of ordinary fermions under these gauge groups are given in Table 3.3. Note that each generation must transform non-trivially under only one of the $SU(3)$'s and one of the $U(1)$'s, and that those charges are the same as that of the SM color, and hypercharge Y (normalized to $Q_{em} = I_3 + Y$). This ensures anomaly cancellation.

At scale $\Lambda \sim 1$ TeV, technicolor, which is included in the model to generate the W and Z masses, is assumed to become strong and generate a condensate (of something which is left unspecified) which breaks the two $SU(3)$'s and the two $U(1)$'s to their diagonal subgroups:

$$SU(3)_s \times SU(3)_w \to SU(3)_c\ , \qquad U(1)_s \times U(1)_w \to U(1)_Y\ , \tag{3.2.32}$$

which we identify with the usual SM color and hypercharge groups. The massless unbroken SU(3) gauge bosons (the gluons G_μ^a) and the massive broken SU(3) gauge bosons (the so called *colorons* C_μ^a) are related to the original $SU(3)_s \times SU(3)_w$ gauge fields $X_{s\mu}^a$ and $X_{w\mu}^a$ by

$$\begin{aligned} C_\mu &= X_{s\mu}\cos\theta_3 - X_{w\mu}\sin\theta_3 \\ G_\mu &= X_{s\mu}\sin\theta_3 + X_{w\mu}\cos\theta_3 \end{aligned} \tag{3.2.33}$$

where we have suppressed the color indices, and

$$\tan\theta_3 = \frac{g_{3w}}{g_{3s}}\ . \tag{3.2.34}$$

The currents to which the gluons and colorons couple to are:

$$g_{3s}J^\mu_{3s}X_{s\mu} + g_{3w}J^\mu_{3w}X_{w\mu} = g_3\left(\cot\theta_3 J^\mu_{3s} - \tan\theta_3 J^\mu_{3w}\right)C_\mu + g_3\left(J^\mu_{3s} + J^\mu_{3w}\right)G_\mu \ , \tag{3.2.35}$$

where

$$\frac{1}{g_3^2} = \frac{1}{g_{3s}^2} + \frac{1}{g_{3w}^2} \ . \tag{3.2.36}$$

Since the quarks carry only one of the $SU(3)$ charges, we can identify

$$J^\mu_3 = J^\mu_{3s} + J^\mu_{3w} \tag{3.2.37}$$

as the QCD color current, and g_3 as the QCD coupling constant.

Similarly, the massless unbroken U(1) gauge boson B_μ and the massive broken U(1) gauge boson Z'_μ are related to the original $U(1)_s \times U(1)_w$ gauge fields $Y_{s\mu}$ and $Y_{w\mu}$ by

$$\begin{aligned} Z'_\mu &= Y_{s\mu}\cos\theta_1 - Y_{w\mu}\sin\theta_1 \\ B_\mu &= Y_{s\mu}\sin\theta_1 + Y_{w\mu}\cos\theta_1 \end{aligned} \tag{3.2.38}$$

where

$$\tan\theta_1 = \frac{g_{1w}}{g_{1s}} \ . \tag{3.2.39}$$

The currents to which the B_μ and Z'_μ couple to are:

$$g_{1s}J^\mu_{1s}Y_{s\mu} + g_{1w}J^\mu_{1w}Y_{w\mu} = g_1\left(\cot\theta_1 J^\mu_{1s} - \tan\theta_1 J^\mu_{1w}\right)Z'_\mu + g_1\left(J^\mu_{1s} + J^\mu_{1w}\right)B_\mu \ , \tag{3.2.40}$$

where

$$\frac{1}{g_1^2} = \frac{1}{g_{1s}^2} + \frac{1}{g_{1w}^2} \ . \tag{3.2.41}$$

Again, since the fermions carry only one of the $U(1)$ charges, we can identify

$$J^\mu_1 = J^\mu_{1s} + J^\mu_{1w} \tag{3.2.42}$$

as the SM hypercharge current, and g_1 as the SM hypercharge coupling constant g'. Note that the interactions of the colorons and the Z' with the third generation fermions are strong, while their interactions with the first and second generation fermions are weak. This results in the formation of a top-condensate which accounts for the large mass of the top quark.[2]

Therefore, the interaction of the Z' in this model with the quarks and leptons is given by

$$\mathcal{L} = g'\left(\cot\theta_1 J^\mu_{1s} - \tan\theta_1 J^\mu_{1w}\right)Z'_\mu \ , \tag{3.2.43}$$

where g' is the SM hypercharge coupling, and

$$\begin{aligned} J^\mu_{1s} &= \frac{1}{6}\left(\bar{t}_L\gamma^\mu t_L + \bar{b}_L\gamma^\mu b_L\right) + \frac{2}{3}\bar{t}_R\gamma^\mu t_R - \frac{1}{3}\bar{b}_R\gamma^\mu b_R - \frac{1}{2}\left(\bar{\tau}_L\gamma^\mu\tau_L + \bar{\nu}_{\tau L}\gamma^\mu\nu_{\tau L}\right) - \bar{\tau}_R\gamma^\mu\tau_R \ , \\ J^\mu_{1w} &= \frac{1}{6}\left(\bar{c}_L\gamma^\mu c_L + \bar{s}_L\gamma^\mu s_L\right) + \frac{2}{3}\bar{c}_R\gamma^\mu c_R - \frac{1}{3}\bar{s}_R\gamma^\mu s_R - \frac{1}{2}\left(\bar{\mu}_L\gamma^\mu\mu_L + \bar{\nu}_{\mu L}\gamma^\mu\nu_{\mu L}\right) - \bar{\mu}_R\gamma^\mu\mu_R \\ &+ \frac{1}{6}\left(\bar{u}_L\gamma^\mu u_L + \bar{d}_L\gamma^\mu d_L\right) + \frac{2}{3}\bar{u}_R\gamma^\mu u_R - \frac{1}{3}\bar{d}_R\gamma^\mu d_R - \frac{1}{2}\left(\bar{e}_L\gamma^\mu e_L + \bar{\nu}_{eL}\gamma^\mu\nu_{eL}\right) - \bar{e}_R\gamma^\mu e_R \ . \end{aligned}$$

[2]The Z'-exchange interaction in the $t\bar{t}$ channel is attractive, but that in the $b\bar{b}$ channel is repulsive. This repulsion is assumed to be strong enough to counter the attraction due to the colorons and prevent the bottom from condensing.

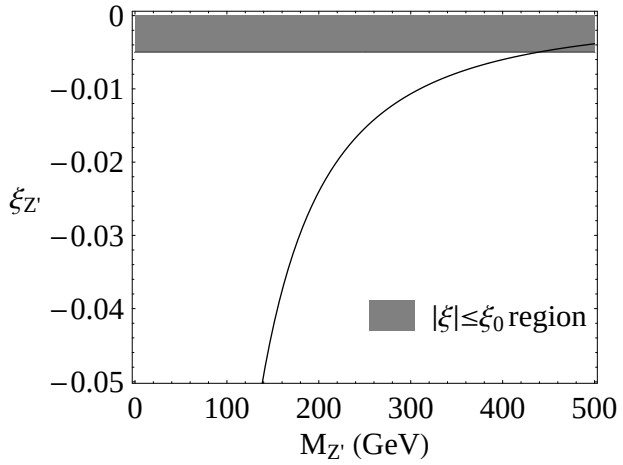

Figure 3.2.5: ξ_{TT} dependence on the Z' mass in the top color assisted technicolor model.

(3.2.44)

The exchange of the Z' leads to the current-current interaction

$$\frac{1}{2}\left(\cot\theta_1 J_{1s} - \tan\theta_1 J_{1w}\right)\left(\cot\theta_1 J_{1s} - \tan\theta_1 J_{1w}\right) \ , \tag{3.2.45}$$

the $J_{1s}J_{1s}$ part of which does not contribute to neutrino oscillations on the Earth, while the $J_{1w}J_{1w}$ part is suppressed relative to the $J_{1w}J_{1s}$ part by a factor of $\tan^2\theta_1 \ll 1$. Therefore, we only need to consider the $J_{1s}J_{1w}$ interaction which only affects the propagation of $\nu_{\tau L}$ (*cf.* Fig. 3.2.2b). The forward scattering amplitude of $\nu_{\tau L}$ against fermion $F = p, n, e$ is given by

$$\begin{aligned}
i\mathcal{M} &= (-ig'\cot\theta_1)(+ig'\tan\theta_1)\langle\nu_{\tau L}|\left(-\frac{1}{2}\,\overline{\nu_\tau}\gamma^\mu P_L\nu_\tau\right)|\nu_{\tau L}\rangle\ \frac{ig_{\mu\nu}}{M_{Z'}^2} \\
&\quad \times\langle F|\left[\overline{u}\gamma^\nu\left(\frac{1}{6}P_L+\frac{2}{3}P_R\right)u + \overline{d}\gamma^\nu\left(\frac{1}{6}P_L-\frac{1}{3}P_R\right)d + \overline{e}\gamma^\nu\left(-\frac{1}{2}P_L-P_R\right)e\right]|F\rangle \\
&\to -\frac{ig'^2}{2M_{Z'}^2}\left(\phi^\dagger_{\nu_\tau}\phi_{\nu_\tau}\right)\left[\frac{1}{2}\left(\frac{1}{6}+\frac{2}{3}\right)(2N_p+N_n)+\frac{1}{2}\left(\frac{1}{6}-\frac{1}{3}\right)(N_p+2N_n)+\frac{1}{2}\left(-\frac{1}{2}-1\right)N_e\right] \\
&= -\frac{ig'^2}{2M_{Z'}^2}\left(\phi^\dagger_{\nu_\tau}\phi_{\nu_\tau}\right)\left(\frac{3}{4}N_p+\frac{1}{4}N_n-\frac{3}{4}N_e\right) \\
&= -\frac{ig'^2}{8M_{Z'}^2}\left(\phi^\dagger_{\nu_\tau}\phi_{\nu_\tau}\right)N_n \\
&\approx -i\left(\frac{g'^2}{M_{Z'}^2}\right)\frac{N}{8}\left(\phi^\dagger_{\nu_\tau}\phi_{\nu_\tau}\right) \ = \ -iV_{\nu_\tau}\left(\phi^\dagger_{\nu_\tau}\phi_{\nu_\tau}\right) \ .
\end{aligned} \tag{3.2.46}$$

Note that the angle θ_1 has vanished from this expression and the only unknown parameter here is the Z' mass.

The effective potentials felt by the different neutrino flavors are

$$V_{\nu_e} \ = \ V_{\nu_\mu} \ = \ 0 \ , \qquad V_{\nu_\tau} \ = \ +\frac{N}{8}\frac{g'^2}{M_{Z'}^2} \ , \tag{3.2.47}$$

and the effectivie ξ is

$$\xi_{TT} = \frac{V_{\nu_\tau} - V_{\nu_\mu}}{V_{CC}} = \frac{1}{2}\frac{(g'/M_{Z'})^2}{(g/M_W)^2} = \frac{1}{2}\tan^2\theta_W \frac{M_W^2}{M_{Z'}^2} = \frac{1}{2}\sin^2\theta_W \frac{M_Z^2}{M_{Z'}^2} \; . \tag{3.2.48}$$

The dependence of ξ_{TT} on the Z' mass is shown in Fig. 3.2.5. The limit $|\xi_{TT}| \leq \xi_0 = 0.005$ in this case translates to:

$$M_{Z'} \geq M_Z \sqrt{\frac{\sin^2\theta_W}{2\xi_0}} \approx 440\,\mathrm{GeV} \; . \tag{3.2.49}$$

This potential limit from the measurement of ξ is much weaker than what is already available from precision electroweak data [45], or from the direct search for $p\bar{p} \to Z'X \to \tau^+\tau^- X$ at CDF mentioned earlier [60].

3.3 Generation Non-Diagonal Leptoquarks

Leptoquarks are particles carrying both baryon number B, and lepton number L. They occur in various extensions of the SM such as Grand Unification Theories (GUT's) or Extended Technicolor (ETC). In GUT models, the quarks and leptons are placed in the same multiplet of the GUT group. The massive gauge bosons which correspond to the broken generators of the GUT group which change quarks into leptons, and vice versa, are vector leptoquarks. In ETC models, the technicolor interaction will bind the techniquarks and the technileptons into scalar or vector bound states. These leptoquark states couple to the ordinary quarks and leptons through ETC interactions.

The interactions of leptoquarks with ordinary matter can be described in a model-independent fashion by an effective low-energy Lagrangian as discussed in Ref. [63]. Assuming the fermionic content of the SM, the most general dimensionless $SU(3)_C \times SU(2)_L \times U(1)_Y$ invariant couplings of scalar and vector leptoquarks satisfying baryon and lepton number conservation is given by:

$$\mathcal{L} = \mathcal{L}_{F=2} + \mathcal{L}_{F=0} \; , \tag{3.3.1}$$

where

$$\begin{aligned}
\mathcal{L}_{F=2} &= \Big[g_{1L}\,\overline{q_L^c} i\tau_2 \ell_L + g_{1R}\,\overline{u_R^c} e_R\Big] S_1 + \tilde{g}_{1R}\Big[\overline{d_R^c} e_R\Big]\tilde{S}_1 \\
&\quad + g_{3L}\Big[\overline{q_L^c} i\tau_2 \vec{\tau} \ell_L\Big]\vec{S}_3 \\
&\quad + \Big[g_{2L}\,\overline{d_R^c}\gamma^\mu \ell_L + g_{2R}\,\overline{q_L^c}\gamma^\mu e_R\Big] V_{2\mu} + \tilde{g}_{2L}\Big[\overline{u_R^c}\gamma^\mu \ell_L\Big]\tilde{V}_{2\mu} + h.c. \; ,
\end{aligned} \tag{3.3.2}$$

$$\begin{aligned}
\mathcal{L}_{F=0} &= \Big[h_{2L}\,\overline{u_R}\ell_L + h_{2R}\,\overline{q_L} i\tau_2 e_R\Big] S_2 + \tilde{h}_{2L}\Big[\overline{d_R}\ell_L\Big]\tilde{S}_2 \\
&\quad + \Big[h_{1L}\,\overline{q_L}\gamma^\mu \ell_L + h_{1R}\,\overline{d_R}\gamma^\mu e_R\Big] V_{1\mu} + \tilde{h}_{1R}\Big[\overline{u_R}\gamma^\mu e_R\Big]\tilde{V}_{1\mu} \\
&\quad + h_{3L}\Big[\overline{q_L}\vec{\tau}\gamma^\mu \ell_L\Big]\vec{V}_{3\mu} + h.c. \; .
\end{aligned} \tag{3.3.3}$$

Here, the scalar and vector leptoquark fields are denoted by S and V, respectively, their subscripts indicating the dimension of their $SU(2)_L$ representation. The same index is attached to

their respective coupling constants, the g's and h's, with the extra subscript L or R indicating the chirality of the lepton involved in the interaction. For simplicity, color, weak isospin, and generation indices have been suppressed. The leptoquarks $S_1, \tilde{S}_1, \vec{S}_3, V_2, \tilde{V}_2$ carry fermion number $F = 3B + L = -2$, while the leptoquarks $S_2, \tilde{S}_2, V_1, \tilde{V}_1, \vec{V}_3$ have $F = 0$.

Rewriting the fermion doublets and the leptoquark multiplets in terms of the individual component fields, Eqs. (3.3.2) and (3.3.3) are expanded as follows:

$$\begin{aligned}
\mathcal{L}_{F=2} &= \Big[g_{1L}(\overline{u_L^c}e_L - \overline{d_L^c}\nu_L) + g_{1R}(\overline{u_R^c}e_R)\Big]S_1^0 + \tilde{g}_{1R}\Big[\overline{d_R^c}e_R\Big]\tilde{S}_1^0 \\
&\quad + \Big[g_{2L}(\overline{d_R^c}\gamma^\mu e_L) + g_{2R}(\overline{d_L^c}\gamma^\mu e_R)\Big]V_{2\mu}^+ + \Big[g_{2L}(\overline{d_R^c}\gamma^\mu \nu_L) + g_{2R}(\overline{u_L^c}\gamma^\mu e_R)\Big]V_{2\mu}^- \\
&\quad + \tilde{g}_{2L}\Big[(\overline{u_R^c}\gamma^\mu e_L)\tilde{V}_{2\mu}^+ + (\overline{u_R^c}\gamma^\mu \nu_L)\tilde{V}_{2\mu}^-\Big] \\
&\quad + g_{3L}\Big[-\sqrt{2}(\overline{d_L^c}e_L)S_3^+ - (\overline{u_L^c}e_L + \overline{d_L^c}\nu_L)S_3^0 + \sqrt{2}(\overline{u_L^c}\nu_L)S_3^-\Big] + h.c.\,, \qquad (3.3.4)
\end{aligned}$$

$$\begin{aligned}
\mathcal{L}_{F=0} &= \Big[h_{2L}(\overline{u_R}e_L) + h_{2R}(\overline{u_L}e_R)\Big]S_2^+ + \Big[h_{2L}(\overline{u_R}\nu_L) - h_{2R}(\overline{d_L}e_R)\Big]S_2^- \\
&\quad + \tilde{h}_{2L}\Big[(\overline{d_R}e_L)\tilde{S}_2^+ + (\overline{d_R}\nu_L)\tilde{S}_2^-\Big] \\
&\quad + \Big[h_{1L}(\overline{u_L}\gamma^\mu \nu_L + \overline{d_L}\gamma^\mu e_L) + h_{1R}(\overline{d_R}\gamma^\mu e_R)\Big]V_{1\mu}^0 + \tilde{h}_{1R}\Big[\overline{u_R}\gamma^\mu e_R\Big]\tilde{V}_{1\mu}^0 \\
&\quad + h_{3L}\Big[\sqrt{2}(\overline{u_L}\gamma^\mu e_L)V_{3\mu}^+ + (\overline{u_L}\gamma^\mu \nu_L - \overline{d_L}\gamma^\mu e_L)V_{3\mu}^0 + \sqrt{2}(\overline{d_L}\gamma^\mu \nu_L)V_{3\mu}^-\Big] + h.c. \qquad (3.3.5)
\end{aligned}$$

Superscripts indicate the weak isospin of each field, not the electromagnetic charge. For fields with subscript 1, the superscript 0 is redundant and may be dropped. The quantum numbers and couplings of the various leptoquarks fields are summarized in Table 3.4. Note that the scalar $\tilde{S}_1$ and the vector $\tilde{V}_{1\mu}$ do not couple to the neutrinos, so they are irrelevant to our discussion and will not be considered further. The isospin plus components of the remaining leptoquarks, namely S_2^+, $\tilde{S}_2^+$, S_3^+, $V_{2\mu}^+$, $\tilde{V}_{2\mu}^+$, and $V_{3\mu}^+$, do not couple to the neutrinos either, but we will keep them in our Lagrangian since their coupling constants are common with the other components that do couple, and are important in understanding how the couplings are constrained by neutrinoless experiments.

Since the leptoquarks must distinguish among different generation fermions to contribute to neutrino oscillation matter effects, we generalize their interactions by allowing the coupling constants to depend on the generations of the quarks and leptons that couple to each leptoquark:

$$\begin{aligned}
\mathcal{L}_{F=2} &= \Big[g_{1L}^{ij}(\overline{u_{iL}^c}e_{jL} - \overline{d_{iL}^c}\nu_{jL}) + g_{1R}^{ij}(\overline{u_{iR}^c}e_{jR})\Big]S_1^0 \\
&\quad + \Big[g_{2L}^{ij}(\overline{d_{iR}^c}\gamma^\mu e_{jL}) + g_{2R}^{ij}(\overline{d_{iL}^c}\gamma^\mu e_{jR})\Big]V_{2\mu}^+ + \Big[g_{2L}^{ij}(\overline{d_{iR}^c}\gamma^\mu \nu_{jL}) + g_{2R}^{ij}(\overline{u_{iL}^c}\gamma^\mu e_{jR})\Big]V_{2\mu}^- \\
&\quad + \tilde{g}_{2L}^{ij}\Big[(\overline{u_{iR}^c}\gamma^\mu e_{jL})\tilde{V}_{2\mu}^+ + (\overline{u_{iR}^c}\gamma^\mu \nu_{jL})\tilde{V}_{2\mu}^-\Big] \\
&\quad + g_{3L}^{ij}\Big[-\sqrt{2}(\overline{d_{iL}^c}e_{jL})S_3^+ - (\overline{u_{iL}^c}e_{jL} + \overline{d_{iL}^c}\nu_{jL})S_3^0 + \sqrt{2}(\overline{u_{iL}^c}\nu_{jL})S_3^-\Big] + h.c.\,, \qquad (3.3.6)
\end{aligned}$$

Leptoquark		Spin	F	$SU(3)_C$	I_3	Y	Q_{em}	Allowed Couplings
S_1	S_1^0	0	-2	$\bar{3}$	0	$\frac{1}{3}$	$\frac{1}{3}$	$g_{1L}(\overline{u_L^c}e_L - \overline{d_L^c}\nu_L)$, $g_{1R}(\overline{u_R^c}e_R)$
$\tilde{S}_1$	$\tilde{S}_1^0$	0	-2	$\bar{3}$	0	$\frac{4}{3}$	$\frac{4}{3}$	$\tilde{g}_{1R}(\overline{d_R^c}e_R)$
$V_{2\mu}$	$V_{2\mu}^+$	1	-2	$\bar{3}$	$+\frac{1}{2}$	$\frac{5}{6}$	$\frac{4}{3}$	$g_{2L}(\overline{d_R^c}\gamma^\mu e_L)$, $g_{2R}(\overline{d_L^c}\gamma^\mu e_R)$
	$V_{2\mu}^-$				$-\frac{1}{2}$		$\frac{1}{3}$	$g_{2L}(\overline{d_R^c}\gamma^\mu \nu_L)$, $g_{2R}(\overline{u_L^c}\gamma^\mu e_R)$
$\tilde{V}_{2\mu}$	$\tilde{V}_{2\mu}^+$	1	-2	$\bar{3}$	$+\frac{1}{2}$	$-\frac{1}{6}$	$\frac{1}{3}$	$\tilde{g}_{2L}(\overline{u_R^c}\gamma^\mu e_L)$
	$\tilde{V}_{2\mu}^-$				$-\frac{1}{2}$		$-\frac{2}{3}$	$\tilde{g}_{2L}(\overline{u_R^c}\gamma^\mu \nu_L)$
$\vec{S}_3$	S_3^+	0	-2	$\bar{3}$	$+1$	$\frac{1}{3}$	$\frac{4}{3}$	$-\sqrt{2}g_{3L}(\overline{d_L^c}e_L)$
	S_3^0				0		$\frac{1}{3}$	$-g_{3L}(\overline{u_L^c}e_L + \overline{d_L^c}\nu_L)$
	S_3^-				-1		$-\frac{2}{3}$	$\sqrt{2}g_{3L}(\overline{u_L^c}\nu_L)$
S_2	S_2^+	0	0	3	$+\frac{1}{2}$	$\frac{7}{6}$	$\frac{5}{3}$	$h_{2L}(\overline{u_R}e_L), h_{2R}(\overline{u_L}e_R)$
	S_2^-				$-\frac{1}{2}$		$\frac{2}{3}$	$h_{2L}(\overline{u_R}\nu_L), -h_{2R}(\overline{d_L}e_R)$
$\tilde{S}_2$	$\tilde{S}_2^+$	0	0	3	$+\frac{1}{2}$	$\frac{1}{6}$	$\frac{2}{3}$	$\tilde{h}_{2L}(\overline{d_R}e_L)$
	$\tilde{S}_2^-$				$-\frac{1}{2}$		$-\frac{1}{3}$	$\tilde{h}_{2L}(\overline{d_R}\nu_L)$
$V_{1\mu}$	$V_{1\mu}^0$	1	0	3	0	$\frac{2}{3}$	$\frac{2}{3}$	$h_{1L}(\overline{u_L}\gamma^\mu\nu_L + \overline{d_L}\gamma^\mu e_L)$, $h_{1R}(\overline{d_R}\gamma^\mu e_R)$
$\tilde{V}_{1\mu}$	$\tilde{V}_{1\mu}^0$	1	0	3	0	$\frac{5}{3}$	$\frac{5}{3}$	$\tilde{h}_{1R}(\overline{u_R}\gamma^\mu e_R)$
$\vec{V}_{3\mu}$	$V_{3\mu}^+$	1	0	3	$+1$	$\frac{2}{3}$	$\frac{5}{3}$	$\sqrt{2}h_{3L}(\overline{u_L}\gamma^\mu e_L)$
	$V_{3\mu}^0$				0		$\frac{2}{3}$	$h_{3L}(\overline{u_L}\gamma^\mu\nu_L - \overline{d_L}\gamma^\mu e_L)$
	$V_{3\mu}^-$				-1		$-\frac{1}{3}$	$\sqrt{2}h_{3L}(\overline{d_L}\gamma^\mu\nu_L)$

Table 3.4: Quantum numbers of scalar and vector leptoquarks with $SU(3)_C \times SU(2)_L \times U(1)_Y$ invariant couplings to quark-lepton pairs ($Q_{\rm em} = I_3 + Y$).

$$
\begin{aligned}
\mathcal{L}_{F=0} \;=\; & \Big[h_{2L}^{ij}(\overline{u_{iR}}e_{jL}) + h_{2R}^{ij}(\overline{u_{iL}}e_{jR})\Big]S_2^+ + \Big[h_{2L}^{ij}(\overline{u_{iR}}\nu_{jL}) - h_{2R}^{ij}(\overline{d_{iL}}e_{jR})\Big]S_2^- \\
& + \tilde{h}_{2L}^{ij}\Big[(\overline{d_{iR}}e_{jL})\tilde{S}_2^+ + (\overline{d_{iR}}\nu_{jL})\tilde{S}_2^-\Big] \\
& + \Big[h_{1L}^{ij}(\overline{u_{iL}}\gamma^\mu\nu_{jL} + \overline{d_{iL}}\gamma^\mu e_{jL}) + h_{1R}^{ij}(\overline{d_{iR}}\gamma^\mu e_{jR})\Big]V_{1\mu}^0 \\
& + h_{3L}^{ij}\Big[\sqrt{2}(\overline{u_{iL}}\gamma^\mu e_{jL})V_{3\mu}^+ + (\overline{u_{iL}}\gamma^\mu\nu_{jL} - \overline{d_{iL}}\gamma^\mu e_{jL})V_{3\mu}^0 + \sqrt{2}(\overline{d_{iL}}\gamma^\mu\nu_{jL})V_{3\mu}^-\Big] + h.c.\,.
\end{aligned}
\tag{3.3.7}
$$

Here, i is the quark generation number, and j is the lepton generation number. Summation over repeated indices is assumed. The interactions that contribute to neutrino oscillation matter effects are those with indices $(ij) = (12)$ and $(ij) = (13)$. It is often assumed in the literature that generation non-diagonal couplings are absent to account for the non-observation of flavor changing neutral currents and lepton flavor violation. However, the constraints from such rare processes are always on *products of different* (ij)*-couplings* and not on the *individual* non-diagonal couplings by themselves. For instance, non-observation of the decay $K_L \to \bar{e}\mu$ constrains the product of (12) and (21) couplings, but not the (12) and (21) couplings separately, which allows one of them to be sizable if the other is small. Constraints on the individual (12) and (13) couplings actually come from precision measurements of *flavor conserving* processes, such as $R_\pi = \Gamma(\pi \to \mu\nu_\mu)/\Gamma(\pi \to e\nu_e)$ which constrains the square of the (12) coupling, and those constraints are not yet that strong [64].

In the following, we calculate the effective value of ξ induced by the exchange of these leptoquarks. The leptoquark fields are naturally grouped into pairs from the way they couple to the

quarks and leptons: $(S_1, \vec{S}_3)$, $(S_2, \tilde{S}_2)$, $(V_2, \tilde{V}_2)$, and $(V_1, \vec{V}_3)$. We treat each of these pairs in turn, and then discuss the potential bounds on the leptoquark couplings and masses.

3.3.1 S_1 and $\vec{S}_3$ leptoquarks

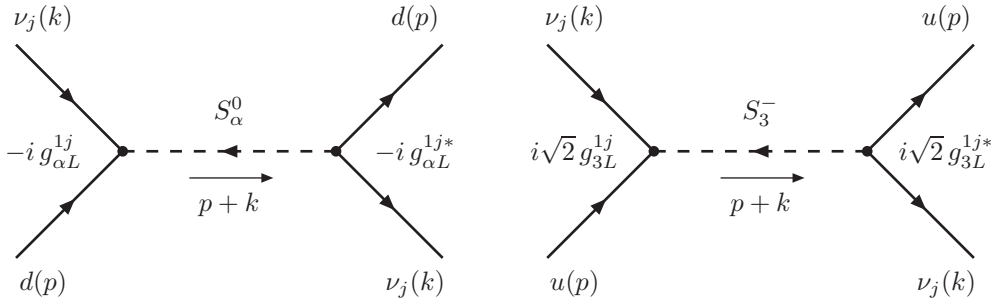

$(a)\ \alpha = 1, 3$ $\qquad$ (b)

Figure 3.3.1: Diagrams contributing to neutrino oscillation matter effects from the exchange of (a) S_1^0 or the isospin 0 component of $\vec{S}_3$, and (b) the isospin -1 component of $\vec{S}_3$. The EM charge $Q_{em} = I_3 + Y$ for S_1^0 and S_3^0 are $+\frac{1}{3}$, while that for S_3^- is $-\frac{2}{3}$.

The $(ij) = (12)$ and (13) interactions of the leptoquarks S_1 and $\vec{S}_3$ are, respectively,

$$\mathcal{L} = -g_{1L}^{12}(\overline{d_L^c}\nu_{\mu L})S_1 - g_{1L}^{13}(\overline{d_L^c}\nu_{\tau L})S_1 + h.c.\ , \tag{3.3.8}$$

and

$$\mathcal{L} \;=\; g_{3L}^{12}\left[-(\overline{d_L^c}\nu_{\mu L})S_3^0 + \sqrt{2}(\overline{u_L^c}\nu_{\mu L})S_3^-\right] + g_{3L}^{13}\left[-(\overline{d_L^c}\nu_{\tau L})S_3^0 + \sqrt{2}(\overline{u_L^c}\nu_{\tau L})S_3^-\right] + h.c. \tag{3.3.9}$$

The interactions described by Eqs. (3.3.8) and (3.3.9) can be written in a common general form as

$$\mathcal{L} = \lambda\,(\overline{q^c}P_L\,\nu)S + \lambda^*(\overline{\nu}P_R\,q^c)\bar{S}\ , \tag{3.3.10}$$

where $q = u$ or d. The Feynman diagrams contributing to neutrino oscillation matter effects are shown in Fig. 3.3.1. At momenta much smaller than the mass of the leptoquark, the corresponding matrix element is

$$i\mathcal{M} = (-i)^2|\lambda|^2\langle\nu, q|\,(\overline{\nu}P_R\,q^c)\left(\frac{-i}{M_S^2}\right)(\overline{q^c}P_L\,\nu)\,|\nu, q\rangle\ . \tag{3.3.11}$$

Using the Fiertz rearrangement

$$(\overline{\nu}P_R\,q^c)\,(\overline{q^c}P_L\,\nu) \;=\; -\frac{1}{2}\,(\overline{\nu}\gamma^\mu P_L\,\nu)\,(\overline{q^c}\gamma_\mu P_R\,q^c) \;=\; +\frac{1}{2}\,(\overline{\nu}\gamma^\mu P_L\,\nu)\,(\overline{q}\gamma_\mu P_L\,q)\ , \tag{3.3.12}$$

we obtain

$$i\mathcal{M} = \frac{i|\lambda|^2}{2M_S^2}\,\langle\nu|\overline{\nu}\gamma^\mu P_L\nu|\nu\rangle\,\langle q|\overline{q}\gamma_\mu P_L q|q\rangle \to i\frac{|\lambda|^2}{4M_S^2}\,N_q\left(\phi_\nu^\dagger\phi_\nu\right) = -iV_\nu\left(\phi_\nu^\dagger\phi_\nu\right)\ , \tag{3.3.13}$$

where

$$V_\nu \equiv -\frac{N_q}{4}\frac{|\lambda|^2}{M_S^2}\ . \tag{3.3.14}$$

Applying this expression to the S_1 case, the effective potential for the neutrino of generation number j is:

$$V_{\nu_j} \;=\; -\frac{N_d}{4}\frac{\left|g_{1L}^{1j}\right|^2}{M_{S_1}^2} \;=\; -\frac{(N_p+2N_n)}{4}\frac{\left|g_{1L}^{1j}\right|^2}{M_{S_1}^2} \;\approx\; -\frac{3N}{4}\frac{\left|g_{1L}^{1j}\right|^2}{M_{S_1}^2}\;, \tag{3.3.15}$$

The effective ξ is then

$$\xi_{S_1} \;=\; \frac{V_{\nu_3}-V_{\nu_2}}{V_{CC}} \;=\; +3\,\frac{(\,|g_{1L}^{12}|^2-|g_{1L}^{13}|^2\,)/M_{S_1}^2}{g^2/M_W^2}\;. \tag{3.3.16}$$

For the $\vec{S}_3$ case, the effective potential is

$$\begin{aligned} V_{\nu_j} \;&=\; -\frac{N_d}{4}\frac{|g_{3L}^{1j}|^2}{M_{S_3^0}^2}-\frac{N_u}{2}\frac{|g_{3L}^{1j}|^2}{M_{S_3^-}^2} \\ &=\; -|g_{3L}^{1j}|^2\left[\frac{(N_p+2N_n)}{4M_{S_3^0}^2}-\frac{(2N_p+N_n)}{2M_{S_3^-}^2}\right] \\ &\approx\; -\frac{3N}{4}\left|g_{3L}^{1j}\right|^2\left(\frac{1}{M_{S_3^0}^2}+\frac{2}{M_{S_3^-}^2}\right)\;, \end{aligned} \tag{3.3.17}$$

and the effective ξ is

$$\xi_{\vec{S}_3} \;=\; \frac{V_{\nu_3}-V_{\nu_2}}{V_{CC}} \;=\; +3\,\frac{|g_{3L}^{12}|^2-|g_{3L}^{13}|^2}{g^2/M_W^2}\left(\frac{1}{M_{S_3^0}^2}+\frac{2}{M_{S_3^-}^2}\right)\;. \tag{3.3.18}$$

In the case of degenerate mass, $M_{S_3^0}=M_{S_3^-}\equiv M_{S_3}$, we have

$$\xi_{\vec{S}_3} \;=\; +9\,\frac{(\,|g_{3L}^{12}|^2-|g_{3L}^{13}|^2\,)/M_{S_3}^2}{g^2/M_W^2}\;. \tag{3.3.19}$$

3.3.2 S_2 and $\tilde{S}_2$ leptoquarks

The relevant interactions are

$$\mathcal{L}=h_{2L}^{12}(\overline{u_R}\nu_{\mu L})S_2^- + h_{2L}^{13}(\overline{u_R}\nu_{\tau L})S_2^- + h.c. \tag{3.3.20}$$

for S_2^- and

$$\mathcal{L}=\tilde{h}_{2L}^{12}(\overline{d_R}\nu_{\mu L})\tilde{S}_2^- + \tilde{h}_{2L}^{13}(\overline{d_R}\nu_{\tau L})\tilde{S}_2^- + h.c. \tag{3.3.21}$$

for $\tilde{S}_2^-$ leptoquarks. Both (3.3.20) and (3.3.21) can be written in a common general form as

$$\mathcal{L}=\lambda\,(\overline{q}P_L\,\nu)S+\lambda^*(\overline{\nu}P_R\,q)\bar{S}\;, \tag{3.3.22}$$

where $q=u$ or d. The Feynman diagram contributing to neutrino oscillation matter effects is shown in Fig. 3.3.2a. For momenta much smaller than the mass of the leptoquark, the corresponding matrix element is

$$i\mathcal{M}=(-i)^2|\lambda|^2\langle\nu,q|\,(\overline{\nu}P_R\,q)\left(\frac{-i}{M_S^2}\right)(\overline{q}P_L\,\nu)\,|\nu,q\rangle\;. \tag{3.3.23}$$

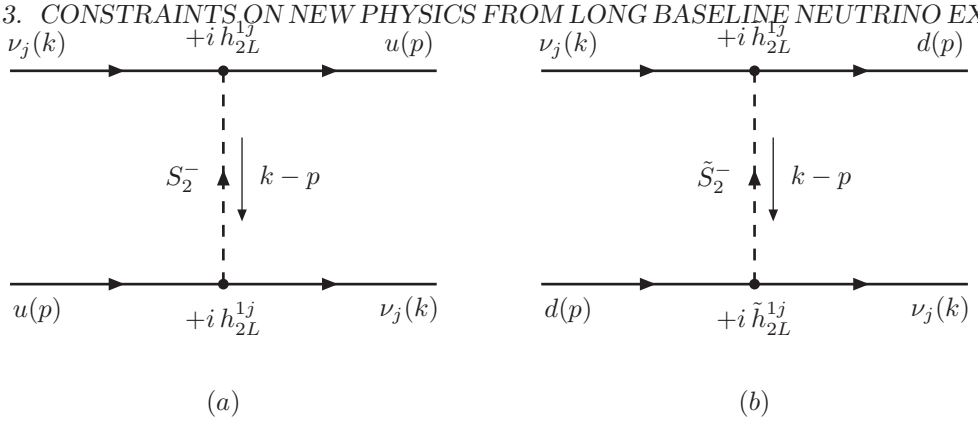

Figure 3.3.2: Diagrams contributing to neutrino oscillation matter effects from the exchange of (a) S_2^-, and (b) $\tilde{S}_2^-$.

Using the Fiertz identity given in Eq. (3.3.12) again, we obtain

$$i\mathcal{M} = -i\frac{|\lambda|^2}{2M_S^2}\,\langle\nu|\overline{\nu}\gamma^\mu P_L\,\nu|\nu\rangle\,\langle q|\overline{q}\gamma_\mu P_R\,q|q\rangle \to -i\frac{|\lambda|^2}{4M_S^2}N_q\left(\phi_\nu^\dagger\phi_\nu\right) = -iV_\nu\left(\phi_\nu^\dagger\phi_\nu\right)\ , \tag{3.3.24}$$

where

$$V_\nu \;=\; +\frac{N_q}{4}\frac{|\lambda|^2}{M_S^2}\,. \tag{3.3.25}$$

Applying this expression to the S_2^- case, the effective potential for the neutrino of generation number j is

$$V_{\nu_j} \;=\; +\frac{N_u}{4}\frac{\left|h^{1j}_{2L}\right|^2}{M^2_{S_2^-}} \;=\; +\frac{(2N_p+N_n)}{4}\frac{\left|h^{1j}_{2L}\right|^2}{M^2_{S_2^-}} \;\approx\; +\frac{3N}{4}\frac{\left|h^{1j}_{2L}\right|^2}{M^2_{S_2^-}}\,, \tag{3.3.26}$$

and the effective ξ is

$$\xi_{S_2^-} \;=\; \frac{V_{\nu_3}-V_{\nu_2}}{V_{CC}} \;=\; -3\,\frac{(\,|h^{12}_{2L}|^2-|h^{13}_{2L}|^2\,)/M^2_{S_2^-}}{g^2/M_W^2}\,. \tag{3.3.27}$$

The effective potential for the $\tilde{S}_2^-$ case is

$$V_{\nu_j} \;=\; +\frac{N_d}{4}\frac{|\tilde{h}^{1j}_{2L}|^2}{M^2_{\tilde{S}_2^-}} \;=\; +\frac{(N_p+2N_n)}{4}\frac{|\tilde{h}^{1j}_{2L}|^2}{M^2_{\tilde{S}_2^-}} \;\approx\; +\frac{3N}{4}\frac{|\tilde{h}^{1j}_{2L}|^2}{M^2_{\tilde{S}_2^-}}\,, \tag{3.3.28}$$

and the effective ξ is

$$\xi_{\tilde{S}_2^-} \;=\; \frac{V_{\nu_3}-V_{\nu_2}}{V_{CC}} \;=\; -3\,\frac{(\,|\tilde{h}^{12}_{2L}|^2-|\tilde{h}^{13}_{2L}|^2\,)/M^2_{\tilde{S}_2^-}}{g^2/M_W^2}\,. \tag{3.3.29}$$

3.3.3 V_2 and $\tilde{V}_2$

The relevant interactions for V_2^- are

$$\mathcal{L} = g^{12}_{2L}(\overline{d^c_R}\gamma^\mu\nu_{\mu L})V^-_{2\mu} + g^{13}_{2L}(\overline{d^c_R}\gamma^\mu\nu_{\tau L})V^-_{2\mu} + h.c. \tag{3.3.30}$$

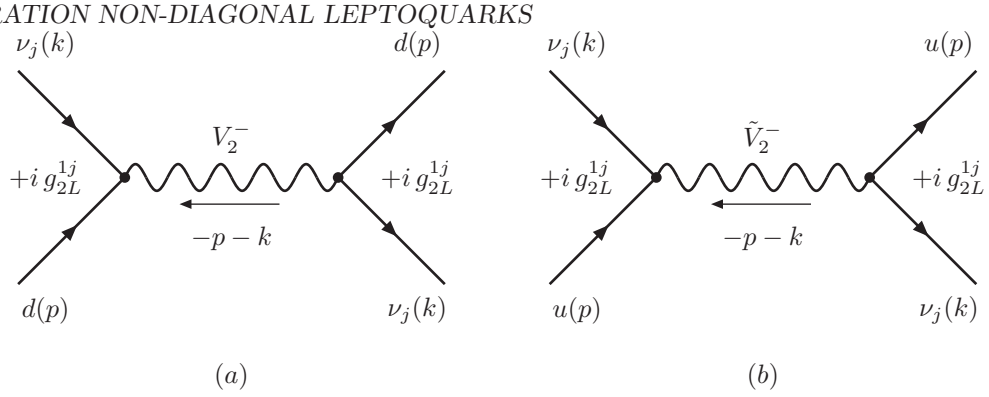

Figure 3.3.3: Diagrams contributing to neutrino oscillation matter effects from the exchange of

and those for $\tilde{V}_2^-$ are

$$\mathcal{L} = \tilde{g}_{2L}^{12}(\overline{u_R^c}\gamma^\mu\nu_{\mu L})\tilde{V}_{2\mu}^- + \tilde{g}_{2L}^{13}(\overline{u_R^c}\gamma^\mu\nu_{\tau L})\tilde{V}_{2\mu}^- + h.c. \tag{3.3.31}$$

Both (3.3.30) and (3.3.31) can be written in a common general form as

$$\mathcal{L} = \lambda\,(\overline{q^c}\gamma^\mu P_L\,\nu)V_\mu + \lambda^*(\overline{\nu}\gamma^\mu P_L\,q^c)\bar{V}_\mu\ . \tag{3.3.32}$$

The Feynman diagrams contributing to neutrino oscillation matter effects are shown in Fig. 3.3.3. For momenta much smaller than the mass of the leptoquark the corresponding matrix element is

$$i\mathcal{M} = (-i)^2|\lambda|^2\langle\nu,q|\,(\overline{\nu}\gamma^\mu P_L\,q^c)\left(\frac{i}{M_V^2}\right)(\overline{q^c}\gamma_\mu P_L\,\nu)\,|\nu,q\rangle\ . \tag{3.3.33}$$

Using the Fiertz rearrangement

$$(\overline{\nu}\gamma^\mu P_L\,q^c)\,(\overline{q^c}\gamma_\mu P_L\,\nu)\ =\ (\overline{\nu}\gamma^\mu P_L\,\nu)\,(\overline{q^c}\gamma_\mu P_L\,q^c)\ =\ -\,(\overline{\nu}\gamma^\mu P_L\,\nu)\,(\overline{q}\gamma_\mu P_R\,q)\ , \tag{3.3.34}$$

we obtain

$$i\mathcal{M} = i\frac{|\lambda|^2}{M_V^2}\,\langle\nu|\overline{\nu}\gamma^\mu P_L\,\nu|\nu\rangle\,\langle q|\overline{q}\gamma_\mu P_R\,q|q\rangle \to i\frac{|\lambda|^2}{2M_V^2}N_q\left(\phi_\nu^\dagger\phi_\nu\right) = -iV_\nu\left(\phi_\nu^\dagger\phi_\nu\right)\ , \tag{3.3.35}$$

where

$$V_\nu \equiv -\frac{N_q}{2}\frac{|\lambda|^2}{M_V^2}\ . \tag{3.3.36}$$

Applying this to the V_2^- case, the effective potential for the neutrino of generation number j is

$$V_{\nu_j}\ =\ -\frac{N_d}{2}\frac{\left|g_{2L}^{1j}\right|^2}{M_{V_2^-}^2}\ =\ -\frac{(N_p+2N_n)}{2}\frac{\left|g_{2L}^{1j}\right|^2}{M_{V_2^-}^2}\ \approx\ -\frac{3N}{2}\frac{\left|g_{2L}^{1j}\right|^2}{M_{V_2^-}^2}\ . \tag{3.3.37}$$

The effective ξ is

$$\xi_{V_2^-}\ =\ \frac{V_{\nu_3}-V_{\nu_2}}{V_{CC}}\ =\ +6\,\frac{(\ |g_{2L}^{12}|^2-|g_{2L}^{13}|^2\ )/M_{V_2^-}^2}{g^2/M_W^2}\ . \tag{3.3.38}$$

The effective potential for the $\tilde{V}_2^-$ case is

$$V_{\nu_j} \;=\; -\frac{N_u}{2}\frac{|\tilde{g}_{2L}^{12}|^2}{M^2_{\tilde{V}_2^-}} \;=\; -\frac{(2N_p+N_n)}{2}\frac{|\tilde{g}_{2L}^{12}|^2}{M^2_{\tilde{V}_2^-}} \;\approx\; -\frac{N_u}{2}\frac{|\tilde{g}_{2L}^{12}|^2}{M^2_{\tilde{V}_2^-}}\;. \tag{3.3.39}$$

The effective ξ is

$$\xi_{\tilde{V}_2^-} \;=\; \frac{V_{\nu_3}-V_{\nu_2}}{V_{CC}} \;=\; +6\,\frac{(\,|\tilde{g}_{2L}^{12}|^2-|\tilde{g}_{2L}^{13}|^2\,)/M^2_{\tilde{V}_2^-}}{g^2/M_W^2}\;. \tag{3.3.40}$$

3.3.4 V_1 and $\vec{V}_3$ leptoquarks

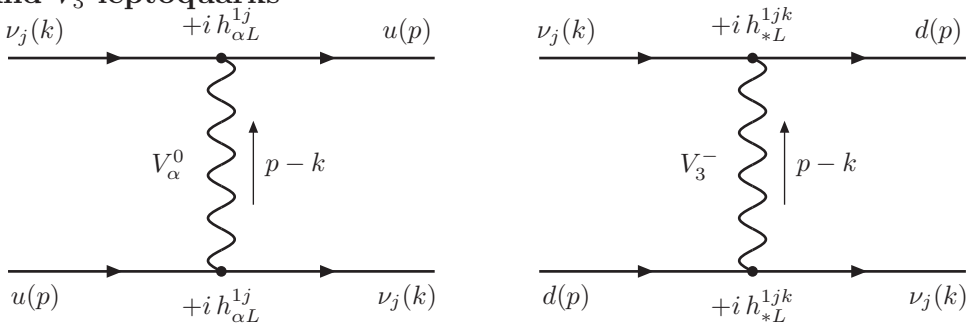

$(a)\ \alpha=1,3$ $\qquad$ (b)

Figure 3.3.4: Diagrams contributing to neutrino oscillation matter effects from the exchange of (a) V_1^0 or the isospin 0 component of $\vec{V}_3$, and (b) the isospin -1 component of $\vec{V}_3$. The EM charges $Q_{em}=I_3+Y$ for V_1^0 and V_3^0 are $+\frac{2}{3}$, while that for V_3^- is $-\frac{1}{3}$.

The relevant interactions for V_1 are

$$\mathcal{L} = h^{12}_{1L}(\overline{u_L}\gamma^\mu\nu_{\mu L})V_{1\mu} + h^{13}_{1L}(\overline{u_L}\gamma^\mu\nu_{\tau L})V_{1\mu} + h.c. \tag{3.3.41}$$

and those for $\vec{V}_3$ are

$$\begin{aligned}\mathcal{L} \;&=\; h^{12}_{3L}\left[(\overline{u_L}\gamma^\mu\nu_{\mu L})V^0_{3\mu} + \sqrt{2}(\overline{d_L}\gamma^\mu\nu_{\mu L})V^-_{3\mu}\right] \\ &\quad + h^{13}_{3L}\left[(\overline{u_L}\gamma^\mu\nu_{\tau L})V^0_{3\mu} + \sqrt{2}(\overline{d_L}\gamma^\mu\nu_{\tau L})V^-_{3\mu}\right] + h.c.\end{aligned} \tag{3.3.42}$$

The interactions described by Eqs. (3.3.41) and (3.3.42) can be written in a common general form as

$$\mathcal{L} = \lambda\,(\overline{q}\gamma^\mu P_L\,\nu)V + \lambda^*(\overline{\nu}\gamma^\mu P_L\,q)\bar{V}\;. \tag{3.3.43}$$

The Feynman diagrams contributing to neutrino oscillation matter effects are shown in Fig. 3.3.4. For momenta much smaller than the mass of the leptoquark the corresponding matrix element is

$$i\mathcal{M} = (-i)^2|\lambda|^2\langle\nu,q|\,(\overline{\nu}\gamma^\mu P_L\,q)\left(\frac{i}{M_V^2}\right)(\overline{q}\gamma_\mu P_L\,\nu)\,|\nu,q\rangle\;. \tag{3.3.44}$$

Using the Fiertz identity given in Eq. (3.3.34) again, we find

$$i\mathcal{M} = -i\frac{|\lambda|^2}{M_V^2}\,\langle\nu|\overline{\nu}\gamma^\mu P_L\,\nu|\nu\rangle\,\langle q|\overline{q}\gamma_\mu P_L\,q|q\rangle \to -i\frac{|\lambda|^2}{2M_V^2}N_q\left(\phi^\dagger_\nu\phi_\nu\right) = -iV_\nu\left(\phi^\dagger_\nu\phi_\nu\right)\;, \tag{3.3.45}$$

where

$$V_\nu \equiv +\frac{N_q}{2}\frac{|\lambda|^2}{M_V^2}\,. \tag{3.3.46}$$

Applying this result to the V_1 case, effective potential is

$$V_{\nu_j} \;=\; +\frac{N_u}{2}\frac{\left|h_{1L}^{1j}\right|^2}{(M_{V_1})^2} \;=\; +\frac{(2N_p+N_n)}{2}\frac{\left|h_{1L}^{1j}\right|^2}{(M_{V_1})^2} \;\approx\; +\frac{3N}{2}\frac{\left|h_{1L}^{1j}\right|^2}{(M_{V_1})^2}\,. \tag{3.3.47}$$

The effective ξ is

$$\xi_{V_1} \;=\; \frac{V_{\nu_3}-V_{\nu_2}}{V_{CC}} \;=\; -6\,\frac{(\,|h_{1L}^{12}|^2-|h_{1L}^{13}|^2\,)/M_{V_1}^2}{g^2/M_W^2}\,. \tag{3.3.48}$$

The effective potential for the $\vec{V}_3$ case is

$$\begin{aligned} V_{\nu_j} &= +\frac{N_u}{2}\frac{\left|h_{3L}^{1j}\right|^2}{M_{V_3^0}^2}+N_d\,\frac{\left|h_{3L}^{1j}\right|^2}{M_{V_3^-}^2} \\ &= +\left|h_{3L}^{1j}\right|^2\left[\frac{(2N_p+N_n)}{2M_{V_3^0}^2}+\frac{(N_p+2N_n)}{M_{V_3^-}^2}\right] \\ &\approx +\frac{3N}{2}\,\left|h_{3L}^{1j}\right|^2\left(\frac{1}{M_{V_3^0}^2}+\frac{2}{M_{V_3^-}^2}\right)\,. \end{aligned} \tag{3.3.49}$$

The effective ξ is

$$\xi_{\vec{V}_3} \;=\; \frac{V_{\nu_3}-V_{\nu_2}}{V_{CC}} \;=\; -6\,\frac{|h_{3L}^{12}|^2-|h_{3L}^{13}|^2}{g^2/M_W^2}\left(\frac{1}{M_{V_3^0}^2}+\frac{2}{M_{V_3^-}^2}\right)\,. \tag{3.3.50}$$

In the case of degenerate mass, $M_{V_3^0}=M_{V_3^-}\equiv M_{V_3}$, we have

$$\xi_{\vec{V}_3} \;=\; -18\,\frac{(\,|h_{3L}^{12}|^2-|h_{3L}^{13}|^2\,)/M_{V_3}^2}{g^2/M_W^2}\,. \tag{3.3.51}$$

3.3.5 Constraints on the Leptoquark Couplings and Masses

Assuming a common mass for leptoquarks in the same $SU(2)_L$ weak-isospin multiplet, the effective ξ due to the exchange of any particular type of leptoquark can be written in the form

$$\xi_{LQ} = C_{LQ}\,\frac{\delta\lambda_{LQ}^2/M_{LQ}^2}{g^2/M_W^2} = \frac{C_{LQ}}{4\sqrt{2}G_F}\left(\frac{\delta\lambda_{LQ}^2}{M_{LQ}^2}\right)\,. \tag{3.3.52}$$

Here, C_{LQ} is a constant prefactor, and $\delta\lambda_{LQ}^2$ represents

$$\delta\lambda_{LQ}^2 = |\lambda_{LQ}^{12}|^2-|\lambda_{LQ}^{13}|^2\,, \tag{3.3.53}$$

LQ	C_{LQ}	$\delta\lambda^2_{LQ}$	upper bound from $\lvert\xi\rvert \le \xi_0$	current bounds from Ref. [64]
S_1	$+3$	$\lvert g^{12}_{1L}\rvert^2 - \lvert g^{13}_{1L}\rvert^2$	1.1×10^{-3}	$(g^{12}_{1L})^2 \le 0.008 \quad (R_\pi)$ $(g^{13}_{1L})^2 \le 0.7 \quad (\tau \to \pi\nu)$
$\vec{S}_3$	$+9$	$\lvert g^{12}_{3L}\rvert^2 - \lvert g^{13}_{3L}\rvert^2$	3.7×10^{-4}	$(g^{12}_{3L})^2 \le 0.008 \quad (R_\pi)$ $(g^{13}_{3L})^2 \le 0.7 \quad (\tau \to \pi\nu)$
S_2	-3	$\lvert h^{12}_{2L}\rvert^2 - \lvert h^{13}_{2L}\rvert^2$	1.1×10^{-3}	$(h^{12}_{2L})^2 \le 1 \quad (\mu N \to \mu X)$
$\tilde{S}_2$	-3	$\lvert \tilde{h}^{12}_{2L}\rvert^2 - \lvert \tilde{h}^{13}_{2L}\rvert^2$	1.1×10^{-3}	$(\tilde{h}^{12}_{2L})^2 \le 2 \quad (\mu N \to \mu X)$
V_2	$+6$	$\lvert g^{12}_{2L}\rvert^2 - \lvert g^{13}_{2L}\rvert^2$	5.5×10^{-4}	$(g^{12}_{2L})^2 \le 1 \quad (\mu N \to \mu X)$
$\tilde{V}_2$	$+6$	$\lvert \tilde{g}^{12}_{2L}\rvert^2 - \lvert \tilde{g}^{13}_{2L}\rvert^2$	5.5×10^{-4}	$(\tilde{g}^{12}_{2L})^2 \le 5 \quad (\mu N \to \mu X)$
V_1	-6	$\lvert h^{12}_{1L}\rvert^2 - \lvert h^{13}_{1L}\rvert^2$	5.5×10^{-4}	$(h^{12}_{1L})^2 \le 0.004 \quad (R_\pi)$ $(h^{13}_{1L})^2 \le 0.1 \quad (D \to \mu\nu)$
$\vec{V}_3$	-18	$\lvert h^{12}_{3L}\rvert^2 - \lvert h^{13}_{3L}\rvert^2$	1.8×10^{-4}	$(h^{12}_{3L})^2 \le 0.004 \quad (R_\pi)$ $(h^{13}_{3L})^2 \le 0.1 \quad (D \to \mu\nu)$

Table 3.5: Constraints on the leptoquark couplings with all the leptoquark masses set to 100 GeV. To obtain the bounds for a different leptoquark mass M_{LQ}, simply rescale these numbers with the factor $(M_{LQ}/100\ \text{GeV})^2$.

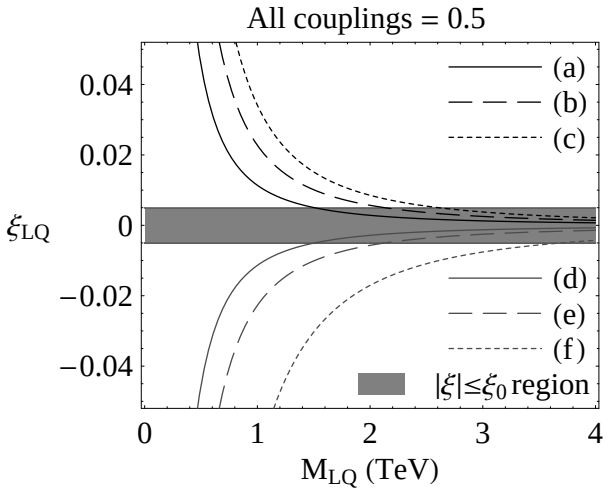

where λ^{ij}_{LQ} is a generic coupling constant. The values of C_{LQ} and $\delta\lambda^2_{LQ}$ for the different types of leptoquark are listed in the first two columns of Table 3.5. In Fig. 3.3.4, we show how ξ_{LQ} depend on the leptoquark mass M_{LQ} for the choice $\sqrt{\delta\lambda^2_{LQ}} = 0.5$, where we have assumed $\delta\lambda^2_{LQ} > 0$. To obtain the picture for the case when $\delta\lambda^2_{LQ} < 0$, the vertical axis of the graph should be flipped. The constraint $|\xi_{LQ}| \le \xi_0$ translates into:

$$M_{LQ} \ge M_W \sqrt{\frac{|\delta\lambda^2_{LQ}|}{g^2}} \sqrt{\frac{|C_{LQ}|}{\xi_0}} = \sqrt{\frac{|C_{LQ}||\delta\lambda^2_{LQ}|}{4\sqrt{2} G_F\, \xi_0}} \approx \sqrt{|C_{LQ}||\delta\lambda^2_{LQ}|} \times (1700\,\text{GeV})\,. \qquad (3.3.54)$$

The resulting bounds are shown in Fig. 3.3.4, where the regions of the $(M_{LQ}, \sqrt{|\delta\lambda^2_{LQ}|})$ parameter space below each of the lines will be excluded. One can also fix the leptoquark mass and obtain

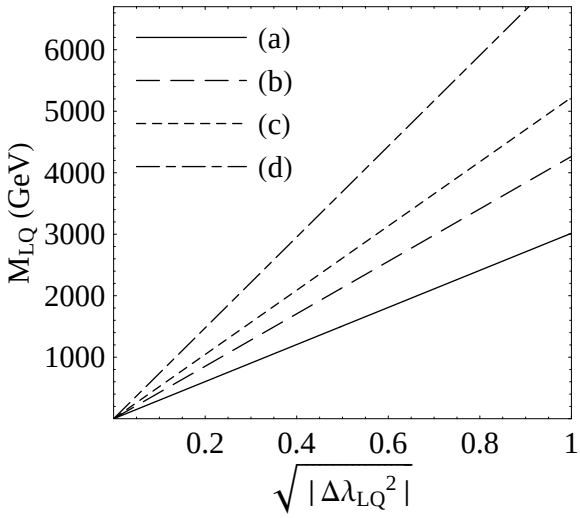

Process	(ij)	LQ	Assumptions	95% CL bound	Reference
$p\bar{p} \to LQ\,\overline{LQ}\,X \to (j\nu)(j\nu)X$	$(**)$	S	$\beta = 0^{(a)}$	117 GeV	CDF [66]
$p\bar{p} \to LQ\,\overline{LQ}\,X \to (j\nu)(j\nu)X$	$(**)$	S	$\beta = 0$	135 GeV	D0 [67]
$p\bar{p} \to LQ\,\overline{LQ}\,X \to (j\mu)(j\mu)X$ $p\bar{p} \to LQ\,\overline{LQ}\,X \to (j\mu)(j\nu)X$	$(*2)$	S	$\beta = 0.5$	208 GeV	CDF [68]
$p\bar{p} \to LQ\,\overline{LQ}\,X \to (j\mu)(j\mu)X$ $p\bar{p} \to LQ\,\overline{LQ}\,X \to (j\mu)(j\nu)X$	$(*2)$	S	$\beta = 0.5$	204 GeV	D0 [69]
$p\bar{p} \to LQ\,\mu\,X \to (j\mu)\mu\,X$	$(*2)$	S	$\beta = 0.5,\ \lambda = 1^{(b)}$	226 GeV$^{(c)}$	D0 [70]
$p\bar{p} \to LQ\,\overline{LQ}\,X \to (j\tau)(j\tau)X$	$(*3)$	V	minimal coupling [72]	251 GeV	CDF [71]

Table 3.6: Direct search limits on the Leptoquark mass from the Tevatron. $^{(a)}\beta$ is the assumed branching fraction $B(LQ \to q\ell) = 1 - B(LQ \to q\nu)$, and $^{(b)}\lambda$ is the Yukawa coupling of the Leptoquark with the quark-lepton pair. $^{(c)}$Combined bound with the pair production data.

upper bounds on the leptoquark couplings:

$$|\delta\lambda^2_{LQ}| \;\le\; \left(\frac{4\sqrt{2}G_F\,\xi_0}{|C_{LQ}|}\right) M^2_{LQ} \;=\; \frac{3.3\times10^{-3}}{|C_{LQ}|}\left(\frac{M_{LQ}}{100\,\mathrm{GeV}}\right)^2 . \tag{3.3.55}$$

The values when $M_{LQ} = 100\,\mathrm{GeV}$ are listed in the third column of Table 3.5. The bounds for a different choice of leptoquark mass M_{LQ} can be obtained by multiplying by a factor of $(M_{LQ}/100\mathrm{GeV})^2$. This result can be compared with various indirect bounds from rare processes which are listed in the last column of Table 3.5. As can be seen, the limits from $|\xi| \le \xi_0$ can significantly improve existing bounds.

Limits on leptoquark masses from direct searches at the Tevatron are listed in Table 3.6. Bounds from LEP and LEP II are weaker due to their smaller center of mass energies. Since neutrino oscillation is only sensitive to leptoquarks with $(ij) = (12)$ and/or $(ij) = (13)$ couplings, we only quote limits which apply to leptoquarks with *only* those particular couplings, that is, leptoquarks that decay into a first generation quark, and either a second or third generation lepton. Though it is usually stated in collider analyses that leptoquarks are assumed to decay

into a quark-lepton pair of one particular generation, it is often the case that the jets coming from the quarks are not flavor tagged. Analyses that look for the leptoquark in the quark-neutrino decay channel are of course blind to the flavor of the neutrino. Therefore, the bounds listed apply to leptoquarks with generation non-diagonal couplings also.

As can be seen from Table 3.6, the mass bounds from the Tevatron are typically around 200 GeV and are mostly independent of the leptoquark-quark-lepton coupling λ. This independence is due to the dominance of the strong interaction processes, $q\bar{q}$ annihilation and gluon fusion, in the leptoquark pair-production cross sections, and the fact that heavy leptoquarks decay without a displaced vertex even for very small values of λ: the decay widths of scalar and vector leptoquarks with leptoquark-quark-lepton coupling λ are given by $\lambda^2 M_{LQ}/16\pi$ and $\lambda^2 M_{LQ}/24\pi$, respectively, which correspond to lifetimes of $O(10^{-21})$ seconds for $M_{LQ} = O(10^2)$ GeV, and $\lambda = O(10^{-2})$. In contrast, the potential bound on M_{LQ} from neutrino oscillation, Eq. (3.3.54), depends on the coupling $\sqrt{|C_{LQ}||\delta\lambda^2_{LQ}|}$, but can be expected to be stronger than the existing ones for $\sqrt{|C_{LQ}||\delta\lambda^2_{LQ}|}$ as small as 0.1.

Bounds on leptoquarks with $(ij) = (12)$ couplings can also be obtained from bounds on contact interactions of the form

$$\mathcal{L} = \pm\frac{4\pi}{(\Lambda^{\pm}_{q\mu})^2}\left(\bar{q}\gamma^\mu P_X q\right)\left(\bar{\mu}\gamma_\mu P_L \mu\right) \ , \tag{3.3.56}$$

where $X = L$ or R, and $q = u$ or d. For instance, at energies much lower than the leptoquark mass, the exchange of the S_1 leptoquark leads to the interaction

$$\mathcal{L}_{S_1} = +\frac{|g^{12}_{1L}|^2}{2M^2_{S_1}}\left(\bar{u}\gamma^\mu P_L u\right)\left(\bar{\mu}\gamma_\mu P_L \mu\right) \ . \tag{3.3.57}$$

The remaining cases are listed in Table 3.7. The 95% CL lower bounds on the $\Lambda^{\pm}_{q\ell}$'s from CDF can be found in Ref. [58], and the cases relevant to our discussion are listed in Table 3.8. These bounds translate into bounds on the leptoquark masses and couplings listed in Table 3.7. Clearly, the potential bounds from $|\xi| < \xi_0$, also listed in Table 3.7, are much stronger. It should be noted, though, that the results of Ref. [58] are from Tevatron Run I, and we can expect the Run II results to improve these bounds. Indeed, Ref. [59] from D0, which we cited earlier in the Z' section, analyzes the Run II data for contact interactions of the form

$$\mathcal{L} = \pm\frac{4\pi}{(\Lambda^{\pm})^2}\left(\bar{u}\gamma^\mu P_X u + \bar{d}\gamma^\mu P_X d\right)\left(\bar{\mu}\gamma_\mu P_L \mu\right) \ , \qquad X = L \text{ or } R \ , \tag{3.3.58}$$

and places 95% CL lower bounds on the $\Lambda^{\pm}$'s in the $4 \sim 7$ TeV range. While these are not exactly the interactions induced by leptoquarks, we can nevertheless expect that the bounds on the $\Lambda^{\pm}_{q\mu}$'s will be in a similar range, and thereby conclude that the Run II data will roughly double the lower bounds from Run I. Even then, Table 3.7 indicates that the potential bounds from $|\xi| < \xi_0$ will be much stronger.

The prospects for leptoquark discovery at the LHC are discussed in Refs. [62, 73]. At the LHC, leptoquarks can be pair-produced via gluon fusion and quark-antiquark annihilation, or singly-produced with an accompanying lepton via quark-gluon fusion. The pair-production cross section is dominated by gluon fusion, which does not involve the leptoquark-quark-lepton coupling λ, and is therefore independent of the details assumed for the leptoquark interactions. Once produced,

LQ	Induced Interaction	CDF 95% CL [58]	$\lvert\xi\rvert < \xi_0$
S_1	$+\frac{\lvert g_{1L}^{12}\rvert^2}{2M_{S_1}^2}\,(\bar{u}\gamma^\mu P_L u)\,(\bar{\mu}\gamma_\mu P_L \mu)$	$\frac{M_{S_1}}{\lvert g_{1L}^{12}\rvert} \geq 0.68\,\text{TeV}$	$\frac{M_{S_1}}{\sqrt{\delta g_{1L}^2}} \geq 3.0\,\text{TeV}$
S_2	$-\frac{\lvert h_{2L}^{12}\rvert^2}{2M_{S_2}^2}\,(\bar{u}\gamma^\mu P_R u)\,(\bar{\mu}\gamma_\mu P_L \mu)$	$\frac{M_{S_2}}{\lvert h_{2L}^{12}\rvert} \geq 0.72\,\text{TeV}$	$\frac{M_{S_2}}{\sqrt{\delta h_{2L}^2}} \geq 3.0\,\text{TeV}$
$\tilde{S}_2$	$-\frac{\lvert \tilde{h}_{2L}^{12}\rvert^2}{2M_{\tilde{S}_2}^2}\,(\bar{d}\gamma^\mu P_R d)\,(\bar{\mu}\gamma_\mu P_L \mu)$	$\frac{M_{\tilde{S}_2}}{\lvert \tilde{h}_{2L}^{12}\rvert} \geq 0.38\,\text{TeV}$	$\frac{M_{\tilde{S}_2}}{\sqrt{\delta \tilde{h}_{2L}^2}} \geq 3.0\,\text{TeV}$
S_3	$+\frac{\lvert g_{3L}^{12}\rvert^2}{2M_{S_3}^2}\,(\bar{u}\gamma^\mu P_L u + 2\,\bar{d}\gamma^\mu P_L d)\,(\bar{\mu}\gamma_\mu P_L \mu)$	—	$\frac{M_{\tilde{S}_3}}{\sqrt{\delta \tilde{g}_{3L}^2}} \geq 5.2\,\text{TeV}$
V_1	$-\frac{\lvert h_{1L}^{12}\rvert^2}{M_{V_1}^2}\,(\bar{d}\gamma^\mu P_L d)\,(\bar{\mu}\gamma_\mu P_L \mu)$	$\frac{M_{V_1}}{\lvert h_{1L}^{12}\rvert} \geq 0.48\,\text{TeV}$	$\frac{M_{V_1}}{\sqrt{\delta h_{1L}^2}} \geq 4.3\,\text{TeV}$
V_2	$+\frac{\lvert g_{2L}^{12}\rvert^2}{M_{V_2}^2}\,(\bar{d}\gamma^\mu P_R d)\,(\bar{\mu}\gamma_\mu P_L \mu)$	$\frac{M_{V_2}}{\lvert g_{2L}^{12}\rvert} \geq 0.56\,\text{TeV}$	$\frac{M_{V_2}}{\sqrt{\delta g_{2L}^2}} \geq 4.3\,\text{TeV}$
$\tilde{V}_2$	$+\frac{\lvert \tilde{g}_{2L}^{12}\rvert^2}{M_{\tilde{V}_2}^2}\,(\bar{u}\gamma^\mu P_R u)\,(\bar{\mu}\gamma_\mu P_L \mu)$	$\frac{M_{\tilde{V}_2}}{\lvert \tilde{g}_{2L}^{12}\rvert} \geq 0.85\,\text{TeV}$	$\frac{M_{\tilde{V}_2}}{\sqrt{\delta \tilde{g}_{2L}^2}} \geq 4.3\,\text{TeV}$
V_3	$-\frac{\lvert h_{3L}^{12}\rvert^2}{M_{V_1}^2}\,(2\,\bar{u}\gamma^\mu P_L u + \bar{d}\gamma^\mu P_L d)\,(\bar{\mu}\gamma_\mu P_L \mu)$	—	$\frac{M_{\tilde{V}_3}}{\sqrt{\delta \tilde{h}_{3L}^2}} \geq 7.4\,\text{TeV}$

Table 3.7: The quark-muon interactions induced by leptoquark exchange, and the bounds from CDF [58] compared with potential bounds from neutrino oscillations. Only the couplings that also contribute to neutrino oscillation are listed. Analysis of the Tevatron Run II data is expected to improve the CDF bound by a factor of two.

$(q\mu)$ chirality	$\Lambda_{u\mu}^+$ (TeV)	$\Lambda_{u\mu}^-$ (TeV)	$\Lambda_{d\mu}^+$ (TeV)	$\Lambda_{d\mu}^-$ (TeV)
(LL)	3.4	4.1	2.3	1.7
(RL)	3.0	3.6	2.0	1.9

Table 3.8: The 95% CL lower bound on the compositeness scale from CDF [58]. Results from D0 [59] do not provide limits for cases where the muons couple to only u or d, but we expect the bounds to be in the range $4 \sim 7$ TeV.

each leptoquark will decay into a lepton plus jet, regardless of whether the coupling is generation diagonal or not. The leptoquark width in this decay depends on λ, but it is too narrow compared to the calorimeter resolution for the λ-dependence to be of relevance in the analyses. Therefore, though the analyses of Refs. [62, 73] assume specific values of λ and generation diagonal couplings, we expect their conclusions to apply equally well to different λ-values and generation non-diagonal cases: for $\beta = B(LQ \to q\ell) = 0.5$, the expected sensitivity is up to $M_{LQ} \approx 1\,\text{TeV}$ with 30^{-1} fb of data [73]. Again, in contrast, the the potential bound from neutrino oscillation, Eq. (3.3.54), depends on the coupling $\sqrt{|C_{LQ}||\delta\lambda_{LQ}^2|}$. If $\sqrt{|C_{LQ}||\delta\lambda_{LQ}^2|} = O(1)$, then Eq. (3.3.54) will be competitive with the expected LHC bound.

3.4 SUSY Standard Model with R-parity Violation

Let us next consider contributions from R-parity violating couplings. Assuming the particle content of the Minimal Supersymmetric Standard Model (MSSM), the most general R-parity

violating superpotential (involving only tri-linear couplings) has the form [46]

$$W_{\not R} = \frac{1}{2}\lambda_{ijk}\hat{L}_i\hat{L}_j\hat{E}_k + \lambda'_{ijk}\hat{L}_i\hat{Q}_j\hat{D}_k + \frac{1}{2}\lambda''_{ijk}\hat{U}_i\hat{D}_j\hat{D}_k \ , \tag{3.4.1}$$

where $\hat{L}_i$, $\hat{E}_i$, $\hat{Q}_i$, $\hat{D}_i$, and $\hat{U}_i$ are the left-handed MSSM superfields defined in the usual fashion, and the subscripts $i, j, k = 1, 2, 3$ are the generation indices. (Note, however, that in some references, such as Ref. [47], the isospin singlet superfields $\hat{E}_i$, $\hat{D}_i$, and $\hat{U}_i$ are defined to be right-handed, so the corresponding left-handed fields in Eq. (3.4.1) appear with a superscript c indicating charge-conjugation.) $SU(2)_L$ gauge invariance requires the couplings λ_{ijk} to be antisymmetric in the first two indices:

$$\lambda_{ijk} \ = \ -\lambda_{jik} \ , \tag{3.4.2}$$

whereas $SU(3)$ gauge invariance requires the couplings λ''_{ijk} to be antisymmetric in the latter two:

$$\lambda''_{ijk} \ = \ -\lambda''_{ikj} \ . \tag{3.4.3}$$

These conditions reduce the number of R-parity violating couplings in Eq. (3.4.1) to 45 (9 λ_{ijk}, 27 λ'_{ijk}, and 9 λ''_{ijk}). The purely baryonic operator $\hat{U}_i\hat{D}_j\hat{D}_k$ is irrelevant to our discussion on neutrino oscillation so we will not consider the λ''_{ijk} couplings further. We also neglect possible bilinear R-parity violating couplings which have the effect of mixing the neutrinos with the neutral higgsino; their effect on neutrino oscillation has been discussed extensively by many authors [47, 74, 75].

3.4.1 $\hat{L}\hat{L}\hat{E}$ couplings

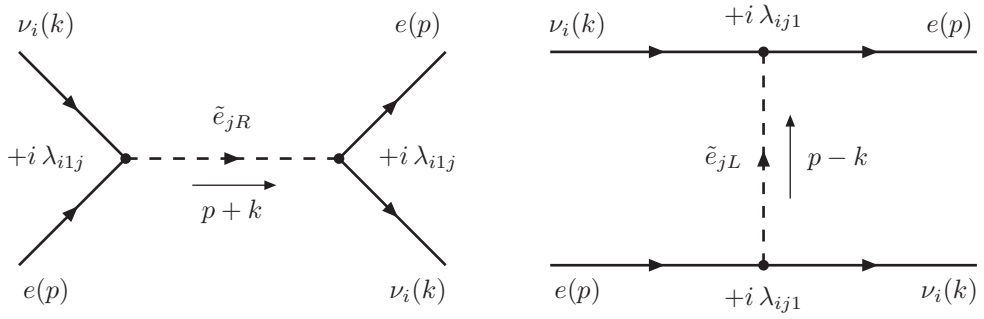

Figure 3.4.1: LLE interactions that contribute to neutrino oscillation matter effects..

The $\hat{L}\hat{L}\hat{E}$ part of the R-parity violating Lagrangian, Eq. (3.4.1), expressed in terms of the component fields is

$$\mathcal{L}_{LLE} \ = \ \lambda_{ijk}\left[\tilde{\nu}_{iL}\overline{e_{kR}}e_{jL} + \tilde{e}_{jL}\overline{e_{kR}}\nu_{iL} + \tilde{e}^*_{kR}\overline{\nu^c_{iL}}e_{jL}\right] + h.c. \tag{3.4.4}$$

The second and third terms of this Lagrangian, together with their hermitian conjugates, contribute to neutrino oscillation matter effects. The corresponding Feynman diagrams are shown in Fig 3.4.1. Since λ_{ijk} is antisymmetric under $i \leftrightarrow j$, it follows that $i \neq j$. Calculations similar to those for the scalar leptoquarks yield

$$V_{\tilde{e}}(\nu_i) = \frac{N_e}{4}\left(\sum_{j\neq i}\frac{|\lambda_{ij1}|^2}{M^2_{\tilde{e}_{jL}}} - \sum_j \frac{|\lambda_{i1j}|^2}{M^2_{\tilde{e}_{jR}}}\right) \ , \tag{3.4.5}$$

or if we write everything out explicitly:

$$\begin{aligned} V_{\tilde{e}}(\nu_2) &= \frac{N_e}{4}\left(\frac{|\lambda_{211}|^2}{M^2_{\tilde{e}_{1L}}}+\frac{|\lambda_{231}|^2}{M^2_{\tilde{e}_{3L}}}-\frac{|\lambda_{211}|^2}{M^2_{\tilde{e}_{1R}}}-\frac{|\lambda_{212}|^2}{M^2_{\tilde{e}_{2R}}}-\frac{|\lambda_{213}|^2}{M^2_{\tilde{e}_{3R}}}\right) , \\ V_{\tilde{e}}(\nu_3) &= \frac{N_e}{4}\left(\frac{|\lambda_{311}|^2}{M^2_{\tilde{e}_{1L}}}+\frac{|\lambda_{321}|^2}{M^2_{\tilde{e}_{2L}}}-\frac{|\lambda_{311}|^2}{M^2_{\tilde{e}_{1R}}}-\frac{|\lambda_{312}|^2}{M^2_{\tilde{e}_{2R}}}-\frac{|\lambda_{313}|^2}{M^2_{\tilde{e}_{3R}}}\right) . \end{aligned} \tag{3.4.6}$$

The effective ξ is

$$\begin{aligned} \xi_{\tilde{e}} &= \frac{V_{\tilde{e}}(\nu_3)-V_{\tilde{e}}(\nu_2)}{V_{CC}} \\ &= \frac{1}{g^2/M_W^2}\left(-\sum_{j=1,3}\frac{|\lambda_{2j1}|^2}{M^2_{\tilde{e}_{jL}}}-\sum_{j=1,2}\frac{|\lambda_{3j1}|^2}{M^2_{\tilde{e}_{jL}}}+\sum_{j=1}^{3}\frac{|\lambda_{21j}|^2-|\lambda_{31j}|^2}{M^2_{\tilde{e}_{jR}}}\right) \\ &= \frac{1}{g^2/M_W^2}\left[\left(\,|\lambda_{211}|^2-|\lambda_{311}|^2\,\right)\left(\frac{1}{M^2_{\tilde{e}_{1R}}}-\frac{1}{M^2_{\tilde{e}_{1L}}}\right)\right. \\ &\qquad \left.+|\lambda_{231}|^2\left(\frac{1}{M^2_{\tilde{e}_{2L}}}-\frac{1}{M^2_{\tilde{e}_{3L}}}\right)+\frac{|\lambda_{212}|^2-|\lambda_{312}|^2}{M^2_{\tilde{e}_{2R}}}+\frac{|\lambda_{213}|^2-|\lambda_{313}|^2}{M^2_{\tilde{e}_{3R}}}\right] . \end{aligned} \tag{3.4.7}$$

For degenerate s-electron masses $M_{\tilde{e}_{jL}} = M_{\tilde{e}_{jR}} \equiv M_{\tilde{e}_j}$, we have

$$\xi_{\tilde{e}} = \frac{1}{g^2/M_W^2}\left(\frac{|\lambda_{231}|^2+|\lambda_{122}|^2-|\lambda_{132}|^2}{M^2_{\tilde{e}_2}}-\frac{|\lambda_{231}|^2-|\lambda_{123}|^2+|\lambda_{133}|^2}{M^2_{\tilde{e}_3}}\right) , \tag{3.4.8}$$

where we have used $\lambda_{ijk} = -\lambda_{jik}$ to reorder the indices.

3.4.2 $\hat{L}\hat{Q}\hat{D}$ couplings

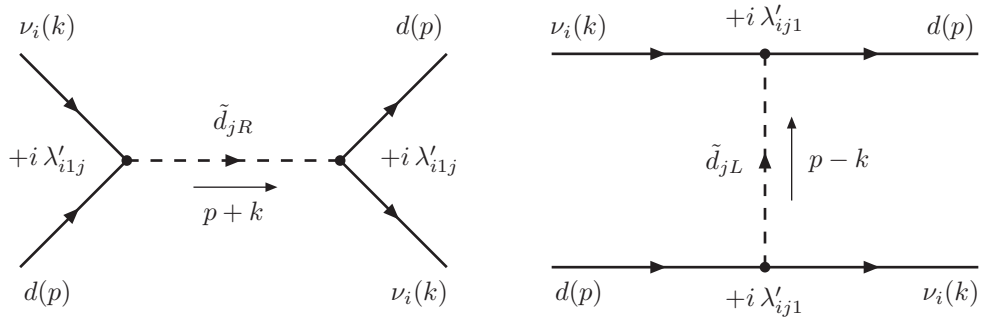

Figure 3.4.2: LQD interactions that contribute to neutrino oscillation matter effects..

The $\hat{L}\hat{Q}\hat{D}$ part of the R-parity violating Lagrangian expressed in terms of the component fields is

$$\begin{aligned} \mathcal{L}_{LQD} &= \lambda'_{ijk}\left[\tilde{\nu}_{iL}\overline{d_{kR}}d_{jL}+\tilde{d}_{jL}\overline{d_{kR}}\nu_{iL}+\tilde{d}^*_{kR}\overline{\nu^c_{iL}}d_{jL}\right. \\ &- \left.\left(\tilde{e}_{iL}\overline{d_{kR}}u_{jL}+\tilde{u}_{jL}\overline{d_{kR}}e_{iL}+\tilde{d}^*_{kR}\overline{e^c_{iL}}u_{jL}\right)\right]+h.c. \end{aligned} \tag{3.4.9}$$

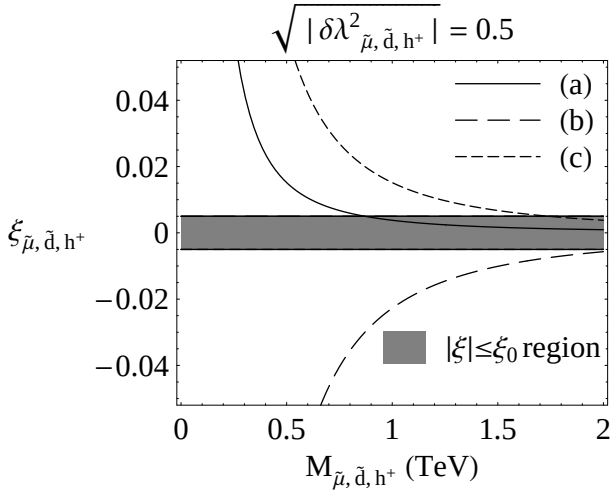

Figure 3.4.3: Dependence of $\xi_{\tilde{\mu},\tilde{d},h}$ on the smuon, sdown, and $h^{\pm}$ masses for (a) $\hat{L}\hat{L}\hat{E}$ R-parity violating interaction; (b) $\hat{L}\hat{Q}\hat{D}$ R-parity violating interaction; and (c) the Zee/Babu-Zee models.

The second and third terms of this Lagrangian, together with their hermitian conjugates, contribute to neutrino oscillation matter effects. The corresponding Feynman diagrams are shown in Fig 3.4.2. Calculations similar to those for the scalar leptoquarks lead to the following effective potential for neutrino flavor ν_i:

$$V_{\tilde{d}}(\nu_i) \;=\; \sum_{j=1}^{3} \frac{N_p + 2N_n}{4} \left(\frac{\left|\lambda'_{ij1}\right|^2}{M^2_{\tilde{d}_{jL}}} - \frac{\left|\lambda'_{i1j}\right|^2}{M^2_{\tilde{d}_{jR}}} \right) \;\approx\; \sum_{j=1}^{3} \frac{3N}{4} \left(\frac{\left|\lambda'_{ij1}\right|^2}{M^2_{\tilde{d}_{jL}}} - \frac{\left|\lambda'_{i1j}\right|^2}{M^2_{\tilde{d}_{jR}}} \right) . \tag{3.4.10}$$

The effective ξ is

$$\begin{aligned} \xi_{\tilde{d}} \;&=\; \frac{V_{\tilde{d}}(\nu_3) - V_{\tilde{d}}(\nu_2)}{V_{CC}} \\ &=\; -3 \sum_{j=1}^{3} \frac{\left(\left|\lambda'_{2j1}\right|^2 - \left|\lambda'_{3j1}\right|^2 \right) / M^2_{\tilde{d}_{jL}} - \left(\left|\lambda'_{21j}\right|^2 - \left|\lambda'_{31j}\right|^2 \right) / M^2_{\tilde{d}_{jR}}}{g^2/M_W^2} . \end{aligned} \tag{3.4.11}$$

For degenerate d-squark masses $M_{\tilde{d}_{jL}} = M_{\tilde{d}_{jR}} \equiv M_{\tilde{d}_j}$, we have

$$\xi_{\tilde{d}} = -3 \sum_{j=1}^{3} \frac{\left(\left|\lambda'_{2j1}\right|^2 - \left|\lambda'_{3j1}\right|^2 + \left|\lambda'_{21j}\right|^2 - \left|\lambda'_{31j}\right|^2 \right) / M^2_{\tilde{d}_j}}{g^2/M_W^2} . \tag{3.4.12}$$

3.4.3 Constraints on the R-parity Violating Couplings and Squark/Slepton Masses

To illustrate our result for R-parity violating interactions, we simplify the analysis by assuming that only the λ_{122} and λ_{132} couplings are non-zero for the $\hat{L}\hat{L}\hat{E}$ case, and only the λ'_{211} and λ'_{311} couplings are non-zero for the $\hat{L}\hat{Q}\hat{D}$ case. Under these assumptions, only the smuon, $\tilde{e}_2 = \tilde{\mu}$, contributes in the first case, and only the sdown, $\tilde{d}_1 = \tilde{d}$, contributes in the latter. The

corresponding ξ's are

$$\begin{aligned} \xi_{\tilde{\mu}} &= +\frac{\delta\lambda^2_{\tilde{\mu}}/M^2_{\tilde{\mu}}}{(g/M_W)^2} = +\frac{1}{4\sqrt{2}G_F}\left(\frac{\delta\lambda^2_{\tilde{\mu}}}{M^2_{\tilde{\mu}}}\right) , \\ \xi_{\tilde{d}} &= -6\,\frac{\delta\lambda^2_{\tilde{d}}/M^2_{\tilde{d}}}{(g/M_W)^2} = -\frac{6}{4\sqrt{2}G_F}\left(\frac{\delta\lambda^2_{\tilde{d}}}{M^2_{\tilde{d}}}\right) , \end{aligned} \tag{3.4.13}$$

where

$$\begin{aligned} \delta\lambda^2_{\tilde{\mu}} &\equiv |\lambda_{122}|^2 - |\lambda_{132}|^2 , \\ \delta\lambda^2_{\tilde{d}} &\equiv |\lambda'_{211}|^2 - |\lambda'_{311}|^2 . \end{aligned} \tag{3.4.14}$$

Fig. 3.4.3 shows how $\xi_{\tilde{\mu}}$ and $\xi_{\tilde{d}}$ depend on masses of the smuon and the sdown for a specific choice of couplings: $\sqrt{\delta\lambda^2_{\tilde{\mu}}} = \sqrt{\delta\lambda^2_{\tilde{d}}} = 0.5$ (we have assumed $\delta\lambda^2_{\tilde{d}}$ and $\delta\lambda^2_{\tilde{\mu}}$ to be positive). The bound $|\xi| \leq \xi_0 = 0.005$ translates into:

$$\begin{aligned} M_{\tilde{\mu}} &\geq \sqrt{|\delta\lambda^2_{\tilde{\mu}}|}\sqrt{\frac{1}{4\sqrt{2}G_F\xi_0}} \approx \sqrt{|\delta\lambda^2_{\tilde{\mu}}|} \times (1700\,\mathrm{GeV}) , \\ M_{\tilde{d}} &\geq \sqrt{|\delta\lambda^2_{\tilde{d}}|}\sqrt{\frac{6}{4\sqrt{2}G_F\xi_0}} \approx \sqrt{|\delta\lambda^2_{\tilde{d}}|} \times (4300\,\mathrm{GeV}) . \end{aligned} \tag{3.4.15}$$

The resulting graphs for the lower mass bounds are shown in Fig. 3.4.4. The regions of the $\left(M_{\tilde{\mu}}, \sqrt{|\delta\lambda^2_{\tilde{\mu}}|}\right)$ and $\left(M_{\tilde{d}}, \sqrt{|\delta\lambda^2_{\tilde{d}}|}\right)$ parameter spaces below each of the lines are excluded. One can also fix the smuon and sdown masses and obtain upper bounds on the R-parity violating couplings:

$$\begin{aligned} \sqrt{|\delta\lambda^2_{\tilde{\mu}}|} &\leq \sqrt{4\sqrt{2}G_F\,\xi_0}\,M_{\tilde{\mu}} = (0.057)\left(\frac{M_{\tilde{\mu}}}{100\,\mathrm{GeV}}\right) , \\ \sqrt{|\delta\lambda^2_{\tilde{d}}|} &\leq \sqrt{\frac{4\sqrt{2}G_F\,\xi_0}{6}}\,M_{\tilde{d}} = (0.023)\left(\frac{M_{\tilde{d}}}{100\,\mathrm{GeV}}\right) . \end{aligned} \tag{3.4.16}$$

These relations are actually more useful than Eq. (3.4.15) since if the smuon and sdown exist, their masses will be measured/constrained by searches for their pair-production at the LHC, independently of the size of possible R-parity violating couplings.

Current bounds on R-parity violating couplings come from a variety of sources [47, 48]. The current indirect bounds of the four couplings under consideration from low-energy experiments are listed in Table 3.9. Comparison with Eq. (3.4.16) shows that the bounds on λ_{122} and λ_{132} are already fairly tight, and neutrino oscillation will do little to improve them. On the other hand, the bounds on λ'_{211} and λ'_{311} can potentially be improved by factors of roughly 2.5 and 5, respectively.

Bounds on R-parity violating couplings from ep and $p\bar{p}$ colliders come from searches for s-channel resonant production of sparticles. The bounds from the ep collider HERA necessarily involve the couplings λ'_{1jk} since the squark must couple to the first generation lepton (electron or positron) [76, 77, 78, 79] so we will not discuss them here. The bound from the Tevatron

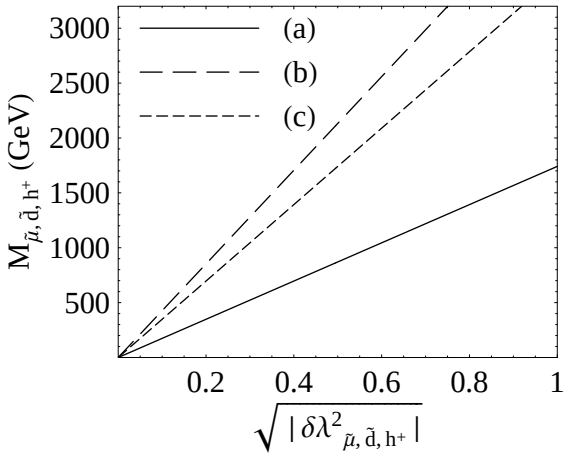

Figure 3.4.4: Lower bounds on (a) the smuon mass in the $\hat{L}\hat{L}\hat{E}$ R-parity violating interaction model, (b) the sdown mass in the $\hat{L}\hat{Q}\hat{D}$ R-parity violating interaction model, and (c) the $h^{\pm}$ mass in the Zee/Babu-Zee models, respectively.

Coupling	Current 2σ Bound	Observable/Process
$\lvert\lambda_{122}\rvert$	$0.05\left(\frac{M_{\tilde{\mu}_R}}{100\,\mathrm{GeV}}\right)$	V_{ud} from nuclear β decay/muon decay
$\lvert\lambda_{132}\rvert$	$0.07\left(\frac{M_{\tilde{\mu}_R}}{100\,\mathrm{GeV}}\right)$	$R_\tau = \frac{\Gamma(\tau^- \to e^-\bar{\nu}_e\nu_\tau)}{\Gamma(\tau^- \to \mu^-\bar{\nu}_\mu\nu_\tau)}$
$\lvert\lambda_{122}\lambda^*_{132}\rvert$	$(2.2\times10^{-3})\left(\frac{M_{\tilde{\nu}_R}}{100\,\mathrm{GeV}}\right)^2$	$\tau \to 3\mu$
$\lvert\lambda'_{211}\rvert$	$0.06\left(\frac{M_{\tilde{d}_R}}{100\,\mathrm{GeV}}\right)$	$R_\pi = \frac{\Gamma(\pi^- \to e^-\bar{\nu}_e)}{\Gamma(\pi^- \to \mu^-\bar{\nu}_\mu)}$
$\lvert\lambda'_{311}\rvert$	$0.12\left(\frac{M_{\tilde{d}_R}}{100\,\mathrm{GeV}}\right)$	$R_{\tau\pi} = \frac{\Gamma(\tau^- \to \pi^-\nu_\tau)}{\Gamma(\pi^- \to \mu^-\nu_\mu)}$

Table 3.9: Current 2σ bounds on R-parity violating couplings from Ref. [47]. These bounds assume that each coupling is non-zero only one at a time.

comes from the analysis of D0 which looked for the R-parity violating processes $d\bar{u} \to \tilde{\mu}$ or $d\bar{d} \to \tilde{\nu}_\mu$, which occur if $\lambda'_{211} \neq 0$, followed by the decay of the slepton via the R-parity conserving processes $\tilde{\mu} \to \tilde{\chi}^0_{1,2,3,4}\,\mu$ or $\tilde{\nu}_\mu \to \tilde{\chi}^\pm_{1,2}\,\mu$ [80]. The neutralinos and charginos produced in these processes cascade decay down to the $\tilde{\chi}^0_1$ (the assumed lightest supersymmetric particle, or LSP) which decays via a virtual smuon, muon-sneutrino, or squark though the R-parity violating λ'_{211} coupling again into a muon and two jets, giving 2 muons in the final state. The bound on the value of λ'_{211} from this analysis depends in a complicated manner on all the masses of the particles involved in the processes. If one uses a minimal supergravity (mSUGRA) framework [81] with $\tan\beta = 5$, $\mu < 0$, and $A_0 = 0$, then the 95% bound is $\lambda'_{211} \leq 0.1$ assuming $M_{\tilde{\mu}} = 363\,\mathrm{GeV}$ [80]. A similar bound would result from Eq. (3.4.16) if $M_{\tilde{d}} = 460\,\mathrm{GeV}$. However, since squarks are generically much heavier than sleptons [81], the existing D0 bound is effectively stronger than the potential bound from $|\xi| \leq \xi_0$.

3.5 Extended Higgs Models

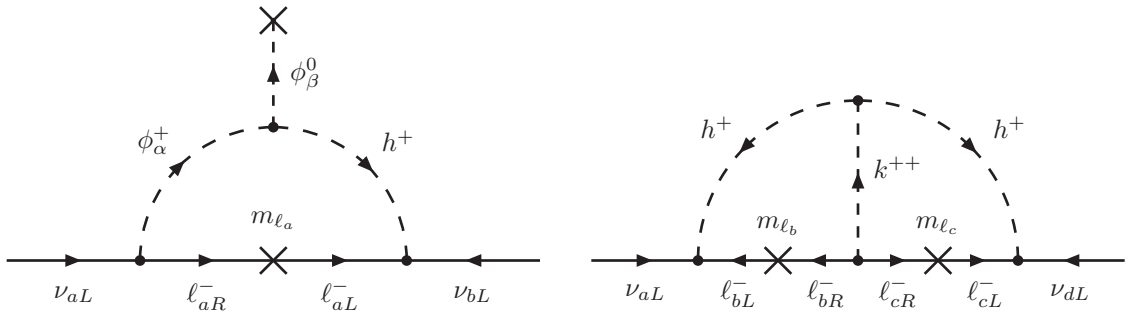

Figure 3.5.1: Diagrams which generate the Majorana masses and mixings of the neutrino in the (a) Zee [82] and (b) Babu-Zee [83] models.

Most models, including the Standard Model (SM) and its various extensions, possess Higgs sectors which distinguish among the different generation fermions. The models discussed in section 3.2 are necessarily so, and so are the Zee [82] and Babu-Zee [83] models of neutrino mass, as well as various triplet Higgs models [84]. As representative cases, we consider the effect of the singlet Higgs in the Zee and Babu-Zee models, and that of a triplet Higgs with hypercharge $Y = +1$ ($Q_{em} = I_3 + Y$).

3.5.1 Singlet Higgs in the Zee and Babu-Zee Models

In the Zee [82] and Babu-Zee [83] models, an isosinglet scalar h^+ with hypercharge $Y = +1$ is introduced, which couples to left-handed lepton doublets as

$$\mathcal{L}_h \;=\; \lambda_{ab} \left(\ell^{\rm T}_{aL} C\, i\sigma_2\, \ell_{bL} \right) h^+ + h.c. \;=\; \lambda_{ab} \left(\overline{\ell^c_{aL}}\, i\sigma_2\, \ell_{bL} \right) h^+ + h.c.\,, \tag{3.5.1}$$

where (ab) are flavor indices: $a, b = e, \mu, \tau$. The hypercharge assignment prohibits the $h^\pm$ fields from having a similar interaction with the quarks. Due to $SU(2)$ gauge invariance, the couplings λ_{ab} are antisymmetric: $\lambda_{ab} = -\lambda_{ba}$. This interaction is analogous to the R-parity violating $\hat{L}\hat{L}\hat{E}$ coupling with $h^\pm$ playing the role of the slepton.

In the Zee model [82], in addition to the $h^\pm$, two or more $SU(2)$ doublets ϕ_α ($\alpha = 1, 2, \cdots$) with hypercharge $Y = -\frac{1}{2}$ are introduced which couple to the $h^\pm$ via

$$\mathcal{L}_{\phi\phi h} \;=\; M_{\alpha\beta} \left(\phi^{\rm T}_\alpha\, i\tau_2\, \phi_\beta \right) h^+ + h.c.\,, \tag{3.5.2}$$

and to the fermions in the usual fashion. The couplings $M_{\alpha\beta}$ are antisymmetric, just like λ_{ab}, which necessitates the introduction of more than one doublet. In this model, Majorana masses and mixings of the neutrinos are generated at one-loop as shown in Fig. 3.5.1a. The extra doublets can also contribute to neutrino oscillation depending on their Yukawa couplings to the leptons, but we will assume that their effect is negligible compared to that of the $h^\pm$.

In the Babu-Zee model [83], in addition to the $h^\pm$, another isosinglet scalar k^{++} with hypercharge $Y = +2$ is introduced which couples to the right-handed leptons and $h^\pm$ via

$$\mathcal{L}_k \;=\; \lambda'_{ab} \left(\overline{e^c_{aR}}\, e_{bR} \right) k^{++} - M\, h^+ h^+ k^{--} + h.c.\,, \tag{3.5.3}$$

where $\lambda'_{ab} = \lambda'_{ba}$. In this model, Majorana masses and mixings of the neutrinos are generated at the two-loop level as shown in Fig. 3.5.1b. In this case, the extra scalar, k, does not contribute to neutrino oscillation.

Expanding Eq. (3.5.1), we obtain

$$\mathcal{L} \;=\; 2\left[\,\lambda_{e\mu}\left(\overline{\nu^c_{eL}}\mu_L - \overline{\nu^c_{\mu L}}e_L\right) + \lambda_{e\tau}\left(\overline{\nu^c_{eL}}\tau_L - \overline{\nu^c_{\tau L}}e_L\right) + \lambda_{\mu\tau}\left(\overline{\nu^c_{\mu L}}\tau_L - \overline{\nu^c_{\tau L}}\mu_L\right)\right] h^+ + h.c. \quad (3.5.4)$$

Keeping only the terms that are relevant for neutrino oscillation matter effects, we have

$$-2\left(\,\lambda_{e\mu}\,\overline{\nu^c_{\mu L}}\,e_L + \lambda_{e\tau}\,\overline{\nu^c_{\tau L}}\,e_L\right) h^+ + h.c. \quad (3.5.5)$$

The corresponding Feynman diagram is shown in Fig. 3.5.2.

Calculations similar to those for the S_1 leptoquark yield

$$V_{\nu_\mu} \;=\; -N\,\frac{|\lambda_{e\mu}|^2}{M_h^2}\,, \qquad V_{\nu_\tau} \;=\; -N\,\frac{|\lambda_{e\tau}|^2}{M_h^2}\,, \quad (3.5.6)$$

and

$$\xi_h \;=\; \frac{V_{\nu_\tau} - V_{\nu_\mu}}{V_{CC}} \;=\; 4\,\frac{(|\lambda_{e\mu}|^2 - |\lambda_{e\tau}|^2)/M_h^2}{(g/M_W)^2} \;=\; +\frac{1}{\sqrt{2}G_F}\left(\frac{\delta\lambda_h^2}{M_h^2}\right)\,, \quad (3.5.7)$$

where we have defined $\delta\lambda_h^2 \equiv |\lambda_{e\mu}|^2 - |\lambda_{e\tau}|^2$. The dependence of ξ_h on the $h^\pm$ mass is plotted in Fig. 3.4.3 for the case $\sqrt{\delta\lambda_h^2} = 0.5$, where we have assumed $\delta\lambda_h^2 > 0$. The bound $|\xi| \le \xi_0 = 0.005$ translates into

$$\left|\frac{\delta\lambda_h^2}{M_h^2}\right| \;\le\; \sqrt{2}G_F\,\xi_0 \;=\; (8.2\times10^{-8})\,\mathrm{GeV}^{-2}\,, \quad (3.5.8)$$

or

$$M_h \;\ge\; \sqrt{\frac{|\delta\lambda_h^2|}{\sqrt{2}G_F\,\xi_0}} \;\approx\; \sqrt{|\delta\lambda_h^2|}\times(3500\,\mathrm{GeV})\,. \quad (3.5.9)$$

This result is represented graphically in Fig. 3.4.4. The region of the $(M_h, \sqrt{|\delta\lambda_h^2|})$ parameter space below the constructed line would be excluded.

A constraint on the exact same combination of the couplings and mass of the $h^\pm$ as above exists from τ decay data: The measured value of the $\tau^- \to \nu_\tau e^- \bar{\nu}_e$ branching fraction imposes the constraint [85]

$$\left|\frac{\delta\lambda_h^2}{M_h^2}\right| \;\le\; (3.4\times10^{-8})\,\mathrm{GeV}^{-2}\,, \quad (3.5.10)$$

which is clearly stronger than Eq. (3.5.8).

3.5.2 Triplet Higgs with $Y = +1$

We denote the components of an isotriplet Higgs with hypercharge $Y = +1$ as

$$\begin{bmatrix} \Delta^{++} \\ \Delta^{+} \\ \Delta^{0} \end{bmatrix}\,. \quad (3.5.11)$$

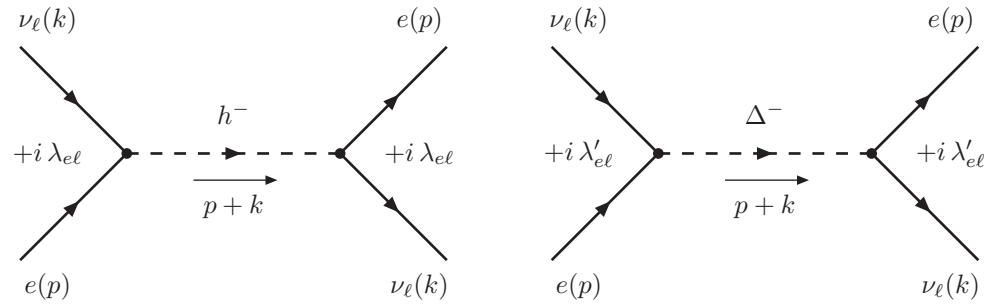

Figure 3.5.2: Contribution to neutrino oscillation matter effects from a singly-charged Higgs in the Zee, Babu-Zee, and $Y = 1$ Triplet Higgs models.

Model	Stronger than existing bounds?	Competitive with LHC?
Gauged $L_e - L_\mu$ and $L_e - L_\tau$	No	—
Gauged $B - 3L_\tau$	Yes	Yes
Topcolor Assisted Technicolor	No	—
Leptoquarks	Yes	Yes*
R-parity violation	No	—
Zee, Babu-Zee, Triplet Higgs	No	—

Table 3.10: The result of our survey. The potential bound from $|\xi| \leq \xi_0 = 0.005$ is compared with existing bounds, and the expected bounds from the LHC. If the existing bound is already stronger, no comparison with the LHC bound is made. *The leptoquark bound will be competitive with the LHC, provided that $\sqrt{|C_{LQ}||\delta\lambda^2_{LQ}|} = O(1)$.

It is customary to write this in 2×2 matrix form:

$$\Delta \;\equiv\; \frac{1}{\sqrt{2}}\left[\Delta^0\left(\frac{\sigma_1 - i\sigma_2}{\sqrt{2}}\right) + \Delta^+\sigma_3 + \Delta^{++}\left(\frac{\sigma_1 + i\sigma_2}{\sqrt{2}}\right)\right] \;=\; \begin{bmatrix} \Delta^+/\sqrt{2} & \Delta^{++} \\ \Delta^0 & -\Delta^+/\sqrt{2} \end{bmatrix} . \quad (3.5.12)$$

The coupling of Δ to the leptons is then

$$\mathcal{L}_\Delta \;=\; \sqrt{2}\lambda'_{ab}\left(\ell^{\rm T}_{aL} C\, i\sigma_2\, \Delta\, \ell_{bL}\right) + h.c. \;=\; \sqrt{2}\lambda'_{ab}\left(\overline{\ell^c_{aL}}\, i\sigma_2\, \Delta\, \ell_{bL}\right) + h.c. \quad (3.5.13)$$

This time, the couplings are symmetric in the flavor indices $\lambda'_{ab} = \lambda'_{ba}$, and the factor of $\sqrt{2}$ is thrown in for latter convenience. Expanding out, we find

$$\mathcal{L}_\Delta \;=\; \lambda'_{ab}\left[\sqrt{2}\left(\overline{\nu^c_{aL}}\nu_{bL}\right)\Delta^0 - \left(\overline{\nu^c_{aL}}e_{bL} + \overline{e^c_{aL}}\nu_{bL}\right)\Delta^+ - \sqrt{2}\left(\overline{e^c_{aL}}e_{bL}\right)\Delta^{++}\right] + h.c. \quad (3.5.14)$$

and the terms relevant to neutrino oscillation in matter are:

$$-2\left(\lambda'_{ee}\,\overline{\nu^c_{eL}}\,e_L + \lambda'_{e\mu}\,\overline{\nu^c_{\mu L}}\,e_L + \lambda'_{e\tau}\,\overline{\nu^c_{\tau L}}\,e_L\right)\Delta^+ + h.c. \quad (3.5.15)$$

Of these, the λ'_{ee} term does not affect ξ, while the other terms are precisely the same as those listed in Eq. (3.5.5). So without further calculations, we can conclude that all the results of the previous subsection apply in this case also.

Chapter 4

Constraints on R-parity violation from recent Belle/Babar data

In this chapter we discuss possible constraints on R-parity violation from recently announced Belle/Babar results on the $B \to \tau\nu$ branching fraction, and the bounds on $\tau^- \to \ell^- K_S^0$ ($\ell = e$ or μ) from Babar.

4.1 Introduction

Measurements of rare decay processes which are small or absent within the Standard Model (SM) provide windows to new physics. During the past year, new measurements and bounds on the decays $B \to \tau\nu_\tau$ [86, 87] and $\tau \to \ell K_S^0$ ($\ell = e$ or μ) [88] have been announced from Babar and Belle. We discuss what constraints can be placed on new physics from these results using R-parity violating supersymmetry (SUSY) as an example, partially updating the analyses of Dreiner et al. from 2002 [89] and 2006 [90].

4.2 $B \to \tau\nu_\tau$

4.2.1 Experimental Value

Babar recently reported their measurement of the $B \to \tau\nu_\tau$ branching fraction, using 383×10^6 $B\bar{B}$ pairs and two different methods to reconstruct the tagged B, as

$$\begin{aligned} \mathcal{B}(B \to \tau\nu_\tau)_{\text{Babar}-\text{hadronic}} &= \left(1.8\,^{+0.9}_{-0.8}\,(\text{stat.}) \pm 0.4\,(\text{bkg.}) \pm 0.2\,(\text{syst.})\right) \times 10^{-4}\,, \\ \mathcal{B}(B \to \tau\nu_\tau)_{\text{Babar}-\text{semileptonic}} &= \left(0.9 \pm 0.6\,(\text{stat.}) \pm 0.1\,(\text{syst.})\right) \times 10^{-4}\,, \end{aligned} \tag{4.2.1}$$

with the combined value given by [86]

$$\mathcal{B}(B \to \tau\nu_\tau)_{\text{Babar}} = \left(1.2 \pm 0.4\,(\text{stat.}) \pm 0.3\,(\text{bkg.}) \pm 0.2\,(\text{syst.})\right) \times 10^{-4}\,. \tag{4.2.2}$$

Belle also reported a new measurement of $\mathcal{B}(B \to \tau\nu_\tau)$ using 657×10^6 $B\bar{B}$ pairs and semileptonic tagging as [87]

$$\mathcal{B}(B \to \tau\nu_\tau)_{\text{Belle}-\text{semileptonic}} = \left(1.65\,^{+0.38}_{-0.37}\,(\text{stat.})\,^{+0.35}_{-0.37}\,(\text{syst.})\right) \times 10^{-4}\,. \tag{4.2.3}$$

A previous 2006 Belle result using 449×10^6 $B\bar{B}$ pairs and hadronic tagging yielded [91]

$$\mathcal{B}(B \to \tau\nu_\tau)_{\text{Belle-hadronic}} \;=\; \left(1.79\,^{+0.56}_{-0.49}\,(\text{stat.})\,^{+0.46}_{-0.51}\,(\text{syst.})\right) \times 10^{-4}\,. \tag{4.2.4}$$

Incorporating all these results, the world average for the branching fraction as of August 2009 is [92]

$$\mathcal{B}(B \to \tau\nu_\tau)_{\text{exp}} \;=\; (\,1.51 \pm 0.33\,) \times 10^{-4}\,. \tag{4.2.5}$$

4.2.2 Standard Model Value

In the Standard Model (SM), the decay $B \to \tau\nu_\tau$ proceeds via s-channel W-exchange which at low energies is described by the effective Lagrangian

$$\mathcal{L}_W \;=\; -\sqrt{2}\,G_F V_{ub}\big(\,\overline{u}\gamma^\mu(1-\gamma_5)b\,\big)\big(\,\overline{\tau}_L\gamma_\mu\nu_{\tau L}\,\big) \;+\; h.c.\,. \tag{4.2.6}$$

This leads to the SM prediction

$$\mathcal{B}(B \to \tau\nu_\tau) \;=\; \left|\sqrt{2}\,G_F V_{ub} m_\tau\right|^2 \frac{m_B}{16\pi}\left(1-\frac{m_\tau^2}{m_B^2}\right)^2 f_B^2 \tau_B\,, \tag{4.2.7}$$

where the B-decay constant f_B is normalized as

$$\big\langle 0\big|\,\bar{u}(x)\gamma^\mu\gamma_5 b(x)\,\big|B^-(p)\big\rangle \;=\; ip^\mu f_B\, e^{-ipx}\,. \tag{4.2.8}$$

Unlike decays into electrons or muons, the chirality-flip factor $(m_\tau/m_B)^2 \approx 0.1$ is not small, but the decay is nevertheless suppressed due to the smallness of $|V_{ub}|$.

If we wish to compare the experimental value, Eq. (4.2.5), against this SM expression instead of using it to extract $|V_{ub}|f_B$, we must obtain the values of $|V_{ub}|$ and f_B from other sources. The extraction of $|V_{ub}|$ from charmless semileptonic B-decays ($B \to \pi\ell\nu$ with $\ell = e$ or μ) is difficult requiring considerable theoretical input [116, 93, 94, 95]. The value quoted in the 2008 Review of Particle Properties [116, 93] is

$$|V_{ub}|_{\text{RPP}} \;=\; (\,3.95 \pm 0.35\,) \times 10^{-3}\,, \tag{4.2.9}$$

with the error dominated by theoretical uncertainty. Note that in using this value as the SM value of $|V_{ub}|$, we are assuming that new physics will not affect charmless semileptonic B-decay. The value of f_B is obtained from unquenched lattice QCD. The HPQCD collaboration reports [96]

$$f_B \;=\; 0.216 \pm 0.022\ \text{GeV}\,. \tag{4.2.10}$$

As can be seen, both $|V_{ub}|$ and f_B suffer from uncertainties on the order of 10%. Substituting Eqs. (4.2.9) and (4.2.10) into Eq. (4.2.7), we find

$$\mathcal{B}(B \to \tau\nu)_{\text{SM}} \;=\; (\,1.29 \pm\, 0.35) \times 10^{-4}\,. \tag{4.2.11}$$

The UTfit [92] and CKMfit [97] collaborations constrain this branching fraction with global SM fits and respectively find

$$\begin{aligned} \mathcal{B}(B \to \tau\nu)_{\text{UTfit}} \;&=\; (\,0.81 \pm\, 0.12) \times 10^{-4}\,, \\ \mathcal{B}(B \to \tau\nu)_{\text{CKMfit}} \;&=\; (\,0.92\,^{+0.10}_{-0.11}) \times 10^{-4}\,, \end{aligned} \tag{4.2.12}$$

as the SM value. Though the errors are much smaller, and the central values in disagreement with the experimental value by almost 2σ, we use neither of these values and adhere to Eq. (4.2.11) since the presence of new physics that would shift $B \to \tau\nu$ away from the SM may affect other observables used in the global fits as well.

4.2.3 Constraint on New Physics

The fractional errors on both the experimental value, Eq. (4.2.5), and the SM prediction, Eq. (4.2.11), are large. However, the constraint on new physics is not necessarily weak since the SM amplitude itself is suppressed by V_{ub} requiring new physics effects to be equally suppressed. We follow Dobrescu and Kronfeld [98] and assume that new physics effects can be expressed in a model independent way with the effective Lagrangian

$$\mathcal{L}_{\rm new} \;=\; \frac{C_A}{M^2}\big(\,\overline{u}\gamma^\mu\gamma_5 b\,\big)\big(\,\overline{\tau}_L\gamma_\mu\nu_L\,\big) + \frac{C_P}{M^2}\big(\,\overline{u}\gamma_5 b\,\big)\big(\,\overline{\tau}_R\nu_L\,\big) + h.c. \tag{4.2.13}$$

where M is the scale of new physics, and C_A and C_P are constants that may be complex in general. Only these operators will cause the decay amplitude from new physics to interfere with that from the SM shifting $\sqrt{2}\,G_F V_{ub} m_\tau$ in Eq. (4.2.7) to

$$\sqrt{2}\,G_F V_{ub} m_\tau \;\to\; \sqrt{2}\,G_F V_{ub} m_\tau + \frac{1}{M^2}\left(C_A m_\tau - \frac{C_P m_B^2}{m_b}\right)\,, \tag{4.2.14}$$

where the u quark mass has been neglected. Assuming that there is no correlation between the experimental and SM values, Eqs. (4.2.5) and (4.2.11), we find

$$\frac{\mathcal{B}(B\to\tau\nu)_{\rm exp}}{\mathcal{B}(B\to\tau\nu)_{\rm SM}} \;=\; 1.17 \pm 0.41\,, \tag{4.2.15}$$

which translates to

$$\left|\,1 + \frac{1}{\sqrt{2}\,G_F V_{ub} M^2}\left(C_A - C_P\frac{m_B^2}{m_b m_\tau}\right)\right|^2 \;=\; 1.17 \pm 0.41\,. \tag{4.2.16}$$

In the standard CKM parametrization we have $V_{ub} = |V_{ub}|e^{-i\delta}$, where δ is the CP violating phase [128]. Therefore,

$$\left|\,1 + \frac{1}{\sqrt{2}\,G_F V_{ub} M^2}\left(C_A - C_P\frac{m_B^2}{m_b m_\tau}\right)\right|^2 \;\approx\; 1 + 2\,\frac{{\rm Re}\left[e^{i\delta}(C_A - C_P m_B^2/m_b m_\tau)\right]}{\sqrt{2}\,G_F|V_{ub}|M^2} \tag{4.2.17}$$

Setting

$$C \;\equiv\; {\rm Re}\left[e^{i\delta}\big(C_A - C_P m_B^2/m_b m_\tau\big)\right]\,, \tag{4.2.18}$$

the above bound becomes

$$\frac{C}{\sqrt{2}\,G_F|V_{ub}|M^2} \;=\; \Big[(1.53\pm0.14)\times 10^3\Big]\,C\left(\frac{100\,{\rm GeV}}{M}\right)^2 \;=\; 0.09 \pm 0.20\,, \tag{4.2.19}$$

or

$$C\left(\frac{100\,{\rm GeV}}{M}\right)^2 \;=\; 0.00006 \pm 0.00013\,. \tag{4.2.20}$$

The 2σ (95%) range of this ratio is therefore

$$-0.00020 \;<\; C\left(\frac{100\,{\rm GeV}}{M}\right)^2 \;<\; 0.00032\,, \qquad (95\%\ {\rm C.L.})\,. \tag{4.2.21}$$

The bound on the scale of new physics M will depend on the sign of C:

$$\begin{array}{ll} M/\sqrt{+C} \;\geq\; 6\ {\rm TeV} & \text{if } C>0\,, \\ M/\sqrt{-C} \;\geq\; 7\ {\rm TeV} & \text{if } C<0\,, \end{array} \qquad (95\%\ {\rm C.L.})\,. \tag{4.2.22}$$

4.2.4 Constraints on R-parity violation

The new physics to which the above bounds apply must distinguish among fermion flavors since it must affect $B \to \tau\nu_\tau$ without affecting $B \to \pi\ell\nu_\ell$ ($\ell = e$ or μ). As an example, we consider R-parity violating supersymmetry (SUSY), the superpotential of which is given by [99, 47]

$$W_{\not R} = \frac{1}{2}\lambda_{ijk}\hat{L}_i\hat{L}_j\hat{E}_k + \lambda'_{ijk}\hat{L}_i\hat{Q}_j\hat{D}_k + \frac{1}{2}\lambda''_{ijk}\hat{U}_i\hat{D}_j\hat{D}_k \ . \tag{4.2.23}$$

Here i, j, k are generation indices, while $SU(2)$-weak isospin and $SU(3)$-color indices are suppressed. The coefficients λ_{ijk} are antisymmetric in the first two indices, while λ''_{ijk} are antisymmetric in the latter two. Consequently, there are 9 independent LLE couplings, 27 independent LQD couplings, and 9 independent UDD couplings. The decay $B \to \pi\ell\nu_\ell$ ($\ell = e$ or μ) can be affected by the coupling combinations $\lambda'_{i1k}\lambda'^*_{i3k}$ ($i = 1$ or 2, k arbitrary) and $\lambda_{ijj}\lambda'^*_{i13}$ ($j = 1$ or 2, $i = 3$ or $3 - j$) so these are assumed to be sufficiently small. The coupling combinations which affect $B \to \tau\nu_\tau$ are shown in Figure 4.2.1. The decay can proceed either via t-channel sdown exchange, or via s-channel selectron exchange.

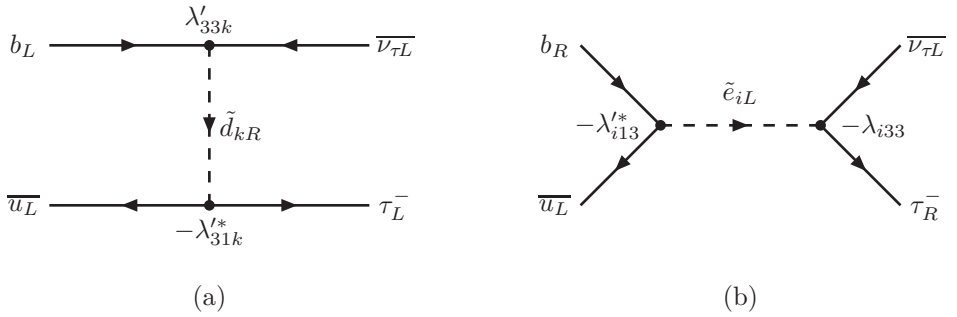

Figure 4.2.1: Possible R-parity violating contributions to $B^- \to \tau^-\bar{\nu}_\tau$. The index is $k = 1$, 2, or 3 in (a), while $i = 1$ or 2 in (b) due to the anti-symmetry of λ_{ijk} in the first two indices.

t-channel sdown exchange

t-channel exchange of $\tilde{d}_{kR}$ ($k = 1, 2$, or 3) is described by the effective operator

$$\mathcal{L}_{\tilde{d}_{kR}} \ = \ -\frac{\lambda'_{33k}\lambda'^*_{31k}}{M^2_{\tilde{d}_{kR}}}\left(\overline{u_L}\tau_L^c\right)\left(\overline{\nu^c_{\tau L}}b_L\right) \ . \tag{4.2.24}$$

A Fierz transformation allows us to rewrite

$$\left(\overline{u_L}\tau_L^c\right)\left(\overline{\nu^c_{\tau L}}b_L\right) \ = \ -\frac{1}{2}\left(\overline{u_L}\gamma_\mu b_L\right)\left(\overline{\nu^c_{\tau L}}\gamma^\mu\tau_L^c\right) \ = \ +\frac{1}{4}\left(\overline{u}\gamma_\mu(1-\gamma_5)b\right)\left(\overline{\tau}_L\gamma^\mu\nu_{\tau L}\right) . \tag{4.2.25}$$

The relevant part of the operator Eq. (4.2.24) is therefore

$$+\frac{\lambda'_{33k}\lambda'^*_{31k}}{4M^2_{\tilde{d}_{kR}}}\left(\overline{u}\gamma_\mu\gamma_5 b\right)\left(\overline{\tau}_L\gamma^\mu\nu_{\tau L}\right) . \tag{4.2.26}$$

Comparison with Eqs. (4.2.13) and (4.2.18) leads to the identifications

$$M \;=\; M_{\tilde{d}_{kR}}\,, \qquad C_A \;=\; \frac{\lambda'_{33k}\lambda'^{*}_{31k}}{4}\,, \qquad C \;=\; \mathrm{Re}\left[e^{i\delta}C_A\right] \;=\; \frac{\mathrm{Re}\left[e^{i\delta}\lambda'_{33k}\lambda'^{*}_{31k}\right]}{4}\,. \tag{4.2.27}$$

Allowing only one sdown contribution to be non-zero at a time, the bounds of Eq. (4.2.21) translate to

$$-0.0008 \;<\; \mathrm{Re}\left[e^{i\delta}\lambda'_{33k}\lambda'^{*}_{31k}\right]\left(\frac{100\,\mathrm{GeV}}{M_{\tilde{d}_{kR}}}\right)^2 \;<\; +0.0013\,, \qquad (95\%\ \mathrm{C.L.})\,. \tag{4.2.28}$$

The bounds on the sdown mass are

$$\begin{array}{ll} \dfrac{M_{\tilde{d}_{kR}}}{\sqrt{+\mathrm{Re}\left[e^{i\delta}\lambda'_{33k}\lambda'^{*}_{31k}\right]}} \;\geq\; 3\ \mathrm{TeV} & \text{if } \mathrm{Re}\left[e^{i\delta}\lambda'_{33k}\lambda'^{*}_{31k}\right] > 0\,, \\ \dfrac{M_{\tilde{d}_{kR}}}{\sqrt{-\mathrm{Re}\left[e^{i\delta}\lambda'_{33k}\lambda'^{*}_{31k}\right]}} \;\geq\; 4\ \mathrm{TeV} & \text{if } \mathrm{Re}\left[e^{i\delta}\lambda'_{33k}\lambda'^{*}_{31k}\right] < 0\,, \end{array} \qquad (95\%\ \mathrm{C.L.})\,. \tag{4.2.29}$$

s-channel selectron exchange

s-channel exchange of $\tilde{e}_{iL}$ ($i = 1$ or 2) is described by the effective operator

$$\mathcal{L}_{\tilde{e}_{iL}} \;=\; \frac{\lambda_{i33}\lambda'^{*}_{i13}}{M^2_{\tilde{e}_{iL}}}\big(\,\overline{u}_L b_R\,\big)\big(\,\overline{\tau}_R\nu_{\tau L}\,\big) \;=\; \frac{\lambda_{i33}\lambda'^{*}_{i13}}{2M^2_{\tilde{e}_{iL}}}\big(\,\overline{u}(1+\gamma_5)b\,\big)\big(\,\overline{\tau}_R\nu_{\tau L}\,\big)\,, \tag{4.2.30}$$

the relevant part of which is

$$\frac{\lambda_{i33}\lambda'^{*}_{i13}}{2M^2_{\tilde{e}_{iL}}}\big(\,\overline{u}\gamma_5 b\,\big)\big(\,\overline{\tau}_R\nu_{\tau L}\,\big)\,. \tag{4.2.31}$$

Comparison with Eqs. (4.2.13) and (4.2.18) leads to the identifications

$$M \;=\; M_{\tilde{e}_{iL}}\,, \qquad C_P \;=\; \frac{\lambda_{i33}\lambda'^{*}_{i13}}{2}\,, \qquad C \;=\; \frac{m_B^2}{m_b m_\tau}\mathrm{Re}\left[-e^{i\delta}C_P\right] \;=\; \frac{m_B^2}{2m_b m_\tau}\mathrm{Re}\left[-e^{i\delta}\lambda_{i33}\lambda'^{*}_{i13}\right]\,. \tag{4.2.32}$$

The factor $m_B^2/m_b m_\tau$ is equal to [100]

$$\frac{m_B^2}{m_b m_\tau} \;=\; \frac{(\,5.27917 \pm 0.00029\ \mathrm{GeV}\,)^2}{(\,1.77684 \pm 0.00017\ \mathrm{GeV}\,)(\,4.79\,^{+0.19}_{-0.08}\ \mathrm{GeV}\,)} \;=\; 3.27\,^{+0.06}_{-0.12}\,, \tag{4.2.33}$$

where we have used the pole mass for m_b. Allowing only one selectron contribution to be non-zero at a time, the bounds of Eq. (4.2.21) translate to

$$-0.00012 \;<\; \mathrm{Re}\left[-e^{i\delta}\lambda_{i33}\lambda'^{*}_{i13}\right]\left(\frac{100\,\mathrm{GeV}}{M_{\tilde{e}_{iL}}}\right)^2 \;<\; +0.00020\ \,, \qquad (95\%\ \mathrm{C.L.})\,. \tag{4.2.34}$$

The corresponding bounds on the selectron mass are

$$\begin{array}{ll} \dfrac{M_{\tilde{e}_{iL}}}{\sqrt{+\mathrm{Re}\left[-e^{i\delta}\lambda_{i33}\lambda'^{*}_{i13}\right]}} \;\geq\; 7\ \mathrm{TeV} & \text{if } \mathrm{Re}\left[-e^{i\delta}\lambda_{i33}\lambda'^{*}_{i13}\right] > 0\,, \\ \dfrac{M_{\tilde{e}_{iL}}}{\sqrt{-\mathrm{Re}\left[-e^{i\delta}\lambda_{i33}\lambda'^{*}_{i13}\right]}} \;\geq\; 9\ \mathrm{TeV} & \text{if } \mathrm{Re}\left[-e^{i\delta}\lambda_{i33}\lambda'^{*}_{i13}\right] < 0\,, \end{array} \qquad (95\%\ \mathrm{C.L.})\,. \tag{4.2.35}$$

4.3 $\tau^- \to \ell^- K_S^0$

4.3.1 Experimental Bounds on Lepton Flavor Violating τ Decays

Babar recently reported their measurements for tau lepton-flavor-violating decays $\tau^- \to \ell^- K_S^0$ ($\ell = e$ or μ) using a data sample corresponding to an integrated luminosity of $469\,\text{fb}^{-1}$. The upper limits on the branching fractions for the two channels, at 90% confidence level, are [88]

$$\begin{array}{rcl} \mathcal{B}(\tau^- \to \mu^- K_S^0)_{\text{Babar}} & < & 4.0 \times 10^{-8}\,, \\ \mathcal{B}(\tau^- \to e^- K_S^0)_{\text{Babar}} & < & 3.3 \times 10^{-8}\,, \end{array} \qquad (90\%\ \text{C.L.})\,. \tag{4.3.1}$$

These supercede the previous 90% bounds from Belle based on $281\,\text{fb}^{-1}$ of data, which were [101]

$$\begin{array}{rcl} \mathcal{B}(\tau^- \to \mu^- K_S^0)_{\text{Belle}} & < & 4.9 \times 10^{-8}\,, \\ \mathcal{B}(\tau^- \to e^- K_S^0)_{\text{Belle}} & < & 5.6 \times 10^{-8}\,, \end{array} \qquad (90\%\ \text{C.L.})\,. \tag{4.3.2}$$

For the sake of comparison with the bounds from $B \to \tau\nu$ we derived in the previous section, and also with the previous bounds from Ref. [90], we will use the 95% confidence level bounds from Babar, which can be read off from Fig. 4 of Ref. [88] as

$$\begin{array}{rcl} \mathcal{B}(\tau^- \to \mu^- K_S^0)_{\text{Babar}} & < & 5.2 \times 10^{-8}\,, \\ \mathcal{B}(\tau^- \to e^- K_S^0)_{\text{Babar}} & < & 4.3 \times 10^{-8}\,, \end{array} \qquad (95\%\ \text{C.L.})\,. \tag{4.3.3}$$

Since there exist no SM contribution to these processes, these bounds translate directly into bounds on new physics.

4.3.2 Constraints on R-parity violation

As in the $B \to \tau\nu_\tau$ analysis, we use R-parity violating SUSY as an example. Possible contributions to the process $\tau^- \to \ell^- K_S^0$ from R-parity violation are shown in Figure 4.3.1. The decay can proceed either via sup exchange, or sneutrino exchange.

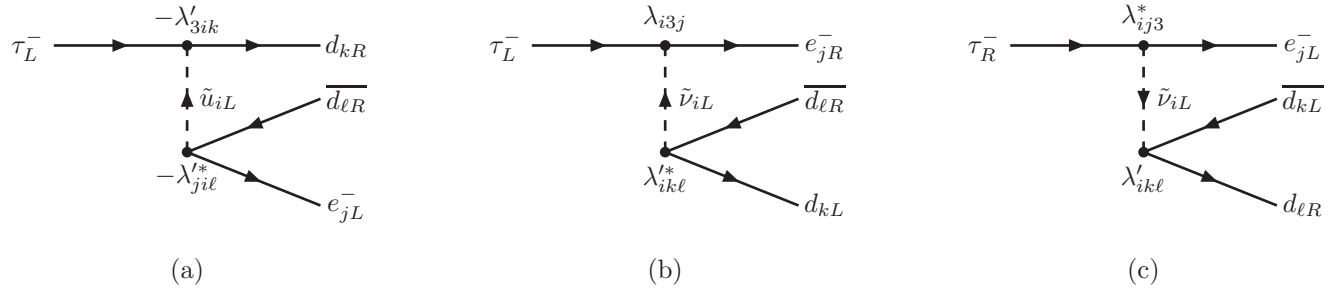

Figure 4.3.1: Possible R-parity violating contributions to $\tau^- \to \ell^- K_S^0$, ($\ell = e$ or μ). The indices are $j = 1$ or 2, $(k\ell) = (12)$ or (21). The index i for the sup exchange diagram can take on any value from 1 to 3, but that in the sneutrino exchange diagrams is restricted due to the antisymmetry of λ_{ijk} in the first two indices and only two values are possible for each diagram: $i = 1$ or 2 in (b), and $i = 3$ or $3 - j$ in (c).

sup exchange

For definiteness, let us first consider the decay $\tau^- \to \mu^- K_S^0$ via the sup exchange subprocess $\tau_L^- \to \mu_L^- \overline{s_R} d_R$ or $\tau_L^- \to \mu_L^- \overline{d_R} s_R$ shown in Figure 4.3.1(a). The indices for these subprocesses are $j = 2$ with $(k\ell) = (12)$ or (21). The effective operator induced by $\tilde{u}_{iL}$ ($i = 1, 2$, or 3) exchange is

$$\mathcal{L}_{\tilde{u}_{iL}} \;=\; \frac{\lambda'_{3ik}\lambda'^*_{2i\ell}}{M^2_{\tilde{u}_{iL}}} \big(\,\overline{d_{kR}}\tau_L\,\big)\big(\,\overline{\mu_L} d_{\ell R}\,\big)\;. \tag{4.3.4}$$

A Fierz transformation allows us to rewrite

$$\big(\,\overline{d_{kR}}\tau_L\,\big)\big(\,\overline{\mu_L} d_{\ell R}\,\big) \;=\; \frac{1}{2}\big(\,\overline{d_{kR}}\gamma_\mu d_{\ell R}\,\big)\big(\,\overline{\mu_L}\gamma^\mu \tau_L\,\big) \;=\; \frac{1}{4}\big(\,\overline{d_k}\gamma_\mu(1+\gamma_5) d_\ell\,\big)\big(\,\overline{\mu_L}\gamma^\mu \tau_L\,\big)\;, \tag{4.3.5}$$

and the part of the operator relevant for the decay in question is

$$\frac{\lambda'_{3ik}\lambda'^*_{2i\ell}}{4M^2_{\tilde{u}_{iL}}} \big(\,\overline{d_k}\gamma_\mu\gamma_5 d_\ell\,\big)\big(\,\overline{\mu_L}\gamma^\mu \tau_L\,\big)\;. \tag{4.3.6}$$

The matrix element of $\overline{d_\ell}\gamma^\mu\gamma_5 d_k$ between the vacuum and the $K_S^0 = (K^0 + \overline{K^0})/\sqrt{2}$ state can be expressed as

$$\big\langle K_S^0(p)\big|\,\overline{d_\ell}(x)\gamma^\mu\gamma_5 d_k(x)\,\big|0\big\rangle \;=\; -\frac{i}{\sqrt{2}}\, p^\mu f_{K^0}\, e^{ipx}\;, \tag{4.3.7}$$

where the K^0 decay constant f_{K^0} is defined as

$$\big\langle 0\big|\,\overline{s}(x)\gamma^\mu\gamma_5 d(x)\,\big|K^0(p)\big\rangle \;=\; \big\langle 0\big|\,\overline{d}(x)\gamma^\mu\gamma_5 s(x)\,\big|\overline{K^0}(p)\big\rangle \;=\; ip^\mu f_{K^0}\, e^{-ipx}\;. \tag{4.3.8}$$

The $\tau^- \to \mu^- K_S^0$ branching fraction due to the operator Eq. (4.3.6) is then expressed as [90]

$$\mathcal{B}(\tau^- \to \mu^- K_S^0) \;=\; \frac{|\lambda'_{3ik}\lambda'^*_{2i\ell}|^2}{M^4_{\tilde{u}_{iL}}}\; \frac{\sqrt{\Lambda(m_\tau^2, m_\mu^2, m_K^2)}\Big[\,(m_\tau^2 - m_\mu^2)^2 - m_K^2(m_\tau^2 + m_\mu^2)\,\Big]}{1024\pi\, m_\tau^3}\,(f_{K^0})^2\,\tau_\tau\;, \tag{4.3.9}$$

where

$$\Lambda(a,b,c) \;\equiv\; a^2 + b^2 + c^2 - 2ab - 2bc - 2ca\;. \tag{4.3.10}$$

Invoking isospin symmetry, we assume that f_{K^0} is equal to the decay constant of the charged Kaons $f_{K^\pm} = 0.1555 \pm 0.0008\,\mathrm{GeV}$ [102] and find

$$\mathcal{B}(\tau^- \to \mu^- K_S^0) \;=\; (\,0.1561 \pm 0.0017\,)\;|\lambda'_{3ik}\lambda'^*_{2i\ell}|^2 \left(\frac{100\,\mathrm{GeV}}{M_{\tilde{u}_{iL}}}\right)^4\;. \tag{4.3.11}$$

Then, the 95% Babar bound, Eq. (4.3.3), translates to

$$\sqrt{|\lambda'_{3ik}\lambda'^*_{2i\ell}|}\left(\frac{100\,\mathrm{GeV}}{M_{\tilde{u}_{iL}}}\right) \;<\; 0.024\;, \qquad \text{or} \qquad \frac{M_{\tilde{u}_{iL}}}{\sqrt{|\lambda'_{3ik}\lambda'^*_{2i\ell}|}} \;>\; 4.2\,\mathrm{TeV}\;, \qquad (95\%\ \mathrm{C.L.})\;. \tag{4.3.12}$$

Similarly, the branching fraction of $\tau^- \to e^- K_S^0$ proceeding via the subprocesses $\tau_L^- \to e_L^- \overline{s_R} d_R$ and $\tau_L^- \to e_L^- \overline{d_R} s_R$ is given by

$$\mathcal{B}(\tau^- \to e^- K_S^0) \;=\; \frac{|\lambda'_{3ik}\lambda'^*_{1i\ell}|^2}{M^4_{\tilde{u}_{iL}}}\; \frac{\sqrt{\Lambda(m_\tau^2, m_e^2, m_K^2)}\Big[\,(m_\tau^2 - m_e^2)^2 - m_K^2(m_\tau^2 + m_e^2)\,\Big]}{1024\pi\, m_\tau^3}\,(f_{K^0})^2\,\tau_\tau$$

$$= \ (\,0.1581 \pm 0.0017\,)\ |\lambda'_{3i1}\lambda'^{*}_{1i2}|^2 \left(\frac{100\,\mathrm{GeV}}{M_{\tilde{u}_{iL}}}\right)^4 . \tag{4.3.13}$$

The constraint from the 95% Babar bound, Eq. (4.3.3), is then

$$\sqrt{|\lambda'_{3ik}\lambda'^{*}_{1i\ell}|}\left(\frac{100\,\mathrm{GeV}}{M_{\tilde{u}_{iL}}}\right) \ < \ 0.023\,, \qquad \text{or} \qquad \frac{M_{\tilde{u}_{iL}}}{\sqrt{|\lambda'_{3ik}\lambda'^{*}_{1i\ell}|}} \ > \ 4.4\,\mathrm{TeV}\,, \qquad (95\%\ \mathrm{C.L.})\,. \tag{4.3.14}$$

sneutrino exchange

Next, we consider the decay $\tau^- \to \mu^- K^0_S$ via the sneutrino exchange subprocess $\tau^-_L \to \mu^-_R \overline{s_R} d_L$ or $\tau^-_L \to \mu^-_R \overline{d_R} s_L$ shown in Figure 4.3.1(b). The indices for these subprocesses are $j = 2$ with $(k\ell) = (12)$ or (21). The effective operator induced by $\tilde{\nu}_{iL}$ ($i = 1$ or 2) exchange is

$$\mathcal{L}_{\tilde{\nu}_{iL}} \ = \ \frac{\lambda_{i32}\lambda'^{*}_{ik\ell}}{M^2_{\tilde{\nu}_{iL}}}\big(\,\overline{\mu_R}\tau_L\,\big)\big(\,\overline{d_{kL}}d_{\ell R}\,\big) \ = \ \frac{\lambda_{i32}\lambda'^{*}_{ik\ell}}{2M^2_{\tilde{\nu}_{iL}}}\big(\,\overline{\mu_R}\tau_L\,\big)\big(\,\overline{d_k}(1+\gamma_5)d_\ell\,\big)\,. \tag{4.3.15}$$

The part of this operator that is relevant for the decay is

$$\frac{\lambda_{i3j}\lambda'^{*}_{ik\ell}}{2M^2_{\tilde{\nu}_{iL}}}\big(\,\overline{\mu_R}\tau_L\,\big)\big(\,\overline{d_k}\gamma_5 d_\ell\,\big)\,, \tag{4.3.16}$$

leading to the branching fraction [90]

$$\mathcal{B}(\tau^- \to \mu^- K^0_S) \ = \ \frac{|\lambda_{i32}\lambda'^{*}_{ik\ell}|^2}{M^4_{\tilde{\nu}_{iL}}}\ \frac{\sqrt{\Lambda(m_\tau^2, m_\mu^2, m_K^2)}\Big(\,m_\tau^2 + m_\mu^2 - m_K^2\,\Big)m_K^2}{256\pi\, m_\tau^3}\ \xi^2 (f_{K^0})^2\,\tau_\tau\,, \tag{4.3.17}$$

where the factor ξ is defined as:

$$\xi \ \equiv \ \frac{m_K}{m_d + m_s} \ \approx \ \frac{m_K}{m_s} \ = \ \frac{(496.614 \pm 0.024\,\mathrm{MeV})}{(105\,^{+25}_{-35}\,\mathrm{MeV})} \ = \ 4 \sim 7\,. \tag{4.3.18}$$

Here, we have used the $\overline{\mathrm{MS}}$ mass at $\mu = 2\,\mathrm{GeV}$ for m_s. The error introduced by the neglect of m_d is only about 5%. Allowing ξ to sweep this range, we find

$$\mathcal{B}(\tau^- \to \mu^- K^0_S) \ = \ \big(\,0.8 \sim 2.4\,\big)\,|\lambda_{i32}\lambda'^{*}_{ik\ell}|^2 \left(\frac{100\,\mathrm{GeV}}{M_{\tilde{\nu}_{iL}}}\right)^4\,, \tag{4.3.19}$$

and Eq. (4.3.3) translates to

$$\sqrt{|\lambda_{i32}\lambda'^{*}_{ik\ell}|}\left(\frac{100\,\mathrm{GeV}}{M_{\tilde{\nu}_{iL}}}\right) \ < \ 0.012 \sim 0.016\,, \qquad \frac{M_{\tilde{\nu}_{iL}}}{\sqrt{|\lambda_{i32}\lambda'^{*}_{ik\ell}|}} \ > \ (6 \sim 8)\,\mathrm{TeV}\,, \qquad (95\%\ \mathrm{C.L.})\,. \tag{4.3.20}$$

The branching fraction due to the subprocesses $\tau^-_R \to \mu^-_L \overline{s_L} d_R$ or $\tau^-_R \to \mu^-_L \overline{d_L} s_R$ shown in Figure 4.3.1(c) is the same as Eq. (4.3.17) except with the coupling constants replaced by the combination $\lambda_{i23}\lambda'^{*}_{ik\ell}$ with $i = 1$ or 3, to which the exact same bounds apply.

The analysis for the decay $\tau^- \to e^- K_S^0$ proceeds in an exactly analogous fashion and the results are

$$\sqrt{|\lambda_{i31}\lambda'^*_{ik\ell}|}\left(\frac{100\,\mathrm{GeV}}{M_{\tilde{\nu}_{iL}}}\right) \;<\; 0.011 \sim 0.015\,, \qquad \frac{M_{\tilde{\nu}_{iL}}}{\sqrt{|\lambda_{i31}\lambda'^*_{ik\ell}|}} \;>\; (7 \sim 9)\,\mathrm{TeV}\,, \qquad (95\%\ \mathrm{C.L.})\,, \tag{4.3.21}$$

with $i = 1$ or 2. The same bounds apply to $\lambda_{i13}\lambda'^*_{ik\ell}$ with $i = 2$ or 3.

$\lambda'\lambda'$	decay	sparticle	new bound	previous bound [Ref] (year)	Product of single-coupling 2σ bounds
$(31k)(33k)$	$B \to \tau\nu_\tau$	$\tilde{d}_{kR}$	$-0.8 \times 10^{-3} < \mathrm{Re}[e^{i\delta}\lambda'\lambda'^*] < 1.3 \times 10^{-3}$	N/A	0.03 $[R_{\tau\pi}][R_\tau^Z]$
(211)(312)	$\tau^- \to \mu^- K_S^0$	$\tilde{u}_{1L}$	$\lvert\lambda'\lambda'^*\rvert < 5.8 \times 10^{-4}$	2.4×10^{-3} [90] (2006)	0.004 $[R_\pi][R_{\tau\pi}]$
(212)(311)		$\tilde{u}_{1L}$			0.004 $[R_\pi][R_{\tau\pi}]$
(221)(322)		$\tilde{u}_{2L}$			0.03 $[R_{D^0}][R_{D_s}(\tau\mu)]$
(222)(321)		$\tilde{u}_{2L}$			0.03 $[R_{D^0}][R_{D_s}(\tau\mu)]$
(231)(332)		$\tilde{u}_{3L}$			0.3 $[R_\mu^Z][R_\tau^Z]$
(232)(331)		$\tilde{u}_{3L}$			0.3 $[R_\mu^Z][R_\tau^Z]$
(111)(312)	$\tau^- \to e^- K_S^0$	$\tilde{u}_{1L}$	$\lvert\lambda'\lambda'^*\rvert < 5.2 \times 10^{-4}$	2.3×10^{-3} [90] (2006)	4×10^{-5} $[\beta\beta0\nu][R_{\tau\pi}]$
(112)(311)		$\tilde{u}_{1L}$			0.002 $[V_{us}, R_\pi][R_{\tau\pi}]$
(121)(322)		$\tilde{u}_{2L}$			0.01 $[Q_W(^{133}\mathrm{Cs})][R_{D_s}(\tau\mu)]$
(122)(321)		$\tilde{u}_{2L}$			0.06 $[R_{D^+}][R_{D_s}(\tau\mu)]$
(131)(332)		$\tilde{u}_{3L}$			0.02 $[Q_W(^{133}\mathrm{Cs})][R_\tau^Z]$
(132)(331)		$\tilde{u}_{3L}$			0.2 $[A_{\mathrm{FB}}^s][R_\tau^Z]$
$\lambda\lambda'$	decay	sparticle	new bound	previous bound [Ref] (year)	Product of single-coupling 2σ bounds
(133)(113)	$B \to \tau\nu_\tau$	$\tilde{e}_{1L}$	$-1.2 \times 10^{-4} < \mathrm{Re}[-e^{i\delta}\lambda\lambda'^*] < 2.0 \times 10^{-4}$	$-6 \times 10^{-4} < \mathrm{Re}[\lambda\lambda'^*] < 1 \times 10^{-3}$	0.002 $[R_\tau][V_{ud}, R_\pi]$
(233)(213)		$\tilde{e}_{2L}$		[89] (2002)	0.003 $[R_\tau][R_\pi]$
(123)(112)	$\tau^- \to \mu^- K_S^0$	$\tilde{\nu}_{1L}$	$\lvert\lambda'\lambda'^*\rvert < (1.5 \sim 2.6) \times 10^{-4}$	1.0×10^{-3} [90] (2006)	0.001 $[V_{ud}][R_\pi, Q_W(^{133}\mathrm{Cs})]$
(123)(121)		$\tilde{\nu}_{1L}$			0.001 $[V_{ud}][Q_W(^{133}\mathrm{Cs})]$
(132)(112)		$\tilde{\nu}_{1L}$			0.002 $[R_\tau][V_{ud}, R_\pi]$
(132)(121)		$\tilde{\nu}_{1L}$			0.002 $[R_\tau][Q_W(^{133}\mathrm{Cs})]$
(232)(212)		$\tilde{\nu}_{2L}$			0.003 $[R_\tau][R_\pi]$
(232)(221)		$\tilde{\nu}_{2L}$			0.005 $[R_\tau][R_{D^0}]$
(233)(312)		$\tilde{\nu}_{3L}$			0.003 $[R_\tau][R_{\tau\pi}]$
(233)(321)		$\tilde{\nu}_{3L}$			0.02 $[R_\tau][R_{D_s}(\tau\mu)]$
(123)(212)	$\tau^- \to e^- K_S^0$	$\tilde{\nu}_{2L}$	$\lvert\lambda'\lambda'^*\rvert < (1.3 \sim 2.3) \times 10^{-4}$	9.7×10^{-4} [90] (2006)	0.002 $[V_{ud}][R_\pi]$
(123)(221)		$\tilde{\nu}_{2L}$			0.003 $[V_{ud}][R_{D^0}]$
(131)(112)		$\tilde{\nu}_{1L}$			0.002 $[R_\tau][V_{ud}, R_\pi]$
(131)(121)		$\tilde{\nu}_{1L}$			0.002 $[R_\tau][Q_W(^{133}\mathrm{Cs})]$
(133)(312)		$\tilde{\nu}_{3L}$			0.003 $[R_\tau][R_{\tau\pi}]$
(133)(321)		$\tilde{\nu}_{3L}$			0.02 $[R_\tau][R_{D_s}(\tau\mu)]$
(231)(212)		$\tilde{\nu}_{2L}$			0.003 $[R_\tau][R_\pi]$
(231)(221)		$\tilde{\nu}_{2L}$			0.005 $[R_\tau][R_{D^0}]$

Table 4.1: The 2σ (95% C.L.) bounds on R-parity violating couplings with the mediating sparticle masses set to 100 GeV. The indices on λ have be reordered using the anti-symmetry in the first two indices. The rightmost column shows the product of the 2σ single-coupling bounds listed in Table **??**. The observables that provide the individual constraints are in shown in brackets.

Chapter 5

Single-Coupling Bounds on R-parity violating Supersymmetry, an update

We update the single-coupling bounds on R-parity violating supersymmetry using the most up to date data as of October 2009. In addition to the data listed in the 2009 Review of Particle Properties [116], we utilize a new determination of the weak charge of cesium-133 [103], and preliminary τ-decay branching fractions from Babar [104]. Analysis of semileptonic D-decay is improved by the inclusion of experimentally measured form-factors into the calculation of the Standard Model predictions.

5.1 Introduction

R-parity violating supersymmetry (SUSY) interactions [99, 47] provide a convenient framework for quantifying quark- and lepton-flavor violating effects that new physics beyond the Standard Model (SM) may have, independently of whether SUSY truly exists in nature or not. Consequently, various authors have used a variety of flavor sensitive observables to constrain the sizes of these couplings [47, 117, 118, 119, 120, 105, 121, 122, 123, 89, 124, 125]. We update the single-coupling bounds, namely the bounds on the individual R-parity violating couplings when only that particular coupling is assumed to be non-zero, using the most up to date precision data available as of October 2009. These include various lepton and meson decay ratios, CKM matrix elements, and the weak charge of atomic nuclei.

The superpotential of R-partiy violating SUSY interactions is given by [99, 47]

$$W_{\not R} = \frac{1}{2}\lambda_{ijk}\hat{L}_i\hat{L}_j\hat{E}_k + \lambda'_{ijk}\hat{L}_i\hat{Q}_j\hat{D}_k + \frac{1}{2}\lambda''_{ijk}\hat{U}_i\hat{D}_j\hat{D}_k \ . \tag{5.1.1}$$

Here i, j, k are generation indices, while $SU(2)$-weak isospin and $SU(3)$-color indices are suppressed. The coefficients λ_{ijk} are antisymmetric in the first two indices, while λ''_{ijk} are antisymmetric in the latter two. Consequently, there are 9 independent LLE couplings, 27 independent LQD couplings, and 9 independent UDD couplings. The λ''_{ijk} couplings lead to baryon number violating effects and are already very strongly constrained by proton decay [47], either individually [126] or in products with the λ_{ijk} and λ'_{ijk} couplings [127], so they will not be considered here.

The explicit forms of the LLE and LQD interactions in terms of four-component spinors are

$$\begin{aligned}\mathcal{L}_{LLE} &= \lambda_{(i<j)k}\left[\left(\tilde{\nu}_{iL}\overline{e_{kR}}e_{jL}+\tilde{e}_{jL}\overline{e_{kR}}\nu_{iL}+\tilde{e}^*_{kR}\overline{\nu^c_{iL}}e_{jL}\right)-\left(\tilde{\nu}_{jL}\overline{e_{kR}}e_{iL}+\tilde{e}_{iL}\overline{e_{kR}}\nu_{jL}+\tilde{e}^*_{kR}\overline{\nu^c_{jL}}e_{iL}\right)\right]+h.c.\\ \mathcal{L}_{LQD} &= \lambda'_{ijk}\left[\left(\tilde{\nu}_{iL}\overline{d_{kR}}d_{jL}+\tilde{d}_{jL}\overline{d_{kR}}\nu_{iL}+\tilde{d}^*_{kR}\overline{\nu^c_{iL}}d_{jL}\right)-\left(\tilde{e}_{iL}\overline{d_{kR}}u_{jL}+\tilde{u}_{jL}\overline{d_{kR}}e_{iL}+\tilde{d}^*_{kR}\overline{e^c_{iL}}u_{jL}\right)\right]+h.c.\end{aligned} \tag{5.1.2}$$

Note that the charge-conjugated chiral fermion fields are denoted $f^c_{L/R}=(f_{L/R})^c=(f^c)_{R/L}$. The exchange of squarks or sleptons mediate interactions among the SM fermions, and the strength of these interactions will be proportional to the ratio of coupling constant squared to the exchanged sparticle mass squared. To simplify or notation, we follow Ref. [47] and define

$$r_{ijk}(\tilde{\ell}) \equiv \frac{1}{4\sqrt{2}G_F}\frac{|\lambda_{ijk}|^2}{M^2_{\tilde{\ell}}}\,, \qquad r'_{ijk}(\tilde{q}) \equiv \frac{1}{4\sqrt{2}G_F}\frac{|\lambda'_{ijk}|^2}{M^2_{\tilde{q}}}\,. \tag{5.1.3}$$

Shifts in various observables will be expresses in terms of these dimensionless parameter combinations. The final bounds on the coupling constant will be shown with all the sparticle masses set to 100 GeV.

In the following sections, we look at the bounds from μ and τ leptonic decays, $\tau \to \pi\nu$ and π decays, CKM unitarity, semi-leptonic D and leptonic D_s decays, the weak charge of cesium-133, and neutrinoless double beta decay. For analyses involving τ-decay, the impact of preliminary τ-decay data from Babar [104] is discussed. The analysis of semi-leptonic D decay is improved by a new calculation of the Standard Model (SM) predictions, which include the effects of experimentally determined form-factors. The analysis of the weak charge of cesium-133 corrects an error in Ref. [47]. Bounds from Z-peak observables are not updated since no new data have been generated since the 2005 review by Barbier et al. [47].

5.2 μ and τ Decay

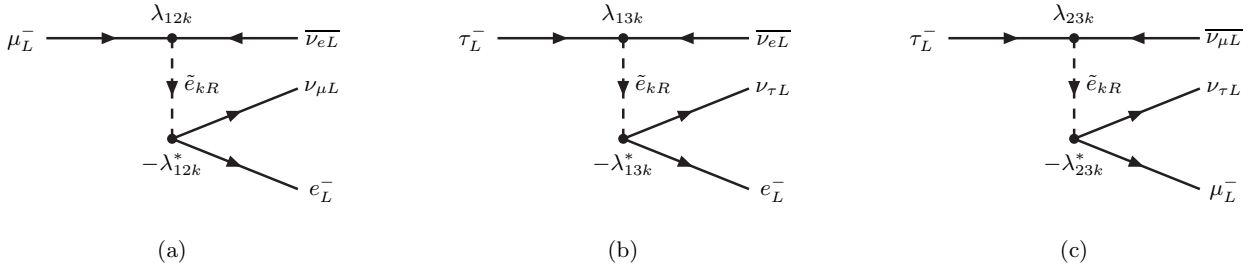

Figure 5.2.1: Possible R-parity violating contributions to (a) $\mu^- \to e^-\overline{\nu_e}\nu_\mu$, (b) $\tau^- \to e^-\overline{\nu_e}\nu_\tau$, and (c) $\tau^- \to \mu^-\overline{\nu_\mu}\nu_\tau$.

The LLE couplings λ_{ijk} affect the decays $\mu^- \to e^-\overline{\nu_e}\nu_\mu$, $\tau^- \to e^-\overline{\nu_e}\nu_\tau$, and $\tau^- \to \mu^-\overline{\nu_\mu}\nu_\tau$ via the processes shown in Fig. 5.2.1. The operator induced by the exchange of $\tilde{e}_{kR}$ $(k=1,2,3)$ via

the coupling $\lambda_{(i<j)k}$ is

$$-\frac{|\lambda_{(i<j)k}|^2}{M^2_{\tilde{e}_{kR}}}\big(\,\overline{\nu^c_{iL}}e_{jL}\,\big)\big(\,\overline{e_{iL}}\nu^c_{jL}\,\big) \quad \stackrel{\text{Fierz}}{\longrightarrow} \quad -\frac{|\lambda_{(i<j)k}|^2}{2M^2_{\tilde{e}_{kR}}}\big(\,\overline{\nu_{jL}}\gamma^\mu e_{jL}\,\big)\big(\,\overline{e_{iL}}\gamma_\mu\nu_{iL}\,\big)\;. \tag{5.2.1}$$

This will interfere with the SM operator

$$-\frac{4G_F}{\sqrt{2}}\big(\,\overline{\nu_{jL}}\gamma^\mu e_{jL}\,\big)\big(\,\overline{e_{iL}}\gamma_\mu\nu_{iL}\,\big)\;, \qquad (i<j)\;, \tag{5.2.2}$$

shifting the effective coupling to

$$\frac{4G_F}{\sqrt{2}} \;\to\; \frac{4G_F}{\sqrt{2}}\Big[\,1+r_{(i<j)k}(\tilde{e}_{kR})\,\Big]\;. \tag{5.2.3}$$

In particular, λ_{12k} will shift the muon decay constant G_μ to

$$G_\mu \;\to\; G_F\Big[\,1+r_{12k}(\tilde{e}_{kR})\,\Big]\;, \tag{5.2.4}$$

and this shift will also affect other observables to be discussed later. The ratios

$$R_{\tau\mu} \;=\; \frac{\Gamma(\tau^-\to\mu^-\overline{\nu_\mu}\nu_\tau)}{\Gamma(\mu^-\to e^-\overline{\nu_e}\nu_\mu)} \qquad \text{and} \qquad R_\tau \;=\; \frac{\Gamma(\tau^-\to e^-\overline{\nu_e}\nu_\tau)}{\Gamma(\tau^-\to\mu^-\overline{\nu_\mu}\nu_\tau)} \tag{5.2.5}$$

will be shifted to

$$\begin{aligned} R_{\tau\mu} &= [R_{\tau\mu}]_{\rm SM}\Big[1+2\Big\{r_{23k}(\tilde{e}_{kR})-r_{12k}(\tilde{e}_{kR})\Big\}\Big]\;,\\ R_\tau &= [R_\tau]_{\rm SM}\Big[1+2\Big\{r_{13k}(\tilde{e}_{kR})-r_{23k}(\tilde{e}_{kR})\Big\}\Big]\;. \end{aligned} \tag{5.2.6}$$

The SM predictions for the decay widths including radiative corrections [108, 109] are:

$$\begin{aligned} \Gamma(\tau\to\mu\,\bar{\nu}_\mu\,\nu_\tau\,(\gamma))_{\rm SM} &= \frac{g^4}{64M_W^4}\,\frac{m_\tau^5}{96\pi^3}\,f\!\left(\frac{m_\mu^2}{m_\tau^2}\right)\delta_W^\tau\,\delta_\gamma^\tau\;,\\ \Gamma(\tau\to e\,\bar{\nu}_e\,\nu_\tau\,(\gamma))_{\rm SM} &= \frac{g^4}{64M_W^4}\,\frac{m_\tau^5}{96\pi^3}\,f\!\left(\frac{m_e^2}{m_\tau^2}\right)\delta_W^\tau\,\delta_\gamma^\tau\;,\\ \Gamma(\mu\to e\,\bar{\nu}_e\,\nu_\mu\,(\gamma))_{\rm SM} &= \frac{g^4}{64M_W^4}\,\frac{m_\mu^5}{96\pi^3}\,f\!\left(\frac{m_e^2}{m_\mu^2}\right)\delta_W^\mu\,\delta_\gamma^\mu \;=\; \frac{1}{\tau_\mu}\;, \end{aligned} \tag{5.2.7}$$

in which $f(x)$ is the phase space factor

$$f(x) = 1-8x+8x^3-x^4-12x^2\ln x\;, \tag{5.2.8}$$

δ_W^ℓ is the W propagator correction

$$\delta_W^\ell = \left(1+\frac{3}{5}\frac{m_\ell^2}{M_W^2}\right), \tag{5.2.9}$$

	phase space	W propagator	photon
$\Gamma(\tau \to \mu\,\bar{\nu}_\mu\,\nu_\tau)$	$f(m_\mu^2/m_\tau^2) = 0.9726$	$\delta_W^\tau = 1.0003$	$\delta_\gamma^\tau = 0.9957$
$\Gamma(\tau \to e\,\bar{\nu}_e\,\nu_\tau)$	$f(m_e^2/m_\tau^2) = 1.0000$		
$\Gamma(\mu \to e\,\bar{\nu}_e\,\nu_\mu)$	$f(m_e^2/m_\mu^2) = 0.9998$	$\delta_W^\mu = 1.0000$	$\delta_\gamma^\mu = 0.9958$

Table 5.1: The corrections to the leptonic decay widths of the τ and μ.

δ_γ^ℓ is the radiative correction from photons

$$\delta_\gamma^\ell = 1 + \frac{\alpha(m_\ell)}{2\pi}\left(\frac{25}{4} - \pi^2\right)\,, \tag{5.2.10}$$

and the values of the running QED coupling constant at the relevant energies are [109]

$$\begin{aligned} \alpha^{-1}(m_\mu) &= \alpha^{-1} - \frac{2}{3\pi}\ln\frac{m_\mu}{m_e} + \frac{1}{6\pi} \approx 136.0\,, \\ \alpha^{-1}(m_\tau) &\approx 133.3\,. \end{aligned} \tag{5.2.11}$$

The numerical values of these corrections are shown in Table 5.1. The SM predictions for the ratios are therefore

$$\begin{aligned} [R_{\tau\mu}]_{\rm SM} &= \frac{\Gamma(\tau \to \mu\,\bar{\nu}_\mu\,\nu_\tau\,(\gamma))_{\rm SM}}{\Gamma(\mu \to e\,\bar{\nu}_e\,\nu_\mu\,(\gamma))_{\rm SM}} = \frac{m_\tau^5}{m_\mu^5}\,\frac{f(m_\mu^2/m_\tau^2)}{f(m_e^2/m_\mu^2)}\,\frac{\delta_W^\tau}{\delta_W^\mu}\,\frac{\delta_\gamma^\tau}{\delta_\gamma^\mu} = 1.309 \times 10^6\,, \\ [R_\tau]_{\rm SM} &= \frac{\Gamma(\tau \to e\,\bar{\nu}_e\,\nu_\tau\,(\gamma))_{\rm SM}}{\Gamma(\tau \to \mu\,\bar{\nu}_\mu\,\nu_\tau\,(\gamma))_{\rm SM}} = \frac{f(m_e^2/m_\tau^2)}{f(m_\mu^2/m_\tau^2)} = 1.028\,. \end{aligned} \tag{5.2.12}$$

The experimental values of these ratios from the Review of Particle Properties [116] are

$$\begin{aligned} R_{\tau\mu} &= \frac{\tau_\mu}{\tau_\tau}\,\mathcal{B}(\tau \to \mu\,\bar{\nu}_\mu\,\nu_\tau\,(\gamma)) = \frac{(2.197034 \pm 0.000021) \times 10^{-6}\,{\rm s}}{(290.6 \pm 1.0) \times 10^{-15}\,{\rm s}}\,(17.36 \pm 0.05)\% \\ &= (1.312 \pm 0.006) \times 10^6\,, \\ R_\tau &= \frac{\mathcal{B}(\tau \to e\,\bar{\nu}_e\,\nu_\tau\,(\gamma))}{\mathcal{B}(\tau \to \mu\,\bar{\nu}_\mu\,\nu_\tau\,(\gamma))} = \frac{(17.85 \pm 0.05)\%}{(17.36 \pm 0.05)\%} = 1.028 \pm 0.004\,. \end{aligned} \tag{5.2.13}$$

The effect of a -13% correlation between $\mathcal{B}(\tau \to e\,\bar{\nu}_e\,\nu_\tau\,(\gamma))$ and $\mathcal{B}(\tau \to \mu\,\bar{\nu}_\mu\,\nu_\tau\,(\gamma))$ on the error on R_τ is small. Allowing only one of the λ's to be non-zero at a time, comparison of Eqs. (5.2.6), (5.2.12), and (5.2.13) places the following 2σ bounds:

$$\begin{aligned} |\lambda_{12k}|\left(\frac{100\,{\rm GeV}}{M_{\tilde{e}_{kR}}}\right) &< 0.05\,[R_{\tau\mu}]\,, \\ |\lambda_{13k}|\left(\frac{100\,{\rm GeV}}{M_{\tilde{e}_{kR}}}\right) &< 0.05\,[R_\tau]\,, \\ |\lambda_{23k}|\left(\frac{100\,{\rm GeV}}{M_{\tilde{e}_{kR}}}\right) &< 0.05\,[R_\tau]\,,\ 0.06\,[R_{\tau\mu}]\,. \end{aligned} \tag{5.2.14}$$

A new but still preliminary value of R_τ from Babar was announced at ICHEP 2008 [104] as

$$[R_\tau]_{\rm Babar2008} = \frac{1}{0.9796 \pm 0.0038} = 1.021 \pm 0.004\,. \tag{5.2.15}$$

Including this value will change the world average to

$$R_\tau \;=\; 1.025 \pm 0.003\;,$$

and the corresponding 2σ bounds will be

$$|\lambda_{13k}| \left(\frac{100\,\mathrm{GeV}}{M_{\tilde{e}_{kR}}}\right) \;<\; 0.03\;[R_\tau]\;, \qquad |\lambda_{23k}| \left(\frac{100\,\mathrm{GeV}}{M_{\tilde{e}_{kR}}}\right) \;<\; 0.05\;[R_\tau]\;. \tag{5.2.16}$$

We see that the bound on λ_{13k} will be tightened.

5.3 π and τ Decay

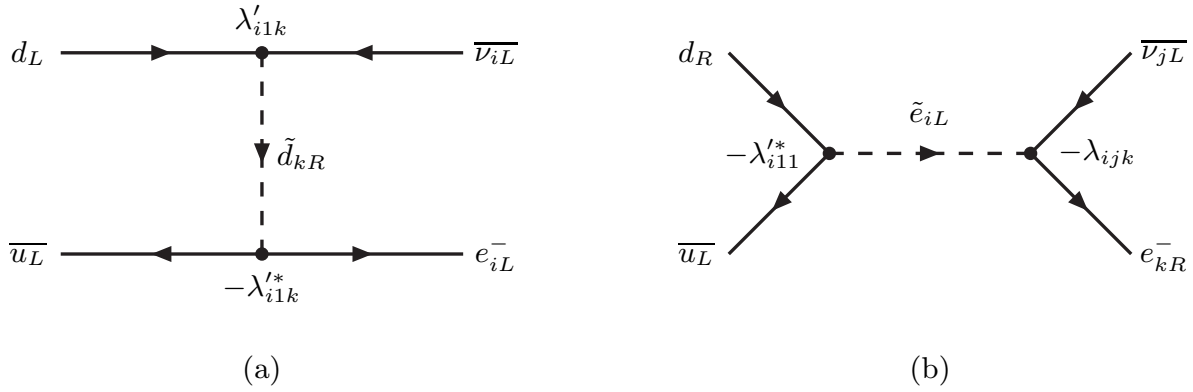

Figure 5.3.1: Possible R-parity violating contributions to $\pi^- \to \ell^- \overline{\nu_\ell}$ ($\ell = e_1 = e$, or $e_2 = \mu$) that interfere with the SM amplitude. The indices are $i = 1$ or 2, $k = 1$, 2, or 3 in (a); while $(jk) = (11)$ or (22), with $i = 3 - j$ or 3 in (b) due to the anti-symmetry of λ_{ijk} in the first two indices. The interference of (b) with the SM amplitude is suppressed due to the smallness of the electron mass.

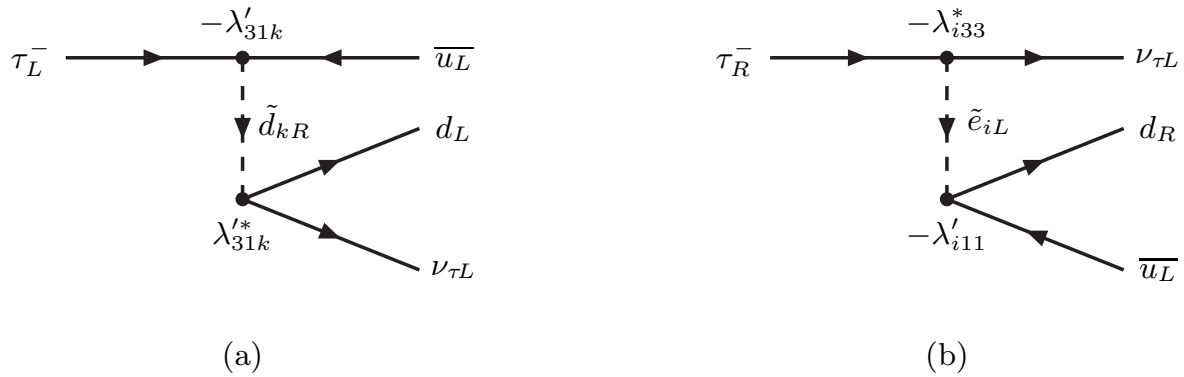

Figure 5.3.2: Possible R-parity violating contributions to the decay $\tau^- \to \pi^- \nu_\tau$.

Possible R-parity violating contributions to the decay $\pi^- \to \ell^- \overline{\nu_\ell}$ ($\ell = e$ or μ) are shown in Fig. 5.3.1, and those to $\tau^- \to \pi^- \nu_\tau$ are shown in Fig. 5.3.2. Since we are only interested in

placing bounds on the individual R-parity violating couplings separately, we will ignore the (b) diagrams in both cases.

The processes of Fig. 5.3.1(a) and Fig. 5.3.2(a) induce the following operators:

$$\begin{aligned}
5.3.1(a): \quad & -\frac{|\lambda'_{i1k}|^2}{M^2_{\tilde{d}_{kR}}}\big(\,\overline{\nu^c_{iL}}d_{jL}\,\big)\big(\,\overline{u_L}e^c_{iL}\,\big) \quad \stackrel{\text{Fierz}}{\longrightarrow} \quad -\frac{|\lambda_{i1k}|^2}{2M^2_{\tilde{d}_{kR}}}\big(\,\overline{\nu^c_{iL}}\gamma^\mu e^c_{iL}\,\big)\big(\,\overline{u_L}\gamma_\mu d_L\,\big) \\
& \qquad\qquad\qquad\qquad\qquad\quad = \quad -\frac{|\lambda_{i1k}|^2}{2M^2_{\tilde{d}_{kR}}}\big(\,\overline{e_{iL}}\gamma^\mu \nu_{iL}\,\big)\big(\,\overline{u_L}\gamma_\mu d_L\,\big)\,, \\
5.3.2(a): \quad & -\frac{|\lambda'_{31k}|^2}{M^2_{\tilde{d}_{kR}}}\big(\,\overline{\tau^c_L}u_L\,\big)\big(\,\overline{d_L}\nu^c_{\tau L}\,\big) \quad \stackrel{\text{Fierz}}{\longrightarrow} \quad -\frac{|\lambda_{31k}|^2}{2M^2_{\tilde{d}_{kR}}}\big(\,\overline{\tau^c_L}\gamma^\mu \nu^c_{\tau L}\,\big)\big(\,\overline{d_L}\gamma_\mu u_L\,\big) \\
& \qquad\qquad\qquad\qquad\qquad\quad = \quad -\frac{|\lambda_{31k}|^2}{2M^2_{\tilde{d}_{kR}}}\big(\,\overline{\nu_{\tau L}}\gamma^\mu \tau_L\,\big)\big(\,\overline{d_L}\gamma_\mu u_L\,\big)\,.
\end{aligned} \tag{5.3.1}$$

These interfere with the SM operators given by

$$-\frac{4G_F}{\sqrt{2}}V_{ud}\big(\,\overline{e_{iL}}\gamma^\mu\nu_{iL}\,\big)\big(\,\overline{u_L}\gamma_\mu d_L\,\big)\,, \qquad \text{and} \qquad -\frac{4G_F}{\sqrt{2}}V^*_{ud}\big(\,\overline{\nu_{\tau L}}\gamma^\mu\tau_L\,\big)\big(\,\overline{d_L}\gamma_\mu u_L\,\big)\,, \tag{5.3.2}$$

and shift the π-decay widths to

$$\Gamma(\pi^-\to\ell_i^-\overline{\nu_{\ell_i}}) \;=\; \big[\,\Gamma(\pi^-\to\ell_i^-\overline{\nu_{\ell_i}})\,\big]_{\rm SM}\left[\,1+\frac{2}{|V_{ud}|}\,r'_{i1k}(\tilde{d}_{kR})\,\right]\,, \tag{5.3.3}$$

while the τ-decay width is shifted by

$$\Gamma(\tau^-\to\pi^-\nu_\tau) \;=\; \big[\,\Gamma(\tau^-\to\pi^-\nu_\tau)\,\big]_{\rm SM}\left[\,1+\frac{2}{|V_{ud}|}\,r'_{31k}(\tilde{d}_{kR})\,\right]\,. \tag{5.3.4}$$

Here, we have neglected any relative phase between the SM and RPV contributions. The ratios

$$\begin{aligned}
R_\pi &= \frac{\Gamma(\pi^-\to e^-\overline{\nu_e})}{\Gamma(\pi^-\to\mu^-\overline{\nu_\mu})}\,, \\
R_{\tau\pi} &= \frac{\Gamma(\tau^-\to\pi^-\nu_\tau)}{\Gamma(\pi^-\to\mu^-\overline{\nu_\mu})}\,,
\end{aligned} \tag{5.3.5}$$

are shifted to

$$\begin{aligned}
R_\pi &= [R_\pi]_{\rm SM}\left[\,1+\frac{2}{|V_{ud}|}\left\{r'_{11k}(\tilde{d}_{kR})-r'_{21k}(\tilde{d}_{kR})\right\}\right]\,, \\
R_{\tau\pi} &= [\,R_{\tau\pi}\,]_{\rm SM}\left[\,1+\frac{2}{|V_{ud}|}\left\{\,r'_{21k}(\tilde{d}_{kR})-r'_{31k}(\tilde{d}_{kR})\,\right\}\right]\,.
\end{aligned} \tag{5.3.6}$$

At tree level, the SM prediction for the π-decay widths is given by

$$[\,\Gamma(\pi^-\to\ell^-\,\overline{\nu_\ell})\,]_{\rm SM,tree} \;=\; \Big(\sqrt{2}G_F|V_{ud}|\Big)^2\,\frac{m_\ell^2 m_\pi}{16\pi}\left(1-\frac{m_\ell^2}{m_\pi^2}\right)^2 f_\pi^2\,, \tag{5.3.7}$$

while that of τ-decay into $\pi\,\nu_\tau$ is

$$[\,\Gamma(\tau^-\to\pi^-\,\nu_\tau)\,]_{\rm SM,tree} \;=\; \left(\sqrt{2}G_F|V_{ud}|\right)^2\,\frac{m_\tau^3}{32\pi}\left(1-\frac{m_\pi^2}{m_\tau^2}\right)^2 f_\pi^2\,, \tag{5.3.8}$$

where the pion decay constant f_π is normalized as

$$\langle 0|\,\bar u\gamma_\mu\gamma_5 d\,(0)\,|\pi^-(\mathbf{q})\rangle = i\,q_\mu f_\pi\,. \tag{5.3.9}$$

Taking ratios, we find

$$\begin{aligned}
[\,R_\pi\,]_{\rm SM,tree} &= \frac{[\,\Gamma(\pi^-\to e^-\,\overline{\nu_e})\,]_{\rm SM,tree}}{[\,\Gamma(\pi^-\to\mu^-\,\overline{\nu_\mu})\,]_{\rm SM,tree}} \;=\; \frac{m_e^2}{m_\mu^2}\,\frac{(1-m_e^2/m_\pi^2)^2}{(1-m_\mu^2/m_\pi^2)^2} \;=\; 1.283\times10^{-4}\,,\\
[\,R_{\tau\pi}\,]_{\rm SM,tree} &= \frac{[\,\Gamma(\tau^-\to\pi^-\,\nu_\tau)\,]_{\rm SM,tree}}{[\,\Gamma(\pi^-\to\mu^-\,\overline{\nu_\mu})\,]_{\rm SM,tree}} \;=\; \frac{m_\tau^3}{2m_\mu^2 m_\pi}\,\frac{(1-m_\pi^2/m_\tau^2)^2}{(1-m_\mu^2/m_\pi^2)^2} \;=\; 9.756\times10^3
\end{aligned} \tag{5.3.10}$$

Radiative corrections to these relations have been calculated in Ref. [110] and modify them to

$$\begin{aligned}
[\,R_\pi\,]_{\rm SM} &= [\,R_\pi\,]_{\rm SM,tree}\,(1+\delta R_\pi)\;,\\
[\,R_{\tau\pi}\,]_{\rm SM} &= [\,R_{\tau\pi}\,]_{\rm SM,tree}\,(1+\delta R_{\tau\pi})\;,
\end{aligned} \tag{5.3.11}$$

with

$$\delta R_\pi = -0.0374\pm0.0001\,,\qquad \delta R_{\tau\pi} = +0.0016^{+0.0009}_{-0.0014}\,. \tag{5.3.12}$$

The uncertainty in these corrections is due to the uncertainty from strong interaction effects. Therefore,

$$\begin{aligned}
[\,R_\pi\,]_{\rm SM} &= 1.235\times10^{-4}\,,\\
[\,R_{\tau\pi}\,]_{\rm SM} &= 9.771^{+0.009}_{-0.013}\times10^3\,.
\end{aligned} \tag{5.3.13}$$

On the other hand, the current experimental values are [116]

$$\begin{aligned}
R_\pi &= \frac{\mathcal{B}(\pi\to e\,\bar\nu_e\,(\gamma))}{\mathcal{B}(\pi\to\mu\,\bar\nu_\mu\,(\gamma))} \;=\; \frac{(0.01230\pm0.00004)\%}{(99.98770\pm0.00004)\%} \;=\; (1.230\pm0.004)\times10^{-4}\,,\\
R_{\tau\pi} &= \frac{\tau_\pi}{\tau_\tau}\,\frac{\mathcal{B}(\tau\to\pi\,\nu_\tau\,(\gamma))}{\mathcal{B}(\pi\to\mu\,\bar\nu_\mu\,(\gamma))}\\
&= \frac{(2.6033\pm0.0005)\times10^{-8}\mathrm{s}}{(290.6\pm1.0)\times10^{-15}\mathrm{s}}\,\frac{(10.91\pm0.07)\%}{(99.98770\pm0.00004)\%} \;=\; (9.775\pm0.071)\times10^3\,.
\end{aligned} \tag{5.3.14}$$

The magnitude of the CKM matrix element V_{ud} is [128],

$$|V_{ud}| \;=\; 0.97418\pm0.00027\,. \tag{5.3.15}$$

Comparison of Eqs. (5.3.6), (5.3.13) and (5.3.14) leads to the following 2σ bounds assuming only one of the couplings is non-zero at a time:

$$|\lambda'_{11k}|\left(\frac{100\,\mathrm{GeV}}{M_{\tilde d_{kR}}}\right) \;<\; 0.03\;[R_\pi]\,,$$

$$
\begin{aligned}
|\lambda'_{21k}| \left(\frac{100\,\mathrm{GeV}}{M_{\tilde{d}_{kR}}} \right) &< 0.06\ [R_\pi]\ ,\ 0.07\ [R_{\tau\pi}]\ , \\
|\lambda'_{31k}| \left(\frac{100\,\mathrm{GeV}}{M_{\tilde{d}_{kR}}} \right) &< 0.06\ [R_{\tau\pi}]\ .
\end{aligned} \tag{5.3.16}
$$

Another preliminary result announced at ICHEP 2008 from Babar [104] was

$$
\left[\frac{\mathcal{B}(\tau^- \to \pi^- \nu_\tau)}{\mathcal{B}(\tau^- \to e^- \bar{\nu}_e \nu_\tau)} \right]_{\mathrm{Babar2008}} = 0.5945 \pm 0.0063\ . \tag{5.3.17}
$$

Using the current world average value of $\mathcal{B}(\tau^- \to e^- \bar{\nu}_e \nu_\tau) = (17.85 \pm 0.05)\%$ [116] we find

$$
\left[\mathcal{B}(\tau^- \to \pi^- \nu_\tau) \right]_{\mathrm{Babar2008}} = 10.61 \pm 0.12\ . \tag{5.3.18}
$$

Including this value will shift the world average to

$$
\mathcal{B}(\tau^- \to \pi^- \nu_\tau) = 10.83 \pm 0.06\ , \tag{5.3.19}
$$

and the ratio $R_{\tau\pi}$ to

$$
R_{\tau\pi} = (9.703 \pm 0.063) \times 10^3\ . \tag{5.3.20}
$$

The error will be reduced somewhat and the central value shifted down by about 1σ. The 2σ bounds will become

$$
|\lambda'_{21k}| \left(\frac{100\,\mathrm{GeV}}{M_{\tilde{d}_{kR}}} \right) < 0.04\ [R_{\tau\pi}]\ , \qquad |\lambda'_{31k}| \left(\frac{100\,\mathrm{GeV}}{M_{\tilde{d}_{kR}}} \right) < 0.08\ [R_{\tau\pi}]\ , \tag{5.3.21}
$$

the change mostly due to the shift in the central value of $R_{\tau\pi}$.

5.4 CKM unitarity

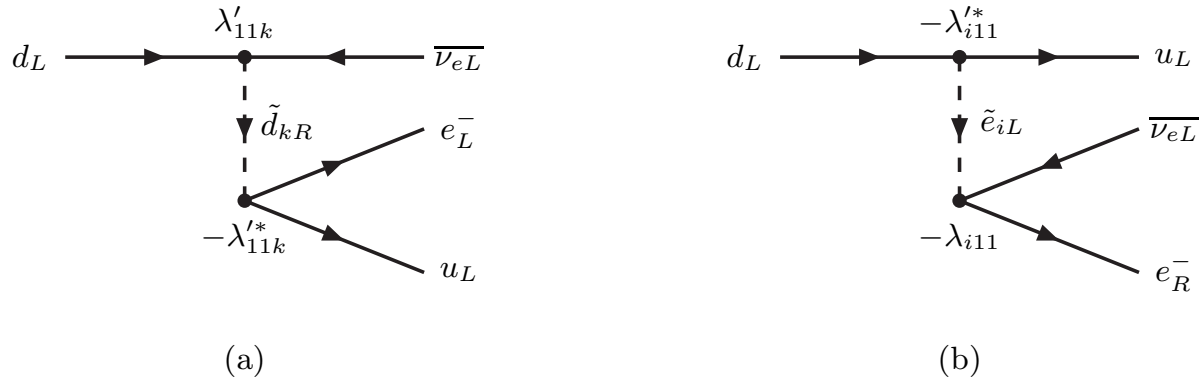

Figure 5.4.1: Possible R-parity violating contributions to nuclear beta decay.

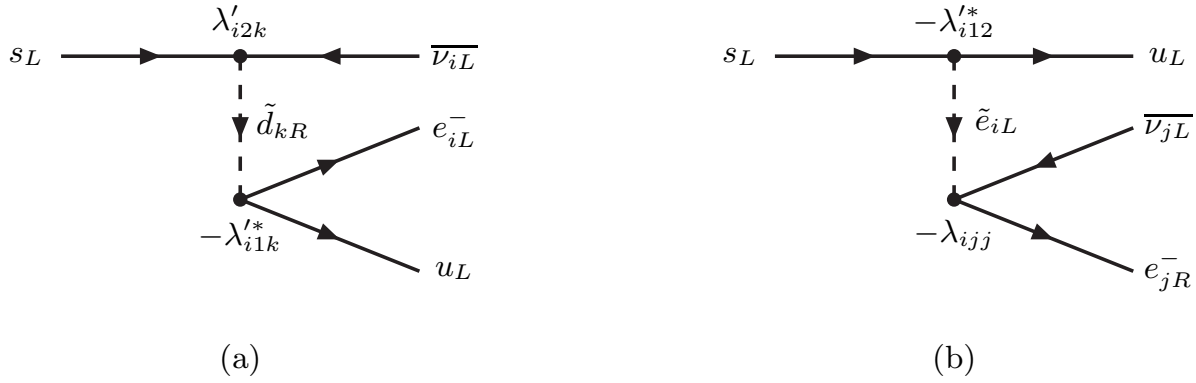

Figure 5.4.2: Possible R-parity violating contributions to semileptonic K-decay.

The SM values of the CKM matrix elements V_{ud}, V_{us}, and V_{ub} must satisfy the unitarity relation

$$|V_{ud}^{\rm SM}|^2 + |V_{us}^{\rm SM}|^2 + |V_{ub}^{\rm SM}|^2 \;=\; 1 \; . \tag{5.4.1}$$

Deviation of the measured values from this relation could be a sign of new physics. The value of $|V_{ud}|$, cited above in Eq. (5.3.15), is obtained from the comparison of superallowed $0^+ \to 0^+$ nuclear beta decays and muon decay [128], the former used to extract the product $G_F V_{ud}$ and the latter used to cancel the G_F. The SM operators relevant for these decays are

$$-\frac{4G_F}{\sqrt{2}} V_{ud}^{\rm SM} \big(\overline{u_L}\gamma^\mu d_L\big)\big(\overline{e_L}\gamma_\mu \nu_{eL}\big) \; , \qquad \text{and} \qquad -\frac{4G_F}{\sqrt{2}} \big(\overline{\nu_{\mu L}}\gamma^\mu \mu_L\big)\big(\overline{e_L}\gamma_\mu \nu_{eL}\big) \; . \tag{5.4.2}$$

Any new physics amplitude which interferes with these operators will affect the extracted value of V_{ud}. The first operator is the same as the operator responsible for the decay $\pi^- \to e^- \overline{\nu_e}$. The RPV amplitudes which interfere with this are the same as those shown in Fig. 5.3.1 except with the u_L lines pointing toward the future as shown in Fig. 5.4.1. Since Fig. 5.4.1(b) depends on two different RPV couplings (its interference is also suppressed by the electron mass) we will only consider Fig. 5.4.1(a) for which the corresponding operator is

$$-\frac{|\lambda'_{11k}|^2}{M^2_{\tilde{d}_{kR}}} \big(\overline{u_L} e^c_L\big)\big(\overline{\nu^c_{eL}} d_L\big) \quad \stackrel{\rm Fierz}{\longrightarrow} \quad +\frac{|\lambda'_{11k}|^2}{2M^2_{\tilde{d}_{kR}}} \big(\overline{u_L}\gamma^\mu d_L\big)\big(\overline{\nu^c_{eL}}\gamma_\mu e^c_L\big) \;=\; -\frac{|\lambda'_{11k}|^2}{2M^2_{\tilde{d}_{kR}}} \big(\overline{u_L}\gamma^\mu d_L\big)\big(\overline{e_L}\gamma_\mu \nu_{eL}\big) \; . \tag{5.4.3}$$

We have already discussed muon decay in section 5.2 where we found that G_F will be shifted by $r_{12k}(\tilde{e}_{kR})$, *cf.* Eq. (5.2.4). Therefore, the shift in V_{ud} will be

$$|V_{ud}|^2 \;=\; |V_{ud}^{\rm SM}|^2 \left[1 + \frac{2}{|V_{ud|}}\, r'_{11k}(\tilde{d}_{kR}) - 2\, r_{12k}(\tilde{e}_{kR})\right] \; . \tag{5.4.4}$$

The values of V_{us} and V_{ub} extracted from semi-leptonic K and B decays are [128, 93]

$$\begin{aligned} |V_{us}| &= 0.2255 \pm 0.0019 \; , \\ |V_{ub}| &= (3.95 \pm 0.35) \times 10^{-3} \; . \end{aligned} \tag{5.4.5}$$

The RPV diagrams that contribute to semi-leptonic K-decay are shown in Fig. 5.4.2. Similar diagrams contribute to semi-leptonic B-decay. None of these diagrams depend on a single RPV coupling so we may neglect them and assume

$$V_{us} \;=\; V_{us}^{\rm SM}\,, \qquad V_{ub} \;=\; V_{ub}^{\rm SM}\,. \tag{5.4.6}$$

Then,

$$\left[1+\frac{2}{|V_{ud}|}\,r'_{11k}(\tilde{d}_{kR})-2\,r_{12k}(\tilde{e}_{kR})\right] \;=\; \frac{|V_{ud}|^2}{1-|V_{us}|^2-|V_{ub}|^2} \;=\; 0.9999\pm 0.0011\,. \tag{5.4.7}$$

The 2σ bounds on the couplings are

$$|\lambda'_{11k}|\left(\frac{100\,{\rm GeV}}{M_{\tilde{d}_{kR}}}\right) \;<\; 0.03\;[V_{ud}]\,, \qquad |\lambda_{12k}|\left(\frac{100\,{\rm GeV}}{M_{\tilde{e}_{kR}}}\right) \;<\; 0.03\;[V_{ud}]\,. \tag{5.4.8}$$

5.5 Semi-leptonic D and leptonic D_s-decay

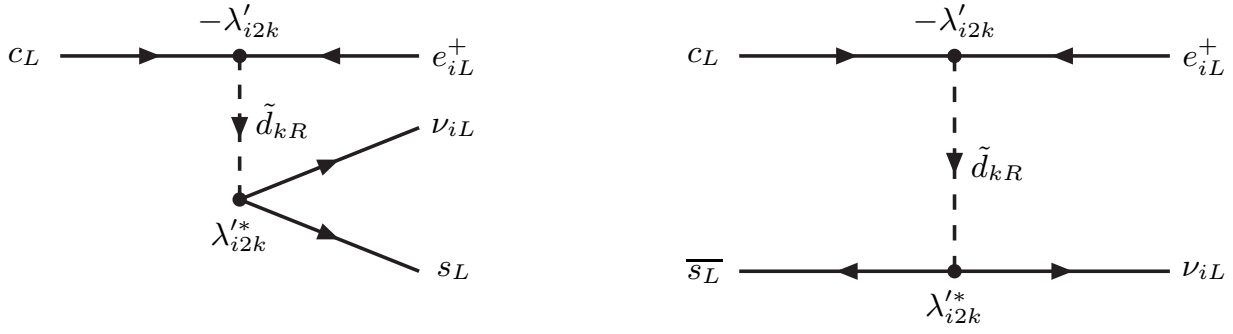

Figure 5.5.1: Possible R-parity violating contributions to semileptonic D-decay and leptonic D_s-decay.

The process shown in Fig. 5.5.1(a) affects semileptonic D-decay, while that in Fig. 5.5.1(b) affects leptonic D_s-decay. They are both described by the same operator given by

$$-\frac{|\lambda'_{i2k}|^2}{M^2_{\tilde{d}_{kR}}}\big(\,\overline{e^c_{iL}}c_L\,\big)\big(\,\overline{s_L}\nu^c_{iL}\,\big) \quad\stackrel{\rm Fierz}{\longrightarrow}\quad -\frac{|\lambda_{i2k}|^2}{2M^2_{\tilde{d}_{kR}}}\big(\,\overline{e^c_{iL}}\gamma^\mu\nu^c_{iL}\,\big)\big(\,\overline{s_L}\gamma_\mu c_L\,\big) \;=\; -\frac{|\lambda_{i2k}|^2}{2M^2_{\tilde{d}_{kR}}}\big(\,\overline{\nu_{iL}}\gamma^\mu e_{iL}\,\big)\big(\,\overline{s_L}\gamma_\mu c_L\,\big)\,. \tag{5.5.1}$$

This interferes with the SM operator

$$-\frac{4G_F}{\sqrt{2}}V^*_{cs}\big(\,\overline{\nu_{iL}}\gamma^\mu e_{iL}\,\big)\big(\,\overline{s_L}\gamma_\mu c_L\,\big)\,, \tag{5.5.2}$$

shifting the D and D_s decay widths by

$$\frac{\Gamma(D\to K\ell_i\nu_{\ell_i})}{\big[\,\Gamma(D\to K\ell_i\nu_{\ell_i})\,\big]_{\rm SM}} \;=\; \frac{\Gamma(D\to K^*\ell_i\nu_{\ell_i})}{\big[\,\Gamma(D\to K^*\ell_i\nu_{\ell_i})\,\big]_{\rm SM}} \;=\; \frac{\Gamma(D_s\to \ell_i\nu_{\ell_i})}{\big[\,\Gamma(D_s\to \ell_i\nu_{\ell_i})\,\big]_{\rm SM}} \;=\; 1+\frac{2}{|V_{cs}|}\,r'_{i2k}(\tilde{d}_{kR})\,, \tag{5.5.3}$$

where we have neglected any relative phase between the SM and RPV contributions. Following Ref. [47], we define the ratios

$$\begin{aligned} R_{D^0} &= \frac{\mathcal{B}(D^0 \to \mu^+ \nu_\mu K^-)}{\mathcal{B}(D^0 \to e^+ \nu_e K^-)} , \\ R_{D^+} &= \frac{\mathcal{B}(D^+ \to \mu^+ \nu_\mu \overline{K^0})}{\mathcal{B}(D^+ \to e^+ \nu_e \overline{K^0})} , \\ R^*_{D^+} &= \frac{\mathcal{B}(D^+ \to \mu^+ \nu_\mu \overline{K^*}(892)^0)}{\mathcal{B}(D^+ \to e^+ \nu_e \overline{K^*}(892)^0)} , \end{aligned} \tag{5.5.4}$$

the shifts of which are

$$\frac{R_{D^0}}{[R_{D^0}]_{\rm SM}} = \frac{R_{D^+}}{[R_{D^+}]_{\rm SM}} = \frac{R^*_{D^+}}{[R^*_{D^+}]_{\rm SM}} = 1 + \frac{2}{|V_{cs}|} \left\{ r'_{22k}(\tilde{d}_{kR}) - r'_{12k}(\tilde{d}_{kR}) \right\} . \tag{5.5.5}$$

The experimental values of these ratios are currently [116]

$$\begin{aligned} R_{D^0} &= \frac{(3.32 \pm 0.13) \times 10^{-2}}{(3.61 \pm 0.05) \times 10^{-2}} = 0.92 \pm 0.04 , \\ R_{D^+} &= \frac{(9.4 \pm 0.8) \times 10^{-2}}{(8.50 \pm 0.26) \times 10^{-2}} = 1.1 \pm 0.1 , \\ R^*_{D^+} &= \frac{(5.4 \pm 0.5) \times 10^{-2}}{(5.51 \pm 0.31) \times 10^{-2}} = 0.98 \pm 0.10 . \end{aligned} \tag{5.5.6}$$

Calculating the SM predictions of these ratios requires knowledge of the form-factors for the matrix elements [129]

$$\langle K | \, \overline{s} \gamma^\mu (1 - \gamma_5) c \, | D \rangle \qquad \text{and} \qquad \langle K^* | \, \overline{s} \gamma^\mu (1 - \gamma_5) c \, | D \rangle , \tag{5.5.7}$$

for which good experimental data now exist from FOCUS [130, 131, 132], Belle [133], Babar [134], and CLEO [135, 136]. Details of our calculation are presented in the appendix. The results are:

$$\begin{aligned} \left[R_{D^0} \right]^{-1}_{\rm SM} = \left[R_{D^+} \right]^{-1}_{\rm SM} &= 1.04 \pm 0.02 \; (1\sigma) , \quad 1.04^{+0.02}_{-0.06} \; (2\sigma) , \\ \left[R^*_{D^+} \right]^{-1}_{\rm SM} &= 1.060^{+0.002}_{-0.003} \; (1\sigma) , \quad 1.060^{+0.005}_{-0.007} \; (2\sigma) . \end{aligned} \tag{5.5.8}$$

The analysis of Ref. [47] used the value of $(1.03)^{-1}$ without any errors for all three ratios. This would be the value of R_{D^0} and R_{D^+} if form factors are ignored and the D and the K treated as point particles with the interaction $(K^\dagger \overleftrightarrow{\partial_\mu} D) W^\mu$, and it lies within our calculated range above. For the ratio $R^*_{D^+}$, if form factors are ignored and the D and the K^* treated as point particles with the interaction $K^{*\dagger}_\mu D \, W^\mu$, its value would be $(1.12)^{-1}$, which illustrates the importance of taking form-factors into account. The value of $|V_{cs}|$, also extracted from D semileptonic decays and D_s leptonic decays [128], is

$$|V_{cs}| = 1.04 \pm 0.06 , \tag{5.5.9}$$

and for our current purpose we can set it to one. In comparing Eqs. (5.5.5), (5.5.6), and (5.5.8), we allow the SM predictions to scan the entire 2σ range of Eq. (5.5.8) and pick up the weakest bounds on the couplings. The resulting 2σ bounds are

$$|\lambda'_{12k}| \left(\frac{100 \, {\rm GeV}}{M_{\tilde{d}_{kR}}} \right) < 0.2 \; [R_{D^0}] , \; 0.2 \; [R_{D^+}] , \; 0.2 \; [R^*_{D^+}] ,$$

$$|\lambda'_{22k}| \left(\frac{100\,\text{GeV}}{M_{\tilde{d}_{kR}}}\right) \;<\; 0.1\;[R_{D^0}]\;,\; 0.4\;[R_{D^+}]\;,\;\; 0.3\;[R^*_{D^+}]\;. \tag{5.5.10}$$

Next, define

$$R_{D_s}(\tau\mu) \;=\; \frac{\mathcal{B}(D_s^+ \to \tau^+\nu_\tau)}{\mathcal{B}(D_s^+ \to \mu^+\nu_\mu)}\;. \tag{5.5.11}$$

The shift of this ratio is

$$\frac{R_{D_s}(\tau\mu)}{\big[\,R_{D_s}(\tau\mu)\,\big]_{\rm SM}} \;=\; 1 + \frac{2}{|V_{cs}|}\left\{r'_{32k}(\tilde{d}_{kR}) - r'_{22k}(\tilde{d}_{kR})\right\}\;. \tag{5.5.12}$$

The current experimental value is

$$R_{D_s}(\tau\mu) \;=\; \frac{(6.6 \pm 0.5)\times 10^{-2}}{(6.3 \pm 0.5)\times 10^{-3}} \;=\; 10.5 \pm 1.1\;, \tag{5.5.13}$$

while the tree-level SM prediction is

$$R_{D_s}(\tau\mu) \;=\; \frac{m_\tau^2}{m_\mu^2}\frac{(1-m_\tau^2/m_{D_s}^2)^2}{(1-m_\mu^2/m_{D_s}^2)^2} \;=\; 9.76 \pm 0.03\;. \tag{5.5.14}$$

Comparison of the two leads to the 2σ bounds given by

$$|\lambda'_{22k}| \left(\frac{100\,\text{GeV}}{M_{\tilde{d}_{kR}}}\right) \;<\; 0.2\;[R_{D_s}(\tau\mu)]\;, \qquad |\lambda'_{32k}| \left(\frac{100\,\text{GeV}}{M_{\tilde{d}_{kR}}}\right) \;<\; 0.3\;[R_{D_s}(\tau\mu)]\;. \tag{5.5.15}$$

5.6 Atomic Parity Violation

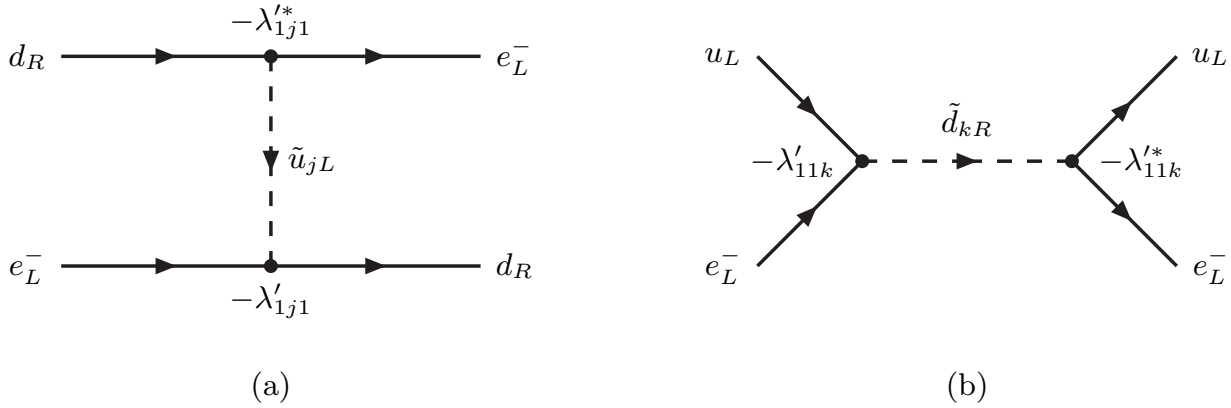

Figure 5.6.1: Possible R-parity violating contributions to atomic parity violation.

The diagrams shown in Fig. (5.6.1) lead to the following effective couplings between the quarks and the electron:

$$(a):\qquad \frac{|\lambda'_{11k}|^2}{M^2_{\tilde{d}_{kR}}}\big(\overline{e^c_L}u_L\big)\big(\overline{u_L}e^c_L\big) \quad\stackrel{\text{Fierz}}{\longrightarrow}\quad -\frac{|\lambda'_{11k}|^2}{2M^2_{\tilde{d}_{kR}}}\big(\overline{e^c_L}\gamma_\mu e^c_L\big)\big(\overline{u_L}\gamma^\mu u_L\big) \;=\; \frac{|\lambda'_{11k}|^2}{2M^2_{\tilde{d}_{kR}}}\big(\overline{e_L}\gamma_\mu e_L\big)\big(\overline{u_L}\gamma^\mu u_L\big)\;,$$

$$(b): \qquad \frac{|\lambda'_{1j1}|^2}{M^2_{\tilde{u}_{jL}}}\big(\overline{e_L}d_R\big)\big(\overline{d_R}e_L\big) \quad \stackrel{\text{Fierz}}{\longrightarrow} \quad -\frac{|\lambda'_{1j1}|^2}{2M^2_{\tilde{u}_{jL}}}\big(\overline{e_L}\gamma^\mu e_L\big)\big(\overline{d_R}\gamma_\mu d_R\big)\ . \tag{5.6.1}$$

The parity violating parts of these interactions are

$$\begin{aligned}(a): \qquad & -\frac{|\lambda'_{11k}|^2}{8M^2_{\tilde{d}_{kR}}}\Big[\big(\overline{e}\gamma_\mu\gamma_5 e\big)\big(\overline{u}\gamma^\mu u\big)+\big(\overline{e}\gamma_\mu e\big)\big(\overline{u}\gamma^\mu\gamma_5 u\big)\Big]\ ,\\ (b): \qquad & \frac{|\lambda'_{1j1}|^2}{8M^2_{\tilde{u}_{jL}}}\Big[\big(\overline{e}\gamma_\mu\gamma_5 e\big)\big(\overline{d}\gamma^\mu d\big)-\big(\overline{e}\gamma_\mu e\big)\big(\overline{d}\gamma^\mu\gamma_5 d\big)\Big]\ .\end{aligned} \tag{5.6.2}$$

The parity violating SM interactions, on the other hand, are

$$\frac{G_F}{\sqrt{2}}\sum_{q=u,d}\Big[C_{1q}\big(\overline{e}\gamma_\mu\gamma_5 e\big)\big(\overline{q}\gamma^\mu q\big)+C_{2q}\big(\overline{e}\gamma_\mu e\big)\big(\overline{q}\gamma^\mu\gamma_5 q\big)\Big]\ , \tag{5.6.3}$$

with

$$\begin{aligned} C_{1u} &= -\frac{1}{2}+\frac{4}{3}s^2\ , \qquad C_{2u} = -\frac{1}{2}+2s^2\ ,\\ C_{1d} &= +\frac{1}{2}-\frac{2}{3}s^2\ , \qquad C_{2d} = +\frac{1}{2}-2s^2\ , \end{aligned} \tag{5.6.4}$$

at tree-level, s^2 being the shorthand for $\sin^2\theta_W$. The weak charge of an atomic nucleus with Z protons and N neutrons is given by

$$Q_W(Z,N) \;=\; -2\Big[C_{1u}(2Z+N)+C_{1d}(Z+2N)\Big] \;=\; (1-4s^2)Z-N\ . \tag{5.6.5}$$

Note that $(2Z+N)$ and $(Z+2N)$ are respectively the number of up and down quarks in the nucleus. Since the presence of the above R-parity violating couplings will shift the C_1 couplings to

$$\begin{aligned} C_{1u} &\to C_{1u}-r'_{11k}(\tilde{d}_{kR})\ ,\\ C_{1d} &\to C_{1d}+r'_{1j1}(\tilde{u}_{jL})\ , \end{aligned} \tag{5.6.6}$$

the weak charge will be shifted by

$$\delta Q_W(Z,N) \;=\; +2\Big[(2Z+N)\,r'_{11k}(\tilde{d}_{kR})-(Z+2N)\,r'_{1j1}(\tilde{u}_{jL})\Big]\ . \tag{5.6.7}$$

Furthermore, since the quantity that is actually measured in atomic parity violation (APV) experiments is the product $G_F Q_W$, and Q_W is extracted by setting G_F equal to the muon decay constant G_μ, the LLE coupling $r_{12k}(\tilde{e}_{kR})$ can also affect Q_W via Eq. (5.2.4):

$$\frac{G_F Q_W}{G_\mu} \;=\; Q_W\big[\,1-r_{12k}(\tilde{e}_{kR})\,\big]\ . \tag{5.6.8}$$

For cesium-133, the total shift will be

$$\delta Q_W(55,78) \;=\; 376\,r'_{11k}(\tilde{d}_{kR})-422\,r'_{1j1}(\tilde{u}_{jL})-Q_W(55,78)\,r_{12k}(\tilde{e}_{kR})\ . \tag{5.6.9}$$

(This formula differs from that provided on page 82 of Ref. [47] which contains a typo: the factor of -2 on the right-hand-side should not be there. This error seems to have propagated into the bounds listed in Eq. (6.47) on the same page. We correct for this error in quoting the bounds from Ref. [47] in Table 5.3.) The latest experimental value of the weak charge of cesium-133 is [103]

$$Q_W({}^{133}_{55}\mathrm{Cs}) \;=\; -73.16 \pm 0.29 \pm 0.20 \;=\; -73.16 \pm 0.35 \; . \tag{5.6.10}$$

On the other hand, the SM value provided in the Review of Particle Properties [116] is

$$\left[\, Q_W({}^{133}_{55}\mathrm{Cs}) \,\right]_{\mathrm{SM}} \;=\; -73.16 \pm 0.03 \; , \tag{5.6.11}$$

which is based on a global fit to all electroweak observables with radiative corrections only from within the SM. Assuming further radiative corrections from new physics is negligibly small, and saturating the difference between the two with the RPV contributions, we find the following 2σ bounds:

$$\lambda'_{11k} \left(\frac{100\,\mathrm{GeV}}{M_{\tilde{d}_{kR}}} \right) \;<\; 0.04 \; [Q_W] \; , \qquad \lambda'_{1j1} \left(\frac{100\,\mathrm{GeV}}{M_{\tilde{u}_{jL}}} \right) \;<\; 0.03 \; [Q_W] \; , \qquad \lambda_{12k} \left(\frac{100\,\mathrm{GeV}}{M_{\tilde{e}_{kR}}} \right) \;<\; 0.08 \; [Q_W] \; . \tag{5.6.12}$$

5.7 Gluino Exhange contribution to Neutrinoless Double Beta Decay

As discussed by Hirsch, Klapdor-Kleingrothaus, and Kovalenko in Ref. [146], many subprocesses involving supersymmetric particles can contribute to neutrinoless double beta decay when the R-parity violating coulping λ'_{111} is non-zero. We begin by looking at the gluino exchange processes which are shown in Fig. 5.7.1.

The operators corresponding to the diagrams of Fig. 5.7.1 are

$$\begin{aligned}
1(a): \qquad & \frac{1}{2} \frac{8\pi\alpha_s}{M_{\tilde{g}}} \frac{\left(\lambda'^{*}_{111}\right)^2}{M^4_{\tilde{u}_L}} \sum_{a=1}^{8} \left[T^{(a)}\right]^{\alpha}{}_{\beta} \left[T^{(a)}\right]^{\gamma}{}_{\delta} \left(\overline{u_L}_{\alpha} u^c_{L\gamma}\right) \left(\overline{e_L} d^{\beta}_R\right) \left(\overline{e_L} d^{\delta}_R\right) \; , \\
1(b): \qquad & \frac{1}{2} \frac{8\pi\alpha_s}{M_{\tilde{g}}} \frac{\left(\lambda'^{*}_{111}\right)^2}{M^4_{\tilde{d}_R}} \sum_{a=1}^{8} \left[T^{(a)}\right]^{\alpha}{}_{\beta} \left[T^{(a)}\right]^{\gamma}{}_{\delta} \left(\overline{u_L}_{\alpha} e^c_L\right) \left(\overline{u_L}_{\gamma} e^c_L\right) \left(\overline{d_R}^{\beta} d^{c\delta}_R\right) \; , \\
1(c): \qquad & -\frac{8\pi\alpha_s}{M_{\tilde{g}}} \frac{\left(\lambda'^{*}_{111}\right)^2}{M^2_{\tilde{d}_R} M^2_{\tilde{u}_L}} \sum_{a=1}^{8} \left[T^{(a)}\right]^{\alpha}{}_{\beta} \left[T^{(a)}\right]^{\gamma}{}_{\delta} \left(\overline{u_L}_{\alpha} d^{\delta}_R\right) \left(\overline{u_L}_{\gamma} e^c_L\right) \left(\overline{e_L} d^{\beta}_R\right) \; ,
\end{aligned} \tag{5.7.1}$$

where $\alpha_s = g_3^2/4\pi$, $T^{(a)} = \lambda^{(a)}/2$ $(a = 1, 2, \cdots, 8)$ are the generators of $SU(3)$, $\lambda^{(a)}$ being the Gell-Mann matrices, and α, β, γ, δ are color indices. The factors of $1/2$ preceding the expressions for diagrams (a) and (b) are symmetry factors.

A sequence of Fierz transformations will render the fermion hexalinears into the following

forms:

$$\begin{aligned}
1(a): &\quad \big(\overline{u_{L\alpha}} u^c_{L\gamma}\big)\big(\overline{e_L} d^\beta_R\big)\big(\overline{e_L} d^\delta_R\big) \quad \stackrel{\text{Fierz}}{\longrightarrow} \quad \left[\frac{1}{4}\big(\overline{u_{L\alpha}} d^\delta_R\big)\big(\overline{u_{L\gamma}} d^\beta_R\big) - \frac{1}{16}\big(\overline{u_{L\alpha}}\sigma_{\mu\nu} d^\delta_R\big)\big(\overline{u_{L\gamma}}\sigma^{\mu\nu} d^\beta_R\big)\right]\big(\overline{e_L} e^c_L\big) + \cdots \\
1(b): &\quad \big(\overline{u_{L\alpha}} e^c_L\big)\big(\overline{u_{L\gamma}} e^c_L\big)\big(\overline{d_R}^\beta d^{c\delta}_R\big) \quad \stackrel{\text{Fierz}}{\longrightarrow} \quad \left[\frac{1}{4}\big(\overline{u_{L\alpha}} d^\delta_R\big)\big(\overline{u_{L\gamma}} d^\beta_R\big) - \frac{1}{16}\big(\overline{u_{L\alpha}}\sigma_{\mu\nu} d^\delta_R\big)\big(\overline{u_{L\gamma}}\sigma^{\mu\nu} d^\beta_R\big)\right]\big(\overline{e_L} e^c_L\big) + \cdots \\
1(c): &\quad \big(\overline{u_{L\alpha}} d^\delta_R\big)\big(\overline{u_{L\gamma}} e^c_L\big)\big(\overline{e_L} d^\beta_R\big) \quad \stackrel{\text{Fierz}}{\longrightarrow} \quad -\frac{1}{2}\big(\overline{u_{L\alpha}} d^\delta_R\big)\big(\overline{u_{L\gamma}} d^\beta_R\big)\big(\overline{e_L} e^c_L\big) + \cdots
\end{aligned} \tag{5.7.2}$$

The ellipses denote terms proportional to $\big(\overline{e_L}\sigma_{\mu\nu} e^c_L\big)$ which do not contribute to $0^+ \to 0^+$ transitions. Note, though it may not be manifest, that the right-hand sides of the expressions for (a) and (b) are symmetric under the interchanges $\alpha \leftrightarrow \gamma$ and $\beta \leftrightarrow \delta$ since the left-hand sides are obviously so. (Can be shown via a Fierz transformation.)

Ref. [146] uses Eq. (31), namely

$$\sum_a \big[\lambda^{(a)}\big]^\alpha{}_\beta \big[\lambda^{(a)}\big]^\gamma{}_\delta \;=\; \frac{16}{9}\,\delta^\alpha_\delta\,\delta^\gamma_\beta - \frac{1}{3}\sum_a \big[\lambda^{(a)}\big]^\alpha{}_\delta \big[\lambda^{(a)}\big]^\gamma{}_\beta\,, \tag{5.7.3}$$

and drops the contribution of the second term on the right-hand side since it will lead to a product of color-octet currents. However, the neglected terms can be rewritten as products of color-singlet currents since another Fierz transformation can interchange the pairing of the quark fields. What this means physically is that even when the quarks exchange color, the nucleons do not have to since the color-changed quarks can be exchanged between the two nucleons and thereby nullify the color exchange. To see this, it is more convenient to use Eq. (32) of Ref. [146], rewritten as:

$$\sum_a \big[\lambda^{(a)}\big]^\alpha{}_\beta \big[\lambda^{(a)}\big]^\gamma{}_\delta \;=\; 2\,\delta^\alpha_\delta\,\delta^\gamma_\beta - \frac{2}{3}\,\delta^\alpha_\beta\,\delta^\gamma_\delta\,. \tag{5.7.4}$$

The first term on the right-hand side clearly leads to color-singlet currents, but the second term does so too for (a) and (b) due to the symmetry under the interchanges $\alpha \leftrightarrow \gamma$ and $\beta \leftrightarrow \delta$ mentioned above. Therefore,

$$\begin{aligned}
&\sum_a \big[\lambda^{(a)}\big]^\alpha{}_\beta \big[\lambda^{(a)}\big]^\gamma{}_\delta \left[\frac{1}{4}\big(\overline{u_{L\alpha}} d^\delta_R\big)\big(\overline{u_{L\gamma}} d^\beta_R\big) - \frac{1}{16}\big(\overline{u_{L\alpha}}\sigma_{\mu\nu} d^\delta_R\big)\big(\overline{u_{L\gamma}}\sigma^{\mu\nu} d^\beta_R\big)\right] \\
&\quad = \quad \frac{4}{3}\left[\frac{1}{4}\big(\overline{u_{L\alpha}} d^\alpha_R\big)\big(\overline{u_{L\beta}} d^\beta_R\big) - \frac{1}{16}\big(\overline{u_{L\alpha}}\sigma_{\mu\nu} d^\alpha_R\big)\big(\overline{u_{L\beta}}\sigma^{\mu\nu} d^\beta_R\big)\right] \\
&\quad = \quad \frac{1}{3}\left[\big(\overline{u_L} d_R\big)\big(\overline{u_L} d_R\big) - \frac{1}{4}\big(\overline{u_L}\sigma_{\mu\nu} d_R\big)\big(\overline{u_L}\sigma^{\mu\nu} d_R\big)\right] \\
&\quad = \quad \frac{1}{12}\left[J_{PS}\cdot J_{PS} - \frac{1}{4}\,J_{T\mu\nu}\cdot J^{\mu\nu}_T\right]\,.
\end{aligned} \tag{5.7.5}$$

For (c), we need another Fierz transformation:

$$-\frac{1}{2}\big(\overline{u_{L\alpha}} d^\delta_R\big)\big(\overline{u_{L\gamma}} d^\beta_R\big) \quad \stackrel{\text{Fierz}}{\longrightarrow} \quad \frac{1}{4}\big(\overline{u_{L\alpha}} d^\beta_R\big)\big(\overline{u_{L\gamma}} d^\delta_R\big) + \frac{1}{16}\big(\overline{u_{L\alpha}}\sigma_{\mu\nu} d^\beta_R\big)\big(\overline{u_{L\gamma}}\sigma^{\mu\nu} d^\delta_R\big)\,. \tag{5.7.6}$$

Therefore,

$$\begin{aligned}
&\sum_a \left[\lambda^{(a)}\right]^\alpha{}_\beta \left[\lambda^{(a)}\right]^\gamma{}_\delta \left[-\frac{1}{2}\left(\overline{u_{L\alpha}} d_R^\delta\right)\left(\overline{u_{L\gamma}} d_R^\beta\right)\right] \\
&= \left[2\,\delta_\delta^\alpha\,\delta_\beta^\gamma - \frac{2}{3}\,\delta_\beta^\alpha\,\delta_\delta^\gamma\right]\left[-\frac{1}{2}\left(\overline{u_{L\alpha}} d_R^\delta\right)\left(\overline{u_{L\gamma}} d_R^\beta\right)\right] \\
&= 2\,\delta_\delta^\alpha\,\delta_\beta^\gamma\left[-\frac{1}{2}\left(\overline{u_{L\alpha}} d_R^\delta\right)\left(\overline{u_{L\gamma}} d_R^\beta\right)\right] - \frac{2}{3}\,\delta_\beta^\alpha\,\delta_\delta^\gamma\left[\frac{1}{4}\left(\overline{u_{L\alpha}} d_R^\beta\right)\left(\overline{u_{L\gamma}} d_R^\delta\right) + \frac{1}{16}\left(\overline{u_{L\alpha}}\sigma_{\mu\nu} d_R^\beta\right)\left(\overline{u_{L\gamma}}\sigma^{\mu\nu} d_R^\delta\right)\right] \\
&= -\left(\overline{u_L} d_R\right)\left(\overline{u_L} d_R\right) - \frac{2}{3}\left[\frac{1}{4}\left(\overline{u_L} d_R\right)\left(\overline{u_L} d_R\right) + \frac{1}{16}\left(\overline{u_L}\sigma_{\mu\nu} d_R\right)\left(\overline{u_L}\sigma^{\mu\nu} d_R\right)\right] \\
&= -\frac{7}{6}\left(\overline{u_L} d_R\right)\left(\overline{u_L} d_R\right) - \frac{1}{24}\left(\overline{u_L}\sigma_{\mu\nu} d_R\right)\left(\overline{u_L}\sigma^{\mu\nu} d_R\right) \\
&= -\frac{1}{6}\left[7\left(\overline{u_L} d_R\right)\left(\overline{u_L} d_R\right) + \frac{1}{4}\left(\overline{u_L}\sigma_{\mu\nu} d_R\right)\left(\overline{u_L}\sigma^{\mu\nu} d_R\right)\right] \\
&= -\frac{1}{24}\left[7\,J_{PS}\cdot J_{PS} + \frac{1}{4}\,J_{T\mu\nu}\cdot J_T^{\mu\nu}\right]\,. \qquad (5.7.7)
\end{aligned}$$

Putting everything together, the contributions of the three diagrams are

$$\begin{aligned}
1(a): &\quad \frac{\pi\alpha_s\left(\lambda'^*_{111}\right)^2}{24\,M_{\tilde g} M^4_{\tilde u_L}}\left[J_{PS}\cdot J_{PS} - \frac{1}{4}\,J_{T\mu\nu}\cdot J_T^{\mu\nu}\right]\left[\,\overline{e}(1+\gamma_5)e^c\,\right]\,, \\
1(b): &\quad \frac{\pi\alpha_s\left(\lambda'^*_{111}\right)^2}{24\,M_{\tilde g} M^4_{\tilde d_R}}\left[J_{PS}\cdot J_{PS} - \frac{1}{4}\,J_{T\mu\nu}\cdot J_T^{\mu\nu}\right]\left[\,\overline{e}(1+\gamma_5)e^c\,\right]\,, \\
1(c): &\quad \frac{\pi\alpha_s\left(\lambda'^*_{111}\right)^2}{24\,M_{\tilde g} M^2_{\tilde d_R} M^2_{\tilde u_L}}\left[7\,J_{PS}\cdot J_{PS} + \frac{1}{4}\,J_{T\mu\nu}\cdot J_T^{\mu\nu}\right]\left[\,\overline{e}(1+\gamma_5)e^c\,\right]\,. \qquad (5.7.8)
\end{aligned}$$

5.8 Neutralino Exhange contribution to Neutrinoless Double Beta Decay

The neutralino exchange diagrams are shown in Fig. 5.8.1. (We only consider the contribution of a single neutralino and drop the index i.) The operators corresponding to the six diagrams are

$$\begin{aligned}
2(a): &\quad \frac{1}{2}\frac{8\pi\alpha_2}{M_\chi}\frac{\left(\lambda'^*_{111}\right)^2}{M^4_{\tilde e_L}}\,\epsilon_L^2(e)\left(\overline{e_L} e^c_{L\gamma}\right)\left(\overline{u_{L\alpha}} d_R^\alpha\right)\left(\overline{u_{L\beta}} d_R^\beta\right)\,, \\
2(b): &\quad \frac{1}{2}\frac{8\pi\alpha_2}{M_\chi}\frac{\left(\lambda'^*_{111}\right)^2}{M^4_{\tilde u_L}}\,\epsilon_L^2(u)\left(\overline{u_{L\alpha}} u^c_{L\beta}\right)\left(\overline{e_L} d_R^\alpha\right)\left(\overline{e_L} d_R^\beta\right)\,, \\
2(c): &\quad \frac{1}{2}\frac{8\pi\alpha_2}{M_\chi}\frac{\left(\lambda'^*_{111}\right)^2}{M^4_{\tilde d_R}}\,\epsilon_R^2(d)\left(\overline{u_{L\alpha}} e^c_L\right)\left(\overline{u_{L\beta}} e^c_L\right)\left(\overline{d_R}^\alpha d_R^{c\beta}\right)\,, \\
2(d): &\quad \frac{8\pi\alpha_2}{M_\chi}\frac{\left(\lambda'^*_{111}\right)^2}{M^2_{\tilde e_L} M^2_{\tilde u_L}}\,\epsilon_L(e)\epsilon_L(u)\left(\overline{u_{L\alpha}} d_R^\alpha\right)\left(\overline{u_{L\beta}} e^c_L\right)\left(\overline{e_L} d_R^\beta\right)\,, \\
2(e): &\quad \frac{8\pi\alpha_2}{M_\chi}\frac{\left(\lambda'^*_{111}\right)^2}{M^2_{\tilde d_R} M^2_{\tilde e_L}}\,\epsilon_L(e)\epsilon_R(d)\left(\overline{u_{L\alpha}} d_R^\alpha\right)\left(\overline{u_{L\beta}} e^c_L\right)\left(\overline{e_L} d_R^\beta\right)\,,
\end{aligned}$$

$$2(f): \qquad \frac{8\pi\alpha_2}{M_\chi}\,\frac{(\lambda'^*_{111})^2}{M^2_{\tilde d_R}M^2_{\tilde u_L}}\,\epsilon_L(u)\epsilon_R(d)\,\big(\overline{u_{L\alpha}}d^\beta_R\big)\big(\overline{u_{L\beta}}e^c_L\big)\big(\overline{e_L}d^\alpha_R\big)\,, \tag{5.8.1}$$

where $\alpha_2 = g_2^2/4\pi$. The factors of 1/2 preceding the expressions for diagrams (a), (b), and (c) are again symmetry factors. The expression for (a) is already in the form of a product of color-singlet currents.

The other fermion hexalinears can be Fierz transformed into the following forms:

$$\begin{aligned}
2(b): \quad & \big(\overline{u_{L\alpha}}u^c_{L\beta}\big)\big(\overline{e_L}d^\alpha_R\big)\big(\overline{e_L}d^\beta_R\big)\\
& \xrightarrow{\text{Fierz}} \left[\frac{1}{4}\big(\overline{u_{L\alpha}}d^\alpha_R\big)\big(\overline{u_{L\beta}}d^\beta_R\big) - \frac{1}{16}\big(\overline{u_{L\alpha}}\sigma_{\mu\nu}d^\alpha_R\big)\big(\overline{u_{L\beta}}\sigma^{\mu\nu}d^\beta_R\big)\right]\big(\overline{e_L}e^c_L\big) + \cdots\\
2(c): \quad & \big(\overline{u_{L\alpha}}e^c_L\big)\big(\overline{u_{L\beta}}e^c_L\big)\big(\overline{d_R}^\alpha d^{c\beta}_R\big)\\
& \xrightarrow{\text{Fierz}} \left[\frac{1}{4}\big(\overline{u_{L\alpha}}d^\alpha_R\big)\big(\overline{u_{L\beta}}d^\beta_R\big) - \frac{1}{16}\big(\overline{u_{L\alpha}}\sigma_{\mu\nu}d^\alpha_R\big)\big(\overline{u_{L\beta}}\sigma^{\mu\nu}d^\beta_R\big)\right]\big(\overline{e_L}e^c_L\big) + \cdots\\
2(d)\;2(e): \quad & \big(\overline{u_{L\alpha}}d^\alpha_R\big)\big(\overline{u_{L\beta}}e^c_L\big)\big(\overline{e_L}d^\beta_R\big)\\
& \xrightarrow{\text{Fierz}} -\frac{1}{2}\big(\overline{u_{L\alpha}}d^\alpha_R\big)\big(\overline{u_{L\beta}}d^\beta_R\big)\big(\overline{e_L}e^c_L\big) + \cdots\\
2(f): \quad & \big(\overline{u_{L\alpha}}d^\beta_R\big)\big(\overline{u_{L\beta}}e^c_L\big)\big(\overline{e_L}d^\alpha_R\big)\\
& \xrightarrow{\text{Fierz}} \left[\frac{1}{4}\big(\overline{u_{L\alpha}}d^\alpha_R\big)\big(\overline{u_{L\beta}}d^\beta_R\big) + \frac{1}{16}\big(\overline{u_{L\alpha}}\sigma_{\mu\nu}d^\alpha_R\big)\big(\overline{u_{L\beta}}\sigma^{\mu\nu}d^\beta_R\big)\right]\big(\overline{e_L}e^c_L\big) + \cdots
\end{aligned} \tag{5.8.2}$$

Therefore, the contributions of the six diagrams are

$$\begin{aligned}
2(a): \quad & \frac{\pi\alpha_2\,(\lambda'^*_{111})^2\,\epsilon^2_L(e)}{2\,M_\chi M^4_{\tilde e_L}}\,\big[J_{PS}\cdot J_{PS}\big]\big[\,\overline{e}(1+\gamma_5)e^c\,\big]\,,\\
2(b): \quad & \frac{\pi\alpha_2\,(\lambda'^*_{111})^2\,\epsilon^2_L(u)}{8\,M_\chi M^4_{\tilde u_L}}\,\left[J_{PS}\cdot J_{PS} - \frac{1}{4}\,J_{T\mu\nu}\cdot J^{\mu\nu}_T\right]\big[\,\overline{e}(1+\gamma_5)e^c\,\big]\,,\\
2(c): \quad & \frac{\pi\alpha_2\,(\lambda'^*_{111})^2\,\epsilon^2_R(d)}{8\,M_\chi M^4_{\tilde d_R}}\,\left[J_{PS}\cdot J_{PS} - \frac{1}{4}\,J_{T\mu\nu}\cdot J^{\mu\nu}_T\right]\big[\,\overline{e}(1+\gamma_5)e^c\,\big]\,,\\
2(d): \quad & -\frac{\pi\alpha_2\,(\lambda'^*_{111})^2\,\epsilon_L(e)\epsilon_L(u)}{2\,M_\chi M^2_{\tilde e_L}M^2_{\tilde u_L}}\,\big[J_{PS}\cdot J_{PS}\big]\big[\,\overline{e}(1+\gamma_5)e^c\,\big]\,,\\
2(e): \quad & -\frac{\pi\alpha_2\,(\lambda'^*_{111})^2\,\epsilon_L(e)\epsilon_R(d)}{2\,M_\chi M^2_{\tilde e_L}M^2_{\tilde d_R}}\,\big[J_{PS}\cdot J_{PS}\big]\big[\,\overline{e}(1+\gamma_5)e^c\,\big]\,,\\
2(f): \quad & \frac{\pi\alpha_2\,(\lambda'^*_{111})^2\,\epsilon_L(u)\epsilon_R(d)}{4\,M_\chi M^2_{\tilde u_L}M^2_{\tilde d_R}}\,\left[J_{PS}\cdot J_{PS} + \frac{1}{4}\,J_{T\mu\nu}\cdot J^{\mu\nu}_T\right]\big[\,\overline{e}(1+\gamma_5)e^c\,\big]\,.
\end{aligned} \tag{5.8.3}$$

5.9 Comparison

Our results are compared with that in Eq. (35) of Ref. [146] in Table 5.2. There are significant differences due to symmetry factors, the inclusion or neglect of the products of color-octet currents, and different color contractions.

Assuming that our results are correct, the neutralino exchange contributions can be collected

Diagram	Ref. [146]	Our result
1(a)	$\frac{1}{9}\left(J_{PS}J_{PS}-\frac{1}{4}J_TJ_T\right)$	$\frac{1}{24}\left(J_{PS}J_{PS}-\frac{1}{4}J_TJ_T\right)$
1(b)	$\frac{1}{9}\left(J_{PS}J_{PS}-\frac{1}{4}J_TJ_T\right)$	$\frac{1}{24}\left(J_{PS}J_{PS}-\frac{1}{4}J_TJ_T\right)$
1(c)	$\frac{2}{9}J_{PS}J_{PS}$	$\frac{1}{24}\left(7\,J_{PS}J_{PS}+\frac{1}{4}J_TJ_T\right)$
2(a)	$J_{PS}J_{PS}$	$\frac{1}{2}J_{PS}J_{PS}$
2(b)	$\frac{1}{12}\left(J_{PS}J_{PS}-\frac{1}{4}J_TJ_T\right)$	$\frac{1}{8}\left(J_{PS}J_{PS}-\frac{1}{4}J_TJ_T\right)$
2(c)	$\frac{1}{12}\left(J_{PS}J_{PS}-\frac{1}{4}J_TJ_T\right)$	$\frac{1}{8}\left(J_{PS}J_{PS}-\frac{1}{4}J_TJ_T\right)$
2(d)	$-\frac{1}{6}J_{PS}J_{PS}$	$-\frac{1}{2}J_{PS}J_{PS}$
2(e)	$-\frac{1}{6}J_{PS}J_{PS}$	$-\frac{1}{2}J_{PS}J_{PS}$
2(f)	$-\frac{1}{6}J_{PS}J_{PS}$	$\frac{1}{4}\left(J_{PS}J_{PS}+\frac{1}{4}J_TJ_T\right)$

Table 5.2: Comparison of our results with those of Ref. [146]. Common factors are not shown.

into the compact form

$$\mathcal{L}_\chi \;=\; \frac{\pi\alpha_2(\lambda'^*_{111})^2}{8M_\chi}\left[\left\{\frac{2\epsilon_L(e)}{M^2_{\tilde{e}_L}}-\frac{\epsilon_L(u)}{M^2_{\tilde{u}_L}}-\frac{\epsilon_R(d)}{M^2_{\tilde{d}_R}}\right\}^2 J_{PS}\cdot J_{PS}-\frac{1}{4}\left\{\frac{\epsilon_L(u)}{M^2_{\tilde{u}_L}}-\frac{\epsilon_R(d)}{M^2_{\tilde{d}_R}}\right\}^2 J_{T\mu\nu}\cdot J_T^{\mu\nu}\right]\left[\,\overline{e}(1+\gamma_5)e^c\,\right]. \tag{5.9.1}$$

This implies that the neutralino contribution will vanish when

$$\frac{\epsilon_L(e)}{M^2_{\tilde{e}_L}} \;=\; \frac{\epsilon_L(u)}{M^2_{\tilde{u}_L}} \;=\; \frac{\epsilon_R(d)}{M^2_{\tilde{d}_R}}\,. \tag{5.9.2}$$

There may be a symmetry reason for this. On the other hand, the gluino exhange contributions put together look like

$$\begin{aligned}\mathcal{L}_{\tilde{g}} \;&=\; \frac{\pi\alpha_s(\lambda'^*_{111})^2}{24\,M_{\tilde{g}}}\left[\left\{\frac{1}{M^4_{\tilde{u}_L}}+\frac{1}{M^4_{\tilde{d}_R}}+\frac{7}{M^2_{\tilde{u}_L}M^2_{\tilde{d}_R}}\right\}J_{PS}\cdot J_{PS}\right.\\ &\qquad\left.-\frac{1}{4}\left\{\frac{1}{M^4_{\tilde{u}_L}}+\frac{1}{M^4_{\tilde{d}_R}}-\frac{1}{M^2_{\tilde{u}_L}M^2_{\tilde{d}_R}}\right\}J_{T\mu\nu}\cdot J_T^{\mu\nu}\right]\left[\,\overline{e}(1+\gamma_5)e^c\,\right]\\ &=\; \frac{\pi\alpha_s(\lambda'^*_{111})^2}{96\,M_{\tilde{g}}}\left[\left\{9\left(\frac{1}{M^2_{\tilde{u}_L}}+\frac{1}{M^2_{\tilde{d}_R}}\right)^2-5\left(\frac{1}{M^2_{\tilde{u}_L}}-\frac{1}{M^2_{\tilde{d}_R}}\right)^2\right\}J_{PS}\cdot J_{PS}\right.\\ &\qquad\left.-\frac{1}{4}\left\{\left(\frac{1}{M^2_{\tilde{u}_L}}+\frac{1}{M^2_{\tilde{d}_R}}\right)^2+3\left(\frac{1}{M^2_{\tilde{u}_L}}-\frac{1}{M^2_{\tilde{d}_R}}\right)^2\right\}J_{T\mu\nu}\cdot J_T^{\mu\nu}\right]\left[\,\overline{e}(1+\gamma_5)e^c\,\right],\end{aligned} \tag{5.9.3}$$

and does not vanish for any choice of the squark masses.

Coupling	Observable	Previous 2σ bound [47]	New 2σ bound	with Babar preliminary [104]
λ_{12k}	V_{ud}	0.05	0.03	
	$R_{\tau\mu}$	0.07	0.05	
	Q_W(Cs)	0.11^*	0.08	
λ_{13k}	R_τ	0.07	0.05	0.03
λ_{23k}	R_τ	0.07	0.05	0.05
	$R_{\tau\mu}$	0.07	0.06	
λ'_{1j1}	Q_W(Cs)	0.03^*	0.03	
λ'_{11k}	V_{ud}	0.02	0.03	
	R_π	0.03	0.03	
	Q_W(Cs)	0.05^*	0.04	
λ'_{12k}	R_{D^0}	$0.27^\dagger$	0.2	
	R_{D^+}	$0.44^\dagger$	0.2	
	$R^*_{D^+}$	$0.23^\dagger$	0.2	
λ'_{21k}	R_π	0.06	0.06	
	$R_{\tau\pi}$	0.08	0.07	0.04
λ'_{22k}	R_{D^0}	$0.21^\dagger$	0.1	
	R_{D^+}	$0.61^\dagger$	0.4	
	$R^*_{D^+}$	$0.38^\dagger$	0.3	
	$R_{D_s}(\tau\mu)$	0.65	0.2	
λ'_{31k}	$R_{\tau\pi}$	0.12	0.06	0.08
λ'_{32k}	$R_{D_s}(\tau\mu)$	0.52	0.3	

Table 5.3: Current single-coupling bounds on various RPV couplings compared with those given in Table 6.1 of Ref. [47]. All sparticle masses have been set to 100 GeV. The values with an asterisk have been corrected for an error in Ref. [47]. Those with a dagger were calculated with the SM prediction fixed to $(1.03)^{-1}$ without any uncertainties.

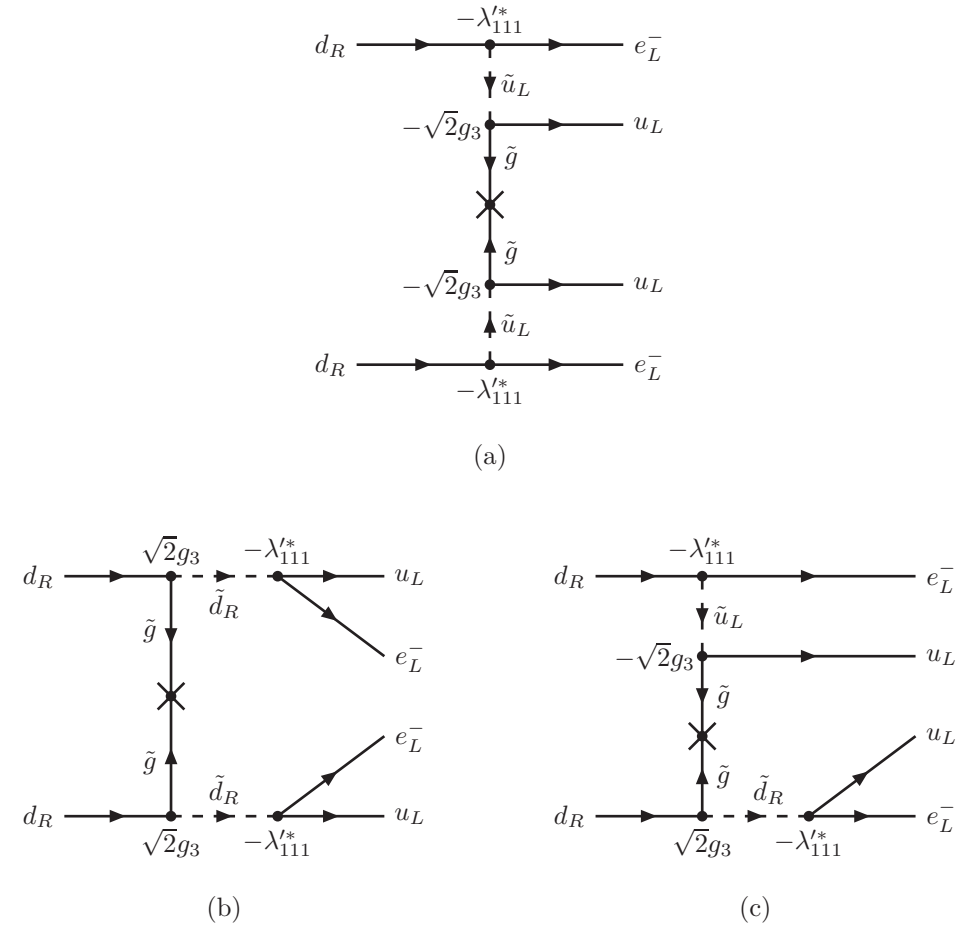

Figure 5.7.1: Contributions of the λ'_{111} coupling to neutrinoless double beta decay via gluino exchange. g_3 is the QCD coupling constant. The cross in each diagram indicates a chirality flip of the gluino.

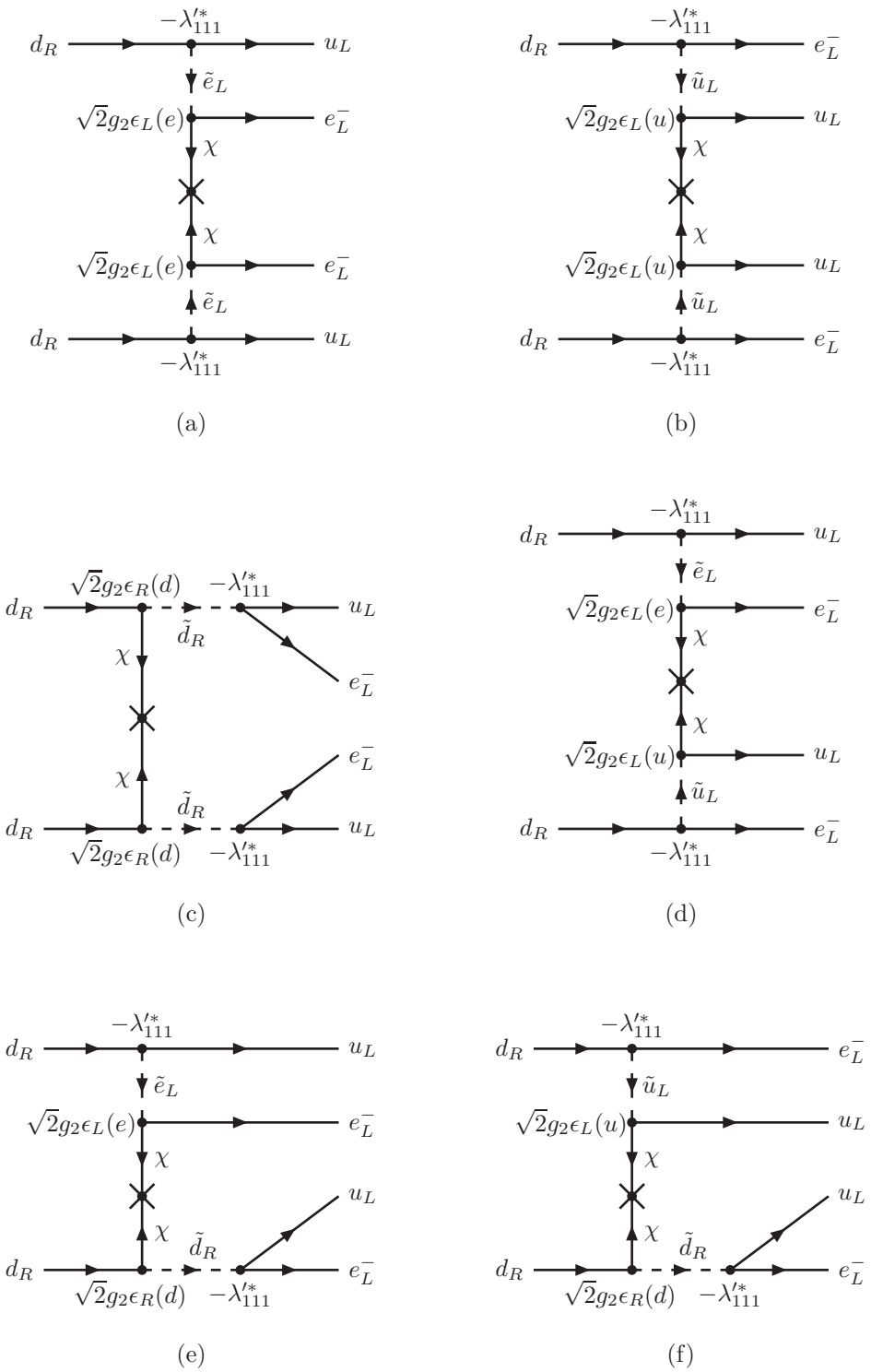

Figure 5.8.1: Contributions of the λ'_{111} coupling to neutrinoless double beta decay via neutralino exchange. g_2 is the $SU(2)_L$ coupling constant. The cross in each diagram indicates a chirality flip of the neutralino.

Chapter 6

Summary

6.1 A Simple Parametrization of Matter Effects on Neutrino Oscillations

We considered the matter effect on neutrino oscillations, and derived simple analytical approximations to the effective mixing angles and effective mass-squared differences in constant density matter. Our results are summarized in Table **??**. These expressions can be utilized in calculating, analyzing, and understanding the behavior of the oscillation probabilities in LBL neutrino oscillation experiments.

The formalism developed in this paper can be further extended to incorporate matter effects due to the violation of universality in neutral current interactions, or additional matter effects due to new interactions. This will be presented in a subsequent paper [33].

6.2 Constraints on New Physics from Long Baseline Neutrino Oscillation

We surveyed the potential constraints on various models of new physics which could be obtained from a hypothetical Fermilab→HyperKamiokande, or similar type of experiment. We assumed that the parameter ξ, defined in Eq. (3.1.4), could be constrained to $|\xi| \leq \xi_0 = 0.005$ at the 99% confidence level. This places a constraint on the couplings and masses of new particles that are exchanged between the neutrinos and matter fermions.

Table 3.10 summarizes our result. Of the models surveyed, the potential bound on gauged $B - 3L_\tau$ from $|\xi| \leq \xi_0$ can be expected to be stronger than the expected bound from the LHC. Bounds on generation non-diagonal leptoquarks can be competitive if $\sqrt{|C_{LQ}||\delta\lambda^2_{LQ}|} = O(1)$. For these cases, neutrino oscillation can be used as an independent check in the event that such new physics is discovered at the LHC.

All the other models are already well constrained by existing experiments, either indirectly by low-energy precision measurements, or by direct searches at colliders. Generically, the couplings and masses of new particles that couple only to leptons are well constrained by lepton universality, while their contribution to neutrino oscillation tend to be suppressed since they only interact with the electrons in matter. This tends to render the existing bound stronger than the potential

bound from $|\xi| \geq \xi_0$.

Topcolor assisted technicolor, and R-parity violating LQD couplings involve interactions with the quarks in matter, but they too belong to the list of already well-constrained models. For the Z' in topcolor assisted technicolor, the proton and electron contributions to neutrino oscillation cancel, just as for the Standard Model Z, and the coupling is also fixed to a small value, which results in a weak bound from $|\xi| \leq \xi_0$. For the LQD coupling, restriction to minimal supergravity provided an extra constraint which strengthened the existing bound.

The fact that only a limited number of models (at least among those we surveyed) can be well constrained by $|\xi| \leq \xi_0$ means, conversely, that if a non-zero ξ is observed in neutrino oscillation, the list of possible new physics that could lead to such an effect is also limited. This could, in principle, help distinguish among possible new physics which have the same type of signature (*e.g.* a leptoquark which may, or may not be generation diagonal) at the LHC.

6.3 Constraints on R-parity violation from recent Belle/Babar data

In Table 4.1 we list the bounds on various R-parity violating coupling combinations obtained in this work against those obtained by Dreiner et al. in 2002 [89] and in 2006 [90]. All sfermion masses have been set to 100 GeV. The bounds from both $B \to \tau\nu_\tau$ and $\tau \to \ell K^0_S$ have all improved by factors of $4 \sim 5$. The corresponding lower bound on the scale of new physics is in the 4 to 10 TeV range if we set all coupling constants to one.

The current single-coupling bounds on the individual R-parity violating couplings that appear in Table 4.1 are listed in Table **??**. The numbers have been updated from those in Table 6.1 on page 110 of Ref. [47] using the most recent data [116, 103, 104]. Detailed derivations will be provided elsewhere [106, 107]. The products of these single-coupling bounds are listed in the rightmost column of Table 4.1 with all sparticle masses set to 100 GeV. As can be seen, the bounds from $B \to \tau\nu_\tau$ and $\tau \to \ell K^0_S$ are much stronger than the products of the single-coupling bounds with the exception of the combination $|\lambda'_{111}\lambda'^*_{312}|$ for which $|\lambda'_{111}|$ is strongly constrained by neutrinoless double beta-decay.

The experimental error on $B \to \tau\nu_\tau$ can be expected to be reduced further as more Belle and Babar data is analyzed. However, unless the theoretical uncertainty of its SM prediction based on charmless semileptonic B decay and lattice calculations can be reduced also, any improvement on the new physics bounds will be limited. The decay $\tau \to \ell K^0_S$, on the other hand, has no SM counterpart, and any reduction of its experimental upper bound will translate directly into an improvement of the bounds on new physics.

6.4 Single-Coupling Bounds on R-parity violating Supersymmetry

We then looked at a variety of single-coupling bounds that can be imposed on R-parity violation from particle decay ratios and atomic parity violation. Our results are summarized in Table 5.3. Compared to the bounds complied in 2004 by Barbier et al. [47], the bounds have steadily improved. For the bounds from observables involving τ-decay, the improvement is due to the results of ALEPH [137] released in 2005. The bounds from observables involving D and D_s decay have improved due to new data from CLEO [135, 138, 139, 140] and Belle [133, 141]. The new

bounds from the weak charge of cesium-133 is due to the reduction of theoretical uncertainty in its extraction from experimental data [103].

Further improvements on the bounds from observables involving τ-decay is expected as analyses of Belle and Babar data get under way, each with hundreds of millions of $\tau^+\tau^-$ pairs, as is evidenced by the effect of the preliminary Babar data from 2008 [104]. The bounds from observables involving π-decay can also be expected to improve considerably in the near future as the PIENU experiment at TRIUMF [142] and the PEN experiment and PSI [143] start their physics runs this year, eventually improving the error on R_π by almost an order of magnitude.

The bound on λ'_{111} from neutrinoless double beta decay will be updated in a subsequent paper [107].

Appendix A

The Jacobi Method

To approximately diagonalize the modified Hamiltonian,

$$H' = \begin{bmatrix} ac_{12}^2c_{13}^2 & ac_{12}s_{12}c_{13}^2 & ac_{12}c_{13}s_{13} \\ ac_{12}s_{12}c_{13}^2 & as_{12}^2c_{13}^2+\delta m_{21}^2 & as_{12}c_{13}s_{13} \\ ac_{12}c_{13}s_{13} & as_{12}c_{13}s_{13} & as_{13}^2+\delta m_{31}^2 \end{bmatrix}, \tag{A.0.1}$$

here we utilize the Jacobi Method. Consider a 2×2 real symmetric matrix

$$M = \begin{bmatrix} \alpha & \beta \\ \beta & \gamma \end{bmatrix}, \qquad \alpha,\beta,\gamma \in \mathbb{R}. \tag{A.0.2}$$

We define a rotation matrix

$$\begin{bmatrix} c_\omega & s_\omega \\ -s_\omega & c_\omega \end{bmatrix}, \qquad \text{where} \qquad c_\omega = cos\omega, \qquad s_\omega = sin\omega, \qquad \tan 2\omega \equiv \frac{2\beta}{\gamma-\alpha}. \tag{A.0.3}$$

Then the matrix M can be diagonalized by

$$R^\dagger MR = \begin{bmatrix} \Lambda_1 & 0 \\ 0 & \Lambda_2 \end{bmatrix}, \qquad \text{with} \qquad \Lambda_1 = \frac{\alpha c_\omega^2-\gamma s_\omega^2}{c_\omega^2-s_\omega^2}, \qquad \Lambda_2 = \frac{\gamma c_\omega^2-\alpha s_\omega^2}{c_\omega^2-s_\omega^2}. \tag{A.0.4}$$

The Jacobi method entails iteratively diagonalizing 2×2 submatrices of a larger matrix in the order that requires the largest rotation angle at each step. To determine which rotations are needed we need to know the relative sizes of each matrix elements. The current bounds for neutrino mixing angles and mass squared differences are

$$\begin{aligned} \sin^2(2\theta_{12}) &= 0.87 \pm 0.03 \\ \sin^2(2\theta_{23}) &= > 0.92 \\ \sin^2(2\theta_{13}) &= < 0.19, \qquad \text{CL} = 90\% \\ \delta m_{21}^2 &= (7.59 \pm 0.20)\times 10^{-5}\text{eV}^2 \\ \delta m_{31}^2 &= (2.43 \pm 0.13)\times 10^{-3}\text{eV}^2. \end{aligned} \tag{A.0.5}$$

We introduce the parameter $\epsilon \equiv \sqrt{\delta m_{21}^2/|\delta m_{31}^2|} = 0.17 - 0.18$ as a basis for the comparison of the matrix elements.

$$H' = \begin{bmatrix} a\mathcal{O}(1) & a\mathcal{O}(1) & a\mathcal{O}(\epsilon) \\ a\mathcal{O}(1) & a\mathcal{O}(\epsilon^2) + \delta m^2_{21} & a\mathcal{O}(\epsilon) \\ a\mathcal{O}(\epsilon) & a\mathcal{O}(\epsilon) & a\mathcal{O}(\epsilon^2) + \delta m^2_{31} \end{bmatrix} \approx \begin{bmatrix} a\mathcal{O}(1) & a\mathcal{O}(1) & a\mathcal{O}(\epsilon) \\ a\mathcal{O}(1) & a\mathcal{O}(\epsilon^2) + \mathcal{O}(\epsilon^3) & a\mathcal{O}(\epsilon) \\ a\mathcal{O}(\epsilon) & a\mathcal{O}(\epsilon) & a\mathcal{O}(\epsilon^2) + \mathcal{O}(\epsilon^5) \end{bmatrix}$$

The angles of the 2×2 rotation matrices are

$$\begin{aligned} \tan 2\phi_{12} &= \frac{2a\mathcal{O}(1)}{(a\mathcal{O}(\epsilon^2) + \delta m^2_{21}) - (a\mathcal{O}(1))} \approx \frac{2a\mathcal{O}(1)}{\delta m^2_{21} - a\mathcal{O}(1)} \\ \tan 2\phi_{23} &= \frac{2a\mathcal{O}(\epsilon)}{(a\mathcal{O}(\epsilon^2) + \delta m^2_{31}) - (a\mathcal{O}(\epsilon^2) + \delta m^2_{21})} \approx \frac{2a\mathcal{O}(\epsilon)}{\delta m^2_{31}} \\ \tan 2\phi_{13} &= \frac{2a\mathcal{O}(\epsilon)}{(a\mathcal{O}(\epsilon^2) + \delta m^2_{31}) - (a\mathcal{O}(1))} \approx \frac{2a\mathcal{O}(\epsilon)}{\delta m^2_{31} - a\mathcal{O}(1)} \,. \end{aligned} \tag{A.0.6}$$

We investigate the rotation angle for five different regions, $a < \delta m^2_{21}$, $a \approx \delta m^2_{21}$, $\delta m^2_{21} < a < \delta m^2_{31}$, and $\delta m^2_{31} < a$, and found that in all cases the Hamiltonian can be approximately diagonalized by a 1-2 rotation followed by a 2-3 rotation.

A.1 $a < \delta m^2_{21}$

$$\begin{aligned} \tan 2\phi_{12} &\approx \frac{a\mathcal{O}(1)}{\delta m^2_{21}} \approx \frac{a\mathcal{O}(1)}{\epsilon^2 \delta m^2_{31}} \approx \frac{a}{\delta m^2_{31}}\mathcal{O}(\epsilon^{-2}) \rightarrow \phi_{12} < 0.03\pi \\ \tan 2\phi_{23} &\approx \frac{a\mathcal{O}(\epsilon)}{\delta m^2_{31}} \approx \frac{a}{\delta m^2_{31}}\mathcal{O}(\epsilon) \rightarrow \phi_{23} < 0.005\pi \\ \tan 2\phi_{13} &\approx \frac{a\mathcal{O}(\epsilon)}{\delta m^2_{31}} \approx \frac{a}{\delta m^2_{31}}\mathcal{O}(\epsilon) \rightarrow \phi_{13} < 0.005\pi, \end{aligned} \tag{A.1.1}$$

so the largest rotation angle is ϕ_{12}.

A.2 $a \approx \delta m^2_{21}$

$$\begin{aligned} \tan 2\phi_{12} &\approx \frac{\delta m^2_{21}}{\delta m^2_{21} - \delta m^2_{21}} \rightarrow \infty \rightarrow \phi_{12} \approx \frac{\pi}{4} \\ \tan 2\phi_{23} &\approx \frac{\delta m^2_{21}\mathcal{O}(\epsilon)}{\delta m^2_{31}} \approx \frac{\delta m^2_{31}\mathcal{O}(\epsilon^3)}{\delta m^2_{31}} \approx \mathcal{O}(\epsilon^3) \rightarrow \phi_{23} \approx 10^{-4}\pi \\ \tan 2\phi_{13} &\approx \frac{\delta m^2_{21}\mathcal{O}(\epsilon)}{\delta m^2_{31} - \delta m^2_{21}} \approx \frac{\delta m^2_{31}\mathcal{O}(\epsilon^3)}{\delta m^2_{31}} \approx \mathcal{O}(\epsilon^3) \rightarrow \phi_{13} \approx 10^{-4}\pi, \end{aligned} \tag{A.2.1}$$

so the largest rotation angle is ϕ_{12}.

A.3 $\delta m^2_{21} < a < \delta m^2_{31}$

$$\begin{aligned}
\tan 2\phi_{12} &\approx -\frac{a\mathcal{O}(1)}{a\mathcal{O}(1)} \approx -\mathcal{O}(1) \to \phi_{12} \approx 0.3\pi \\
\tan 2\phi_{23} &\approx \frac{a\mathcal{O}(\epsilon)}{\delta m^2_{31}} \approx \frac{\epsilon\delta m^2_{31}\mathcal{O}(\epsilon)}{\delta m^2_{31}} \approx \mathcal{O}(\epsilon^2) \to \phi_{23} < 10^{-3}\pi \\
\tan 2\phi_{13} &\approx \frac{a\mathcal{O}(\epsilon)}{\delta m^2_{31}} \approx \frac{\epsilon\delta m^2_{31}\mathcal{O}(\epsilon)}{\delta m^2_{31}} \approx \mathcal{O}(\epsilon^2) \to \phi_{13} < 10^{-3}\pi,
\end{aligned} \tag{A.3.1}$$

so the largest rotation angle is still ϕ_{12}.

A.4 $a \approx \delta m^2_{31}$

The angles are:

$$\begin{aligned}
\tan 2\phi_{12} &\approx \frac{\delta m^2_{31}}{\epsilon^2\delta m^2_{31} - \delta m^2_{31}} \approx -\mathcal{O}(1) \to \phi_{12} \approx 0.3\pi \\
\tan 2\phi_{23} &\approx \frac{\delta m^2_{31}\mathcal{O}(\epsilon)}{\delta m^2_{31}} \approx \mathcal{O}(\epsilon) \to \phi_{23} \approx 10^{-2}\pi \\
\tan 2\phi_{13} &\approx \frac{\delta m^2_{31}\mathcal{O}(\epsilon)}{\delta m^2_{31} - \delta m^2_{31}} \to \infty \to \phi_{13} \approx 0.25\pi
\end{aligned} \tag{A.4.1}$$

So the largest rotation angle is ϕ_{12}.

A.5 $a\mathcal{O}(\epsilon) \approx \delta m^2_{31}$

When $a\mathcal{O}(\epsilon) \approx \delta m^2_{31}$ or $a \approx \delta m^2_{31}\mathcal{O}(\epsilon^{-1})$

$$\begin{aligned}
\tan 2\phi_{12} &\approx \frac{\delta m^2_{31}\mathcal{O}(\epsilon^{-1})}{\delta m^2_{21} - \delta m^2_{31}\mathcal{O}(\epsilon^{-1})} \approx \frac{\delta m^2_{31}\mathcal{O}(\epsilon^{-1})}{\epsilon^2\delta m^2_{31} - \delta m^2_{31}\mathcal{O}(\epsilon^{-1})} \\
&\approx -\frac{\delta m^2_{31}\mathcal{O}(\epsilon^{-1})}{\delta m^2_{31}\mathcal{O}(\epsilon^{-1})} \approx -\mathcal{O}(1) \to \phi_{12} \approx 0.3\pi \\
\tan 2\phi_{23} &\approx \frac{\delta m^2_{31}}{\delta m^2_{31}} \approx \mathcal{O}(1) \to \phi_{23} < 0.25\pi \\
\tan 2\phi_{13} &\approx \frac{\delta m^2_{31}}{\delta m^2_{31} - \delta m^2_{31}\mathcal{O}(\epsilon^{-1})} \approx -\frac{\delta m^2_{31}}{\delta m^2_{31}\mathcal{O}(\epsilon^{-1})} \approx -\mathcal{O}(\epsilon) \to \phi_{13} > 0.4\pi.
\end{aligned} \tag{A.5.1}$$

So the largest rotation angle is ϕ_{13}. Recall that $\sqrt{\delta m^2_{21}/|\delta m^2_{31}|} = \epsilon$ so $\delta m^2_{21} = \epsilon^2\delta m^2_{31}$.

To diagonalize the $(1,2)$ submatrix of H', we define

$$V = \begin{bmatrix} \cos\phi_{12} & \sin\phi_{12} & 0 \\ -\sin\phi_{12} & \cos\phi_{12} & 0 \\ 0 & 0 & 1 \end{bmatrix}, \tag{A.5.2}$$

where

$$\phi_{12} = \frac{1}{2}\tan^{-1}\left[\frac{ac_{13}^2 \sin 2\theta_{12}}{\delta m_{21}^2 - ac_{13}^2 \cos 2\theta_1 2}\right], \qquad \left(0 \le \phi_{12} < \frac{\pi}{2}\right). \tag{A.5.3}$$

Using the 1-2 rotation matrix V, we find

$$\begin{aligned} H'' &= V^\dagger H' V \\ &= \begin{bmatrix} \lambda_1' & 0 & ac_{12}' c_{13} s_{13} \\ 0 & \lambda_2' & as_{12}' c_{13} s_{13} \\ ac_{12}' c_{13} s_{13} & as_{12}' c_{13} s_{13} & as_{13}^2 + \delta m_{31}^2 \end{bmatrix}, \end{aligned} \tag{A.5.4}$$

where

$$c_{12}' = \cos\theta_{12}', \qquad s_{12}' = \sin\theta_{12}', \qquad \theta_{12}' = \theta_{12} + \phi_{12}, \tag{A.5.5}$$

and

$$\begin{aligned} \lambda_1' &= \frac{(ac_{12}^2 c_{13}^2)\cos^2\phi_{12} - (as_{12}^2 c_{13}^2 + \delta m_{21}^2)\sin^2\phi_{12}}{\cos^2\phi_{12} - \sin^2\phi_{12}} \\ \lambda_2' &= \frac{(as_{12}^2 c_{13}^2 + \delta m_{21}^2)\cos^2\phi_{12} - (ac_{12}^2 c_{13}^2)\sin^2\phi_{12}}{\cos^2\phi_{12} - \sin^2\phi_{12}}. \end{aligned} \tag{A.5.6}$$

Again, we follow the same procedure as above and analyze the rotation needed for the five regions , $a < \delta m_{21}^2$, $a \approx \delta m_{21}^2$, $\delta m_{21}^2 < a < \delta m_{31}^2$, and $\delta m_{31}^2 < a$. Since the $(1,2)$ submatrix is already diagonalized, we only need to determine whether the second rotation is $(2,3)$ rotation or $(1,3)$ rotation. From the partially diagonalized Hamiltonian, eq.(A.5.4), the rotation angles are given by

$$\begin{aligned} \tan 2\phi_{23} &= \frac{2as_{12}' c_{13} s_{13}}{as_{13}^2 + \delta m_{31}^2 - \lambda_2'} \\ \tan 2\phi_{13} &= \frac{2ac_{12}' c_{13} s_{13}}{as_{13}^2 + \delta m_{31}^2 - \lambda_1'}. \end{aligned} \tag{A.5.7}$$

A.6 $a < \delta m_{21}^2$ case

The rotation angles required to diagonalize $(1,3)$ or $(2,3)$ submatrices are both very small:

$$\begin{aligned} \tan 2\phi_{23} &\approx \frac{\mathcal{O}(\epsilon^6)}{\mathcal{O}(\epsilon^3)} = \mathcal{O}(\epsilon^3) \\ \tan 2\phi_{13} &\approx \frac{\mathcal{O}(\epsilon^6)}{\mathcal{O}(\epsilon^3)} = \mathcal{O}(\epsilon^3) \end{aligned} \tag{A.6.1}$$

A.7 $\delta m_{21}^2 < a < \delta m_{31}^2$ case

The rotation angles required to diagonalize $(1,3)$ or $(2,3)$ submatrices are

$$\tan 2\phi_{23} \approx \frac{\mathcal{O}(\epsilon^5)}{\mathcal{O}(\epsilon^3)} = \mathcal{O}(\epsilon^2)$$
$$\tan 2\phi_{13} \approx \frac{\mathcal{O}(\epsilon^6)}{\mathcal{O}(\epsilon^3)} = \mathcal{O}(\epsilon^3) \tag{A.7.1}$$

A.8 $a > \delta m^2_{31}$ case

The rotation angles required to diagonalize $(1,3)$ or $(2,3)$ submatrices are

$$\tan 2\phi_{23} \approx \frac{\mathcal{O}(\epsilon^4)}{\mathcal{O}(\epsilon^3)} = \mathcal{O}(\epsilon)$$
$$\tan 2\phi_{13} \approx \frac{\mathcal{O}(\epsilon^6)}{\mathcal{O}(\epsilon^3)} = \mathcal{O}(\epsilon^3) \tag{A.8.1}$$

In all cases, ϕ_{23} is of the same order of magnitude as ϕ_{12} or larger. So we define

$$W = \begin{bmatrix} 1 & 0 & 0 \\ 0 & \cos\phi_{23} & \sin\phi_{23} \\ 0 & -\sin\phi_{23} & \cos\phi_{23} \end{bmatrix}, \tag{A.8.2}$$

where

$$\phi_{23} = \frac{1}{2}\tan^{-1}\left[\frac{2as'_{12}c_{13}s_{13}}{as^2_{13} + \delta m^2_{31} - \lambda'_2}\right]. \tag{A.8.3}$$

Then

$$H''' = R^\dagger_{23} H'' R_{23} = \begin{bmatrix} \lambda''_1 & -ac'_{12}c_{13}s_{13}\sin\phi_{23} & ac'_{12}c_{13}s_{13}\cos\phi_{23} \\ -ac'_{12}c_{13}s_{13}\sin\phi_{23} & \lambda''_2 & 0 \\ ac'_{12}c_{13}s_{13}\cos\phi_{23} & 0 & \lambda''_3 \end{bmatrix}, \tag{A.8.4}$$

where

$$\begin{aligned} \lambda''_1 &= \lambda'_1\,, \\ \lambda''_2 &= \frac{\lambda'_2\cos^2\phi_{23} - (as^2_{13} + \delta m^2_{31})\sin^2\phi_{23}}{\cos^2\phi_{23} - \sin^2\phi_{23}}\,, \\ \lambda''_3 &= \frac{(as^2_{13} + \delta m^2_{31})\cos^2\phi_{23} - \lambda'_2\sin^2\phi_{23}}{\cos^2\phi_{23} - \sin^2\phi_{23}}\,. \end{aligned} \tag{A.8.5}$$

One can repeat the same process to achieve arbitrary precision, but in our case two iterations was sufficient.

A.9 Anti-Neutrino Case

In the case of anti-neutrinos, the matrix needs to be diagonalized is

$$\mathcal{Q}U^{\mathrm{T}}\bar{H}U^*\mathcal{Q}^* = \bar{H}' = \begin{bmatrix} -ac^2_{12}c^2_{13} & -ac_{12}s_{12}c^2_{13} & -ac_{12}c_{13}s_{13} \\ -ac_{12}s_{12}c^2_{13} & -as^2_{12}c^2_{13} + \delta m^2_{21} & -as_{12}c_{13}s_{13} \\ -ac_{12}c_{13}s_{13} & -as_{12}c_{13}s_{13} & -as^2_{13} + \delta m^2_{31} \end{bmatrix}. \tag{A.9.1}$$

Following the general procedure we employed for the neutrinos, we begin by diagonalizing the 1-2 submatrix of $\bar{H}'$. Let

$$V = \begin{bmatrix} \cos\bar{\phi}_{12} & \sin\bar{\phi}_{12} & 0 \\ -\sin\bar{\theta}_{12} & \cos\bar{\theta}'_{12} & 0 \\ 0 & 0 & 1 \end{bmatrix} , \tag{A.9.2}$$

where

$$\tan 2\bar{\phi}_{12} \equiv -\frac{ac_{13}^2 \sin 2\theta_{12}}{\delta m_{21}^2 + ac_{13}^2 \cos 2\theta_{12}} , \quad \left(-\frac{\pi}{2} < \bar{\phi}_{12} \leq 0\right) . \tag{A.9.3}$$

Using V, we find

$$\bar{H}'' = V^\dagger \bar{H}' V = \begin{bmatrix} \bar{\lambda}'_1 & 0 & -a\bar{c}'_{12}c_{13}s_{13} \\ 0 & \bar{\lambda}'_2 & -a\bar{s}'_{12}c_{13}s_{13} \\ -a\bar{c}'_{12}c_{13}s_{13} & -a\bar{s}'_{12}c_{13}s_{13} & -as_{13}^2 + \delta m_{31}^2 \end{bmatrix} \tag{A.9.4}$$

where

$$\bar{c}'_{12} = \cos\bar{\theta}'_{12} , \quad \bar{s}'_{12} = \sin\bar{\theta}'_{12} , \quad \bar{\theta}'_{12} = \theta_{12}\bar{\phi}_{12} , \quad \tan 2\bar{\theta}'_{12} = \frac{\delta m_{21}^2 \sin 2\theta_{12}}{\delta m_{21}^2 \cos 2\theta_{12} + ac_{13}^2} , \tag{A.9.5}$$

and

$$\begin{aligned} \bar{\lambda}'_1 &= \frac{(\delta m_{21}^2 - ac_{13}^2) - \sqrt{(\delta m_{21}^2 + ac_{13}^2)^2 - 4ac_{13}^2 \delta m_{21}^2 s_{12}^2}}{2} \\ \bar{\lambda}'_2 &= \frac{(\delta m_{21}^2 - ac_{13}^2) + \sqrt{(\delta m_{21}^2 + ac_{13}^2)^2 - 4ac_{13}^2 \delta m_{21}^2 s_{12}^2}}{2} . \end{aligned} \tag{A.9.6}$$

Nex, unlike the neutrino case, we diagonalize the 1-3 submatrix of $\bar{H}''$. Let

$$W = \begin{bmatrix} \cos\bar{\phi}_{13} & 0 & \sin\bar{\phi}_{13} \\ 0 & 1 & 0 \\ -\sin\bar{\phi}_{13} & 0 & \cos\bar{\phi}_{13} \end{bmatrix} , \tag{A.9.7}$$

where

$$\tan 2\bar{\phi}_{13} \equiv -\frac{a\bar{c}'_{12} \sin 2\theta_{13}}{\delta m_{31}^2 - as_{13}^2 - \bar{\lambda}'_1} . \tag{A.9.8}$$

The angle $\bar{\phi}_{13}$ is in the fourth quadrant when $\delta m_{31}^2 > 0$, and the first quadrant when $\delta m_{31}^2 < 0$. Using $\bar{R}_{12}$, we find

$$\bar{H}''' = W^\dagger \bar{H}'' W = \begin{bmatrix} \bar{\lambda}''_1 & a\bar{s}'_{12}c_{13}s_{13}\sin\bar{\phi}_{13} & 0 \\ a\bar{s}'_{12}c_{13}s_{13}\sin\bar{\phi}_{13} & \bar{\lambda}''_2 & -a\bar{s}'_{12}c_{13}s_{13}\cos\bar{\phi}_{13} \\ 0 & -a\bar{s}'_{12}c_{13}s_{13}\cos\bar{\phi}_{13} & \bar{\lambda}''_3 \end{bmatrix} , \tag{A.9.9}$$

where

$$\bar{\lambda}''_1 = \bar{\lambda}''_- , \quad \bar{\lambda}''_2 = \bar{\lambda}'_2 , \quad \bar{\lambda}''_3 = \bar{\lambda}''_+ , \qquad \text{if } \delta m_{31}^2 > 0 ,$$

$$\bar{\lambda}''_1 = \bar{\lambda}''_+ \,, \quad \bar{\lambda}''_2 = \bar{\lambda}'_2 \,, \quad \bar{\lambda}''_3 = \bar{\lambda}''_- \,, \qquad \text{if } \delta m^2_{31} < 0 \,. \tag{A.9.10}$$

with

$$\bar{\lambda}''_+ \equiv \frac{\left[(\delta m^2_{31} - a s^2_{13}) + \bar{\lambda}'_1\right] \pm \sqrt{\left[(\delta m^2_{31} - a s^2_{13}) - \bar{\lambda}'_1\right] + 4a^2 \bar{c}'^2_{12} c^2_{13} s^2_{13}}}{2} \,. \tag{A.9.11}$$

Evaluation of the off-diagonal terms of $\bar{H}'''$ reveals that it is approximately diagonalized. Since

$$\begin{aligned} \bar{H}''' &= W^\dagger V^\dagger \mathcal{Q}^\dagger U^\dagger \bar{H} U \mathcal{Q} V W \\ &= \bar{U}'^\dagger \bar{H} \bar{U}' \,, \end{aligned} \tag{A.9.12}$$

where

$$\begin{aligned} & \bar{U}' \\ = \;& U \mathcal{Q} \bar{R}_{12} \bar{R}_{13} \\ = \;& U \bar{R}_{12} \mathcal{Q} \bar{R}_{13} \\ = \;& \begin{bmatrix} 1 & 0 & 0 \\ 0 & c_{23} & s_{23} \\ 0 & -s_{23} & c_{23} \end{bmatrix} \begin{bmatrix} c_{13} & 0 & s_{13} e^{-i\delta} \\ 0 & 1 & 0 \\ -s_{13} e^{i\delta} & 0 & c_{13} \end{bmatrix} \begin{bmatrix} c_{12} & s_{12} & 0 \\ -s_{12} & c_{12} & 0 \\ 0 & 0 & 1 \end{bmatrix} \begin{bmatrix} \bar{c}_{\phi_{12}} & \bar{s}_{\phi_{12}} & 0 \\ -\bar{s}_{\phi_{12}} & \bar{c}_{\phi_{12}} & 0 \\ 0 & 0 & 1 \end{bmatrix} Q \, \bar{R}_{13} \\ = \;& \begin{bmatrix} 1 & 0 & 0 \\ 0 & c_{23} & s_{23} \\ 0 & -s_{23} & c_{23} \end{bmatrix} \begin{bmatrix} c_{13} & 0 & s_{13} e^{-i\delta} \\ 0 & 1 & 0 \\ -s_{13} e^{i\delta} & 0 & c_{13} \end{bmatrix} \begin{bmatrix} \bar{c}'_{12} & \bar{s}'_{12} & 0 \\ -\bar{s}'_{12} & \bar{c}'_{12} & 0 \\ 0 & 0 & 1 \end{bmatrix} \begin{bmatrix} 1 & 0 & 0 \\ 0 & 1 & 0 \\ 0 & 0 & e^{i\delta} \end{bmatrix} \begin{bmatrix} \bar{c}_{\phi_{13}} & 0 & \bar{s}_{\phi_{13}} \\ 0 & 1 & 0 \\ -\bar{s}_{\phi_{13}} & 0 & \bar{c}_{\phi_{13}} \end{bmatrix} \\ = \;& \begin{bmatrix} \bar{U}_{e1} & \bar{U}_{\mu 1} & \bar{U}_{\tau 1} \\ \bar{U}_{e2} & \bar{U}_{\mu 2} & \bar{U}_{\tau 2} \\ \bar{U}_{e3} & \bar{U}_{\mu 3} & \bar{U}_{\tau 3} \end{bmatrix} \end{aligned} \tag{A.9.13}$$

where

$$\begin{aligned} \bar{U}_{e1} &= c_{13} \bar{c}'_{12} \bar{c}_{\phi_{13}} - s_{13} \bar{s}_{\phi_{13}} \\ \bar{U}_{\mu 1} &= c_{13} \bar{s}'_{12} \\ \bar{U}_{\tau 1} &= s_{13} \bar{c}_{\phi_{13}} + c_{13} \bar{c}'_{12} \bar{s}_{\phi_{13}} \\ \bar{U}_{e2} &= -c_{23} \bar{s}'_{12} \bar{c}_{\phi_{13}} - s_{23} (c_{13} \bar{s}_{\phi_{13}} + s_{13} \bar{c}'_{12} \bar{c}_{\phi_{13}}) e^{e\delta} \\ \bar{U}_{\mu 2} &= c_{23} \bar{c}'_{12} - s_{23} s_{13} \bar{s}'_{12} e^{i\delta} \\ \bar{U}_{\tau 2} &= -c_{23} \bar{s}'_{12} \bar{s}_{\phi_{13}} + s_{23} (c_{13} \bar{c}_{\phi_{13}} - s_{13} \bar{c}'_{12} \bar{s}_{\phi_{13}}) e^{i\delta} \\ \bar{U}_{e3} &= s_{23} \bar{s}'_{12} \bar{c}_{\phi_{13}} - c_{23} (c_{13} \bar{s}_{\phi_{13}} + s_{13} \bar{c}'_{12} \bar{c}_{\phi_{13}}) e^{i\delta} \\ \bar{U}_{\mu 3} &= -s_{23} \bar{c}'_{12} - c_{23} s_{13} \bar{s}'_{12} e^{i\delta} \\ \bar{U}_{\tau 3} &= s_{23} \bar{s}'_{12} \bar{s}_{\phi_{13}} + c_{23} (c_{13} \bar{c}_{\phi_{13}} - s_{13} \bar{c}'_{12} \bar{s}_{\phi_{13}}) e^{i\delta} \,. \end{aligned} \tag{A.9.14}$$

Approximated formulae for oscillation probabilities can be obtained by identifying the above matrix with

$$\begin{aligned} \overset{\frown}{U} &= \begin{bmatrix} 1 & 0 & 0 \\ 0 & \overset{\frown}{c}_{23} & \overset{\frown}{s}_{23} \\ 0 & -\overset{\frown}{s}_{23} & \overset{\frown}{c}_{23} \end{bmatrix} \begin{bmatrix} \overset{\frown}{c}_{13} & 0 & \overset{\frown}{s}_{13} e^{-i\overset{\frown}{\delta}} \\ 0 & 1 & 0 \\ -\overset{\frown}{s}_{13} e^{i\overset{\frown}{\delta}} & 0 & \overset{\frown}{c}_{13} \end{bmatrix} \begin{bmatrix} \overset{\frown}{c}_{12} & \overset{\frown}{s}_{12} & 0 \\ -\overset{\frown}{s}_{12} & \overset{\frown}{c}_{12} & 0 \\ 0 & 0 & 1 \end{bmatrix} \\ &= \begin{bmatrix} \overset{\frown}{c}_{12} \overset{\frown}{c}_{13} & \overset{\frown}{s}_{12} \overset{\frown}{c}_{13} & \overset{\frown}{s}_{13} e^{-i\overset{\frown}{\delta}} \\ -\overset{\frown}{s}_{12} \overset{\frown}{c}_{23} - \overset{\frown}{c}_{12} \overset{\frown}{s}_{13} \overset{\frown}{s}_{23} e^{i\overset{\frown}{\delta}} & \overset{\frown}{c}_{12} \overset{\frown}{c}_{23} - \overset{\frown}{s}_{12} \overset{\frown}{s}_{13} \overset{\frown}{s}_{23} e^{i\overset{\frown}{\delta}} & \overset{\frown}{c}_{13} \overset{\frown}{s}_{23} \\ \overset{\frown}{s}_{12} \overset{\frown}{s}_{23} - \overset{\frown}{c}_{12} \overset{\frown}{s}_{13} \overset{\frown}{c}_{23} e^{i\overset{\frown}{\delta}} & -\overset{\frown}{c}_{12} \overset{\frown}{s}_{23} - \overset{\frown}{s}_{12} \overset{\frown}{s}_{13} \overset{\frown}{c}_{23} e^{i\overset{\frown}{\delta}} & \overset{\frown}{c}_{13} \overset{\frown}{c}_{23} \end{bmatrix} . \end{aligned} \tag{A.9.15}$$

Appendix B

Semileptonic D decay ratios with form-factors

The semileptonic decays $D \to K\ell\nu$ ($D^+ \to \overline{K^0}\ell^+\nu_\ell$ or $D^0 \to K^-\ell^+\nu_\ell$) and $D \to K^*\ell\nu$ ($D^+ \to \overline{K}^*(892)^0\ell^+\nu_\ell$ or $D^0 \to K^*(892)^-\ell^+\nu_\ell$) proceed via the SM interaction

$$\mathcal{L} \;=\; -\frac{G_F}{\sqrt{2}} V_{cs}^* \big[\, \bar{s}\gamma_\mu(1-\gamma_5)c \,\big] \big[\, \bar{\nu}\gamma^\mu(1-\gamma_5)\ell \,\big] \;. \tag{B.0.1}$$

For both cases, the hadronic matrix element is expressed in terms of multiple form factors. In this appendix, we calculate the ratios R_{D^0}, R_{D^+}, and $R^*_{D^+}$, defined in Eq. (5.5.4), taking the latest experimental data on these form factors into account.

B.1 $D \to K\ell\nu$

For the decay $D \to K\ell\nu$, the form factors are defined as [129]

$$\langle K|\bar{s}\gamma_\mu(1-\gamma_5)c|D\rangle \;=\; (P_D+P_K)_\mu\, f_+(t) + (P_D-P_K)_\mu\, f_-(t) \;, \tag{B.1.1}$$

where $t = (P_D - P_K)^2$. The decay width in terms of these form factors is

$$\begin{aligned}\Gamma \;=\; \frac{G_F^2|V_{cs}|^2 m_D^3}{24\pi^3} \int_{m_\ell^2}^{(m_D-m_K)^2} dt \Bigg[& \left\{\frac{\lambda^{1/2}(t,m_D^2,m_K^2)}{2m_D^2}\right\}^3 \left(1-\frac{m_\ell^2}{t}\right)^2 \left(1+\frac{m_\ell^2}{2t}\right) |f_+(t)|^2 \\ & + \frac{3}{8}\frac{m_\ell^2}{m_D^2} \left\{\frac{\lambda^{1/2}(t,m_D^2,m_K^2)}{2m_D^2}\right\} \left(1-\frac{m_\ell^2}{t}\right)^2 \frac{t}{m_D^2} \left(\frac{m_D^2-m_K^2}{t}\right)^2 |f_0(t)|^2 \Bigg] \;,\end{aligned} \tag{B.1.2}$$

where we have defined

$$f_0(t) \;\equiv\; f_+(t) + \frac{t}{m_D^2-m_K^2}\, f_-(t) \;, \tag{B.1.3}$$

and

$$\lambda(a,b,c) \;=\; a^2+b^2+c^2-2ab-2bc-2ca \;. \tag{B.1.4}$$

Since $m_e^2 \ll m_D^2$, the scalar form factor term is completely negligible for the electron, and the vector form factor $|f_+(t)|$ can be extracted from the t-dependence of $d\Gamma/dt$. The result is fit by the single-pole function

$$f_+(t) \;=\; \frac{f_+(0)}{1 - t/m^2_{\rm pole}}\,, \tag{B.1.5}$$

where $f_+(0)$ and $m_{\rm pole}$ are adjustable parameters. This form is motivated by the vector meson dominance model [144] which prescribes the following expressions for the form factors [145]:

$$\begin{aligned} f_+(t) &= c_V\,\frac{1}{1 - t/m_V^2}\,, \\ f_0(t) &= c_V + c_S\,\frac{t/m_S^2}{1 - t/m_S^2}\,. \end{aligned} \tag{B.1.6}$$

Here, c_V and c_S are constants, and m_V and m_S are the masses of the lowest lying D_s-mesons with $J^P = 1^-$ and 0^+, respectively. Another popular form used to fit the $f_+(t)$ data is the so-called modified-pole function

$$f_+(t) \;=\; \frac{f_+(0)}{(1 - t/m^2_{D_s^*})(1 - \alpha\, t/m^2_{D_s^*})}\,, \tag{B.1.7}$$

where $m_{D_s^*} = 2112\,\text{MeV}$, and $f_+(0)$ and α are adjustable. The fit values of $m_{\rm pole}$ and α from recent experiments are listed in Table B.1.

Collaboration	Decay Mode	$m_{\rm pole}$ (GeV)	α	$f_-(0)/f_+(0)$	Ref
FOCUS	$D^0 \to K^-\mu^+\nu_\mu$	$1.93 \pm 0.05 \pm 0.03$	$0.28 \pm 0.08 \pm 0.07$	$-1.7^{+1.5}_{-1.4} \pm 0.3$	[13
Belle	$D^0 \to \overline{K}^-\ell^+\nu_\ell$ $(\ell = e, \mu)$	$1.82 \pm 0.04 \pm 0.02$	$0.52 \pm 0.08 \pm 0.06$		[13
Babar	$D^0 \to K^-e^+\nu_e$	$1.884 \pm 0.012 \pm 0.016$	$0.377 \pm 0.023 \pm 0.031$		[13
CLEO	$D^0 \to K^-e^+\nu_e$, $D^+ \to \overline{K}^0 e^+\nu_e$	$1.93 \pm 0.02 \pm 0.01$	$0.30 \pm 0.03 \pm 0.01$		[13

Table B.1: Recent measurements of the $D \to K$ form factors.

The forms of the single-pole and modified-pole functions for the CLEO [136] central values of $m_{\rm pole}$ and α are shown in Fig. B.1.1. They deviate from each other considerably beyond $t \sim 2\,\text{GeV}^2$, where data points are absent due to phase-space suppression. However, due to this same phase-space suppression, it turns out that the R_D ratios are insensitive to this difference in the shape of $f_+(t)$ in this region of t, so we adopt the single-pole form for our purpose.

FOCUS [130], which looked at the muon channel, has determined the ratio $f_-(0)/f_+(0)$, in addition to $m_{\rm pole}$ and α, by performing a two-dimensional fit to $d^2\Gamma/dt\,d\cos\theta_\ell$, where θ_ℓ is the angle between the neutrino and the kaon in the $\mu\nu$ rest-frame. If we adopt the meson-dominance form given in Eq. (B.1.6) for $f_0(t)$, with $c_V = f_+(0)$, this ratio determines $r_0 = c_S/c_V$ as

$$r_0 \;=\; \frac{c_S}{c_V} \;=\; \frac{m_S^2}{m^2_{\rm pole}} + \frac{m_S^2}{m_D^2 - m_K^2}\,\frac{f_-(0)}{f_+(0)}\,. \tag{B.1.8}$$

In the FOCUS analysis, it was assumed that the ratio $f_-(t)/f_+(t)$ was essentially independent of t, which would require $m_S \approx m_{\rm pole}$. However, as noted above, data points do not extend into the regions of t which are phase-space suppressed, thus m_S can be differ significantly from $m_{\rm pole}$ while still maintaining an almost constant ratio $f_-(t)/f_+(t)$ in the regions measured. Indeed, in

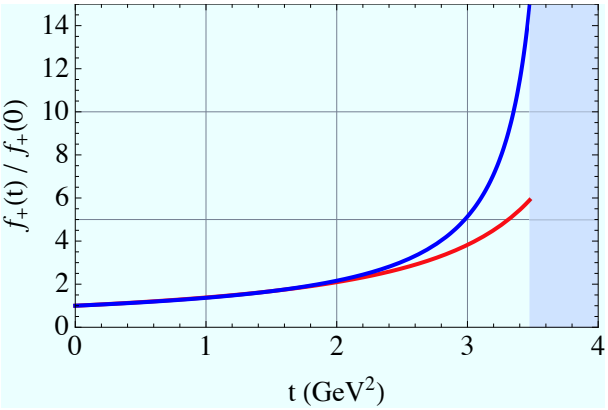

Figure B.1.1: The single-pole function with $m_{\rm pole} = 1.93$ GeV (solid), and the modified-pole function with $\alpha = 0.30$ (dashed). The end-point is at $t = m_D^2 \approx 3.5\,{\rm GeV}^2$.

Fig. B.1.2 we show how this ratio varies with t for the two choices $m_S = m_{\rm pole} = 1930\,{\rm MeV}$ and and $m_S = m(D^*_{s0}(2317)^\pm) = 2317\,{\rm MeV}$ when $f_-(0)/f_+(0) = -1.7$. In the region $t < 2\,{\rm GeV}^2$, the ratio only varies from -1.7 to about -1.5 even for the latter case. Thus, in our calculations, we allow m_S to vary between $m_{\rm pole}$ and $m(D^*_{s0}(2317)^\pm)$.

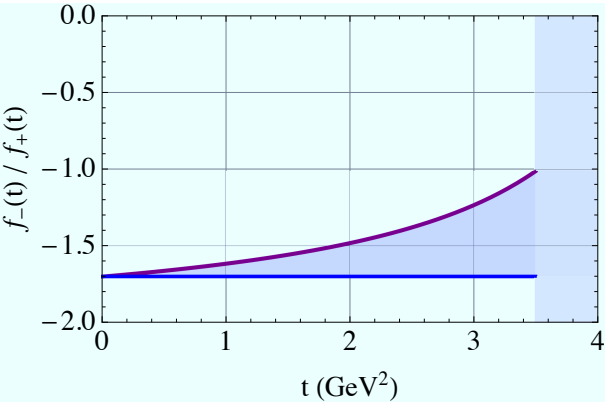

Figure B.1.2: The ratio $f_-(t)/f_+(t)$ with $m_S = m_{\rm pole} = 1930\,{\rm MeV}$ (solid), and $m_S = m(D^*_{s0}(2317)^\pm) = 2317\,{\rm MeV}$ (dashed). The FOCUS central value is used for the value of ratio at $t = 0$.

The form-factors we use are therefore,

$$\begin{aligned} \frac{f_+(t)}{f_+(0)} &= \frac{1}{1 - t/m^2_{\rm pole}}\,, \\ \frac{f_0(t)}{f_+(0)} &= 1 + r_0\,\frac{t/m_S^2}{1 - t/m_S^2}\,. \end{aligned} \tag{B.1.9}$$

For $m_{\rm pole}$ we adopt the FOCUS value of 1.93 GeV, which coincides with the CLEO value. The errors on $m_{\rm pole}$ are small enough as to have no effect on R_D since they only change the form of $f_+(t)$ near the pole. The value of r_0 will depend on the value of the ratio $f_-(0)/f_+(0)$ and our choice of m_S as shown in Fig. B.1.3.

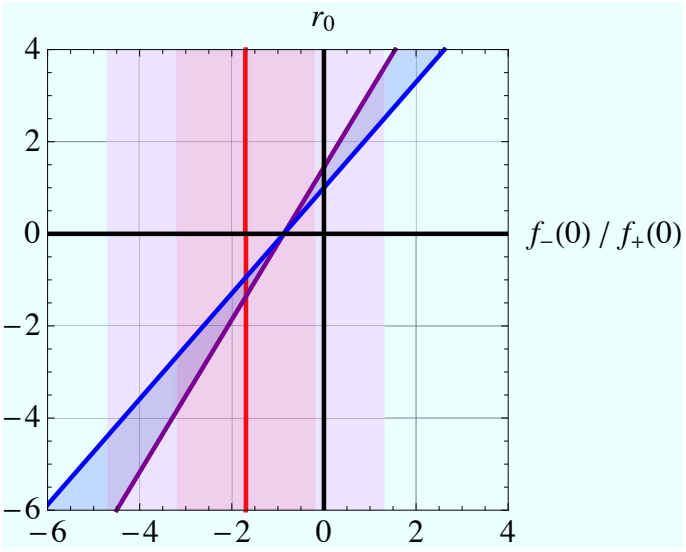

Figure B.1.3: The dependence of r_0 on the ratio $f_-(0)/f_+(0)$ with $m_S = m_{\rm pole} = 1930\,\text{MeV}$ (solid), and $m_S = m(D^*_{s0}(2317)^\pm) = 2317\,\text{MeV}$ (dashed). The shaded bands indicate the one- and two-sigma regions of $f_-(0)/f_+(0)$ as measured by FOCUS [130].

Substituting into Eq. (B.1.2), we obtain the values shown in Fig. B.1.4 for $R_D^{-1} = \Gamma(D \to Ke\nu)/\Gamma(D \to K\mu\nu)$. Reading off from the graph, we assign the following 1σ and 2σ ranges to R_{D^0} and R_{D^+}:

$$(R_{D^0})^{-1} \;=\; (R_{D^+})^{-1} \;=\; 1.04 \pm 0.02\;(1\sigma)\;, \quad 1.04^{+0.02}_{-0.06}\;(2\sigma)\;. \tag{B.1.10}$$

B.2 $D \to K^*\ell\nu$

Next, we consider the decay $D \to K^*\ell\nu_\ell$. The form-factors are defined as [129]

$$\begin{aligned}
&\langle K^*(P_K,\epsilon)|\,\overline{s}\gamma_\alpha(1-\gamma_5)c\,|D(P_D)\rangle \\
&\quad= \;\varepsilon_{\alpha\beta\gamma\delta}P_D^\beta P_K^\gamma \epsilon^{*\delta}\,\frac{2}{m_D+m_{K^*}}\,V(q^2) \\
&\qquad +i\left\{\epsilon^*_\alpha\,(m_D+m_{K^*})\;A_1(q^2) - \frac{(\epsilon^*\cdot q)}{m_D+m_{K^*}}(P_D+P_K)_\alpha\,A_2(q^2) - \frac{(\epsilon^*\cdot q)}{q^2}\,q_\alpha(2m_{K^*})\,A_3(q^2)\right\} \\
&\qquad +i\,\frac{(\epsilon^*\cdot q)}{q^2}\,q_\alpha(2m_{K^*})\,A_0(q^2)\;,
\end{aligned} \tag{B.2.1}$$

where

$$2m_{K^*}A_3(q^2) \;=\; (m_D+m_{K^*})\,A_1(q^2) - (m_D-m_{K^*})\,A_2(q^2)\;, \qquad A_3(0) \;=\; A_0(0)\;, \tag{B.2.2}$$

and $q^\alpha = (P_D - P_K)^\alpha$. Here, $V(q^2)$ is the contribution of vector intermediate states, while $A_1(q^2)$ and $A_2(q^2)$ are contributions of axial-vector intermediate states. $A_3(q^2)$ combines with $A_1(q^2)$ and $A_2(q^2)$ to maintain the transversality of these axial-vector contributions. $A_0(q^2)$ is

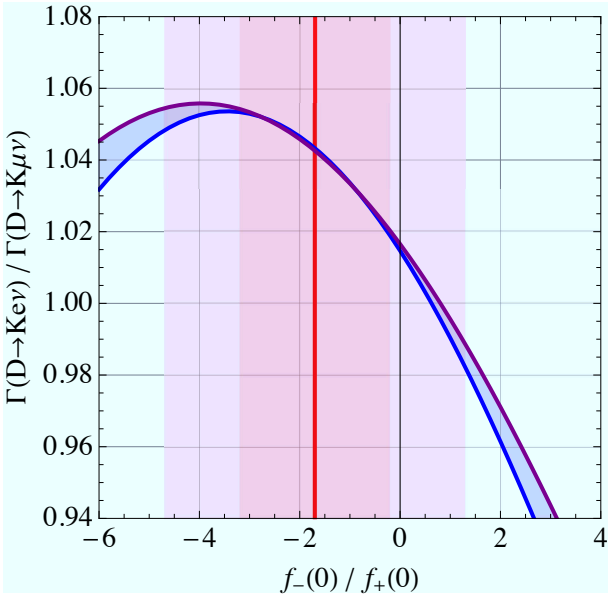

Figure B.1.4: The dependence of $(R_D)^{-1} = \Gamma(D \to Ke\nu)/\Gamma(D \to K\mu\nu)$ on the ratio $f_-(0)/f_+(0)$ with $m_S = m_{\rm pole} = 1930\,\text{MeV}$ (solid), and $m_S = m(D^*_{s0}(2317)^\pm) = 2317\,\text{MeV}$ (dashed). The shaded bands indicate the one- and two-sigma regions of $f_-(0)/f_+(0)$ as measured by FOCUS [130].

the contribution of scalar intermediate states. The condition $A_3(0) = A_0(0)$ is necessary for the cancellation of the poles at $q^2 = 0$. If we rewrite A_3 in terms of A_1 and A_2, the above expression becomes

$$\begin{aligned}
&\langle K^*(P_K,\epsilon)|\,\overline{s}\gamma_\alpha(1-\gamma_5)c\,|D(P_D)\rangle \\
&\quad = \varepsilon_{\alpha\beta\gamma\delta}P_D^\beta P_K^\gamma \epsilon^{*\delta}\,\frac{2}{m_D+m_{K^*}}\,V(q^2) \\
&\qquad +i\left\{(m_D+m_{K^*})\left[\epsilon^*_\alpha - \frac{(\epsilon^*\cdot q)\,q_\alpha}{q^2}\right]A_1(q^2) - \frac{(\epsilon^*\cdot q)}{m_D+m_{K^*}}\left[(P_D+P_K)_\alpha - \frac{(m_D^2-m_{K^*}^2)\,q_\alpha}{q^2}\right]A_2(q^2)\right\} \\
&\qquad +i\,\frac{(\epsilon^*\cdot q)}{q^2}\,q_\alpha(2m_{K^*})\,A_0(q^2)\,,
\end{aligned} \tag{B.2.3}$$

making the transversality of the axial-vector terms manifest. The decay width in terms of these form-factors is

$$\begin{aligned}
\Gamma \;=\; & \frac{G_F^2|V_{cs}|^2 m_D^3}{2^7\pi^3}\int_{m_\ell^2}^{(m_D-m_{K^*})^2} dt \\
&\times\left[\frac{4m_D^2}{3(m_D+m_{K^*})^2}\,\frac{t}{m_D^2}\,\frac{\lambda^{3/2}(m_D^2,m_{K^*}^2,t)}{m_D^6}\left(1+\frac{m_\ell^2}{2t}\right)\left(1-\frac{m_\ell^2}{t}\right)^2 V(t)^2\right. \\
&\quad +\frac{2(m_D+m_{K^*})^2}{3m_D^2}\,\frac{t}{m_D^2}\,\frac{\lambda^{1/2}(m_D^2,m_{K^*}^2,t)}{m_D^2}\left[3+\frac{\lambda(m_D^2,m_{K^*}^2,t)}{4m_{K^*}^2 t}\right]\left(1+\frac{m_\ell^2}{2t}\right)\left(1-\frac{m_\ell^2}{t}\right)^2 A_1(t)^2 \\
&\quad \left.-\frac{(m_D^2-m_{K^*}^2-t)}{3m_{K^*}^2}\,\frac{\lambda^{3/2}(m_D^2,m_{K^*}^2,t)}{m_D^6}\left(1+\frac{m_\ell^2}{2t}\right)\left(1-\frac{m_\ell^2}{t}\right)^2 A_1(t)A_2(t)\right.\,.
\end{aligned}$$

$$+\frac{m_D^4}{6(m_D+m_{K^*})^2 m_{K^*}^2}\,\frac{\lambda^{5/2}(m_D^2,m_{K^*}^2,t)}{m_D^{10}}\left(1+\frac{m_\ell^2}{2t}\right)\left(1-\frac{m_\ell^2}{t}\right)^2 A_2(t)^2$$
$$+\frac{\lambda^{3/2}(m_D^2,m_{K^*}^2,t)}{m_D^6}\,\frac{m_\ell^2}{t}\left(1-\frac{m_\ell^2}{t}\right)^2 A_0(t)^2\Bigg]\,, \qquad \text{(B.2.4)}$$

where $t=q^2$. The $A_0(t)$ contribution, being proportional to m_ℓ^2, cannot be measured at current experimental sensitivities. For the other form-factors, the following expressions motivated by vector-meson-dominance [144] is assumed:

$$V(t) \;=\; V(0)\,\frac{1}{1-t/m_V^2}\,, \qquad A_i(t) \;=\; A_i(0)\,\frac{1}{1-t/m_A^2}\,, \quad (i=1,2,3)\,. \qquad \text{(B.2.5)}$$

The pole masses are taken to be $m_V = m(D_s^{*\pm}) = 2.1\,\text{GeV}$ and $m_A = m(D_{s1}(2460)^\pm) = 2.5\,\text{GeV}$, which are the masses of the lowest lying D_s-mesons with $J^P = 1^-$ and 1^+, respectively. Experimental data is then fit with the ratios $r_v \equiv V(0)/A_1(0)$, and $r_2 \equiv A_2(0)/A_1(0)$. These ratios have been measured by various experiments via the decay sequence $D^+ \to \overline{K^*}(892)^0\ell^+\nu_\ell$, $\overline{K^*}(892)^0 \to K^-\pi^+$, most recently by FOCUS [131], which also measured the decay sequence $D^0 \to K^*(892)^-\mu^+\nu_\mu$, $K^*(892)^- \to \overline{K^0}\pi^-$ [132]. The current world averages are [116]

$$\begin{aligned} r_v \;&=\; \frac{V(0)}{A_1(0)} \;=\; 1.62\pm 0.08\,, \\ r_2 \;&=\; \frac{A_2(0)}{A_1(0)} \;=\; 0.83\pm 0.05\,. \end{aligned} \qquad \text{(B.2.6)}$$

For our purpose, we also need to specify $A_0(t)$ which we assume is of the form

$$A_0(t) \;=\; A_3(0) + c_S\,\frac{t/m_S^2}{1-t/m_S^2}\,, \qquad \text{(B.2.7)}$$

with $m_S = m_{D_s^\pm} = 2.0\,\text{GeV}$, the mass of the lowest lying D_s-meson with $J^P = 0^-$. Normalizing to $A_1(0)$, we have

$$\frac{A_0(t)}{A_1(0)} \;=\; r_3 + r_0\,\frac{t/m_S^2}{1-t/m_S^2}\,, \qquad \text{(B.2.8)}$$

with

$$r_3 \;=\; \frac{(m_D+m_{K^*})}{2m_{K^*}} - \frac{(m_D-m_{K^*})}{2m_{K^*}}\,r_2 \;=\; 1.09\pm 0.03\,. \qquad \text{(B.2.9)}$$

For r_0, we arbitrarily assume that its 1σ range is $r_0 = 0 \pm r_3$. Substituting Eqs. (B.2.5) and (B.2.8) into Eq. (B.2.4), we obtain the values shown in Fig. B.2.1 for the ratio $(R^*_{D^+})^{-1} = \Gamma(D \to K^* e\nu)/\Gamma(D \to K^*\mu\nu)$. Reading off from the graph, we assign the following 1σ and 2σ ranges:

$$(R^*_{D^+})^{-1} \;=\; 1.060^{+0.002}_{-0.003}\;(1\sigma)\,, \qquad 1.060^{+0.005}_{-0.007}\;(2\sigma)\,. \qquad \text{(B.2.10)}$$

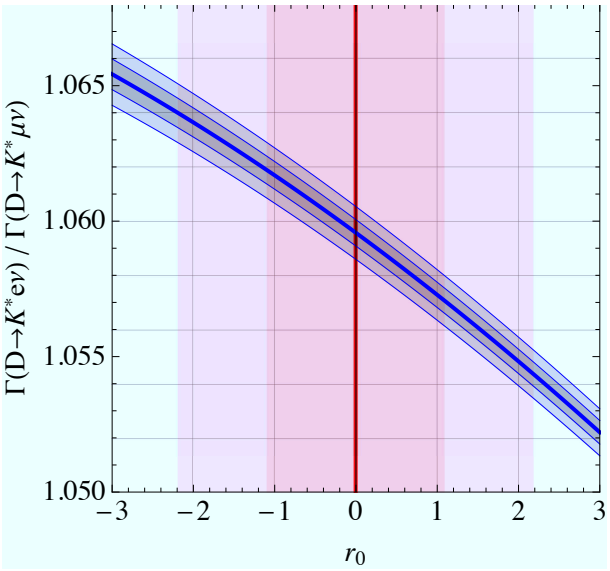

Figure B.2.1: The dependence of $(R^*_{D^+})^{-1} = \Gamma(D \to K^* e\nu)/\Gamma(D \to K^* \mu\nu)$ on the choice of r_0. The wide vertical bands are our assumed one- and two-sigma regions of r_0. The narrow curved bands indicate the one and two-sigma uncertainties due to the error in r_2. The uncertainty due to errors in r_v, m_D, and m_{K^*} are negligible.

Bibliography

[1] M. B. Smy *et al.* [Super-Kamiokande Collaboration], Phys. Rev. D **69**, 011104 (2004) [arXiv:hep-ex/0309011]. S. N. Ahmed *et al.* [SNO Collaboration], Phys. Rev. Lett. **92**, 181301 (2004) [arXiv:nucl-ex/0309004].

[2] T. Araki *et al.* [KamLAND Collaboration], Phys. Rev. Lett. **94**, 081801 (2005) [arXiv:hep-ex/0406035].

[3] Y. Ashie *et al.* [Super-Kamiokande Collaboration], Phys. Rev. Lett. **93**, 101801 (2004) [arXiv:hep-ex/0404034]; Y. Ashie *et al.* [Super-Kamiokande Collaboration], Phys. Rev. D **71**, 112005 (2005) [arXiv:hep-ex/0501064].

[4] M. Apollonio *et al.* [CHOOZ Collaboration], Phys. Lett. B **466**, 415 (1999) [arXiv:hep-ex/9907037]; M. Apollonio *et al.* [CHOOZ Collaboration], Eur. Phys. J. C **27**, 331 (2003) [arXiv:hep-ex/0301017].

[5] M. Fukugita and T. Yanagida, Phys. Lett. B **174**, 45 (1986).

[6] M. H. Ahn *et al.* [K2K Collaboration], Phys. Rev. Lett. **93**, 051801 (2004) [arXiv:hep-ex/0402017], E. Aliu *et al.* [K2K Collaboration], Phys. Rev. Lett. **94**, 081802 (2005) [arXiv:hep-ex/0411038], C. Mariani [K2K Collaboration], arXiv:hep-ex/0505019.

[7] G. Rosa [OPERA Collaboration], Nucl. Phys. Proc. Suppl. **145**, 98 (2005), H. Pessard [OPERA Collaboration], arXiv:hep-ex/0504033.

[8] G. S. Tzanakos [MINOS Collaboration], AIP Conf. Proc. **721**, 179 (2004).

[9] D. Ayres *et al.* [NOvA Collaboration], arXiv:hep-ex/0210005, D. S. Ayres *et al.* [NOvA Collaboration], arXiv:hep-ex/0503053,

[10] Y. Itow *et al.*, arXiv:hep-ex/0106019; Y. Hayato [T2K Collaboration], Nucl. Phys. Proc. Suppl. **143**, 269 (2005), K. Kaneyuki [T2K Collaboration], Nucl. Phys. Proc. Suppl. **145**, 178 (2005), Y. Hayato [T2K Collaboration], Nucl. Phys. Proc. Suppl. **147**, 9 (2005). See also the JHF Neutrino Working Group's home page, http://neutrino.kek.jp/jhfnu/.

[11] M. V. Diwan *et al.*, Phys. Rev. D **68**, 012002 (2003) [arXiv:hep-ph/0303081].

[12] N. Okamura, M. Aoki, K. Hagiwara, Y. Hayato, T. Kobayashi, T. Nakaya and K. Nishikawa, arXiv:hep-ph/0104220; M. Aoki, K. Hagiwara, Y. Hayato, T. Kobayashi, T. Nakaya, K. Nishikawa and N. Okamura, Phys. Rev. D **67**, 093004 (2003) [arXiv:hep-ph/0112338].

[13] H. S. Chen *et al.* [VLBL Study Group H2B-1], arXiv:hep-ph/0104266, Y. F. Wang, K. Whisnant, Z. H. Xiong, J. M. Yang and B. L. Young [VLBL Study Group H2B-4], Phys. Rev. D **65**, 073021 (2002) [arXiv:hep-ph/0111317].

[14] H. Minakata and H. Nunokawa, Phys. Lett. B **413**, 369 (1997) [arXiv:hep-ph/9706281]; V. Barger, D. Marfatia and K. Whisnant, Phys. Lett. B **560**, 75 (2003) [arXiv:hep-ph/0210428].

[15] M. Ishitsuka, T. Kajita, H. Minakata and H. Nunokawa, Phys. Rev. D **72**, 033003 (2005) [arXiv:hep-ph/0504026].

[16] K. Hagiwara, N. Okamura and K. i. Senda, arXiv:hep-ph/0504061.

[17] O. Mena Requejo, S. Palomares-Ruiz and S. Pascoli, Phys. Rev. D **72**, 053002 (2005) [arXiv:hep-ph/0504015]; O. Mena and S. Parke, Phys. Rev. D **72**, 053003 (2005) [arXiv:hep-ph/0505202]; O. Mena, S. Palomares-Ruiz and S. Pascoli, arXiv:hep-ph/0510182.

[18] L. Wolfenstein, Phys. Rev. D **17**, 2369 (1978); R. R. Lewis, Phys. Rev. D **21**, 663 (1980); V. D. Barger, K. Whisnant, S. Pakvasa and R. J. N. Phillips, Phys. Rev. D **22**, 2718 (1980); S. P. Mikheyev and A. Yu. Smirnov, Yad. Fiz. **42**, 1441 (1985), [Sov. J. Nucl. Phys. **42**, 913 (1986)]; S. P. Mikheyev and A. Yu. Smirnov, Nuovo Cimento **C9**, 17 (1986).

[19] P. Lipari, Phys. Rev. D **61**, 113004 (2000) [arXiv:hep-ph/9903481]; V. D. Barger, S. Geer, R. Raja and K. Whisnant, Phys. Lett. B **485**, 379 (2000) [arXiv:hep-ph/0004208].

[20] K. Kimura, A. Takamura and H. Yokomakura, J. Phys. G **29**, 1839 (2003); K. Kimura, A. Takamura and H. Yokomakura, Phys. Rev. D **66**, 073005 (2002) [arXiv:hep-ph/0205295]; K. Kimura, A. Takamura and H. Yokomakura, Phys. Lett. B **537**, 86 (2002) [arXiv:hep-ph/0203099].

[21] J. Arafune, M. Koike and J. Sato, Phys. Rev. D **56**, 3093 (1997) [Erratum-ibid. D **60**, 119905 (1999)] [arXiv:hep-ph/9703351].

[22] M. Freund, Phys. Rev. D **64**, 053003 (2001) [arXiv:hep-ph/0103300].

[23] Z. Maki, M. Nakagawa and S. Sakata, Prog. Theor. Phys. **28**, 870 (1962).

[24] "Neutrino mass, mixing, and flavor change", B. Kayser, in the *Review of Particle Physics*, Phys. Lett. B**592** (2004) 1.

[25] K. Hagiwara and N. Okamura, Nucl. Phys. B **548**, 60 (1999) [arXiv:hep-ph/9811495].

[26] A. M. Dziewonski and D. L. Anderson, Physics of the Earth and Planetary Interiors, **25** (1981) 297–356.

[27] F. Ardellier *et al.* [Double-Chooz Collaboration], arXiv:hep-ex/0405032; F. Dalnoki-Veress [Double-Chooz Collaboration], arXiv:hep-ex/0406070.

[28] F. Suekane [KASKA Collaboration], arXiv:hep-ex/0407016.

[29] V. Barger, D. Marfatia and K. Whisnant, Phys. Rev. D **65**, 073023 (2002) [arXiv:hep-ph/0112119].

[30] M. Aoki, K. Hagiwara and N. Okamura, Phys. Lett. B **554**, 121 (2003) [arXiv:hep-ph/0208223].

[31] K. Hagiwara, Nucl. Phys. Proc. Suppl. **137**, 84 (2004) [arXiv:hep-ph/0410229].

[32] H. Minakata and H. Nunokawa, JHEP **0110**, 001 (2001) [arXiv:hep-ph/0108085].

[33] M. Honda, N. Okamura, and T. Takeuchi, in preparation.

[34] M. Honda, N. Okamura and T. Takeuchi, arXiv:hep-ph/0603268;
M. Honda, Y. Kao, N. Okamura and T. Takeuchi, arXiv:hep-ph/0602115;
M. Honda, Y. Kao, N. Okamura, A. Pronin and T. Takeuchi, arXiv:hep-ph/0610281;
M. Honda, Y. Kao, N. Okamura, A. Pronin and T. Takeuchi, arXiv:0704.0369 [hep-ph].

[35] NUMI Technical Design Handbook,
available at http://www-numi.fnal.gov/numwork/tdh/tdh_index.html

[36] Y. Itow *et al.*, arXiv:hep-ex/0106019;
updated version available at http://neutrino.kek.jp/jhfnu/.

[37] A. Zee, Phys. Lett. B **161**, 141 (1985);
M. Fukugita and T. Yanagida, Phys. Lett. B **206**, 93 (1988).

[38] X. G. He, G. C. Joshi, H. Lew and R. R. Volkas, Phys. Rev. D **43**, R22 (1991);
X. G. He, G. C. Joshi, H. Lew and R. R. Volkas, Phys. Rev. D **44**, 2118 (1991).

[39] E. Ma, Phys. Lett. B **433**, 74 (1998) [arXiv:hep-ph/9709474];
E. Ma and U. Sarkar, Phys. Lett. B **439**, 95 (1998) [arXiv:hep-ph/9807307];
P. B. Pal and U. Sarkar, Phys. Lett. B **573**, 147 (2003) [arXiv:hep-ph/0306088].

[40] E. Ma, D. P. Roy and U. Sarkar, Phys. Lett. B **444**, 391 (1998) [arXiv:hep-ph/9810309].

[41] E. Ma and D. P. Roy, Phys. Rev. D **59**, 097702 (1999); [arXiv:hep-ph/9811266].

[42] L. N. Chang, O. Lebedev, W. Loinaz, and T. Takeuchi, Phys. Rev. D **63**, 074013 (2001) [arXiv:hep-ph/0010118].

[43] E. Ma and D. P. Roy, Phys. Rev. D **58**, 095005 (1998) [arXiv:hep-ph/9806210].

[44] C. T. Hill, Phys. Lett. B **345**, 483 (1995) [arXiv:hep-ph/9411426];
R. S. Chivukula, B. A. Dobrescu and J. Terning, Phys. Lett. B **353**, 289 (1995) [arXiv:hep-ph/9503203];
K. D. Lane and E. Eichten, Phys. Lett. B **352**, 382 (1995) [arXiv:hep-ph/9503433];
G. Buchalla, G. Burdman, C. T. Hill, and D. Kominis, Phys. Rev. D **53**, 5185 (1996) [arXiv:hep-ph/9510376];
K. D. Lane, Phys. Rev. D **54**, 2204 (1996) [arXiv:hep-ph/9602221];
K. D. Lane, Phys. Lett. B **433**, 96 (1998) [arXiv:hep-ph/9805254];
W. Loinaz and T. Takeuchi, Phys. Rev. D **60**, 115008 (1999) [arXiv:hep-ph/9903362].

[45] D. Kominis, Phys. Lett. B **358**, 312 (1995) [arXiv:hep-ph/9506305];
R. S. Chivukula and J. Terning, Phys. Lett. B **385**, 209 (1996) [arXiv:hep-ph/9606233];
Y. Su, G. F. Bonini and K. D. Lane, Phys. Rev. Lett. **79**, 4075 (1997) [arXiv:hep-ph/9706267];
W. Loinaz and T. Takeuchi, Phys. Rev. D **60**, 015005 (1999) [arXiv:hep-ph/9812377];
G. Burdman, K. D. Lane and T. Rador, Phys. Lett. B **514**, 41 (2001) [arXiv:hep-ph/0012073].

[46] L. J. Hall and M. Suzuki, Nucl. Phys. B **231**, 419 (1984);
H. E. Haber and G. L. Kane, Phys. Rept. **117**, 75 (1985);
M. Nowakowski and A. Pilaftsis, Nucl. Phys. B **461**, 19 (1996) [arXiv:hep-ph/9508271];
S. P. Martin, arXiv:hep-ph/9709356.

[47] R. Barbier *et al.*, Phys. Rept. **420**, 1 (2005) [arXiv:hep-ph/0406039].

[48] O. Lebedev, W. Loinaz and T. Takeuchi, Phys. Rev. D **61**, 115005 (2000) [arXiv:hep-ph/9910435];
O. Lebedev, W. Loinaz and T. Takeuchi, Phys. Rev. D **62**, 015003 (2000) [arXiv:hep-ph/9911479].

[49] Z. Maki, M. Nakagawa and S. Sakata, Prog. Theor. Phys. **28**, 870 (1962).

[50] Y. Ashie *et al.* [Super-Kamiokande Collaboration], Phys. Rev. D **71**, 112005 (2005) [arXiv:hep-ex/0501064].

[51] J. Dorenbosch *et al.* [CHARM Collaboration], Phys. Lett. B **180**, 303 (1986);
P. Vilain *et al.* [CHARM-II Collaboration], Phys. Lett. B **320**, 203 (1994).

[52] S. Baek, N. G. Deshpande, X. G. He and P. Ko, Phys. Rev. D **64**, 055006 (2001) [arXiv:hep-ph/0104141];
E. Ma, D. P. Roy and S. Roy, Phys. Lett. B **525**, 101 (2002) [arXiv:hep-ph/0110146];
S. Choubey and W. Rodejohann, Eur. Phys. J. C **40**, 259 (2005) [arXiv:hep-ph/0411190];
W. Rodejohann and M. A. Schmidt, Phys. Atom. Nucl. **69**, 1833 (2006) [arXiv:hep-ph/0507300];
B. Adhikary, Phys. Rev. D **74**, 033002 (2006) [arXiv:hep-ph/0604009];
T. Ota and W. Rodejohann, Phys. Lett. B **639**, 322 (2006) [arXiv:hep-ph/0605231];
E. J. Chun and K. Turzynski, arXiv:hep-ph/0703070.

[53] R. Foot, Mod. Phys. Lett. A **20**, 3035 (2005) [arXiv:hep-ph/0505154].

[54] M. Acciarri *et al.* [L3 Collaboration], Phys. Lett. B **489**, 81 (2000) [arXiv:hep-ex/0005028].

[55] G. Abbiendi *et al.* [OPAL Collaboration], Eur. Phys. J. C **33**, 173 (2004) [arXiv:hep-ex/0309053].

[56] J. Abdallah *et al.* [DELPHI Collaboration], Eur. Phys. J. C **45**, 589 (2006) [arXiv:hep-ex/0512012].

[57] S. Schael *et al.* [ALEPH Collaboration], Eur. Phys. J. C **49**, 411 (2007) [arXiv:hep-ex/0609051].

[58] F. Abe *et al.* [CDF Collaboration], Phys. Rev. Lett. **79**, 2198 (1997).

[59] N. P. Xuan, fermilab-thesis-2005-40, UMI-31-66510.

[60] D. Acosta *et al.* [CDF Collaboration], Phys. Rev. Lett. **95**, 131801 (2005) [arXiv:hep-ex/0506034].

[61] W.-M. Yao et al., Journal of Physics G **33**, 1 (2006), *the Review of Particle Properties* and its 2007 update available at http://pdg.lbl.gov.

[62] ATLAS detector and physics performance. Technical design report. Vol. 2, CERN-LHCC-99-15, ATLAS-TDR-15;
CMS physics : Technical Design Report v.2 : Physics performance, CERN-LHCC-2006-021, CMS-TDR-008-2.

[63] W. Buchmüller, R. Rückl and D. Wyler, Phys. Lett. B **191**, 442 (1987);
J. Blumlein and R. Ruckl, Phys. Lett. B **304**, 337 (1993);
M. Tanabashi, in the Review of Particle Properties [61].

[64] S. Davidson, D. C. Bailey and B. A. Campbell, Z. Phys. C **61**, 613 (1994) [arXiv:hep-ph/9309310];
E. Gabrielli, Phys. Rev. D **62**, 055009 (2000) [arXiv:hep-ph/9911539];
S. Davidson, S. Forte, P. Gambino, N. Rius and A. Strumia, JHEP **0202**, 037 (2002) [arXiv:hep-ph/0112302].

[65] M. Dittmar, A. S. Nicollerat and A. Djouadi, Phys. Lett. B **583**, 111 (2004) [arXiv:hep-ph/0307020].

[66] D. Acosta *et al.* [CDF Collaboration], Phys. Rev. D **71**, 112001 (2005) [Erratum-ibid. D **71**, 119901 (2005)] [arXiv:hep-ex/0410076].

[67] V. M. Abazov *et al.* [D0 Collaboration], Phys. Lett. B **640**, 230 (2006) [arXiv:hep-ex/0607009].

[68] A. Abulencia *et al.* [CDF Collaboration], Phys. Rev. D **73**, 051102 (2006) [arXiv:hep-ex/0512055].

[69] V. M. Abazov *et al.* [D0 Collaboration], Phys. Lett. B **636**, 183 (2006) [arXiv:hep-ex/0601047].

[70] V. M. Abazov *et al.* [D0 Collaboration], Phys. Lett. B **647**, 74 (2007) [arXiv:hep-ex/0612012].

[71] CDF note 8309, "Search for Third Generation Vector Leptoquarks in Run II",
http://www-cdf.fnal.gov/physics/exotic/r2a/20070308.3genvlq/vlq3_public_page_files/lq3_cdfpubnote

[72] J. Blumlein, E. Boos and A. Kryukov, Z. Phys. C **76**, 137 (1997) [arXiv:hep-ph/9610408].

[73] V. A. Mitsou, N. C. Benekos, I. Panagoulias and T. D. Papadopoulou, Czech. J. Phys. **55**, B659 (2005) [arXiv:hep-ph/0411189];
A. Belyaev, C. Leroy, R. Mehdiyev and A. Pukhov, JHEP **0509**, 005 (2005) [arXiv:hep-ph/0502067].

[74] C. S. Aulakh and R. N. Mohapatra, Phys. Lett. B **119**, 136 (1982);
L. J. Hall and M. Suzuki, Nucl. Phys. B **231**, 419 (1984);
I. H. Lee, Nucl. Phys. B **246**, 120 (1984);
J. R. Ellis, G. Gelmini, C. Jarlskog, G. G. Ross and J. W. F. Valle, Phys. Lett. B **150**, 142 (1985);
G. G. Ross and J. W. F. Valle, Phys. Lett. B **151**, 375 (1985);
S. Dawson, Nucl. Phys. B **261**, 297 (1985);
V. D. Barger, G. F. Giudice and T. Han, Phys. Rev. D **40**, 2987 (1989).

[75] R. Hempfling, Nucl. Phys. B **478**, 3 (1996) [arXiv:hep-ph/9511288];
A. G. Akeroyd, M. A. Diaz, J. Ferrandis, M. A. Garcia-Jareno and J. W. F. Valle, Nucl. Phys. B **529**, 3 (1998) [arXiv:hep-ph/9707395];
E. J. Chun, S. K. Kang, C. W. Kim and U. W. Lee, Nucl. Phys. B **544**, 89 (1999) [arXiv:hep-ph/9807327];
E. J. Chun and J. S. Lee, Phys. Rev. D **60**, 075006 (1999) [arXiv:hep-ph/9811201];
D. E. Kaplan and A. E. Nelson, JHEP **0001**, 033 (2000) [arXiv:hep-ph/9901254];
J. C. Romao, M. A. Diaz, M. Hirsch, W. Porod and J. W. F. Valle, Phys. Rev. D **61**, 071703(R) (2000) [arXiv:hep-ph/9907499];
F. Takayama and M. Yamaguchi, Phys. Lett. B **476**, 116 (2000) [arXiv:hep-ph/9910320];
M. Hirsch, M. A. Diaz, W. Porod, J. C. Romao and J. W. F. Valle, Phys. Rev. D **62**, 113008 (2000) [Erratum-ibid. D **65**, 119901 (2002)] [arXiv:hep-ph/0004115];
M. A. Diaz, M. Hirsch, W. Porod, J. C. Romao and J. W. F. Valle, Phys. Rev. D **68**, 013009 (2003) [Erratum-ibid. D **71**, 059904 (2005)] [arXiv:hep-ph/0302021];
E. J. Chun, D. W. Jung, S. K. Kang and J. D. Park, Phys. Rev. D **66**, 073003 (2002) [arXiv:hep-ph/0206030];
E. J. Chun, D. W. Jung and J. D. Park, Phys. Lett. B **557**, 233 (2003) [arXiv:hep-ph/0211310];
D. W. Jung, S. K. Kang, J. D. Park and E. J. Chun, JHEP **0408**, 017 (2004) [arXiv:hep-ph/0407106].

[76] S. Chekanov *et al.* [ZEUS Collaboration], Phys. Rev. D **68**, 052004 (2003) [arXiv:hep-ex/0304008].

[77] S. Chekanov *et al.* [ZEUS Collaboration], Eur. Phys. J. C **44**, 463 (2005) [arXiv:hep-ex/0501070].

[78] C. Adloff *et al.* [H1 Collaboration], Phys. Lett. B **568**, 35 (2003) [arXiv:hep-ex/0305015].

[79] A. Aktas *et al.* [H1 Collaboration], Eur. Phys. J. C **36**, 425 (2004) [arXiv:hep-ex/0403027].

[80] V. M. Abazov *et al.* [D0 Collaboration], Phys. Rev. Lett. **97**, 111801 (2006) [arXiv:hep-ex/0605010].

[81] S. P. Martin, arXiv:hep-ph/9709356.

[82] A. Zee, Phys. Lett. B **93**, 389 (1980) [Erratum-ibid. B **95**, 461 (1980)].

[83] K. S. Babu, Phys. Lett. B **203**, 132 (1988);
A. Zee, Nucl. Phys. B **264**, 99 (1986).

[84] J. F. Gunion and C. Hays, in E. Accomando *et al.*, "Workshop on CP studies and non-standard Higgs physics," arXiv:hep-ph/0608079, chapter 13, pages 497-526;
A. G. Akeroyd and M. Aoki, Phys. Rev. D **72**, 035011 (2005) [arXiv:hep-ph/0506176].

[85] K. S. Babu and C. Macesanu, Phys. Rev. D **67**, 073010 (2003) [arXiv:hep-ph/0212058].

[86] M. Barrett [on behalf of the Babar collaboration], arXiv:0903.4855 [hep-ex].

[87] K. Hara [Belle Collaboration], arXiv:0810.3301 [hep-ex].

[88] B. Aubert *et al.* [Babar Collaboration], Phys. Rev. D **79**, 012004 (2009) [arXiv:0812.3804 [hep-ex]].

[89] H. K. Dreiner, G. Polesello and M. Thormeier, Phys. Rev. D **65**, 115006 (2002) [arXiv:hep-ph/0112228].

[90] H. K. Dreiner, M. Kramer and B. O'Leary, Phys. Rev. D **75**, 114016 (2007) [arXiv:hep-ph/0612278].

[91] K. Ikado *et al.*, Phys. Rev. Lett. **97**, 251802 (2006) [arXiv:hep-ex/0604018].

[92] Unitarity Triangle fit Group (UTfit) http://www.utfit.org

[93] R. Kowalewski and T. Mannel, in Ref. [116].

[94] A. Petrella [Babar Collaboration and Belle Collaboration], arXiv:0903.5180 [hep-ex].

[95] Heavy Flavor Averaging Group (HFAG) http://www.slac.stanford.edu/xorg/hfag/

[96] A. Gray *et al.* [HPQCD Collaboration], Phys. Rev. Lett. **95**, 212001 (2005) [arXiv:hep-lat/0507015].

[97] CKMfitter Group (J. Charles et al.), Eur. Phys. J. C41, 1-131 (2005), [hep-ph/0406184], updated results and plots available at: http://ckmfitter.in2p3.fr

[98] B. A. Dobrescu and A. S. Kronfeld, Phys. Rev. Lett. **100**, 241802 (2008) [arXiv:0803.0512 [hep-ph]].

[99] G. Bhattacharyya, Nucl. Phys. Proc. Suppl. **52A**, 83 (1997) [arXiv:hep-ph/9608415];
G. Bhattacharyya, arXiv:hep-ph/9709395;
S. P. Martin, arXiv:hep-ph/9709356;
H. K. Dreiner, arXiv:hep-ph/9707435.

[100] A. V. Manohar and C. T. Sachrajda, in Ref. [116].

[101] Y. Miyazaki *et al.* [BELLE Collaboration], Phys. Lett. B **639**, 159 (2006) [arXiv:hep-ex/0605025].

[102] J. L. Rosner and S. Stone, in Ref. [116].

[103] S. G. Porsev, K. Beloy and A. Derevianko, Phys. Rev. Lett. **102**, 181601 (2009) [arXiv:0902.0335 [hep-ph]].

[104] S. Banerjee, talk at the 34th International Conference on High Energy Physics, Philadelphia, 29 July-5 August, 2008.

[105] O. Lebedev, W. Loinaz and T. Takeuchi, Phys. Rev. D **61**, 115005 (2000) [arXiv:hep-ph/9910435];
O. Lebedev, W. Loinaz and T. Takeuchi, Phys. Rev. D **62**, 015003 (2000) [arXiv:hep-ph/9911479].

[106] Y. Kao and T. Takeuchi, in preparation.

[107] Y. Kao and T. Takeuchi, in preparation.

[108] T. Kinoshita and A. Sirlin, Phys. Rev. **113**, 1652 (1959); A. Sirlin, Rev. Mod. Phys. **50**, 573 (1978) [Erratum-ibid. **50**, 905 (1978)]; T. van Ritbergen and R. G. Stuart, Phys. Rev. Lett. **82**, 488 (1999) [hep-ph/9808283].

[109] W. J. Marciano and A. Sirlin, Phys. Rev. Lett. **61**, 1815 (1988).

[110] R. Decker and M. Finkemeier, Nucl. Phys. B **438**, 17 (1995) [hep-ph/9403385].

[111] G. Altarelli, G. F. Giudice and M. L. Mangano, Nucl. Phys. B **506**, 29 (1997) [arXiv:hep-ph/9705287].

[112] M. Hirsch, H. V. Klapdor-Kleingrothaus and S. G. Kovalenko, *Prepared for 4th International Symposium on Weak and Electromagnetic Interaction in Nuclei (WEIN 95), Osaka, Japan, 12-16 Jun 1995*

[113] M. Doi, T. Kotani and E. Takasugi, Prog. Theor. Phys. Suppl. **83**, 1 (1985).

[114] S. Bethke, arXiv:0908.1135 [hep-ph].

[115] H. V. Klapdor-Kleingrothaus and I. V. Krivosheina, Mod. Phys. Lett. A **21**, 1547 (2006).

[116] C. Amsler *et al.* [Particle Data Group], "Review of Particle Physics," Phys. Lett. B **667**, 1 (2008).

[117] K. S. Babu and R. N. Mohapatra, Phys. Rev. Lett. **75**, 2276 (1995) [arXiv:hep-ph/9506354];
M. Hirsch, H. V. Klapdor-Kleingrothaus and S. G. Kovalenko, Phys. Rev. D **53**, 1329 (1996) [arXiv:hep-ph/9502385];
A. Faessler, S. Kovalenko, F. Simkovic and J. Schwieger, Phys. Rev. Lett. **78**, 183 (1997) [arXiv:hep-ph/9612357];
A. Faessler, S. Kovalenko and F. Simkovic, Phys. Rev. D **58**, 115004 (1998) [arXiv:hep-ph/9803253].

[118] K. Huitu, J. Maalampi, M. Raidal and A. Santamaria, Phys. Lett. B **430**, 355 (1998) [arXiv:hep-ph/9712249].

[119] G. Bhattacharyya and A. Raychaudhuri, Phys. Rev. D **57**, R3837 (1998) [arXiv:hep-ph/9712245].

[120] S. Baek and Y. G. Kim, Phys. Rev. D **60**, 077701 (1999) [arXiv:hep-ph/9906385].

[121] J. P. Saha and A. Kundu, Phys. Rev. D **66**, 054021 (2002) [arXiv:hep-ph/0205046].

[122] S. Bar-Shalom, G. Eilam and Y. D. Yang, Phys. Rev. D **67**, 014007 (2003) [arXiv:hep-ph/0201244].

[123] B. C. Allanach, A. Dedes and H. K. Dreiner, Phys. Rev. D **60**, 075014 (1999) [arXiv:hep-ph/9906209];
B. C. Allanach, A. Dedes and H. K. Dreiner, Phys. Rev. D **69**, 115002 (2004) [Erratum-ibid. D **72**, 079902 (2005)] [arXiv:hep-ph/0309196].

[124] A. Kundu and S. Nandi, Phys. Rev. D **78**, 015009 (2008) [arXiv:0803.1898 [hep-ph]];
P. Dey, A. Kundu, B. Mukhopadhyaya and S. Nandi, JHEP **0812**, 100 (2008) [arXiv:0808.1523 [hep-ph]].

[125] Y. Kao and T. Takeuchi, arXiv:0909.0042 [hep-ph].

[126] D. Chang and W. Y. Keung, Phys. Lett. B **389**, 294 (1996) [arXiv:hep-ph/9608313];
K. Choi, K. Hwang and J. S. Lee, Phys. Lett. B **428**, 129 (1998) [arXiv:hep-ph/9802323];
G. Bhattacharyya and P. B. Pal, Phys. Lett. B **439**, 81 (1998) [arXiv:hep-ph/9806214].

[127] I. Hinchliffe and T. Kaeding, Phys. Rev. D **47**, 279 (1993);
C. E. Carlson, P. Roy and M. Sher, Phys. Lett. B **357**, 99 (1995) [arXiv:hep-ph/9506328];
A. Y. Smirnov and F. Vissani, Phys. Lett. B **380**, 317 (1996) [arXiv:hep-ph/9601387];
G. Bhattacharyya and P. B. Pal, Phys. Rev. D **59**, 097701 (1999) [arXiv:hep-ph/9809493].

[128] A. Ceccucci, Z. Ligeti and Y. Sakai, in Ref. [116].

[129] M. Wirbel, B. Stech and M. Bauer, Z. Phys. C **29**, 637 (1985);
M. Bauer and M. Wirbel, Z. Phys. C **42**, 671 (1989);
J. D. Richman and P. R. Burchat, Rev. Mod. Phys. **67**, 893 (1995) [arXiv:hep-ph/9508250].

[130] J. M. Link *et al.* [FOCUS Collaboration], Phys. Lett. B **607**, 233 (2005) [arXiv:hep-ex/0410037].

[131] J. M. Link *et al.* [FOCUS Collaboration], Phys. Lett. B **544**, 89 (2002) [arXiv:hep-ex/0207049].

[132] J. M. Link *et al.* [FOCUS Collaboration], Phys. Lett. B **607**, 67 (2005) [arXiv:hep-ex/0410067].

[133] L. Widhalm *et al.* [Belle Collaboration], Phys. Rev. Lett. **97**, 061804 (2006) [arXiv:hep-ex/0604049].

[134] B. Aubert *et al.* [BABAR Collaboration], Phys. Rev. D **76**, 052005 (2007) [arXiv:0704.0020 [hep-ex]].

[135] S. Dobbs *et al.* [CLEO Collaboration], Phys. Rev. D **77**, 112005 (2008) [arXiv:0712.1020 [hep-ex]].

[136] D. Besson *et al.* [CLEO Collaboration], Phys. Rev. D **80**, 032005 (2009) [arXiv:0906.2983 [hep-ex]].

[137] S. Schael *et al.* [ALEPH Collaboration], Phys. Rept. **421**, 191 (2005) [arXiv:hep-ex/0506072].

[138] M. Artuso *et al.* [CLEO Collaboration], Phys. Rev. Lett. **99**, 071802 (2007) [arXiv:0704.0629 [hep-ex]].

[139] T. K. Pedlar *et al.* [CLEO Collaboration], Phys. Rev. D **76**, 072002 (2007) [arXiv:0704.0437 [hep-ex]].

[140] K. M. Ecklund *et al.* [CLEO Collaboration], Phys. Rev. Lett. **100**, 161801 (2008) [arXiv:0712.1175 [hep-ex]].

[141] L. Widhalm *et al.* [Belle Collaboration], Phys. Rev. Lett. **100**, 241801 (2008) [arXiv:0709.1340 [hep-ex]].

[142] C. Malbrunot [PIENU Collaboration], talk at Flavor Physics and CP Violation 2009, Lake Placid, NY, May 27-June 1, 2009. See also `https://pienu.triumf.ca/`.

[143] D. Pocanic *et al.* [PEN Collaboration], arXiv:0909.4358 [hep-ex].

[144] J. J. Sakurai, Phys. Rev. Lett. **22**, 981 (1969).

[145] M. Finkemeier and E. Mirkes, Z. Phys. C **72**, 619 (1996) [arXiv:hep-ph/9601275].

[146] M. Hirsch, H. V. Klapdor-Kleingrothaus and S. G. Kovalenko, Phys. Rev. D **53**, 1329 (1996) [arXiv:hep-ph/9502385];